RNA interference-mediated co-transcriptional gene silencing in fission yeast

Inauguraldissertation

zur
Erlangung der Würde eines Doktors der Philosophie
vorgelegt der
Philosophisch-Naturwissenschaftlichen Fakultät
der Universität Basel

von

Katrina Jane Woolcock

aus Gloucester, UK

Basel, 2012

creative commons

Attribution-Noncommercial-No Derivative Works 2.5 Switzerland

---

You are free:

to Share — to copy, distribute and transmit the work

Under the following conditions:

Attribution. You must attribute the work in the manner specified by the author or licensor (but not in any way that suggests that they endorse you or your use of the work).

Noncommercial. You may not use this work for commercial purposes.

No Derivative Works. You may not alter, transform, or build upon this work.

- For any reuse or distribution, you must make clear to others the license terms of this work. The best way to do this is with a link to this web page.
- Any of the above conditions can be waived if you get permission from the copyright holder.
- Nothing in this license impairs or restricts the author's moral rights.

Your fair dealing and other rights are in no way affected by the above.

This is a human-readable summary of the Legal Code (the full license) available in German:
http://creativecommons.org/licenses/by-nc-nd/2.5/ch/legalcode.de

Disclaimer:
The Commons Deed is not a license. It is simply a handy reference for understanding the Legal Code (the full license) — it is a human-readable expression of some of its key terms. Think of it as the user-friendly interface to the Legal Code beneath. This Deed itself has no legal value, and its contents do not appear in the actual license. Creative Commons is not a law firm and does not provide legal services. Distributing of, displaying of, or linking to this Commons Deed does not create an attorney-client relationship.

Quelle: http://creativecommons.org/licenses/by-nc-nd/2.5/ch/deed.en Datum: 3.4.2009

Genehmigt von der Philosophisch-Naturwissenschaftlichen Fakultät auf Antrag von Prof. Dr. Marc Bühler, Dr. Bas van Steensel und Dr. Dirk Schübeler.

Basel, den 18. September

Prof. Dr. Jörg Schibler
Dekan

Table of Contents

Abbreviations

Ago1	*S. pombe* Argonaute
ARC	Argonaute siRNA chaperone complex
ATF/CREB	activating transcription factor/cAMP response element-binding
BANC	bound by Atf1 under normal conditions
bp	base pairs
ChIP	chromatin immunoprecipitation
CLRC	Clr4-Rik1-Cul4 complex
CTD	C-terminal domain
CTGS	co-transcriptional gene silencing
DamID	DNA adenine methyltransferase identification
DCL	Dicer-like
Dcr1	*S. pombe* Dicer
dsRBD	dsRNA binding domain
dsRNA	double-stranded RNA
endo-siRNA	endogenous siRNA
HDAC	histone deacetylase
HP1	heterochromatin protein 1
LTR	long terminal repeat of retrotransposon
miRNA	microRNA
MVB	multivesicular body
ncRNA	non-coding RNA
NPC	nuclear pore complex
NRDE	nuclear RNAi defective

nt	nucleotides
PAZ	PIWI, Argonaute, and Zwille
piRNA	Piwi-interacting RNA
Piwi	P-element induced wimpy testis
Pol II	RNA polymerase II
Pol IV	RNA polymerase IV
Pol V	RNA polymerase V
pre-miRNA	precursor miRNA
pri-miRNA	primary miRNA
priRNAs	primal RNAs
PTGS	post-transcriptional gene silencing
qPCR	quantitative real-time PCR
RdDM	RNA-directed DNA methylation
Rdp1	*S. pombe* RNA-dependent RNA polymerase
RDRC	RNA-directed RNA polymerase complex
RdRP	RNA-dependent RNA polymerase
RISC	RNA-induced silencing complex
RITS	RNA-induced transcriptional silencing complex
RNAi	RNA interference
RNase III	ribonuclease III
scnRNA	scan RNA
SHREC	Snf2/Hdac-containing repressor complex
siRNA	small interfering RNA
snoRNA	small nucleolar RNA

snRNA	small nuclear RNA
sRNA	small RNA
TF	transcription factor
Tf2	Tf2 LTR retrotransposon
TGS	transcriptional gene silencing
UTR	untranslated region
WAGO	worm-specific AGO
WT	wild type
wtf	with Tf2-type LTRs

Summary

In the last decade or so, RNA interference (RNAi) has gained unanticipated recognition in the fields of RNA biology and gene regulation. It exists in a wide variety of eukaryotic organisms, and various forms of RNAi are involved in diverse biological processes. Furthermore, it has been extensively exploited as an experimental tool and has great potential in therapeutics. At its core, RNAi comprises small non-coding RNAs (sRNAs) in association with Argonaute proteins. The sRNAs are usually produced by cleavage of long double-stranded RNA by the endoribonuclease Dicer enzymes. The sRNAs guide Argonautes to target transcripts via complementary base-pairing, resulting in repression that can occur at various stages of the RNA production process. Perhaps the most well-studied mechanisms of RNAi-mediated repression are those occurring in the cytoplasm at a post-transcriptional level, whereby the target transcript is subject to degradation and/or inhibition of translation. However, well-characterised examples of nuclear RNAi also exist, and usually involve RNAi-mediated chromatin modification such as DNA methylation in plants and histone methylation in protozoa and fungi. These modifications can contribute to heterochromatin formation and inhibit RNA production at the level of transcription. In addition to mediating post-transcriptional and transcriptional gene silencing, recent evidence from several organisms suggests that RNAi can mediate co-transcriptional gene silencing (CTGS), whereby physical association of the RNAi machinery with chromatin can promote degradation of the nascent transcripts and/or inhibit transcription. Such a mode of silencing was first proposed in the fission yeast *Schizosaccharomyces pombe* (*S. pombe*), where the RNAi machinery is thought to repress heterochromatic RNA at a transcriptional and co-transcriptional level. During my PhD, I focused on the association of the RNAi machinery with chromatin in *S. pombe*. Using a sensitive chromatin profiling technique called DamID, I was able to provide the first direct evidence that *S. pombe* Dicer functions *in cis* on chromatin. Secondly, I uncovered a novel role for RNAi in gene regulation outside of the well-studied heterochromatic regions. The evidence presented here shows that the *S. pombe* RNAi machinery is concentrated at nuclear pores where it acts to co-transcriptionally degrade euchromatic RNAs, particularly those from retrotransposon long-terminal repeats, non-coding RNAs and stress response genes bound by the activating transcription factor Atf1. This may keep such features 'poised' for expression, allowing more rapid upregulation under inducing conditions. In addition, I provide evidence that Atf1 has a role in tethering its target genes to nuclear pores and that RNAi-mediated CTGS is

regulated by temperature. Of particular note, Argonaute is not required for targeting the other RNAi components to euchromatin, suggesting that in this case guidance by the sRNA is not responsible for recognition of substrates. I discuss the implications of these results, particularly in the context of RNAi in other eukaryotes.

Introduction

RNA interference

RNA interference (RNAi) was first recognized as a double-stranded RNA (dsRNA)-mediated silencing process in *C. elegans* by Fire and Mello in 1998 (Fire et al., 1998). Soon after this landmark discovery, it was shown in plants that small RNAs (sRNAs) are the guides responsible for silencing (Hamilton and Baulcombe, 1999). Apart from their short length (~20-30 nucleotides (nt)), a defining feature of small silencing RNAs is their association with members of the Argonaute family of effector proteins (Hammond et al., 2001). The sRNAs guide the Argonautes to RNA targets with complementarity, usually inducing silencing (Figure I). Therein lies the beauty of RNAi – the sRNAs are long enough to provide the sequence complexity needed to guide proteins with exquisite specificity to target RNAs. RNA-mediated targeting of RNA was previously thought to be limited to small nuclear RNAs (snRNAs) and small nucleolar RNAs (snoRNAs), which use base complementarity for recognition of RNA substrates in the nucleus, bringing in associated protein partners that mediate RNA splicing and modification, respectively. The discovery of RNAi demonstrated that nature has taken advantage of sRNA-guided targeting in diverse contexts – there may even be an evolutionary link between these sRNA-based pathways. Along with the identification of longer functional non-coding RNAs (ncRNAs), the discovery of RNAi has overturned the traditional perception of RNA as a generally passive messenger between DNA and protein, and placed RNA at the centre of eukaryotic gene regulation.

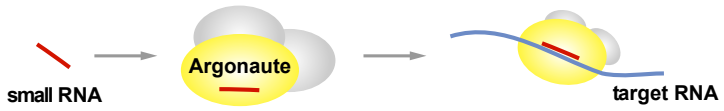

Figure I An Argonaute protein bound to a small RNA forms the minimal RNA-induced silencing complex (RISC), but often associates with accessory proteins to mediate silencing.

My PhD thesis focuses on the role of RNAi in the nucleus of the fission yeast *Schizosaccharomyces pombe* (*S. pombe*). *S. pombe* contains single copies of the major RNAi components Argonaute (Ago1), Dicer (Dcr1), and the RNA-dependent RNA polymerase (Rdp1). Since these are key factors in many RNAi pathways and I have focused particularly on them during my PhD, I will introduce them in some detail below. Broadly, there are three types of small silencing RNAs in eukaryotes: small interfering RNAs (siRNAs), microRNAs (miRNAs),

and Piwi-interacting RNAs (piRNAs). I will introduce these briefly – there are several recent good reviews that discuss each of these pathways in detail (Carthew and Sontheimer, 2009; Ghildiyal and Zamore, 2009; Siomi et al., 2011). I will then follow this with an in-depth introduction to the RNAi pathway in *S. pombe*.

Argonaute

Argonautes, the key effector proteins in RNAi pathways, consist of four domains. Crystal structures, initially from archaea and bacteria, revealed a bilobed structure, with one lobe consisting of the PAZ (PIWI, Argonaute, and Zwille) and N-terminal (N) domains and the other consisting of the PIWI and middle (MID) domains (Ma et al., 2005; Song et al., 2004; Wang et al., 2008b; Wang et al., 2008c; Yuan et al., 2005). The PAZ domain binds the 3' end of the guide RNA, while the MID domain provides a binding pocket for the 5' phosphate. A central cleft allows binding of guide and target RNAs. The PIWI domain adopts an RNase H fold, which contains a catalytic triad (DDE/H motif) that can catalyze guide strand-mediated cleavage of the target RNA ('slicing'). However, not all Argonautes are cleavage competent – some recruit other factors necessary for silencing. *S. pombe* Ago1 does have slicing activity, which is required for siRNA maturation (Buker et al., 2007).

Recently, the first full-length eukaryotic Argonaute crystal structures were reported, including that of human Ago2 (Elkayam et al., 2012; Nakanishi et al., 2012; Schirle and MacRae, 2012) (Figure II). While the overall architecture and the active site structure are conserved with prokaryotes, there are many extended loops and additional secondary structures specific to the eukaryotic Argonautes. Since these insertions are external, they are likely to generate surfaces for interactions with Ago-binding proteins. Although the biological functions of prokaryotic Argonautes are unknown, the conservation of structure implies that all kingdoms of life most likely use this enzyme in fundamentally the same way.

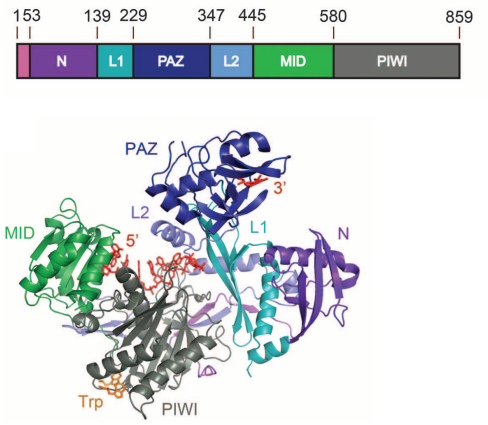

Figure II 2D domain structure and 3D crystal structure of human Ago2. L1 and L2 are linkers. A generic guide RNA (red) can be traced for nucleotides 1-8 and 21. Tryptophan molecules (orange) bind to pockets in the PIWI domain, which may mediate interactions with GW proteins. Adapted from (Schirle and MacRae, 2012).

Most organisms have multiple copies of Argonaute, which can be specialized for different functions. For example, of the 5 Argonaute members in *Drosophila melanogaster* the miRNA pathway predominantly uses AGO1, whereas the siRNA pathway uses AGO2 (Okamura et al., 2004). There are eight, ten and 27 Argonaute paralogues in humans, *Arabidopsis thaliana*, and *C. elegans*, respectively. The Argonaute family of proteins can be split into three subfamilies. Those most similar to *Arabidopsis* Argonaute-1, the Ago clade, are usually involved in siRNA- and miRNA-mediated pathways and are fairly ubiquitously expressed. Members of the Piwi (P-element induced wimpy testis) clade associate with piRNAs and are primarily expressed in the germline. The remaining Argonaute members have been identified so far only in *C. elegans*, and are therefore referred to as worm-specific AGOs, or WAGOs.

Dicer

Dicer proteins are dsRNA-specific ribonucleases of the RNase III family. They usually consist of a PAZ domain, followed by two RNase III domains and a dsRNA binding domain (dsRBD) (Figure II). The N-terminus often contains an RNA helicase domain, which may be important for processivity on long dsRNA substrates (Welker et al., 2011). The helicase/ATPase activity of *S. pombe* Dicer is required for siRNA generation *in vitro* and *in vivo* (Colmenares et al., 2007). The two RNase III domains of Dicer enzymes cleave dsRNA on opposite strands to produce a staggered duplex of ~21-25 nt, with 5' phosphates, 3' hydroxyl groups, and 2-nt 3' overhangs. The distance between the PAZ domain, which anchors the end of the substrate, and the RNase III

domains is thought to act as a ruler to produce sRNAs of characteristic lengths (Macrae et al., 2006). *S. pombe* Dcr1 has an unusual PAZ domain, which may explain the size variability of fission yeast siRNAs compared with other organisms. Interestingly, although *S. cerevisiae* lacks both Dicer and Argonaute homologues, Dicer enzymes were recently identified in some budding yeasts (Drinnenberg et al., 2009). These only have one RNase III domain and are thought to act as dimers, binding cooperatively along the dsRNA substrate such that the distance between consecutive active sites determines the length of the siRNAs (Weinberg et al., 2011). So far, attempts to crystallize the large and complicated metazoan Dicers have failed, and structural insights into the overall architecture have come from electron microscopy studies (Lau et al., 2012) (Figure III).

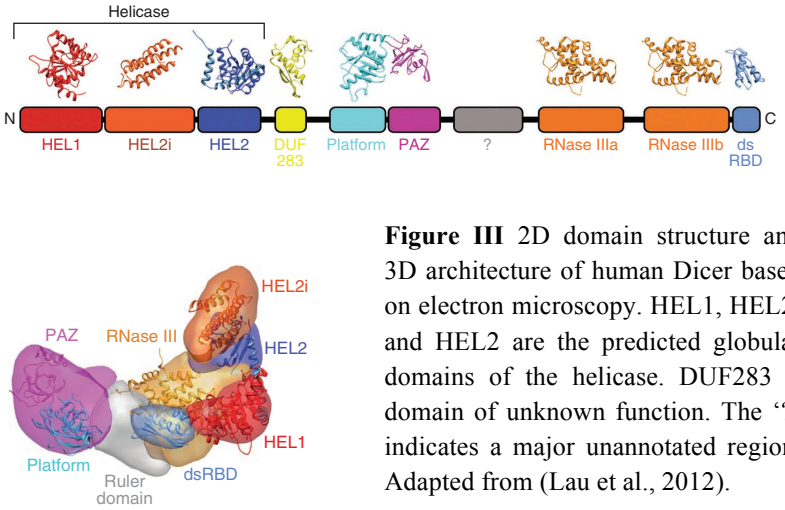

Figure III 2D domain structure and 3D architecture of human Dicer based on electron microscopy. HEL1, HEL2i and HEL2 are the predicted globular domains of the helicase. DUF283 = domain of unknown function. The '?' indicates a major unannotated region. Adapted from (Lau et al., 2012).

Some organisms, such as mammals and *C. elegans*, possess only one Dicer enzyme, which can produce functionally different sRNAs. Others, including *Drosophila* and plants, have several Dicers, which have become specialized for different RNAi pathways. For example, *Drosophila* DCR1 produces miRNAs, whereas DCR2 produces siRNAs (Lee et al., 2004b). In *Arabidopsis*, which has four Dicer-like (DCL) proteins, DCL1 produces miRNAs, and DCL2 makes viral siRNAs (Xie et al., 2004).

RNA-dependent RNA polymerase

In some organisms, RNA-dependent RNA polymerases (RdRPs) are required for amplification of RNAi responses, producing 'secondary' siRNAs. So far, RdRPs have been identified in plants, fungi, protozoa and nematodes. In *C. elegans*, secondary siRNAs are required for the inheritance of RNAi effects (Grishok et al., 2000). In addition, RdRPs are responsible for the phenomenon of 'transitivity' observed in plants and worms, whereby primary siRNAs targeted against one part of a gene promote the production of secondary siRNAs homologous to regions 3' or 5' of the initial target (Sijen et al., 2001; Vaistij et al., 2002). The main route for secondary siRNA production in plants is thought to be unprimed 5' to 3' RNA synthesis starting at the 3' end of target transcripts, followed by Dicer cleavage (Figure IVa). Most *C. elegans* secondary siRNAs, called 22G-RNAs due to their size and 5'G bias, have 5' triphosphates and are predominantly complementary to the target RNA. This suggests that they are produced as individual products in a primer-independent manner on the mRNA template, rather than being Dicer products (Pak and Fire, 2007; Sijen et al., 2007) (Figure IVb). The 22G-RNAs are usually loaded onto members of the WAGO group (Yigit et al., 2006).

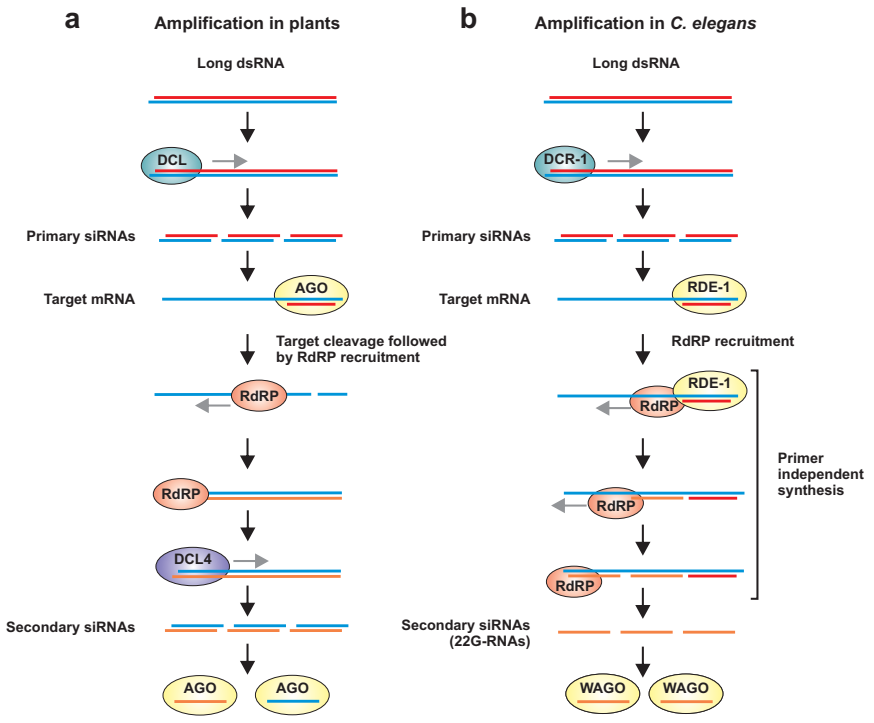

Figure IV Secondary siRNA production in plants and *C. elegans*. (**a**) In plants, a primary siRNA guides target cleavage, which allows RNA synthesis from the 3' end. The resulting dsRNA is cleaved by Dicer-like 4 to give secondary siRNAs of both orientations. (**b**) In *C. elegans*, a primary siRNA bound to the 'primary Argonaute' RDE-1 guides RdRP recruitment. The RdRP mediates primer independent synthesis of secondary siRNAs, which are predominantly antisense to the target. Adapted from (Ghildiyal and Zamore, 2009).

Rdp1-dependent transitivity has also been reported in *S. pombe* (Simmer et al., 2010). Rdp1 has been shown to function in a primer-independent manner *in vitro* (Motamedi et al., 2004; Sugiyama et al., 2005), although all detectable centromeric siRNAs have a 5' monophosphate (Djupedal et al., 2009). Therefore, it is likely that Rdp1 mediates primer-independent second-strand synthesis, creating long dsRNAs that are then cleaved by Dcr1 (Colmenares et al., 2007).

siRNA-mediated silencing

siRNAs are usually derived from long exogenous dsRNAs such as viruses, which are cleaved into ~21 nt sRNAs by Dicer (Bernstein et al., 2001). The strand that directs silencing is called the guide strand while the other, which is destroyed, is called the passenger strand. The guide strand bound to an Argonaute constitutes the minimal mature RNA-induced silencing complex (RISC). siRNAs usually bind to their targets with perfect complementarity and mediate post-transcriptional cleavage of the target RNA by the Piwi domain of the Argonaute. While the role of this pathway is best characterised for the response to exogenous dsRNAs, various endogenous siRNA (endo-siRNA) pathways have been identified, most readily in species possessing RdRPs and more recently in *Drosophila* and mammals (Okamura and Lai, 2008). For example, endo-siRNAs can repress transposable elements in *Drosophila* somatic cells that lack the piRNA pathway (Chung et al., 2008; Czech et al., 2008; Ghildiyal et al., 2008; Kawamura et al., 2008). This pathway depends on the siRNA-generating DCR2 and the predominant siRNA effector AGO2.

miRNA-mediated silencing

miRNAs, around 20-24 nt long, are generally derived from precursor transcripts called primary miRNAs (pri-miRNAs), produced by RNA polymerase II (Pol II) (Lee et al., 2004a). The pri-miRNA is first processed in the nucleus by Drosha, another RNase III endonuclease, to produce a 60-70 nt hairpin pre-miRNA (Lee et al., 2003). The pre-miRNA is exported and cleaved by Dicer in the cytoplasm. In plants, DCL1 fulfils the roles of both Drosha and Dicer in the nucleus. A few miRNAs in *Drosophila* and mammals are nearly fully complementary to their mRNA

targets and can direct cleavage (Yekta et al., 2004). Since plant miRNAs are highly complementary to their targets, it was assumed that this would be the predominant mode of their silencing activity (Rhoades et al., 2002). However, there is also evidence for widespread miRNA-mediated translational repression (Brodersen et al., 2008). In contrast to plants, most miRNAs in *Drosophila* and mammals have limited complementarity, restricted to the 5' 'seed region' (Lewis et al., 2003). The small size of the seed region means that a single miRNA can regulate many different genes. It has been proposed that extensive pairing to a target RNA exposes the small RNA to nucleotidyl transferases and 3'-to-5' exonucleases (unless it is 2'-*O*-methylated at the 3' end), making it unstable (Ameres et al., 2010; Ameres et al., 2011). This provides an explanation for the partial complementarity between animal miRNAs and their targets. The mode of miRNA-mediated repression in animals can involve both repression of translation and degradation of the target mRNA. Several recent papers indicate that repression of translation initiation generally precedes deadenylation and mRNA decay (Bazzini et al., 2012; Bethune et al., 2012; Djuranovic et al., 2012).

piRNA-mediated silencing

First discovered in *Drosophila* (Aravin et al., 2001), ~24-32 nt piRNAs are required for germline development and fertility. They do not require Dicer for their production and bind to members of the Piwi clade of Argonautes. Primary piRNA biogenesis is thought to occur mainly via the processing of long single-stranded transcripts produced from piRNA clusters. Many piRNAs correspond to repetitive sequences such as transposable elements and can mediate their cleavage (Brennecke et al., 2007; Gunawardane et al., 2007). Although *Drosophila* and mammals most likely lack RdRP activity, a mechanism for piRNA amplification does exist in the germline. This is known as the 'ping-pong' cycle and was first proposed based on observations made in *Drosophila* (Brennecke et al., 2007; Gunawardane et al., 2007), which have three Piwi proteins: Piwi, Aubergine (Aub), and AGO3. Piwi and Aub are mainly associated with antisense piRNAs, whereas AGO3 harbours mainly sense piRNAs. Sense and antisense piRNAs targeting individual transposons tend to have overlapping 5' ends separated by exactly 10 nt, the distance that Piwi proteins cleave their targets from the 5' end of the guide. These observations suggested the

following amplification cycle: an Aub-associated piRNA antisense to an expressed transposon mediates cleavage of its target. This results in a new sense piRNA that associates with AGO3. The sense piRNA base pairs with an antisense piRNA cluster transcript, and mediates cleavage to generate another Aub-bound antisense piRNA, identical to the initiator piRNA. The cycle only acts efficiently if a target transcript is present, so will amplify piRNAs targeting active transposons. In this way, it is analogous to RdRP-dependent amplification, which also uses the target transcript to amplify functionally relevant small RNAs. However, in contrast to secondary siRNA production, the ping-pong cycle does not result in transitivity. Signatures of the ping-pong cycle have been found in diverse organisms including zebrafish, *Xenopus laevis* and mammals. Although the exact mechanisms of piRNA-mediated silencing are unclear, they are likely to include both transcriptional and post-transcriptional aspects (Olovnikov et al., 2012) (see discussion).

RNAi-mediated heterochromatin formation

Although the small RNAs described above are thought to predominantly mediate post-transcriptional gene silencing (PTGS) in the cytoplasm, RNAi also has well-characterised roles in heterochromatin formation in plants, *Tetrahymena thermophila*, and *S. pombe*. Heterochromatin was originally distinguished from euchromatin cytologically as regions of chromosomes that do not undergo post-mitotic decondensation, but remain condensed during interphase (Heitz, 1928). Although chromatin has traditionally been classed as either repressive heterochromatin or active euchromatin, it is now clear that chromatin domains are more complex (Filion et al., 2010). Nonetheless, the type of chromatin I will be referring to as heterochromatin is generally characterised by histone hypoacetylation and methylation of histone H3 lysine 9 (H3K9me) (Rea et al., 2000). Di- and trimethylated H3K9 is recognized and bound by the conserved heterochromatin protein 1 (HP1) proteins via their chromodomain (Bannister et al., 2001; Lachner et al., 2001). HP1 proteins also contain a C-terminal chromoshadow domain that is thought to mediate protein-protein interactions, including self-association.

Since heterochromatin is highly compact, and presumably less accessible to the transcription machinery, it has traditionally been viewed as transcriptionally inactive. However, studies in the last decade or so have challenged this assumption. Firstly, with the advent of genome-wide techniques for studying transcription, including next generation sequencing technologies, it has become clear that transcription is more widespread than anticipated, and is not restricted to euchromatin (Kapranov et al., 2007; Wilhelm et al., 2008). Secondly, small RNAs produced from heterochromatic regions are actually essential for the formation of heterochromatin in several organisms (detailed below). In general, these sRNAs guide Argonautes to nascent transcripts and target chromatin modifications.

RNA-directed DNA methylation in plants

RNA-mediated chromatin modification was first observed in plants (Wassenegger et al., 1994). Although the mechanism was not understood at the time, it is now known that small RNAs play a key role in RNA-directed DNA methylation (RdDM) (Figure V) (Matzke et al., 2009; Zhang and Zhu, 2011). Repetitive genomic sequences including transposons and centromeric repeats produce 24 nt siRNAs that target DNA methylation to silence these regions and other loci that are homologous to the siRNAs. Briefly, the plant-specific RNA polymerase IV (Pol IV) transcribes precursors that are processed by the RdRP RDR2 and the Dicer-like DCL3 to produce siRNAs that load onto AGO4 (Herr et al., 2005). Another plant-specific RNA polymerase, Pol V, produces transcripts that presumably act as scaffolds for association of AGO4-siRNA complexes and subsequent chromatin modification (Wierzbicki et al., 2008). The extended C-terminal domain (CTD) of Pol V contains WG/GW repeats that provide a platform for interaction with AGO4 (El-Shami et al., 2007). It is likely that the siRNAs interact with the nascent RNA, although it is possible that they pair with target DNA exposed by Pol V transcription. The de novo methyltransferase DRM2 is thought to be primarily responsible for the DNA methylation (Cao and Jacobsen, 2002). Intriguingly, it was shown recently that RdDM is not a solely nuclear process, as AGO4 is loaded with heterochromatic siRNAs in the cytoplasm and AGO4-mediated slicing is required to produce the mature complex that can enter the nucleus (Ye et al., 2012).

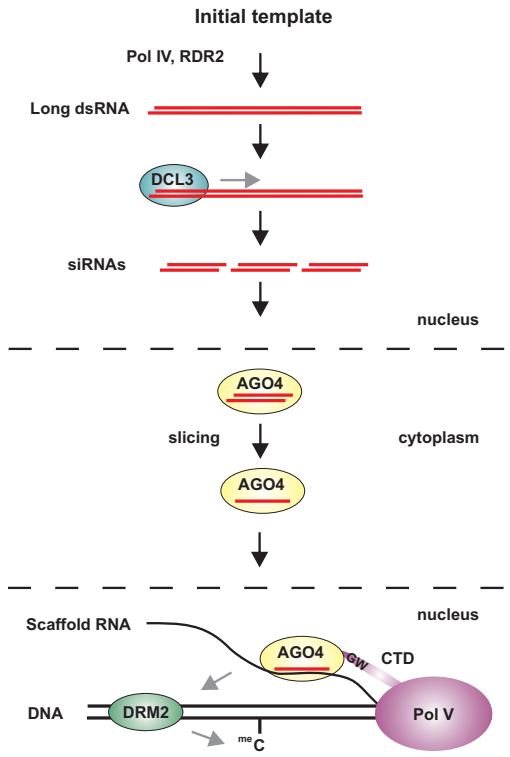

Figure V Model for RNA-directed DNA methylation in plants. Pol IV transcription of repetitive sequences followed by RDR2 activity produces dsRNA substrates for DCL3 in the nucleus. The resulting siRNAs are loaded onto AGO4 in the cytoplasm, where cleavage of the passenger strand occurs. The mature AGO4-siRNA complex can enter the nucleus and target homologous regions, probably by base-pairing with Pol V-dependent transcripts. GW repeats in the C-terminal domain of Pol V stabilise the association of AGO4. Chromatin is subsequently modified by the de novo DNA methyltransferase DRM2.

RNA-directed DNA elimination in *Tetrahymena*

In the ciliated protozoan *Tetrahymena*, an extreme example of RNAi-directed heterochromatin formation leads eventually to DNA elimination of transposon-related sequences from the newly-developing somatic (macronuclear) genome (Kataoka and Mochizuki, 2011) (Figure VI). During sexual conjugation, the whole germline (micronuclear) genome is bidirectionally transcribed, probably by Pol II, and processed in the nucleus by the Dicer Dcl1p to ~28-30 nt 'scan' RNAs (scnRNAs) (Malone et al., 2005; Mochizuki and Gorovsky, 2005). These scnRNAs associate with the Argonaute Twi1p in the cytoplasm. Similar to the situation in plants, Twi1p slicer activity is required for subsequent localization of the Twi1p-scnRNA complex to the parental macronucleus. In this case, Giw1p binds to Twi1p only in the context of the mature complex and mediates its nuclear import (Noto et al., 2010). Once in the parental macronucleus, it is thought that base-pairing interactions between the scnRNAs and nascent non-coding transcripts from the parental macronuclear genome mediate scnRNA degradation. Therefore, this 'scnRNA selection'

leaves only those scnRNAs with no homologous sequences in the parental macronuclear genome. The remaining scnRNAs, still bound to Twi1p, relocate to the newly-developing macronucleus where they target homologous sequences and mediate methylation of H3K9 and H3K27. Subsequent binding of chromodomain proteins marks these regions for excision by a PiggyBac transposase-like protein (Cheng et al., 2010). Therefore, this elegant mechanism ensures elimination of any sequences not present in the parental macronucleus.

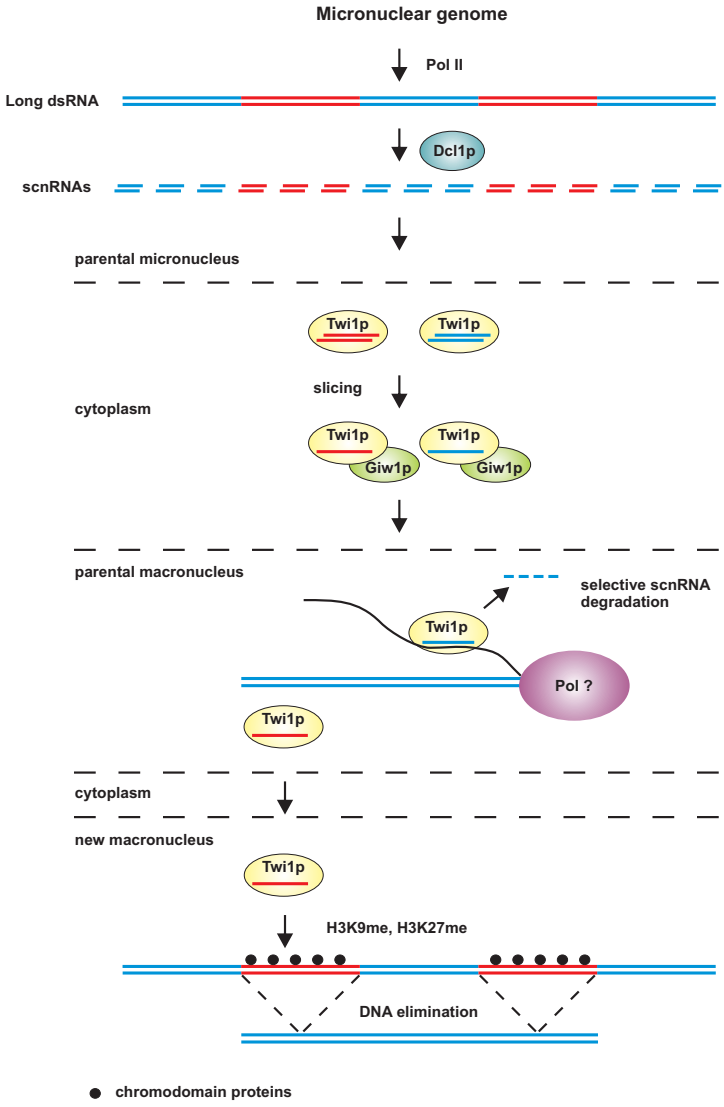

Figure VI Model for RNA-directed DNA elimination in *Tetrahymena*. The whole micronuclear (germline) genome is transcribed and processed by Dcl1p to produce ~28-30 nt scnRNAs. These associate with the Argonaute Twi1p in the cytoplasm, where cleavage of the passenger strand occurs. Giw1p associates with the mature Twi1p-scnRNA complex and mediates its import to the parental macronucleus. Base-pairing with nascent transcripts induces degradation of homologous scnRNAs, leaving only those matching sequences not present in the macronucleus. These scnRNAs, still bound to Twi1p, enter the developing macronucleus and target histone modifications to homologous regions. Subsequent binding by chromodomain proteins directs these regions for elimination. Many details of this process are still unclear.

In the fission yeast *S. pombe*, siRNAs are essential for centromeric heterochromatin assembly (White and Allshire, 2008), as discussed in detail below.

Heterochromatin formation in *S. pombe*

RNAi-mediated heterochromatin formation in *S. pombe* is perhaps the most extensively studied example of nuclear RNAi. All three major regions of heterochromatin in *S. pombe*, the centromeres, mating-type region and telomeres, contain *dg* and/or *dh* repeats that serve as RNAi-dependent heterochromatin nucleation centres. However, the exact mechanisms of silencing differ at each.

Centromeric heterochromatin

In *S. pombe*, the central kinetochore binding site is flanked by innermost repeats (*imr*) which in turn are surrounded by outermost repeats (*otr*) comprising the heterochromatic *dg* and *dh* repeats. Ten years ago, it was shown that all three major components of the RNAi machinery present in *S. pombe*, Ago1, Dcr1 and Rdp1, are essential for the formation of centromeric heterochromatin (Volpe et al., 2002). Loss of RNAi-mediated heterochromatin formation is accompanied by defects in chromosome segregation (Provost et al., 2002). As a result of intense study, the mechanistic details and key components of this process are now quite well-characterised (Figure VII). The RNA-induced transcriptional silencing complex (RITS; consisting of Ago1, Chp1 and Tas3) (Verdel et al., 2004) is loaded, via the Argonaute siRNA chaperone complex (ARC; consisting of Ago1, Arb1 and Arb2) (Buker et al., 2007), with Dcr1-dependent single-stranded siRNAs. RITS is guided to chromatin via base-pairing of the Ago1-bound siRNA with complementary sequences in RNA Pol II nascent transcripts (Buhler et al., 2006). The importance of Pol II in the process is demonstrated by mutants in two different Pol II subunits that are defective in heterochromatin formation but not general transcription (Djupedal et al., 2005; Kato et al., 2005). Once tethered via nascent transcripts, RITS recruits CLRC (Clr4-Rik1-Cul4 complex), a complex containing the sole *S. pombe* H3K9 methyltransferase Clr4 (Bayne et al., 2010). Similar to *Tetrahymena*, RNAi-directed histone methylation provides a binding site for HP1 homologues such as Swi6 and Chp2, and can additionally stabilize binding of RITS via the chromodomain-containing Chp1 component. However, instead of mediating DNA elimination, these HP1 proteins are thought to promote transcriptional gene silencing (TGS; see

below). Clr4 itself also contains a chromodomain that binds H3K9me, which is thought to promote spreading of heterochromatin (Zhang et al., 2008). RITS also helps to recruit the RNA-dependent RNA polymerase complex (RDRC; consisting of Rdp1, Cid12 and Hrr1), amplifying the process by generating more dsRNA substrates for Dcr1 (Motamedi et al., 2004; Sugiyama et al., 2005). Thus, the RNAi machinery acts in a positive feedback loop on centromeric repeats, guaranteeing high levels of H3K9 methylation and rapid turnover of centromeric RNAs into siRNAs. This '*in cis*' model is supported by crosslinking of RITS and RDRC subunits to chromatin (Cam et al., 2005; Motamedi et al., 2004; Noma et al., 2004).

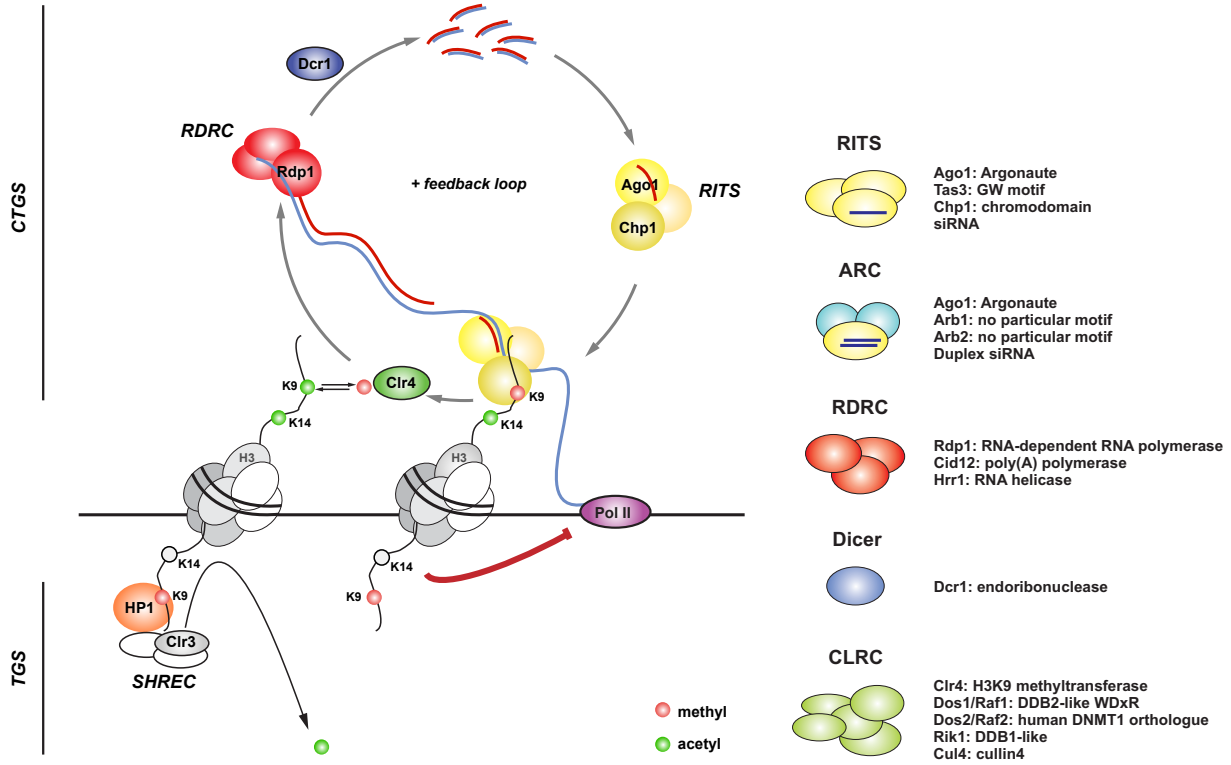

Figure VII Model for RNAi-mediated heterochromatin formation at centromeres in *S. pombe* and the major protein complexes involved. Repression of centromeric transcripts and maintenance of high levels of H3K9me depends on a positive feedback loop. Dcr1-dependent siRNAs from the centromeric repeats guide the RITS complex to nascent Pol II transcripts via complementary base-pairing. RITS recruits the Clr4-containing CLRC complex, which mediates H3K9 methylation. This stabilizes RITS association with chromatin via the Chp1 component. RITS helps to recruit RDRC, and Dcr1 processing of the resulting dsRNA produces more siRNAs, as well as contributing to CTGS. In addition to stabilizing RITS association, H3K9me creates binding sites for HP1 proteins, including Chp2. Chp2 recruits the SHREC complex, containing the HDAC Clr3. Deacetylation of H3K14 by Clr3 reduces transcription. Therefore, tight repression involves a combination of TGS and CTGS.

Whereas in most other eukaryotes tested introduction of an artificial source of siRNAs is sufficient to trigger PTGS of any homologous locus, RNAi-mediated repression and assembly of heterochromatin in *S. pombe* occurs inefficiently *in trans* and depends to some extent on the chromosomal location of the target gene (Buhler et al., 2006; Iida et al., 2008; Simmer et al., 2010). The reason for this *cis*-restriction is not clear.

Transcriptional versus co-transcriptional gene silencing

Repression of heterochromatin involves mechanisms that restrict RNA Pol II access to the DNA, ensuring TGS. In *S. pombe*, this strongly depends on the acetylation level of histone H3 lysine 14 (H3K14). Whereas H3K14 acetylation correlates with active transcription, deacetylation of H3K14 restricts the access of Pol II to heterochromatin and thus limits transcription in *S. pombe* (Sugiyama et al., 2007; Yamada et al., 2005). Deacetylation of H3K14ac occurs downstream of H3K9 methylation and is mediated by the class II histone deacetylase (HDAC) Clr3, a component of the Snf2/Hdac-containing repressor complex (SHREC) (Bjerling et al., 2002; Sugiyama et al., 2007). SHREC can be recruited to heterochromatin by physically interacting with the HP1 Chp2 (Fischer et al., 2009; Motamedi et al., 2008). In addition, Swi6 associates with the class I HDAC Clr6, which has broader specificity (Nicolas et al., 2007; Yamane et al., 2011).

However, the fact that, contrary to the traditional assumption, heterochromatin is not completely inaccessible to the transcription machinery shows that TGS cannot be the only mode of silencing. Indeed, deleting components of the SHREC complex resulted in only partial derepression of centromeric transcripts compared to *clr4*Δ cells (~10-20%), whereas a comparable increase in Pol II occupancy was observed (Motamedi et al., 2008). Therefore, it is likely that the rest of the silencing involves RNAi-mediated co-transcriptional gene silencing (CTGS), by direct degradation of the heterochromatic RNAs as they are transcribed (Buhler et al., 2006; Noma et al., 2004). Other factors are likely to be involved in CTGS. For example, in cells lacking the non-canonical poly(A) polymerase Cid14, heterochromatic transcripts are increased, while the structure of heterochromatin remains intact (Buhler et al., 2007). It is

thought that polyadenylation by Cid14 targets RNA for degradation via the RNA exosome and/or the RNAi pathway. In summary, TGS and CTGS cooperate to ensure tight repression of centromeric transcripts in *S. pombe* (Figure VII).

Mating-type region and telomeres

The RNAi machinery is also required for establishment of heterochromatin at the mating-type region and subtelomeres, but redundant mechanisms ensure maintenance in the absence of RNAi. At the mating-type region, RNAi acts via the *cenH* (centromeric homology) sequence, which has 96% similarity to *dg* and *dh*, to nucleate heterochromatin formation. However, only when RNAi deletions are combined with deletion of Atf1 or Pcr1 is silencing lost (Jia et al., 2004). Atf1 and Pcr1 contain basic leucine zipper (bZIP) DNA binding domains with strong homology to the activating transcription factor/cAMP response element-binding (ATF/CREB) protein family. Atf1 and Pcr1 form a heterodimer and are involved in environmental stress responses. They act in parallel with the RNAi pathway to establish and maintain heterochromatin at the mating-type locus, perhaps by direct recruitment of Clr4/Swi6 (Jia et al., 2004). Interestingly, a role for the *Drosophila* homologue of Atf1, dATF-2, in heterochromatin formation has been shown (Seong et al., 2011).

Genes encoding RecQ type DNA helicases *tlh1* and *tlh2*, located at the ends of chromosome 1 and 2 respectively, have high homology to the *cenH* sequence (Kanoh et al., 2005). The telomeric repeat-binding protein Taz1 and RNAi act redundantly to establish heterochromatin at telomeres, although other yet-to-be-identified factors are also involved (Hansen et al., 2006; Kanoh et al., 2005). Taz1 and Ccq1 may cooperate to recruit SHREC to the telomere ends (Sugiyama et al., 2007).

Establishing interactions of the RNAi machinery with the genome

A controversial question with regard to RNAi-mediated silencing in fission yeast is how the RNAi machinery is brought to certain regions of the genome in the first place. The

interdependence of the RNAi and chromatin modifying pathways due to the positive feedback loop make it difficult to identify the initial trigger. Several possibilities have been proposed: (1) formation of dsRNA by base pairing of sense and antisense centromeric transcripts, (2) folding of single stranded centromeric transcripts into hairpin structures (Djupedal et al., 2009), (3) recruitment of RITS and RDRC by low levels of H3K9me, which are present in RNAi mutants (Partridge et al., 2007), and (4) random association of degradation products with Argonaute (Halic and Moazed, 2010). In the latter model, it was proposed that Dcr1- and Rdp1-independent degradation products, so-called primal RNAs (priRNAs), guide Argonaute to the repeats to begin the amplification process. Consistent with this, the authors found lower levels of H3K9me in *ago1*Δ compared to *dcr1*Δ or *rdp1*Δ cells (Halic and Moazed, 2010). This model has been challenged by the finding that CLRC components, and not RNAi factors, play a critical role in assembling centromeric heterochromatin when Ago1 is physically separated from Tas3-Chp1, and that indistinguishable low levels of H3K9me remain at centromeres in all three RNAi mutants (Shanker et al., 2010). Therefore, how the initial establishment of RNAi-chromatin interactions occurs remains unclear.

Cell cycle regulation of heterochromatin

Several papers provide evidence that transcription of centromeric repeats and production of siRNAs is highest in S phase, corresponding to lower levels of H3K9me and Swi6 (Chen et al., 2008; Kloc et al., 2008). During G2, RITS is recruited and the positive feedback loop establishes robust silencing. It is thought that phosphorylation of H3S10 in mitosis inhibits Swi6 binding, since this mark has been shown to antagonize the binding of chromodomain proteins to H3K9me (Fischle et al., 2005; Hirota et al., 2005). Therefore TGS is somewhat relieved in G1/S, allowing increased transcription and siRNAs. This model provides a possible explanation for the paradox of transcriptionally active heterochromatin, since the transcriptional activity is mainly restricted to S phase. However, it does not provide an explanation for how the positive feedback loop is started.

Roles for nuclear RNAi outside heterochromatin in *S. pombe*

While much is known about the role of RNAi at heterochromatin in fission yeast, relatively little is known about functions in euchromatin. At some regions, Ago1 cooperates with histone variant H2A.Z, Rrp6 (3'-to-5' exoribonuclease component of the nuclear exosome) and Clr4 to silence antisense transcripts (Zofall et al., 2009). At specific meiotic genes, the Mmi1 RNA surveillance machinery can recruit H3K9me and RITS, although their contribution to silencing in vegetative cells appears to be small (Hiriart et al., 2012; Zofall et al., 2012).

At some convergent gene pairs, inefficient transcription termination in G1 results in overlapping transcripts and presumably dsRNA, leading to RNAi-dependent deposition of H3K9me3 and Swi6 (Gullerova and Proudfoot, 2008). Swi6 recruits cohesin (Nonaka et al., 2002), which is then concentrated to the intergenic region, presumably by the action of the Pol II machinery (Lengronne et al., 2004), promoting efficient transcription termination throughout G2. Loss of cohesin in M phase leads again to inefficient transcription termination in G1. Recently, it has been shown that genes encoding RNAi components often occur in co-transcribed convergent gene pairs and participate in an autoregulatory process (Gullerova et al., 2011). Their RNAi-dependent downregulation in G1/S is thought to contribute to relief of centromeric silencing in this phase, while in G2 accumulation of cohesin prevents overlapping transcription and restores their expression to promote centromeric silencing.

Nuclear organisation of the RNAi pathway in *S. pombe*

When I started my PhD, little was known about the subcellular localization of Dcr1, and the microscopy data available contradicted the known role for Dcr1 in the nucleus (Carmichael et al., 2006). Since then, live-cell imaging studies from our lab have shown that GFP-Dcr1 forms nuclear peripheral foci (Emmerth et al., 2010) (Figure VIIIa). Dcr1 appears to be tethered to nuclear pores since in a *nup120*Δ mutant, which shows a pore-clustering phenotype, Dcr1 clusters to one side of the nucleus (Figure VIIIa). The dsRBD was shown to be required for nuclear retention of Dcr1 and consequently centromeric silencing. Subsequent structural studies

revealed that zinc-coordination by the dsRBD is critical for proper folding of the domain and hence for Dcr1 nuclear localization (Barraud et al., 2011) (Figure VIIIb). However, the relevance of Dcr1-pore association was not clear, since no mutant was identified where loss of pore interaction but not loss of nuclear localization occurred. It is possible that interaction between the dsRBD and a pore component (directly or indirectly) is required for nuclear retention.

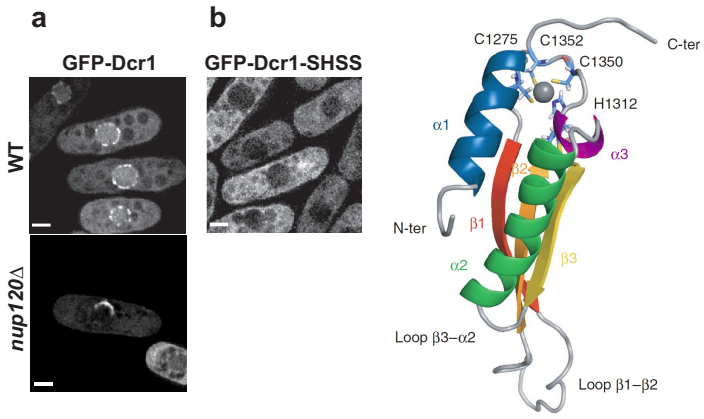

Figure VIII Subcellular localization of Dcr1. (**a**) Fluorescence microscopy of living cells showing the localization of GFP-Dcr1 in wild type and *nup120*Δ cells, in which NPCs cluster. Figure taken from (Emmerth et al., 2010). (**b**) Left: live-cell imaging of the zinc motif mutant GFP-Dcr1-SHSS. Scale bars = 2 µm. Right: cartoon representation of the lowest energy NMR solution structure of the Dcr1 C-terminus. The zinc coordinating residues (CHCC) are shown as sticks in light blue. The zinc ion is shown as a grey sphere. Figure taken from (Barraud et al., 2011).

In recent years, the importance of nuclear organisation in genome regulation has become increasingly apparent. In particular, the nuclear periphery seems to have both repressive and activating properties. Studies in budding yeast suggest that the nuclear periphery between pores is generally a repressive environment, while nuclear pores are important for activation of certain genes (Taddei et al., 2010). Similarly, in metazoan cells, the nuclear lamina is generally a repressive environment whereas genes associated with nuclear pore complexes (NPCs) are generally active or at least moderately transcribed (Kind and van Steensel). There is accumulating evidence from *S. cerevisiae* that transcription factors (TFs) are involved in targeting certain genomic regions to nuclear pores. For example, the upstream regions of genes enriched for some *S. cerevisiae* nuclear pore components have over-representation of the Rap1 binding motif (Casolari et al., 2004). In another study, genetic and biochemical experiments demonstrated a link between the Rap1 activation complex and NPCs (Menon et al., 2005). Several inducible genes, for example *GAL1*, *GAL2*, *INO1*, *HXK1* and *HSP104*, are targeted to the NPC upon activation and, at least in some cases, the gene promoter is required for this (Dieppois et al., 2006; Taddei, 2007). DNA 'zip' codes within the promoters of some genes are

necessary and sufficient for targeting to NPCs (Ahmed et al., 2010; Light et al., 2010). Recently, it was shown that the transcription factor Put3 is required for targeting via one of these zip codes (Brickner et al., 2012). Furthermore, a transcriptional repressor has been implicated in tethering certain genomic regions to the nuclear lamina in mammalian cells (Zullo et al., 2012), suggesting that TF-mediated genome organisation at the nuclear periphery is widespread. In contrast to other eukaryotes, not much is known about the role of nuclear localization in gene regulation in *S. pombe* (Olsson and Bjerling, 2011). The fact that *S. pombe* Dcr1 associates with nuclear pores suggests the intriguing possibility that Dcr1 could be involved in gene regulation in these foci.

Aim of the thesis

The aim of my PhD project was to investigate interactions, beyond those previously characterised, of the RNAi machinery and associated factors with the fission yeast genome. A particular focus was on Dcr1, which cannot be efficiently cross-linked to chromatin. Next, I aimed to characterise the mechanism of recruitment to bound regions and to investigate possible functions of the RNAi machinery at regions outside the well-studied heterochromatic loci.

Results

Part I: RNAi-mediated co-transcriptional gene silencing in euchromatin

Results published in:

- Woolcock K, Gaidatzis D, Punga T, Bühler M (2011). Dicer associates with chromatin to repress genome activity in *Schizosaccharomyces pombe*. ***Nat Struct Mol Biol*** 18(1):94-9.
- Woolcock K, Stunnenberg R, Gaidatzis D, Hotz H-R, Emmerth S, Barraud P, Bühler M (2012). RNA interference keeps Atf1-bound stress response genes in check at nuclear pores. ***Genes Dev*** 26(7):683-92.
    - ∗ Highlighted in Holoch D and Moazed D (2012). RNAi in fission yeast finds new targets and new ways of targeting at the nuclear periphery. ***Genes Dev*** 26(8):741-5.

See Appendix for the above manuscripts.

In order to study the interactions between Dcr1 and the fission yeast genome, I chose to use an alternative chromatin profiling technique called DamID (DNA adenine methyltransferase identification). First developed in *Drosophila* (van Steensel and Henikoff, 2000), DamID involves fusion of the protein of interest to the adenine methyltransferase Dam from *E. coli* (Figure 1A). On interaction of the fusion protein, which is expressed at low levels in addition to the endogenous copy of the protein of interest, with chromatin, Dam methylates the N^6 position of adenine in the sequence context GATC. Methylated fragments can be isolated using methylation-specific restriction enzymes, and then PCR amplified and hybridised to tiling arrays. Comparing the methylation pattern in a strain expressing the fusion protein with that in a strain expressing Dam alone shows which regions of the genome were bound by the protein of interest. DamID has a major advantage over chromatin immunoprecipitation (ChIP) in that the methylation will occur even upon transient, indirect and weak interactions, whereas ChIP requires a robust interaction to achieve cross-linking. The disadvantage is that it is impossible to look at a particular time window, since the methylation will continually accumulate.

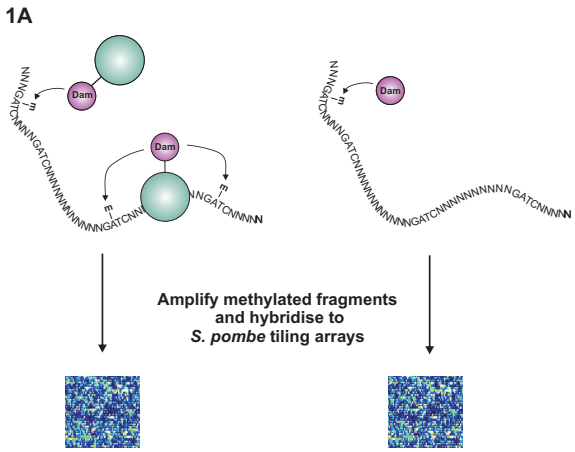

Figure 1A Outline of the DamID technique. The protein of interest is expressed at low levels as a fusion protein with Dam, a DNA adenine methyltransferase from *E. coli*. Therefore Dam leaves methyl marks close to the genomic binding sites. A Dam only control is carried out in parallel.

First, I tested the DamID approach by carrying it out for three proteins for which ChIP in combination with microarrays (ChIP-chip) had already been published; Swi6, Rdp1 and Ago1 (Cam et al., 2005). The DamID showed a good overlap with the ChIP-chip profiles, despite having generally lower enrichments (Figure 1B). I therefore proceeded to carry out DamID for Dcr1. In support of the '*in cis*' model for RNAi-mediated heterochromatin formation, the results showed that Dcr1 is enriched at centromeric regions, although with lower enrichment than for Swi6, Rdp1 and Ago1 (Figure 1C). Dcr1 is not enriched at the other major regions of heterochromatin (Figure 1C). Interestingly, Dcr1 showed enrichment not only at centromeres, but also at several euchromatic regions, particularly loci producing ncRNAs and long terminal repeats of retrotransposons (LTRs) (Figure 1C). A similar pattern was seen at these regions for Rdp1 and Ago1, but not Swi6, suggesting that the core RNAi components might be involved in regulating these regions independently of their role in heterochromatin formation.

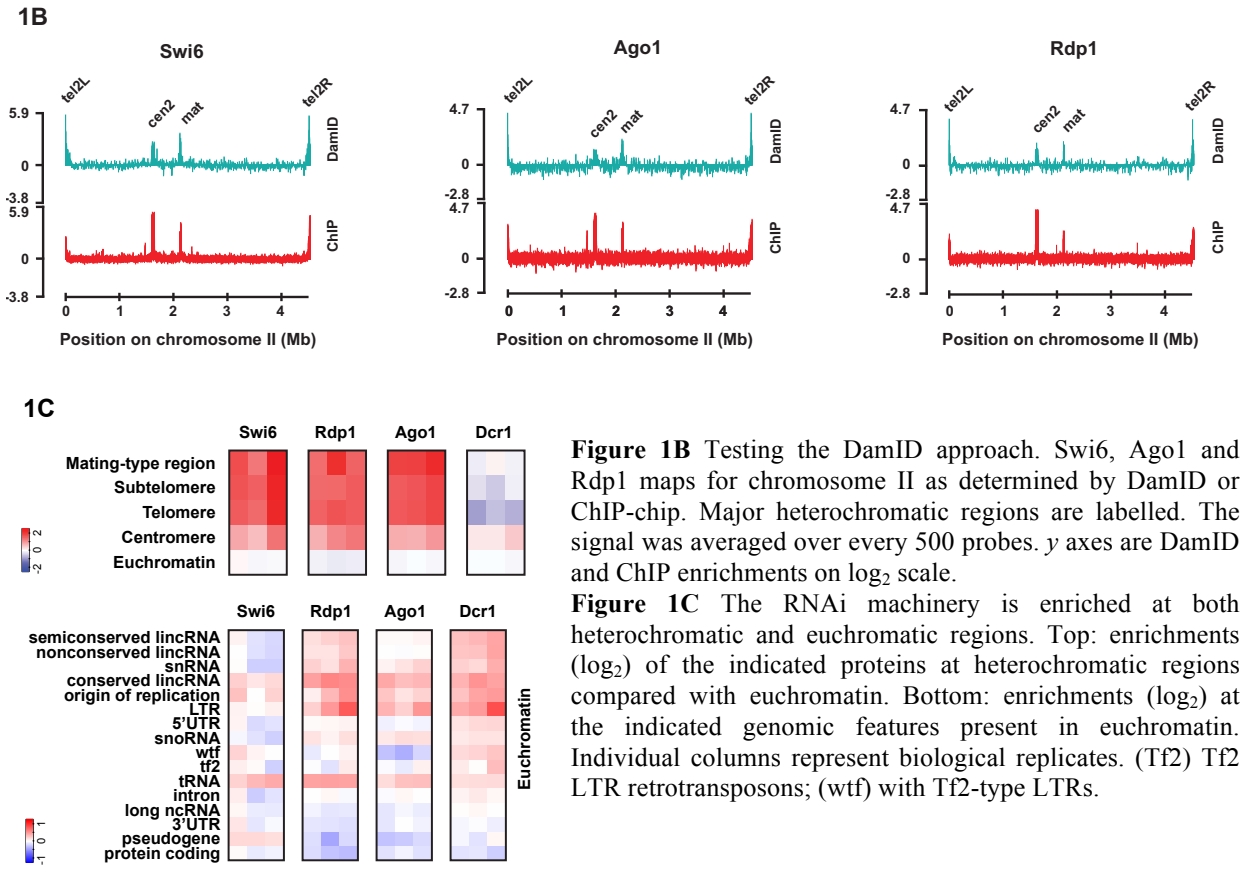

Figure 1B Testing the DamID approach. Swi6, Ago1 and Rdp1 maps for chromosome II as determined by DamID or ChIP-chip. Major heterochromatic regions are labelled. The signal was averaged over every 500 probes. *y* axes are DamID and ChIP enrichments on $\log_2$ scale.

Figure 1C The RNAi machinery is enriched at both heterochromatic and euchromatic regions. Top: enrichments ($\log_2$) of the indicated proteins at heterochromatic regions compared with euchromatin. Bottom: enrichments ($\log_2$) at the indicated genomic features present in euchromatin. Individual columns represent biological replicates. (Tf2) Tf2 LTR retrotransposons; (wtf) with Tf2-type LTRs.

To investigate this possibility, I used quantitative real-time PCR (qPCR) to test several of the bound regions for changes in expression upon deletion of the RNAi components. Indeed, I observed an increase in RNA levels for several loci in all three RNAi mutants (Figure 1D and data not shown), suggesting that RNAi acts to silence these regions. The silencing depends on the RNase III activity of Dcr1 (Figure 1D), therefore I expected to see siRNAs mapping to the silenced regions. Surprisingly, however, very few total or Ago1-bound small RNAs are produced from these regions according to published deep sequencing data (Emmerth et al., 2010; Halic and Moazed, 2010) (data not shown). In addition, RNAi association with these regions does not seem to result in H3K9 methylation and Swi6 binding (Figure 1C and data not shown), suggesting that the silencing mechanism is distinct from that occurring at heterochromatin. This led us to propose a model whereby RNAi-mediated CTGS can also occur on euchromatin, but that any small RNAs produced by such a mechanism are not functional and therefore rapidly degraded (Woolcock et al., 2011).

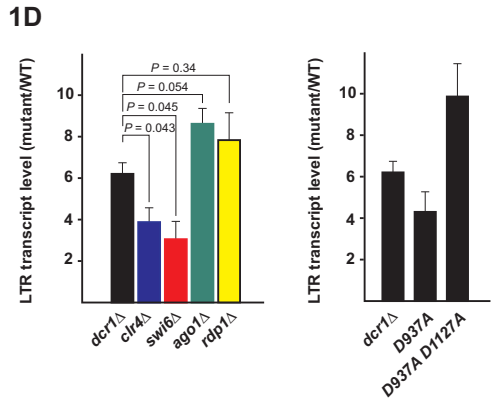

Figure 1D The RNAi machinery contributes to LTR repression. Tf2 LTR transcript levels in the indicated mutant strains. D937A and D1127A are mutated sites in the RNase III catalytic centres of Dcr1. RNA levels were normalized to actin and represented as fold increase compared to wild type. Error bars represent s.e.m., n = 6 biological replicates for *dcr1*Δ, n =3 biological replicates for all other mutants. P values were generated using the Student's t-test.

There had been indications in the literature that RNAi-mediated silencing of certain regions could function to repress neighbouring genes. I therefore hypothesised that LTRs or ncRNAs could create a local concentration of the RNAi machinery, facilitating repression of nearby genes. Indeed, replacing Dcr1-associated ncRNAs or LTRs with the *URA3* gene resulted in upregulation of a nearby gene in some cases (Figure 1E). However, subsequent removal of the *URA3* reversed this effect, suggesting that the upregulation was due to insertion of the *URA3* and not removal of the ncRNA/LTR. Therefore, it seems unlikely that RNAi association with certain

features has an effect on surrounding gene expression. This would make sense if the silencing mechanism does not involve recruitment and spreading of chromatin modifications, but rather direct co-transcriptional degradation of nascent transcripts, as I hypothesise below.

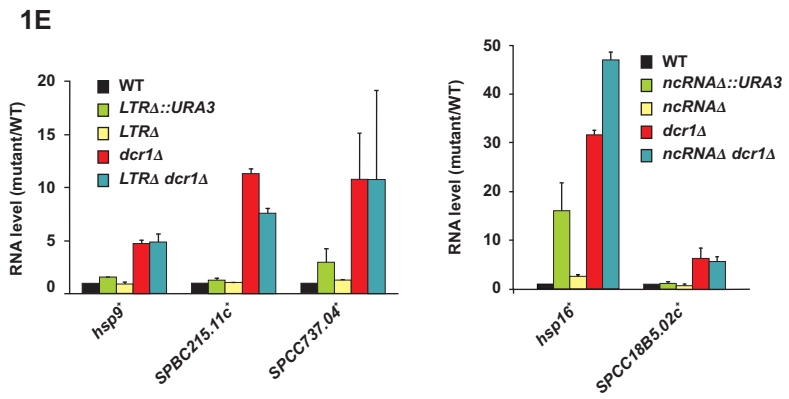

Figure 1E Dcr1 association with LTRs and ncRNAs does not seem to affect nearby gene expression. Several genes that are upregulated in *dcr1*Δ cells and located within 5 kb of an LTR or ncRNA that is enriched by Dam-Dcr1 were assessed for RNA levels in the indicated backgrounds. RNA levels were normalized to actin and shown as fold increase compared to wild type. Error bars represent s.d., $n = 2$ biological replicates.

Part II: Establishment of RNAi-genome interactions

Results published in Woolcock K, Stunnenberg R, Gaidatzis D, Hotz H-R, Emmerth S, Barraud P, Bühler M (2012). RNA interference keeps Atf1-bound stress response genes in check at nuclear pores. ***Genes Dev*** 26(7):683-92.

Several models have suggested that either H3K9 methylation or initial targeting of Ago1 by small RNAs is required to provide the initial trigger for RNAi-mediated heterochromatin formation (Halic and Moazed, 2010; Shanker et al., 2010). Surprisingly, the absence of either Clr4, Rdp1, Ago1 or combinations of these did not alter the binding pattern of Dcr1 (Figure 2A). Similarly, Rdp1 association with euchromatin is independent of Clr4, Ago1 and Dcr1, and some residual Rdp1 association is present at centromeres in all three mutants (Figure 2B). This suggests that siRNA production can potentially occur at these regions independently of H3K9me or other RNAi components, although H3K9me clearly stabilizes the association of RITS and RDRC with heterochromatin and priRNAs may be required to prime the amplification of siRNAs.

Since Dcr1 co-localizes with nuclear pores according to microscopy (Emmerth et al., 2010), I hypothesised that genomic regions shown to be associated with Dcr1 by DamID correspond to regions close to nuclear pores. To test this, I did DamID for Nup85, a scaffold nucleoporin and part of the Nup107-120 complex (Bai et al., 2004), and Amo1, which localizes in a punctate nuclear peripheral pattern that does not overlap with pores (Pardo and Nurse, 2005). Indeed, Nup85 DamID shows a very strong correlation with Dcr1 DamID, whereas Amo1 shows no strong enrichment at any genomic region (Figure 2C). This confirms that the foci seen by microscopy reflect real Dcr1 localization and are not an artefact of Dcr1 overexpression. Furthermore, it indicates that most, if not all, of the interactions between Dcr1 and chromatin occur at pores. In this way, compartmentalisation may be responsible for targeting RNAi components to certain genomic regions and providing substrate specificity.

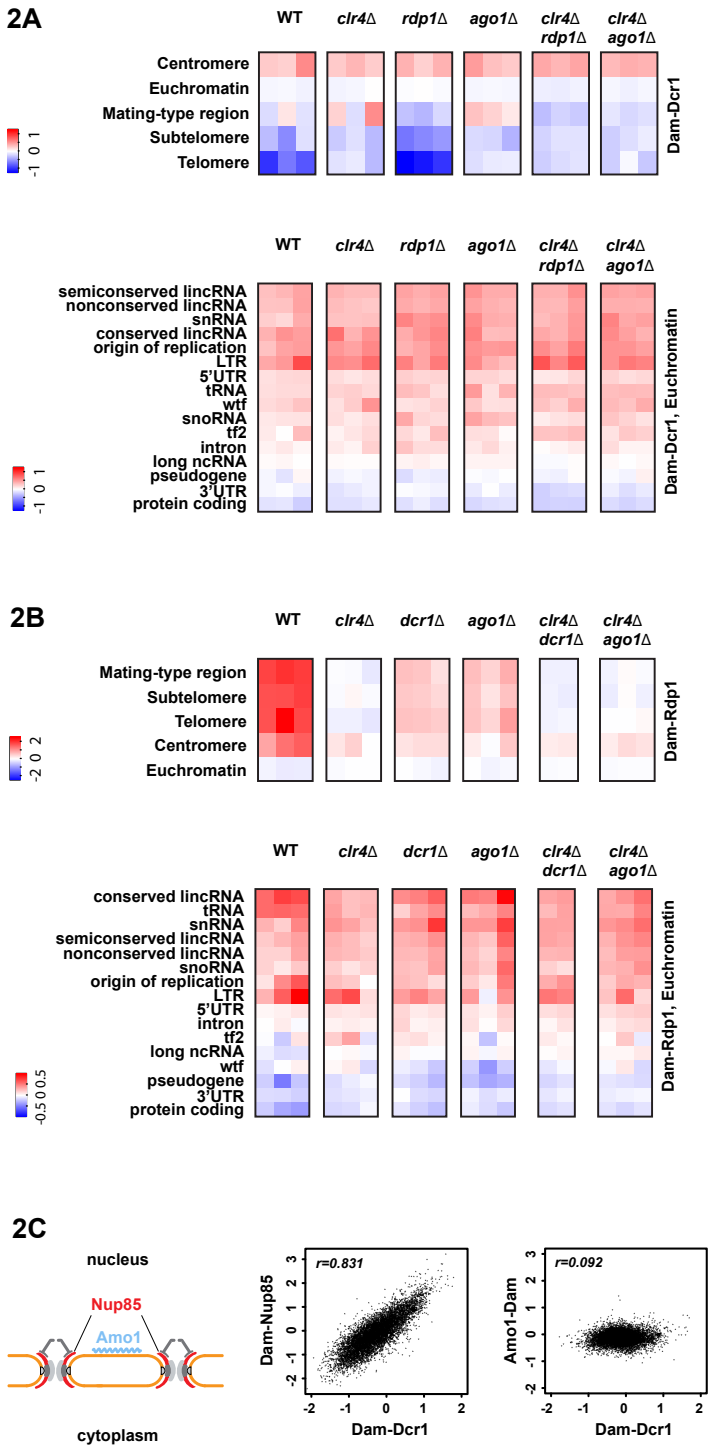

Figure 2 Interactions between chromatin and the RNAi pathway occur at nuclear pore complexes, independently of small RNAs. (**A-B**) Dcr1 and Rdp1 enrichments (log_2) in the mutant backgrounds indicated. Individual columns represent biological replicates. (**C**) Left: representation of Nup85 and Amo1 locations at the nuclear periphery. Right: comparisons of Dcr1 enrichment (log_2) at individual features with Nup85 and Amo1 enrichments (log_2).

Part III: RNAi-mediated regulation of protein-coding genes

Results published in Woolcock K, Stunnenberg R, Gaidatzis D, Hotz H-R, Emmerth S, Barraud P, Bühler M (2012). RNA interference keeps Atf1-bound stress response genes in check at nuclear pores. ***Genes Dev*** 26(7):683-92.

To learn more about the functional relevance of Dcr1 association with euchromatin at nuclear pores, I focused on protein-coding genes. Interestingly, Dcr1 and Nup85 show a preference for promoter regions of genes, as does Rdp1 to a lesser extent, whereas Ago1 does not (Figure 3A). This suggests that Dcr1/Rdp1 may have a role at promoter regions, perhaps affecting transcription, or that genes associated with Dcr1/nuclear pores do so via their promoter regions.

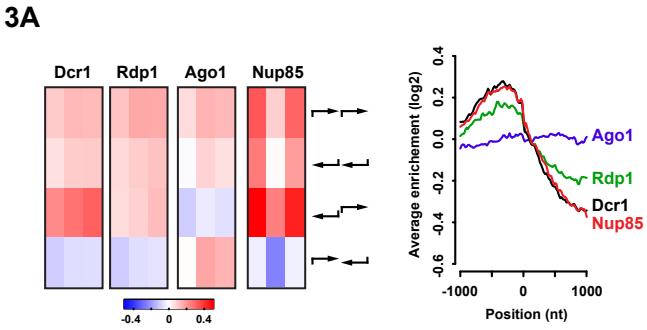

Figure 3A Promoter regions are preferentially associated with Dcr1 and Rdp1 at NPCs. Left: enrichments (log_2) of the indicated proteins at tandem, divergent, and convergent intergenic regions. Individual columns represent biological replicates. Right: average enrichments 1 kb on either side of the beginning of ORFs. One representative replicate shown for each experiment.

Looking at the types of genes with the highest enrichment for Dcr1 and Nup85, I realised that many of them are involved in responses to stressful conditions. However, using GO term analysis did not identify any particular groups of genes that are preferentially enriched, except for around 10 genes with the term 'glucose catabolic process'. Furthermore, previously defined stress response genes, the so-called induced and repressed core environmental stress response (CESR) genes (Chen et al., 2003), did not show a significant preferential enrichment for Nup85 or RNAi components (data not shown). As an alternative way to look at stress response genes, I used previously published ChIP-chip data for Atf1 (Eshaghi et al., 2010), a well-characterised stress response transcription factor also known to be involved in heterochromatin formation at the mating-type region (Jia et al., 2004). Atf1 is thought to be constitutively bound to its targets. Upon stress, Atf1 is phosphorylated by the MAP kinase Sty1 and activates transcription. I focused my analysis on a group of genes that were shown to have Atf1 bound to their probable

promoter regions under normal conditions (Eshaghi et al., 2010), and which I refer to as BANCs, for 'bound by Atf1 under normal conditions'. Nup85 and RNAi components show a strong preference for this group of genes compared to all others, whereas Swi6 and Amo1 do not (Figure 3B). As well as implicating the RNAi machinery in regulation of this group of genes, these results suggest that their association with Atf1, rather than the fact that they are stress response genes, is a defining feature for their preferential association with Nup85/RNAi.

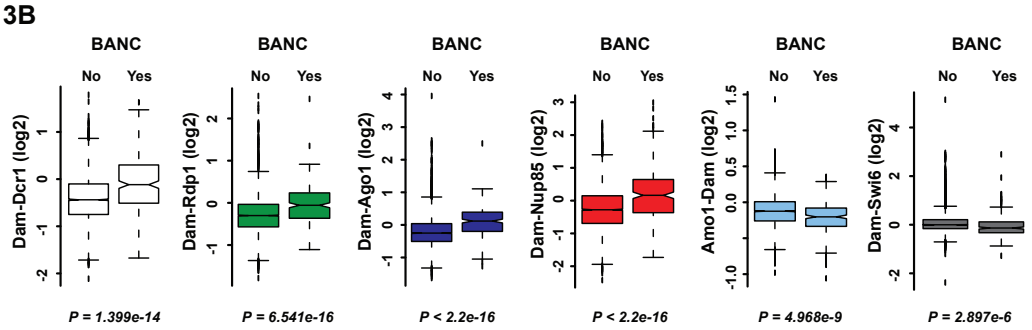

Figure 3B Atf1-bound genes are preferentially associated with the RNAi machinery at NPCs. DamID enrichment at BANCs ('Yes'; 261 genes) compared with all other genes ('No'; 4715 genes) for Dcr1, Rdp1, Ago1, Nup85, Amo1 and Swi6. BANC = bound by Atf1 under normal conditions.

To test whether these genes are regulated by RNAi, I used tiling arrays to compare their expression in wild type and RNAi mutant strains. Indeed, BANCs show preferential upregulation compared to other genes in all three RNAi mutants (Figure 3C). This is not the case for *swi6*Δ, confirming that the upregulation is not an indirect effect of losing heterochromatin, which can be considered a stressful condition (Figure 3C). BANCs are also preferentially upregulated in *clr4*Δ cells (data not shown); however, since Clr4 has been proposed to methylate another component of the pathway (Gerace et al., 2010), this could be an indirect effect. RNA levels of some heat shock genes tested decrease more slowly, after the initial response to elevated temperature, in cells lacking Dcr1 compared to wild type (data not shown). I propose that RNAi-mediated CTGS is occurring at these genes in association with nuclear pores (Woolcock et al., 2012) (Figure 3D). This may help to keep stress response genes in check under normal conditions, allowing more rapid upregulation and export upon their induction, and may contribute to the transient nature of stress responses. Although there is a relative enrichment of Ago1-bound sRNAs mapping to

BANCs, this enrichment remains in *dcr1*Δ (Figure 3E). Therefore, rather than being functional siRNAs, these may simply be degradation products.

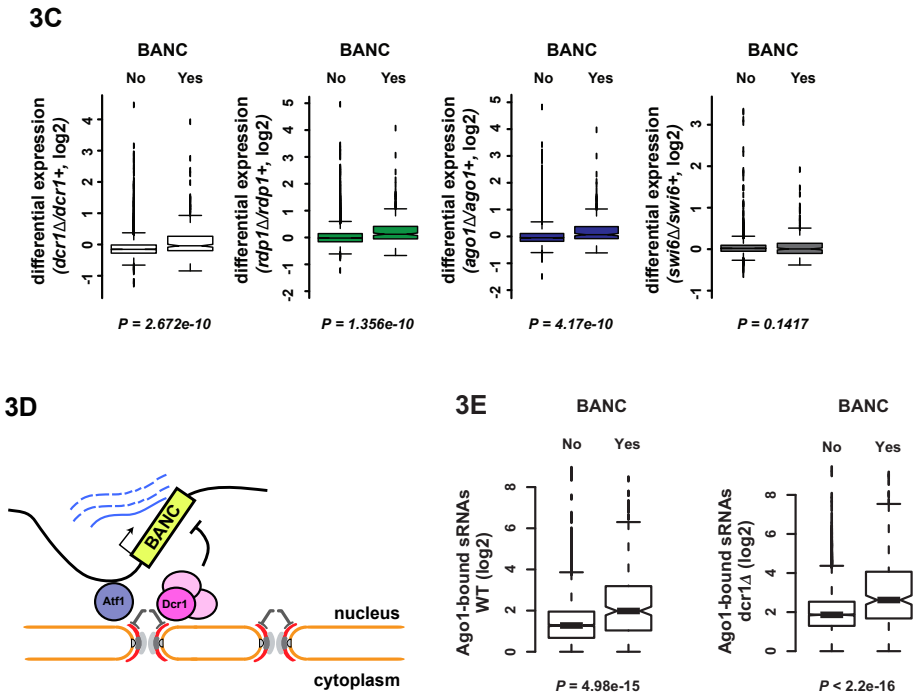

(**C**) RNAi contributes to repression of BANCs. Expression analysis by tiling arrays showing differential expression of BANCs compared with all other genes in the mutants indicated. (**D**) Model for RNAi-mediated CTGS of Atf1-bound genes (BANCs) at nuclear pores. (**E**) Small RNA deep sequencing data (Halic and Moazed, 2010) was reannotated to show the number of Ago1-bound sRNAs at BANCs compared with all other genes in wild type and *dcr1*Δ cells.

Part IV: Further characterisation of the properties and nuclear environment of BANCs

Unpublished observations

To further characterise BANCs, I re-annotated other genome-wide datasets to enable comparison of this group with all other genes. High-throughput sequencing of cDNA (RNA-seq) shows that BANCs have a wide range of transcription under normal conditions, and are generally moderately transcribed (Figure 4A). Pol II ChIP-chip shows a similar picture (Figure 4A).

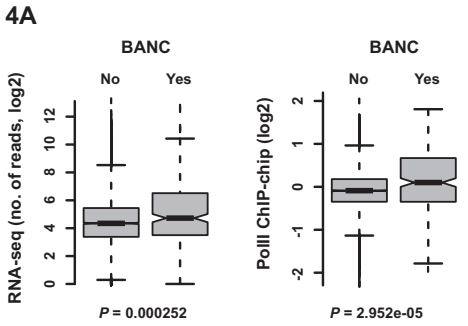

Figure 4A BANCs as a group have average expression levels. Published datasets (Wilhelm et al., 2008) were reanalyzed and annotated to enable comparison of RNA-seq and Pol II ChIP-chip between BANCs and all other genes.

Interestingly, BANCs seem to be generally depleted for histones (Figure 4B) judging by ChIP-chip data. In fact, it is known that certain induced stress response genes in *S. pombe* display a large nucleosome depleted region at their promoters, with an average size of 400 bp under non-induced conditions (Sanso et al., 2011). This supports the idea that BANCs have potential for high levels of transcription even under normal conditions, but are kept in check by repressive mechanisms.

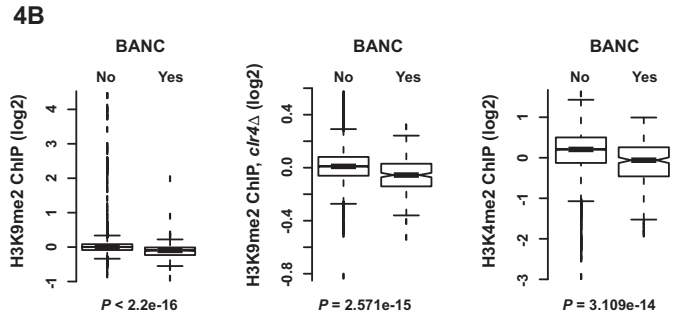

Figure 4B BANCs are generally depleted for histones. Published datasets (Cam et al., 2005) were reannotated to enable comparison of H3K9me2 and H3K4me2 ChIP-chip between BANCs and all other genes.

In addition to the RNAi machinery, other factors that can influence gene expression are enriched at BANCs. For example, the DNA-binding factor Sap1, shown to be recruited by LTRs (Zaratiegui et al., 2011b), also has a preference for BANCs (Figure 4C). Several HDACs, which have a negative impact on transcription, show a similar preference (Figure 4D). Consistent with a contribution to silencing, BANCs are preferentially upregulated in a *clr6-1* HDAC mutant (Figure 4E). Therefore, I believe that nuclear pores provide a special subnuclear environment where various factors come together to influence the expression of genes tethered there.

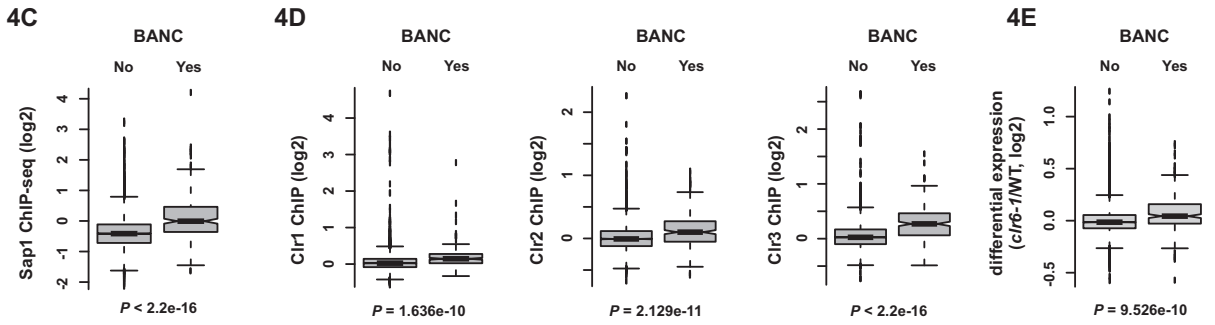

In addition to the RNAi machinery, BANCs are preferentially associated with other repressive factors. Publicly available datasets were reannotated to enable comparison between BANCs and all other genes. (**C**) Sap1 ChIP-seq (Zaratiegui et al., 2011b). (**D**) ChIP-chip for HDACs Clr1, Clr2 and Clr3 (Sugiyama et al., 2007). (**E**) Microarray expression analysis for the *clr6-1* mutant allele (Nicolas et al., 2007).

Part V: Role for transcription factors in genome organisation at nuclear pores

Unpublished observations

The fact that Atf1 binding seems to be a defining feature for preferential Nup85/Dcr1 binding suggested a role for Atf1 itself in the association of BANCs with Nup85/Dcr1. To investigate this, I deleted the *atf1* gene and performed DamID for both Nup85 and Dcr1. Excitingly, the significant preference for BANC association with Nup85 is lost in *atf1*Δ (Figure 5A), demonstrating that Atf1 is either directly or indirectly involved in tethering these genes to nuclear pores. However, to my surprise, Dcr1 preference for BANCs was not significantly abolished (Figure 5B). Therefore, Dcr1 association with BANCs is not simply a consequence of co-localization at nuclear pores, and some other feature of BANCs seems to be recognized by Dcr1 (see discussion).

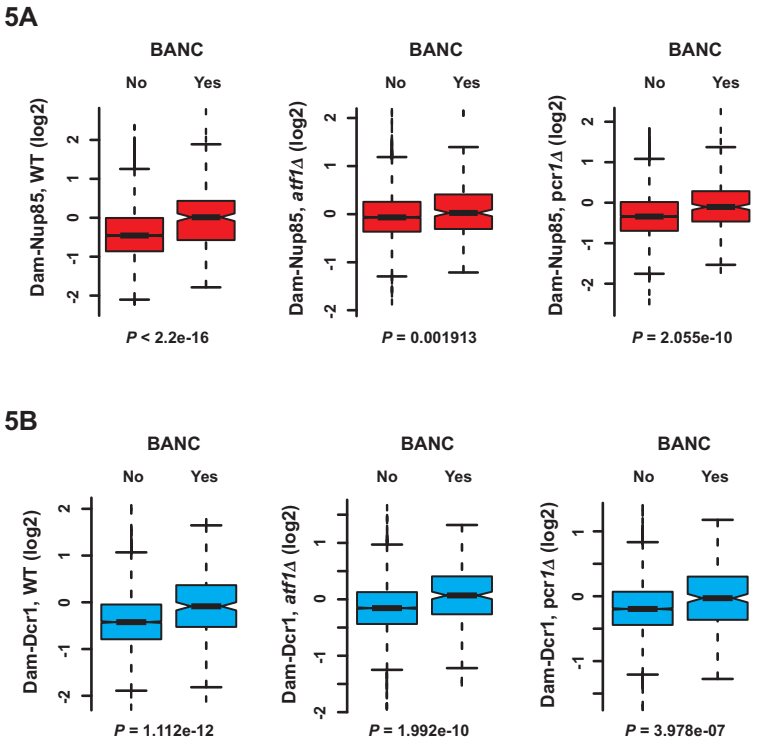

Nup85, but not Dcr1, preference for BANCs is abolished in *atf1*Δ cells. (**A**) Nup85 DamID in wild type, *atf1*Δ and *pcr1*Δ cells. (**B**) Dcr1 DamID in wild type, *atf1*Δ and *pcr1*Δ cells.

Although centromeric regions do not strongly associate with Nup85, the weak interaction that does exist is clearly lost in an *atf1*Δ strain (and to a lesser extent in *pcr1*Δ) (Figure 5C). Similar to BANCs, the association with Dcr1 is not lost (Figure 5C). Nonetheless, Atf1-mediated tethering to the pores may have a function in centromeric heterochromatin formation. Perhaps the interaction occurs transiently in S phase when heterochromatic marks are at their lowest. In support of this idea, chromatin seems to interact more freely with nuclear pores in the absence of H3K9me (Figure 5D). Quantification of centromeric RNA levels shows lower levels in *atf1*Δ *dcr1*Δ double mutants than in *dcr1*Δ single mutants (Kasia Kowalik, personal communication). This suggests that Atf1 promotes transcription of pre-siRNA transcripts. Whether association with nuclear pores is important for this transcriptional activation remains to be determined.

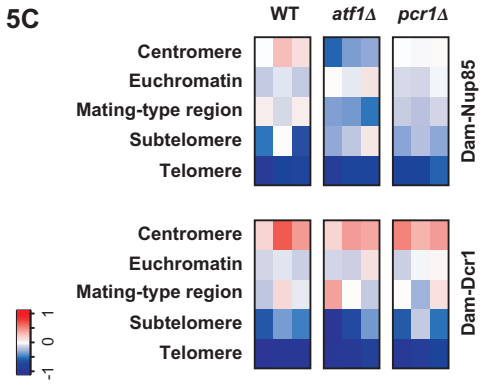

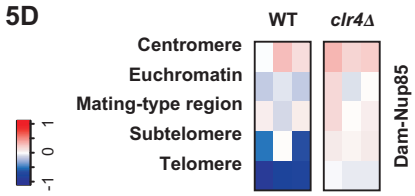

(**C**) Nup85, but not Dcr1, association with centromeres is lost in *atf1*Δ and, to a lesser extent, *pcr1*Δ cells. Nup85 and Dcr1 enrichments (log_2) at heterochromatic regions compared with euchromatin in the indicated backgrounds. (**D**) Loss of H3K9me increases association of heterochromatic regions with Nup85. Nup85 enrichment (log_2) at heterochromatic regions compared to euchromatin in wild type and *clr4*Δ cells.

Part VI: Regulation of RNAi at elevated temperatures

Results published in Woolcock K, Stunnenberg R, Gaidatzis D, Hotz H-R, Emmerth S, Barraud P, Bühler M (2012). RNA interference keeps Atf1-bound stress response genes in check at nuclear pores. ***Genes Dev*** 26(7):683-92.

Since CTGS contributes to repression of Atf1-bound stress response genes under normal conditions, I wondered whether CTGS would be impaired under stress conditions to enable gene induction. One way in which this could occur is via re-localization either of the RNAi machinery or the loci themselves. Results from both DamID and microscopy experiments suggest that the loci do not move upon heat shock (Figure 6A-B). Similarly, Dcr1 localization does not seem to change at short time points after temperature increase, judging by microscopy. This could not be tested by DamID, which is not suitable for studying the dynamics of protein-genome interactions. While it is still possible that another aspect of CTGS is inhibited under stressful conditions, these results support a model whereby CTGS continues to be active after stress but is overcome by strong transcriptional activation of stress response genes.

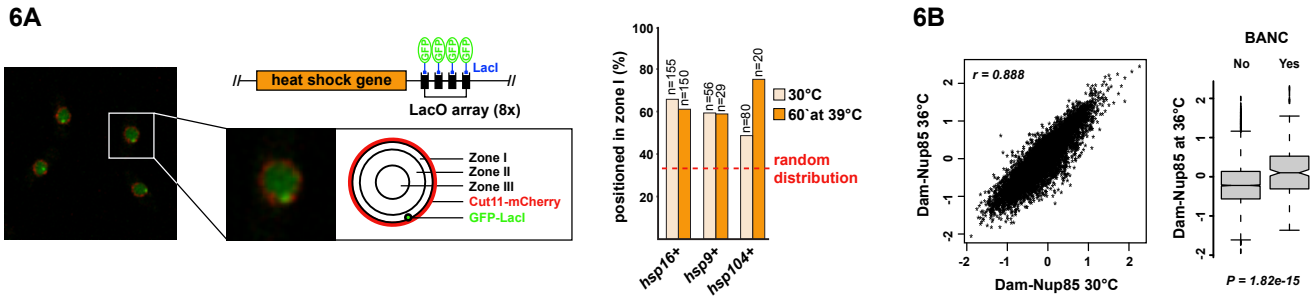

Genes associating with RNAi components do not change their nuclear localization upon temperature increase. (**A**) Left: summary of the LacO/LacI-GFP system used to analyse the location of individual heat-shock genes (Taddei et al., 2004). Live cells with GFP-LacI-marked *lacO::hsp16*$^{+}$ locus and the nuclear membrane marker mCherry-Cut11 were imaged at 30°C (single-plane confocal image). Right: heat shock gene localization was assigned to one of three concentric nuclear zones of equal area. Percentage of cells with the GFP focus at the nuclear periphery (zone I) before and after a 1 h shift to 39°C is shown. Experiments done by Rieka Stunnenberg. (**B**) Comparison of the genome-wide Nup85 DamID enrichment ($\log_2$) at 30°C and 36°C. BANCs remain preferentially enriched for Nup85 at 36°C.

Although Dcr1 localization does not seem to change initially, it was observed that Dcr1 loses its nuclear localization when cells are subjected to higher temperatures for a prolonged period, and

accumulates in patches in the cytoplasm (Figure 6C). This is unlikely to be an artefact of the GFP tag since Cid14-GFP does not show this behaviour (Rieka Stunnenberg, personal communication). Furthermore, the observation is supported by DamID, as the amount of DNA obtained for a Dam-Dcr1 strain is much lower if the cells are grown at higher temperatures, demonstrating overall lower levels of methylation (Figure 6D). Overall protein levels of Dcr1 do not change drastically (data not shown). Loss of Dcr1 from the nucleus may abrogate CTGS and could be responsible for the reactivation of certain heat shock genes after prolonged heat shock, perhaps contributing to thermotolerance.

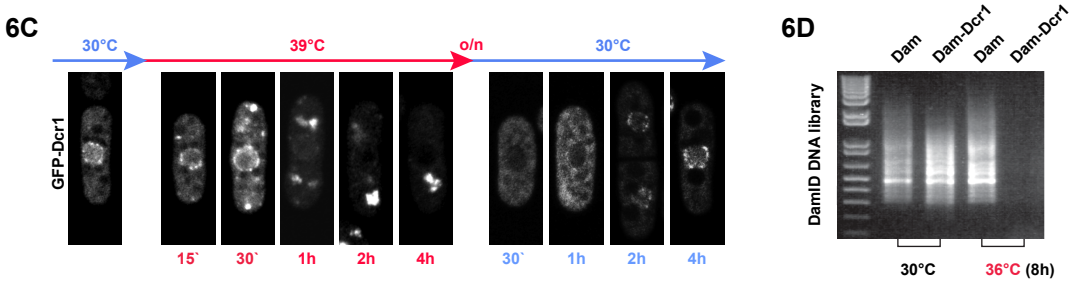

Dcr1 loses its nuclear localization at higher temperatures. (**C**) Fluorescence microscopy of living cells expressing GFP-Dcr1. Cells were grown at 30°C, temperature was shifted to 39°C, and confocal images were taken at the indicated times after this shift. Although not visible here, some nuclear rim signal remains up to 4 h. Recovery of nuclear Dcr1 was monitored over 4 h after shifting the temperature from 39°C (cells having been at this temperature overnight) back to 30°C. Experiments done by Rieka Stunnenberg. (**D**) Much lower DamID library concentrations are obtained from Dam-Dcr1 strains when performed at 36°C compared with 30°C (confirmed by at least four independent replicates).

A likely explanation for loss of nuclear Dcr1 at higher temperatures comes from structural studies of the dsRBD. Structural integrity of the dsRBD is crucial for Dcr1's nuclear retention, and disrupting the coordination of a zinc ion results in relocalization of Dcr1 to the cytoplasm accompanied by loss of centromeric silencing (Barraud et al., 2011). Differential scanning fluorimetry shows that the dsRBD becomes unstable at higher temperatures, beginning to unfold around 34-38°C (Figure 6E). Therefore, unfolding of the dsRBD may cause the loss of nuclear localization at higher temperatures. In support of this idea, BANCs are preferentially upregulated at normal temperatures in strains with a disrupted Dcr1 dsRBD (Figure 6F).

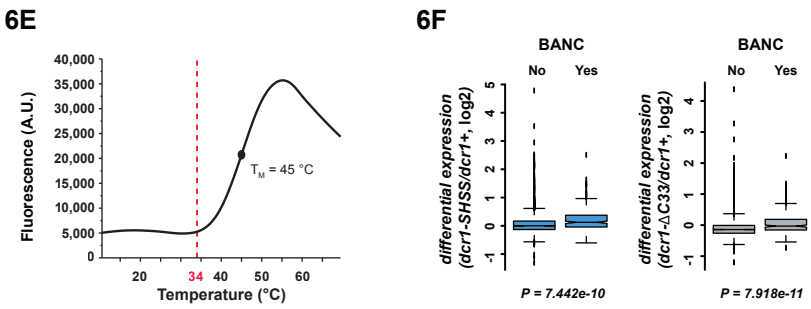

Unfolding of Dcr1's C-terminal domain is likely responsible for the loss of nuclear localization at higher temperatures. (**E**) Thermal unfolding of Dcr1's C-terminal domain (shown in Figure VIIIb) monitored by differential scanning fluorimetry. Dotted line: temperature at which unfolding transition begins. (**F**) Expression analysis by tiling array (Barraud et al., 2011) showing differential expression at BANCs compared with all other genes in a Dcr1 mutant in which the dsRBD can no longer coordinate a zinc ion (*dcr1-SHSS*) and in a Dcr1 mutant lacking the C-terminal 33 amino acids (*dcr1-ΔC33*). Both of these are unable to fold the dsRBD properly and hence lose nuclear retention properties.

Dcr1 may not be the only component to be regulated by temperature. Using DamID, it appears that Rdp1 shows similar behaviour, since DNA levels obtained at the end of the protocol are lower at 39°C compared to 30°C (data not shown). No other Dam fusion proteins tested showed this behaviour. Microscopy for GFP-Rdp1 supports the idea that Rdp1 loses its nuclear localization at elevated temperatures (Rieka Stunnenberg, personal communication). Interestingly, Dcr1 and Rdp1 are large proteins (158 and 139 kDa, respectively) and may unfold more easily at higher temperatures. In conclusion, several components of the RNAi pathway in *S. pombe* may be regulated by a temperature increase.

Part VII: Role of Cid14 in co-transcriptional gene silencing

Results published in:

- Keller C, Woolcock K, Hess D, Bühler M (2010). Proteomic and functional analysis of the noncanonical poly(A) polymerase Cid14. ***RNA*** 16(6):1124-9.
- Keller C, Adaixo R, Stunnenberg R, Woolcock K, Hiller S, Bühler M (2012). $HP1^{Swi6}$ mediates the recognition and destruction of heterochromatic RNA transcripts. ***Mol Cell*** 47(2):215-27. Highlighted in:
    - Ren J and Martienssen RA (2012). Silent decision: HP1 protein escorts heterochromatic RNAs to their destiny. ***EMBO J*** 31(15):3237-8.
    - Schuldt A (2012). Chromatin: RNA eviction by HP1. ***Nat Rev Mol Cell Biol*** 13(8):478-9.
    - Creamer KM and Partridge JF (2012). Should I stay or should I go? Chromodomain proteins seal the fate of heterochromatic transcripts in fission yeast. ***Mol Cell*** 47(2):153-5.

See Appendix for the above manuscripts.

In addition to the studies described above, I contributed to two other manuscripts published by our lab, specifically relating to the role of the non-canonical poly(A) polymerase Cid14 in CTGS. The functional homologue of Cid14 in *S. cerevisiae* polyadenylates nuclear RNAs as part of an exosome-mediated RNA turnover pathway (LaCava et al., 2005; Vanacova et al., 2005; Wyers et al., 2005). In *S. pombe*, Cid14 has previously been implicated in ribosomal RNA processing and heterochromatic gene silencing (Buhler et al., 2007; Buhler et al., 2008; Wang et al., 2008a; Win et al., 2006). Interestingly, heterochromatin remains largely intact in *cid14*Δ cells, despite a loss of silencing, suggesting a role in CTGS (Buhler et al., 2007).

In the first study, comparing genome-wide differential expression in *cid14*Δ cells with published ChIP-chip data for H3K9me2 and Swi6 (Cam et al., 2005), revealed a small set of heterochromatic genes upregulated in *cid14*Δ, most of which are subtelomeric genes (Keller et al., 2010). Subsequently, I used DamID to test whether Cid14 physically associates with chromatin (Keller et al., 2012), since attempts to crosslink it to heterochromatic regions had failed. This revealed an association of Cid14 with the centromeres, mating-type region and telomeres (Figure 7A), supporting a role for Cid14 in the degradation of heterochromatic transcripts. Interestingly, the association of Cid14 with the mating-type region and telomeres was lost in a *swi6*Δ mutant (Figure 7A). The major results from the study revealed that Swi6 binds RNA, primarily via its hinge region, and that this binding competes with H3K9me association (Keller et al., 2012). Similar to *cid14*Δ cells, strains in which Swi6 can no longer bind RNA have

impaired silencing but largely intact heterochromatin, particularly at the mating-type region and telomeres. In combination with the DamID, these findings support a model whereby Swi6 recognises transcripts from heterochromatin, dissociates from H3K9me-marked nucleosomes as a result of RNA binding, and passes the RNA to Cid14, which then initiates degradation (Figure 7B). Cid14 can associate with centromeres independently of Swi6 (Figure 7A). Similarly, Cid14 associates with euchromatic regions, including BANCs, independently of Swi6 (Figure 7C) and may also play a role in CTGS at these regions. Further studies are required to investigate which factors are required for Cid14 association with these regions.

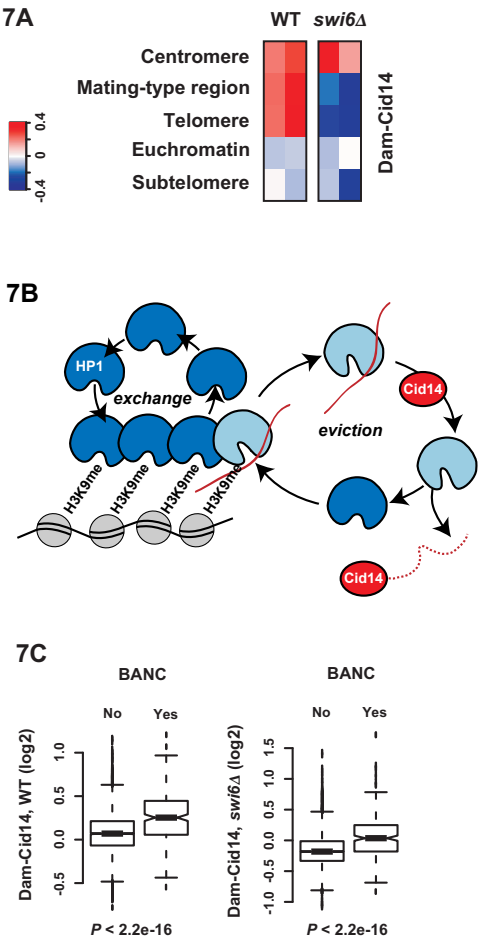

Figure 7 Cid14 may be involved in CTGS at both heterochromatic and euchromatic regions. (**A**) DamID enrichment (log_2) for Cid14 at heterochromatin and euchromatin in wild type and *swi6*Δ cells. (**B**) Model for Swi6-mediated degradation of heterochromatic RNA. Swi6 (blue) associates dynamically with H3K9-methylated nucleosomes. It binds newly synthesized RNA (red) and dissociates as a result of competition between RNA- and H3K9me-binding (light blue). The RNA is then passed to Cid14, which initiates degradation. (**C**) Cid14 associates preferentially with BANCs in both wild type and *swi6*Δ cells.

Discussion & Outlook

Possible mechanisms of CTGS

The results summarized above describe a novel function for the RNAi machinery in repression of euchromatic regions in *S. pombe*. Pol II occupancy (of either S5-P or S2-P forms) (Zaratiegui et al., 2011a) does not significantly change at BANCs in *dcr1*Δ compared to wild type (data not shown). Furthermore, I detected no H3K9me2 enrichment at LTRs and heat shock genes (data not shown), and the lack of Swi6 association implies that H3K9me is not a feature of BANCs (Figure 3B). These observations support a model in which CTGS does not inhibit transcription but rather acts by degrading the nascent transcripts. There are several possibilities that can be envisaged for the exact mechanism of CTGS, which I will outline below (see also Figure 8):

- Slice and torpedo – this mode requires the slicer activity of an Argonaute protein. Small RNAs are not necessarily required for targeting Ago1 to the nascent transcript but are required for cleavage. The creation of a free 5' end would make the downstream RNA fragment susceptible to exonuclease activity, which could catch up with Pol II and force termination, as in the 'torpedo' model for transcription termination (Kim et al., 2004; Teixeira et al., 2004; West et al., 2004).
- Dice and torpedo – in this mode, Dicer would recognize a hairpin formed in the nascent transcript and cleave without the need for Ago1. This could again result in a torpedo-like eviction of Pol II downstream of the cleavage site.
- Dice and trash – in this case Rdp1 would create dsRNA by reverse transcribing the nascent transcript, which is then processed by Dcr1. Small RNAs are again not necessary for targeting but may be required to prime synthesis by Rdp1. It is also possible that bidirectional overlapping transcription creates dsRNA substrates for Dcr1 without the need for Rdp1. Processing by Dcr1 could function in a similar way to exonucleases in the torpedo model, causing premature termination of Pol II.

Careful experiments will be required to test which, if any, of these models is true. Although repression of BANCs as a group of genes requires Dcr1, Rdp1 and Ago1, it could be that different subgroups depend only on one or two components, according to the models above. RNA secondary structures with the potential to be recognized by Dcr1 may be encoded by Dcr1-

associated genes. If torpedo-like events do occur, then Pol II occupancy downstream of the cleavage site is expected to decrease. Furthermore, 5'-to-3' exoribonucleases would be required for degradation of the downstream fragment and Pol II eviction. Since transcription is likely to oppose the deposition of repressive histone marks, loss of Pol II may result in an increase in H3K9me or histone deacetylation. Since BANCs associate with several HDACs, I propose that the repressive factors at NPCs have to be overcome by strong transcriptional activation.

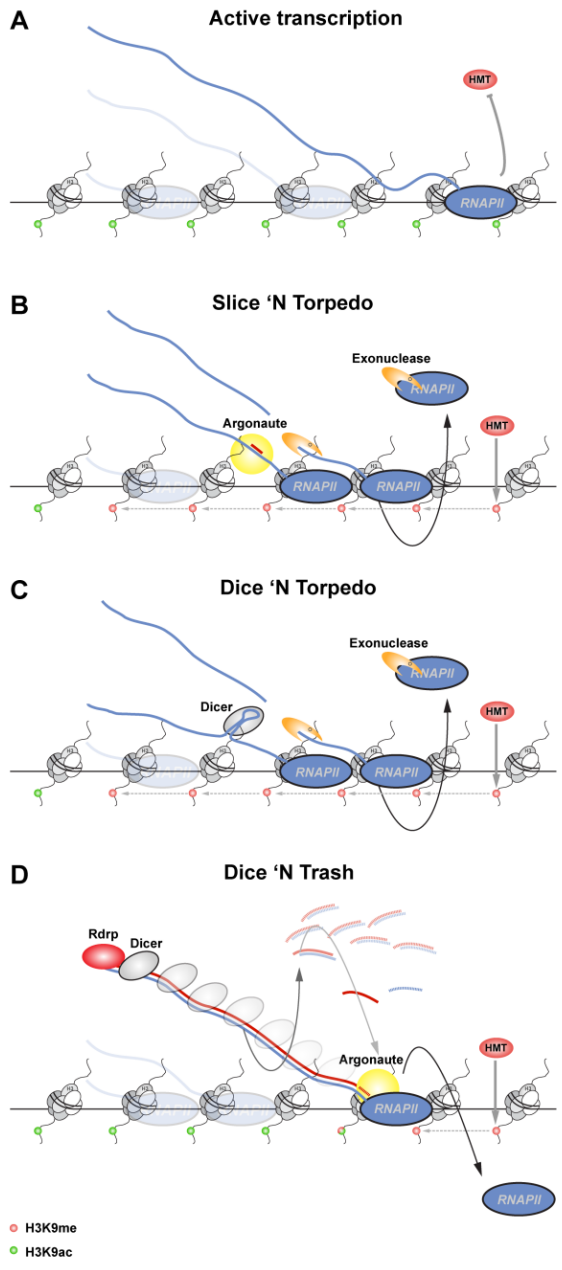

Figure 8 Possible mechanisms for RNAi-mediated co-transcriptional gene silencing. (**A**) Active transcription may oppose repressive modifications such as methylation of H3K9. (**B**) Ago1-mediated slicing of the nascent transcript creates a free 5' end that is subject to degradation by exonucleases, causing eviction of downstream Pol II as in the 'torpedo' model for transcription termination. (**C**) Dcr1 recognises a secondary structure formed in the nascent transcript and cleaves, again resulting in torpedo-like eviction of downstream Pol II. (**D**) Rdp1 creates long dsRNA, perhaps primed by Ago1-bound sRNAs, which are then processed by Dcr1. This may again result in a torpedo-like mechanism.

Nuclear organisation of RNAi

The organisation of RNAi targets at NPCs would be a neat way of separating different RNAi pathways. For example, the dynamic and relatively active environment around pores (Casolari et al., 2004; Kalverda et al., 2010) could create an unfavourable environment for heterochromatin formation, despite the presence of the RNAi components. In contrast, the major regions of heterochromatin do not interact strongly with pores, although it is possible that a transient association plays a role in pre-siRNA transcription at centromeres (see Part V). In some cases, gene association with nuclear pores is known to enhance transcription (Brickner and Walter, 2004; Taddei et al., 2006). While diffusion of mRNAs to NPCs is not thought to be rate limiting for export (Shav-Tal et al., 2004), it could be that NPC localization promotes expression by coordinating transcription and export, as proposed many years ago by the 'gene gating' hypothesis (Blobel, 1985). It seems likely that the localization of BANCs at NPCs keeps them poised for rapid induction and export.

Nuclear pores have been shown to play important regulatory roles in other processes. For example, certain types of DNA damage in *S. cerevisiae* are recruited to pores where repair takes place (Nagai et al., 2008), and incorporation of the nucleoporin Nup210 into the NPC is required for myogenic and neuronal differentiation in mammalian cells (D'Angelo et al., 2012). In higher eukaryotes, many nucleoporins are actually mobile and are found in the nucleoplasm, where they can associate with active genes and stimulate their expression (Capelson et al., 2010; Kalverda et al., 2010). It is possible that the recruitment to active genes occurs due to an affinity of the nucleoporin for certain TFs (discussed below). In summary, accumulating evidence shows that NPCs are not only sophisticated mediators of transport between the nucleus and cytoplasm, but also play regulatory roles in many other processes.

The subnuclear organisation of RNAi in *S. pombe* is reminiscent of the subcellular organisation of RNAi pathways in other organisms. For example, miRNA pathway components were found to associate with endosomes and multivesicular bodies (MVBs) in both human and *Drosophila* cells, and blocking MVB formation impairs miRNA-mediated silencing (Gibbings et al., 2009; Lee et al., 2009). A mitochondrial outer membrane protein, MITOPLD, is involved in formation

of nuage, a perinuclear structure required for piRNA biogenesis and function, in mice (Huang et al., 2011; Watanabe et al., 2011). In *Arabidopsis*, proteins involved in RdDM are concentrated in nuclear Cajal and AB bodies (Li et al., 2008; Li et al., 2006a; Pontes et al., 2006). Finally, components of the RNAi process 'meiotic silencing by unpaired DNA' (MSUD) in *Neurospora crassa* co-localize in a perinuclear region (Alexander et al., 2008; Shiu et al., 2006). Such organisation is likely to enhance the specificity and efficiency of RNAi pathways, and allow better regulation.

The role of transcription factors in genome organisation

The finding that Atf1 is required for preferential association of BANCs with pores supports hypotheses that propose a role for TFs in organising chromatin at pores in other organisms (see introduction). The way in which Atf1 is able to tether its target genes to pores remains unknown. Preliminary biochemical data (TAP purification followed by mass spectrometry) does not reveal any obvious nuclear periphery interaction partners for Atf1 (data not shown). Further biochemical work will be required to determine how Atf1 associates with nuclear pores.

Since Atf1 seems to be involved in tethering its target genes to nuclear pores, I wondered whether other TFs perform a similar function. One way to check this is to look for a preferential association of genomic regions containing known TF motifs with Nup85. Unfortunately, there is no database for *S. pombe* TF motifs, so I used the *S. cerevisiae* Jaspar database. The motif for the *S. cerevisiae* ATF/CREB family transcription factor CST6 is extremely similar to that of Atf1 (TGACGT). Creating a score for association of a certain TF weight matrix with Nup85 DamID (Dimos Gaidatzis, see Additional Methods) gives CST6 a high score, which decreases in *atf1*Δ (Figure 9A), suggesting that this approach is sound. As expected, the score for CST6 does not change between wild type and *atf1*Δ for Dcr1 DamID (Figure 9B). Several other TF motifs have a high score for association with Nup85 and Dcr1, suggesting that these TFs might similarly help tether their target genes to pores. However, deletion of three such TFs does not affect genome association with Nup85 (Kasia Kowalik, personal communication). It is possible that several TFs act redundantly to tether their targets to nuclear pores.

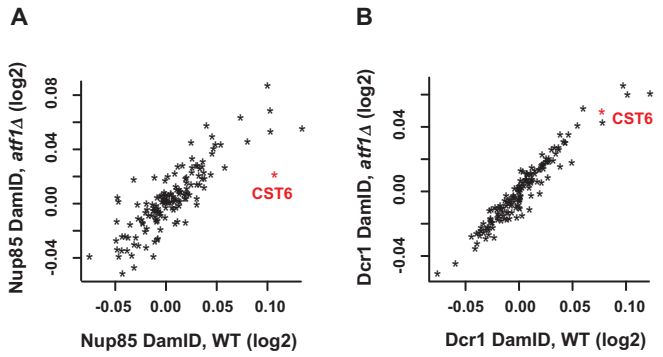

Figure 9 A score is given to each *S. cerevisiae* transcription factor weight matrix according to its preference for either Nup85 (A) or Dcr1 (B) (see Additional Methods for details). CST6 has the same motif as Atf1.

A recent genome-wide chromosome conformation capture study in *S. pombe* revealed significant associations among highly transcribed genes and those with shared GO terms, including metabolic processes and response to stimulus (Tanizawa et al., 2010). The associating genes often contain similar DNA motifs in their promoters. It remains to be seen whether such clustering depends on transcription factors, and whether the associations occur near NPCs. Evidence from mammalian cells that the transcription factor Klf1 mediates preferential co-associations of Klf1-regulated genes (Schoenfelder et al., 2010) suggests that transcription factor-mediated genome organisation may be a widely-conserved phenomenon.

How does Dcr1 recognise its substrates?

The mechanism by which Dcr1 associates with pores is unknown, and again biochemical studies do not reveal any obvious interaction partners (Stephan Emmerth). Surprisingly, while Nup85 preference for BANCs is lost in *atf1*Δ, Dcr1 preference is not. Similarly, centromeres lose their weak association with pores in *atf1*Δ, but Dcr1 remains bound there. These results suggest that, at least to some extent, Dcr1 is found at pores because its targets are localized there. Therefore, it may independently be able to recognize its targets.

I tested several aspects of Dcr1 function for a possible involvement in target recognition (data not shown). Mutating either one or both of the RNase III domains of Dcr1 had almost no effect on Dcr1 association with the genome, as did mutation of a residue important for *in vitro* RNA binding properties of the dsRBD (Barraud et al., 2011). Deletion of *ers1*, which results in loss of

centromeric heterochromatin (Roguev et al., 2008; Rougemaille et al., 2008), similarly had no effect. It was recently shown that Ers1 associates with Swi6 and helps to recruit RDRC to heterochromatin (Hayashi et al., 2012; Rougemaille et al., 2012). Although Ers1 also co-purifies with Dcr1 (Rougemaille et al., 2012), the DamID results suggest that Ers1 has no role in Dcr1 recruitment. Finally, deletion of *abp1*, which also localizes to LTRs and is involved in their repression (Cam et al., 2008), did not change Dcr1 association.

Interestingly, splitting genes into those with high and low expression shows that Dcr1 (and to a lesser extent Nup85) has a preference for more highly transcribed genes (Figure 10). Therefore, RNA level/other transcription factors/Pol II could promote recognition. It will be interesting to test whether the point mutations of Pol II subunits Rpb2 and Rbp7 that affect centromeric silencing (Djupedal et al., 2005; Kato et al., 2005) affect Dcr1 recruitment to chromatin and BANC silencing.

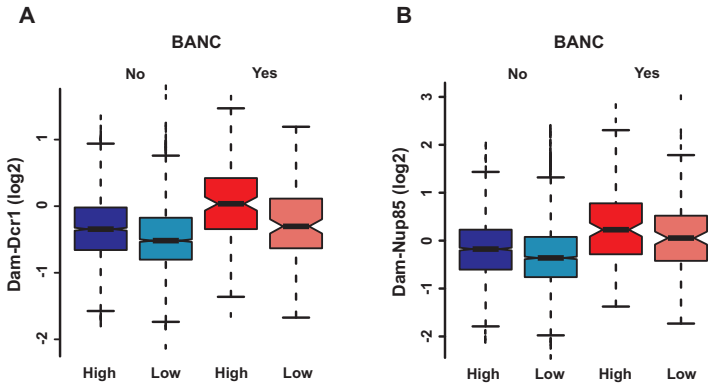

Figure 10 (**A**) Dcr1 preferentially associates with more highly expressed genes. (**B**) Nup85 shows a similar, but less pronounced, trend. BANCs are in red, other genes are in blue. The groups are split into expression either above ('high') or below ('low') the mean expression of all genes according to RNA-seq data (Wilhelm et al., 2008).

Possible conservation of RNAi-mediated TGS/CTGS in other eukaryotes

C. elegans

Work on nuclear RNAi in *C. elegans* is clearly reminiscent of CTGS in fission yeast. Both exogenous and endogenous siRNAs can silence nuclear-retained RNAs or nuclear-localized polycistronic RNAs. The evidence suggests that the siRNAs are mainly generated by RdRPs acting on mRNA templates in the cytoplasm (Guang et al., 2008). The siRNAs associate with the

Argonaute protein NRDE-3 (nuclear RNAi defective-3; lacks residues required for slicer activity) in the cytoplasm and are subsequently transported to the nucleus (Guang et al., 2008). NRDE-3 associates with pre-mRNA that has complementarity to the siRNAs and recruits other NRDE factors, resulting in H3K9 methylation of the surrounding histones (Burkhart et al., 2011; Guang et al., 2010). A reduction in pre-mRNA and a decrease in Pol II occupancy occurs 3' to the site of RNAi, implying a block in transcription elongation (Guang et al., 2010). Nuclear run-on assays confirm an NRDE-2/3-dependent inhibition of RNA Pol II transcription 3' to the site of RNAi. However, it is possible that Pol II inhibition is a secondary consequence of another co-transcriptional silencing activity associated with the NRDE pathway, which could be cleavage/degradation. For example, cleavage of the nascent transcript by a NRDE component or interacting partner could result in exonucleolytic degradation from the unprotected 5' end of the newly-created RNA fragment. The exonuclease would then catch up with Pol II and promote termination, as described for the 'torpedo' model above. If active transcription counteracts H3K9 methylation, eviction of RNA Pol II from chromatin by the torpedo might explain the observed increase in this repressive histone modification. The importance of the H3K9 methylation for silencing is unclear. Indeed, H3K9me occurs throughout the targeted gene, while inhibition of transcription only occurs 3' to the site of RNAi, suggesting that H3K9me is not responsible for silencing (Burkhart et al., 2011). However, chromatin factors have previously been implicated in RNAi-mediated transgene silencing in *C. elegans* (Grishok et al., 2005; Robert et al., 2005). More recently, it was shown that RNAi-mediated heritable silencing in the *C. elegans* germline depends on chromatin factors including the putative H3K9 methyltransferase SET-25 and the HP1 homologue HPL-2 (Ashe et al., 2012; Shirayama et al., 2012). Intriguingly, the nucleoporin *npp-4* affects both transposon silencing in the germline and RNAi-mediated transgene silencing in the soma (Grishok et al., 2005; Vastenhouw et al., 2003).

Drosophila

The existence of nuclear RNAi pathways in other eukaryotes is still debated. Evidence often stems from loss-of-function studies, making it difficult to rule out indirect effects, and the absence of RdRP-mediated amplification means that siRNA levels are likely to be low.

Furthermore, reports on the impact of RNAi pathways on chromatin modification are sometimes contradictory. Nonetheless, in *Drosophila*, endo-siRNAs, which mostly map to transposable elements, have been implicated in heterochromatin formation in somatic cells (Fagegaltier et al., 2009). In addition, there are several interesting links between chromatin and the piRNA pathway. piRNA pathway components have been implicated in H3K9 methylation of chromatin in the soma (Pal-Bhadra et al., 2004). Furthermore, Piwi is distributed along polytene chromosomes and interacts directly with HP1a (Brower-Toland et al., 2007). However, another study showed that HP1 can associate with piRNA clusters in somatic cells independently of both endo-siRNA and piRNA pathways, and provided evidence that Piwi may actually oppose HP1 recruitment at some regions (Moshkovich and Lei, 2010). In the germline, loss of piRNAs is accompanied by a decrease in repressive and an increase in active histone modifications on several upregulated transposons (Klenov et al., 2007). In addition, CpG DNA methylation is impaired in the male germline of some Piwi family mutants in mice (Aravin et al., 2008; Carmell et al., 2007; Kuramochi-Miyagawa et al., 2008). As well as this possible impact of the piRNA pathway on chromatin, there is evidence that heterochromatin can affect piRNA production. For example, mutations in the HP1 homologue Rhino, the H3K9 methyltransferase SetDB1 and a Rhino-interacting protein called Cutoff all impair piRNA generation (Klattenhoff et al., 2009; Pane et al., 2011; Rangan et al., 2011). Therefore, similar to the case in *S. pombe*, it is possible that the small RNA pathway can affect chromatin and, vice versa, chromatin can affect small RNA production.

As mentioned before, CTGS mechanisms may produce small RNAs that are not actually functional and the silencing effect does not necessarily involve chromatin modifications. Therefore, a better way to assess the action of the RNAi machinery in the nucleus is by investigating direct association with the genome. This has been done in *Drosophila* using both polytene chromosome staining and ChIP. In one study, DCR2 and AGO2 were shown to associate with many euchromatic and transcriptionally active loci, including heat shock genes (Cernilogar et al., 2011). Knockdown of DCR2 or AGO2 resulted in upregulation of some of these transcripts. Interestingly, one of these heat shock clusters, the *hsp70* locus, is known to be associated with NPCs (Kurshakova et al., 2007). These results are clearly reminiscent of the

observations in fission yeast, although in contrast to my findings, the association of DCR2 seems to be dependent on the presence of AGO2 in *Drosophila* (Cernilogar et al., 2011). It is important to note that, while the authors show the presence of AGO2-bound small RNAs matching to heat shock loci, which increase upon heat shock, these are not necessarily functional and could simply be degradation products.

Another study looked at AGO2 association using ChIP coupled to massively parallel sequencing (ChIP-seq) and similarly showed association with many euchromatic regions, but not with regions shown to produce endo-siRNAs (Moshkovich et al., 2011). The regions bound by AGO2 overlap with insulator proteins, including CP190 and CTCF (Moshkovich et al., 2011). Since insulator proteins are often involved in organising chromatin at the nuclear periphery (Guelen et al., 2008; Kalverda and Fornerod, 2010; van Bemmel et al., 2010), it is tempting to speculate that the association of the RNAi machinery with the periphery that is seen in fission yeast could be conserved in *Drosophila*. Furthermore, the authors report an AGO2 preference for promoters, similar to what I observed for Dcr1 and Rdp1 in fission yeast.

Other eukaryotes

In contrast to *Drosophila*, where miRNA and siRNA pathways have been roughly segregated into DCR1/AGO1- and DCR2/AGO2-mediated processes, respectively, mammals possess only one Dicer enzyme, loss of which results in early embryonic lethality (Bernstein et al., 2003). Separating the effects of Dicer perturbation on the miRNA pathway and on other RNAi-mediated processes is therefore challenging (Benetti et al., 2008; Sinkkonen et al., 2008). Nonetheless, some reports have implicated Dicer in silencing centromeric repeats in mammals, although there are contradictory findings as to whether changes in chromatin modifications accompany the loss of silencing in Dicer mutants (Fukagawa et al., 2004; Kanellopoulou et al., 2005; Murchison et al., 2005). Thus, it is possible that RNAi in mammals is dispensable for the integrity of heterochromatin but might still contribute to tight repression. A potential example of such repression is the processing of *Alu* RNAs, which incidentally are abundant in heterochromatin, by DICER1 in the human eye (Kaneko et al., 2011). In age-related macular

degeneration, decreased levels of *DICER1* mRNA are responsible for an increase in double-stranded *Alu* RNAs, and subsequent cytotoxicity. The RNA accumulation occurs in both nuclear and cytoplasmic compartments. Using antisense oligonucleotides targeting *Alu* sequences blocks DICER1 reduction-induced cytotoxicity, despite persistent global miRNA expression deficits. Whether such repression occurs in association with chromatin remains to be investigated.

Artificial targeting of siRNAs to promoter regions in human cells can affect transcript levels and induce chromatin modifications in an Argonaute-dependent manner, reminiscent of the observations in *C. elegans* (Janowski et al., 2006; Kim et al., 2006; Morris et al., 2004; Morris et al., 2008; Ting et al., 2005; Weinberg et al., 2006). However, these studies have reported both repressive and activating effects, apparently dependent on the cell context (Janowski et al., 2007; Li et al., 2006b; Schwartz et al., 2008; Ting et al., 2005), and the effect does not always seem to involve chromatin modifications (Janowski et al 2005, Napoli et al 2009). If the effects are co-transcriptional, however, then chromatin modifications are not necessary and could be a consequence of silencing/activation. I believe that efforts to map interactions between the RNAi machinery and mammalian genomes, and to perturb the subcellular localization of RNAi components, will be more informative as to whether endogenous RNAi-mediated TGS/CTGS processes are conserved. Argonaute proteins have been found in the nuclei of mammalian cells (Robb et al., 2005; Weinmann et al., 2009), and a recent study showed interaction of human DICER1 with several nuclear pore components (Ando et al., 2011), providing encouraging hints that such processes exist.

Although *S. cerevisiae* is one of the few eukaryotes lacking the RNAi machinery, there is some evidence that the dsRNA-specific RNase III, Rnt1p, can also have co-transcriptional functions. For example, it was proposed that Rnt1p co-transcriptionally degrades RNAs involved in the glucose-sensing pathway (Lavoie et al., 2012). Furthermore, co-transcriptional cleavage by Rnt1p can ensure proper transcription termination (Ghazal et al., 2009; Rondon et al., 2009), similar to a recently described role for *Arabidopsis* DCL4 (Liu et al., 2012) and the requirement for Dcr1 in transcription termination within *S. pombe* centromeric repeats (Zaratiegui et al.,

2011a). Therefore, co-transcriptional functions of RNase III enzymes may also exist in organisms lacking the RNAi pathway.

Physiological relevance of CTGS

While the above studies strongly hint at a possibly conserved function of nuclear RNAi pathways that is consistent with the concept of CTGS, the physiological relevance of such a mode of genome regulation is not clear. The fact that CTGS in fission yeast seems to occur preferentially at stress response genes near nuclear pores suggests that this mechanism functions to keep certain genes poised for expression, enabling very rapid upregulation and export under stress conditions. This is conceptually similar to the well-studied phenomenon of Pol II pausing at heat shock genes in *Drosophila* (Guertin et al., 2010). The association of DCR2 and AGO2 with heat shock loci in *Drosophila* suggests a similar function, and the results even indicate that DCR2 and AGO2 affect Pol II pausing at these genes (Cernilogar et al., 2011). It is interesting to note that DCR2 and AGO2 are required to compensate for temperature fluctuations in the developing *Drosophila* embryo (Lucchetta et al., 2009). It remains to be seen whether other CTGS mechanisms, like those in *C. elegans*, are also involved in regulating responses to environmental changes. There are already some hints in this direction, for example genes upregulated in several RNAi mutants overlap with those induced upon exposure of *C. elegans* to pathogens or toxins (Welker et al., 2007).

Interestingly, after long periods of elevated temperature, fission yeast Dcr1 leaves the nucleus (Figure 6B), indicating that environmental conditions can regulate the RNAi pathway. This could be required for adapting in the longer term, for example by enabling upregulation of transcripts involved in thermotolerance. However, the loss of Dcr1 from the nucleus upon heat results in a maximum increase in centromeric transcripts of ~5-fold, much less than the 60-100-fold increase seen in *dcr1*Δ cells. Although it was previously reported that silencing of transgenes inserted into heterochromatin is alleviated at higher temperatures (Allshire et al., 1994), we see only a mild increase in *otr1R::ura4*$^{+}$ transcripts after up to 8 h of heat shock (Kasia Kowalik, personal

communication). This suggests that compensatory mechanisms may exist to keep centromeres silent at higher temperatures.

There is also evidence from other organisms that temperature can influence RNAi pathways. For example, RNAi in plants is more efficient at higher temperatures, with levels of siRNAs, but not miRNAs, positively correlating with temperature (Szittya et al., 2003). In contrast, RNAi-mediated silencing of transgenes in the *C. elegans* germline is enhanced by culturing the worms at lower as opposed to higher temperatures (Strome et al., 2001). It is possible that higher or lower temperatures affect pairing of small RNAs with their targets. However, it could be that more sophisticated regulation of RNAi pathways in response to temperature changes, exemplified by the relocalization of fission yeast Dicer, is behind these observations.

Materials & Methods

Part I: RNAi-mediated co-transcriptional gene silencing in euchromatin

For DamID, RNA isolation, cDNA synthesis and quantitative RT-PCR, see the Methods sections of the published manuscripts found in the Appendix (Woolcock et al., 2011; Woolcock et al., 2012). In addition, a detailed DamID bench protocol and R scripts used for analysis have been deposited in the Bühler laboratory protocols database and are available on request.

Replacement and deletion of Dcr1-associated ncRNAs and LTRs

Fission yeast strains were grown at 30°C in YES. All strains (listed in Table 1) were constructed following a standard PCR-based protocol (Bahler et al., 1998). Fragments ~500 bp either side of the LTR or ncRNA were linked by a fusion PCR strategy and transformed into an *LTR*Δ*::URA3* (*C.a.*) or *ncRNA*Δ*::URA3* (*C.a.*) strain, respectively, followed by counter-selection on 5-FOA. The RNA level of the nearby Dcr1-regulated gene (within 5 kb, measuring from the middle of the LTR/ncRNA to the middle of the gene) was then determined by quantitative RT-PCR, done as previously described (Emmerth et al., 2010). Primer pairs used for PCR reactions are listed in Table 2.

Table 1

Strain	Genotype	Source
SPB30	*h+ leu1-32 ade6-M210 ura4DS/E otr1R(SphI)::GFP+/NAT (ura4 promoter and Tadh1 terminator)*	1
SPB830	*h+ leu1-32 ade6-M210 ura4DS/E otr1R(SphI)::GFP+/NAT (ura4 promoter and Tadh1 terminator) dcr1Δ::hph*	2
SPB757	*h+ leu1-32 ade6-M210 ura4DS/E otr1R(SphI)::GFP+/NAT (ura4 promoter and Tadh1 terminator) LTR4480Δ::URA3*	2
SPB760	*h+ leu1-32 ade6-M210 ura4DS/E otr1R(SphI)::GFP+/NAT (ura4 promoter and Tadh1 terminator) LTR4480Δ*	2
SPB831	*h+ leu1-32 ade6-M210 ura4DS/E otr1R(SphI)::GFP+/NAT (ura4 promoter and Tadh1 terminator) LTR4480Δ dcr1Δ::hph*	2
SPB758	*h+ leu1-32 ade6-M210 ura4DS/E otr1R(SphI)::GFP+/NAT (ura4 promoter and Tadh1 terminator) LTR3517Δ::URA3*	2
SPB761	*h+ leu1-32 ade6-M210 ura4DS/E otr1R(SphI)::GFP+/NAT (ura4 promoter and Tadh1 terminator) LTR3517Δ*	2
SPB832	*h+ leu1-32 ade6-M210 ura4DS/E otr1R(SphI)::GFP+/NAT (ura4 promoter and Tadh1 terminator) LTR3517Δ dcr1Δ::hph*	2
SPB759	*h+ leu1-32 ade6-M210 ura4DS/E otr1R(SphI)::GFP+/NAT (ura4 promoter and Tadh1 terminator) LTR1452Δ::URA3*	2
SPB762	*h+ leu1-32 ade6-M210 ura4DS/E otr1R(SphI)::GFP+/NAT (ura4 promoter and Tadh1 terminator) LTR1452Δ*	2

SPB833	*h+ leu1-32 ade6-M210 ura4DS/E otr1R(SphI)::GFP+/NAT (ura4 promoter and Tadh1 terminator) LTR1452Δ dcr1Δ::hph*	2
SPB866	*h+ leu1-32 ade6-M210 ura4DS/E otr1R(SphI)::GFP+/NAT (ura4 promoter and Tadh1 terminator) ncRNA540Δ::URA3*	2
SPB908	*h+ leu1-32 ade6-M210 ura4DS/E otr1R(SphI)::GFP+/NAT (ura4 promoter and Tadh1 terminator) ncRNA.540Δ*	2
SPB929	*h+ leu1-32 ade6-M210 ura4DS/E otr1R(SphI)::GFP+/NAT (ura4 promoter and Tadh1 terminator) ncRNA.540Δ dcr1Δ::hph*	2
SPB867	*h+ leu1-32 ade6-M210 ura4DS/E otr1R(SphI)::GFP+/NAT (ura4 promoter and Tadh1 terminator) ncRNA472Δ::URA3*	2
SPB910	*h+ leu1-32 ade6-M210 ura4DS/E otr1R(SphI)::GFP+/NAT (ura4 promoter and Tadh1 terminator) ncRNA.472Δ*	2
SPB931	*h+ leu1-32 ade6-M210 ura4DS/E otr1R(SphI)::GFP+/NAT (ura4 promoter and Tadh1 terminator) ncRNA.472Δ dcr1Δ::hph*	2

1 = Bühler lab strain collection, 2 = This study

Table 2

Name	**Number**	**Sequence**
hsp9 for	mb1733	GAACAAGGCAAGGAGAAAATGACT
hsp9 rev	mb1734	AATGGATTCCTTGGCCTTGTC
SPBC215.11c for	mb1735	CAGCTTCTTCCGCCGTAGAT
SPBC215.11c rev	mb1736	ACCATGTCGCCAACCTTGA
SPCC737.04 for	mb1739	GGTACGACCGGGAGACGTT
SPCC737.04 rev	mb1740	CAAATGGCGGCCCAACT
hsp16 for	mb3059	AAAGCACCGAGGGTAACCAA
hsp16 rev	mb3060	TGGTACGAGAGAATGAGCCAAA
SPCC18B5.02c for	mb2473	TCAAAGACTTGTGCCGAAAGG
SPCC18B5.02c rev	mb2474	CAAACGAAGAGCGCTTTTGC
act1 for	mb555	TCCTCATGCTATCATGCGTCTT
act1 rev	mb556	CCACGCTCCATGAGAATCTTC

Part II: Establishment of RNAi-genome interactions

See Methods section in the published manuscript found in the Appendix (Woolcock et al., 2012).

Part III: RNAi-mediated regulation of protein-coding genes

See Methods section in the published manuscript found in the Appendix (Woolcock et al., 2012).

Part IV: Further characterisation of the properties and nuclear environment of BANCs

Previously published datasets were reannotated to enable comparison of BANCs with all other genes (Cam et al., 2005; Nicolas et al., 2007; Sugiyama et al., 2007). Deep sequencing datasets (Wilhelm et al., 2008; Zaratiegui et al., 2011b) were reanalysed using the FMI deep sequencing pipeline and annotated to enable comparison of BANCs with all other genes. RNA polymerase II ChIP-chip (Wilhelm et al., 2008) was reanalysed as previously described (Woolcock et al., 2012).

Part V: Role for transcription factors in genome organisation at nuclear pores

Fission yeast strains were grown at 30°C in YES. All strains (listed in Table 3) were constructed following a standard PCR-based protocol (Bahler et al., 1998). DamID was done as previously described (Woolcock et al., 2012).

Table 3

Strain	Genotype	Source
SPB492	*h+ otr1R(SphI)::ura4+ ura4-DS/E ade6-M210 leu1Δ::nmt1(81x)-dam-myc-kan*	1
SPB381	*h+ otr1R(SphI)::ura4+ ura4-DS/E ade6-M210 leu1Δ::nmt1(81x)-dam-myc-dcr1-kan*	1
SPB1151	*h+ otr1R(SphI)::ura4+ ura4-DS/E ade6-M210 leu1Δ::nmt1(81x)-dam-myc-nup85-kan*	2
SPB711	*h+ otr1R(SphI)::ura4+ ura4-DS/E ade6-M210 leu1Δ::nmt1(81x)-dam-myc-kan clr4Δ::nat*	1
SPB1426	*h+ otr1R(SphI)::ura4+ ura4-DS/E ade6-M210 leu1Δ::nmt1(81x)-dam-myc-nup85-kan clr4Δ::nat*	3
SPB1433	*h+ otr1R(SphI)::ura4+ ura4-DS/E ade6-M210 leu1Δ::nmt1(81x)-dam-myc-kan atf1Δ::nat*	3
SPB1434	*h+ otr1R(SphI)::ura4+ ura4-DS/E ade6-M210 leu1Δ::nmt1(81x)-dam-myc-dcr1-kan atf1Δ::nat*	3
SPB1435	*h+ otr1R(SphI)::ura4+ ura4-DS/E ade6-M210 leu1Δ::nmt1(81x)-dam-myc-nup85-kan atf1Δ::nat*	3
SPB1436	*h+ otr1R(SphI)::ura4+ ura4-DS/E ade6-M210 leu1Δ::nmt1(81x)-dam-myc-kan pcr1Δ::nat*	3
SPB1437	*h+ otr1R(SphI)::ura4+ ura4-DS/E ade6-M210 leu1Δ::nmt1(81x)-dam-myc-dcr1-kan pcr1Δ::nat*	3
SPB1438	*h+ otr1R(SphI)::ura4+ ura4-DS/E ade6-M210 leu1Δ::nmt1(81x)-dam-myc-nup85-kan pcr1Δ::nat*	3

1 = (Woolcock et al., 2011), 2 = (Woolcock et al., 2012), 3 = This study

Part VI: Regulation of RNAi at elevated temperatures

See Methods section in the published manuscript found in the Appendix (Woolcock et al., 2012).

Part VII: Role of Cid14 in co-transcriptional gene silencing

See Methods sections in the published manuscripts found in the Appendix (Keller et al., 2012; Keller et al., 2010).

Additional Methods

Motif enrichment analysis in DamID data

Jaspar core fungi (21.12.2011) weight matrices were downloaded from http://jaspar.cgb.ki.se/ and were used to scan the *S. pombe* genome with a minimum meme score of 10. This resulted in a list of 753956 predicted binding sites for 160 transcription factors (TFs). Clustering of the binding sites (in windows of 10 bp) revealed one pair of TFs (MA0338.1 and MA0339.1) with identical binding sites. MA0339.1 was therefore removed from further analysis. To determine if the DamID signal from various experiments can be explained by TF binding, we performed a linear regression (in windows of 1000 bp) using the number of TF binding sites as predictors and the DamID signal as the response variable. The coefficients obtained from the regression were used as the inferred contribution of every TF to the DamID signal.

References

Ahmed, S., Brickner, D.G., Light, W.H., Cajigas, I., McDonough, M., Froyshteter, A.B., Volpe, T., and Brickner, J.H. (2010). DNA zip codes control an ancient mechanism for gene targeting to the nuclear periphery. Nature cell biology *12*, 111-118.

Alexander, W.G., Raju, N.B., Xiao, H., Hammond, T.M., Perdue, T.D., Metzenberg, R.L., Pukkila, P.J., and Shiu, P.K. (2008). DCL-1 colocalizes with other components of the MSUD machinery and is required for silencing. Fungal Genet Biol *45*, 719-727.

Allshire, R.C., Javerzat, J.P., Redhead, N.J., and Cranston, G. (1994). Position effect variegation at fission yeast centromeres. Cell *76*, 157-169.

Ameres, S.L., Horwich, M.D., Hung, J.H., Xu, J., Ghildiyal, M., Weng, Z., and Zamore, P.D. (2010). Target RNA-directed trimming and tailing of small silencing RNAs. Science *328*, 1534-1539.

Ameres, S.L., Hung, J.H., Xu, J., Weng, Z., and Zamore, P.D. (2011). Target RNA-directed tailing and trimming purifies the sorting of endo-siRNAs between the two Drosophila Argonaute proteins. RNA *17*, 54-63.

Ando, Y., Tomaru, Y., Morinaga, A., Burroughs, A.M., Kawaji, H., Kubosaki, A., Kimura, R., Tagata, M., Ino, Y., Hirano, H.*, et al.* (2011). Nuclear pore complex protein mediated nuclear localization of dicer protein in human cells. PloS one *6*, e23385.

Aravin, A.A., Naumova, N.M., Tulin, A.V., Vagin, V.V., Rozovsky, Y.M., and Gvozdev, V.A. (2001). Double-stranded RNA-mediated silencing of genomic tandem repeats and transposable elements in the D. melanogaster germline. Current biology : CB *11*, 1017-1027.

Aravin, A.A., Sachidanandam, R., Bourc'his, D., Schaefer, C., Pezic, D., Toth, K.F., Bestor, T., and Hannon, G.J. (2008). A piRNA pathway primed by individual transposons is linked to de novo DNA methylation in mice. Molecular cell *31*, 785-799.

Ashe, A., Sapetschnig, A., Weick, E.M., Mitchell, J., Bagijn, M.P., Cording, A.C., Doebley, A.L., Goldstein, L.D., Lehrbach, N.J., Le Pen, J.*, et al.* (2012). piRNAs Can Trigger a Multigenerational Epigenetic Memory in the Germline of C. elegans. Cell *150*, 88-99.

Bahler, J., Wu, J.Q., Longtine, M.S., Shah, N.G., McKenzie, A., 3rd, Steever, A.B., Wach, A., Philippsen, P., and Pringle, J.R. (1998). Heterologous modules for efficient and versatile PCR-based gene targeting in Schizosaccharomyces pombe. Yeast *14*, 943-951.

Bai, S.W., Rouquette, J., Umeda, M., Faigle, W., Loew, D., Sazer, S., and Doye, V. (2004). The fission yeast Nup107-120 complex functionally interacts with the small GTPase Ran/Spi1 and is required for mRNA export, nuclear pore distribution, and proper cell division. Mol Cell Biol *24*, 6379-6392.

Bannister, A.J., Zegerman, P., Partridge, J.F., Miska, E.A., Thomas, J.O., Allshire, R.C., and Kouzarides, T. (2001). Selective recognition of methylated lysine 9 on histone H3 by the HP1 chromo domain. Nature *410*, 120-124.

Barraud, P., Emmerth, S., Shimada, Y., Hotz, H.R., Allain, F.H., and Buhler, M. (2011). An extended dsRBD with a novel zinc-binding motif mediates nuclear retention of fission yeast Dicer. The EMBO journal *30*, 4223-4235.

Bayne, E.H., White, S.A., Kagansky, A., Bijos, D.A., Sanchez-Pulido, L., Hoe, K.L., Kim, D.U., Park, H.O., Ponting, C.P., Rappsilber, J.*, et al.* (2010). Stc1: a critical link between RNAi and chromatin modification required for heterochromatin integrity. Cell *140*, 666-677.

Bazzini, A.A., Lee, M.T., and Giraldez, A.J. (2012). Ribosome profiling shows that miR-430 reduces translation before causing mRNA decay in zebrafish. Science *336*, 233-237.

Benetti, R., Gonzalo, S., Jaco, I., Munoz, P., Gonzalez, S., Schoeftner, S., Murchison, E., Andl, T., Chen, T., Klatt, P.*, et al.* (2008). A mammalian microRNA cluster controls DNA methylation and telomere recombination via Rbl2-dependent regulation of DNA methyltransferases. Nature structural & molecular biology *15*, 998.

Bernstein, E., Caudy, A.A., Hammond, S.M., and Hannon, G.J. (2001). Role for a bidentate ribonuclease in the initiation step of RNA interference. Nature *409*, 363-366.

Bernstein, E., Kim, S.Y., Carmell, M.A., Murchison, E.P., Alcorn, H., Li, M.Z., Mills, A.A., Elledge, S.J., Anderson, K.V., and Hannon, G.J. (2003). Dicer is essential for mouse development. Nature genetics *35*, 215-217.

Bethune, J., Artus-Revel, C.G., and Filipowicz, W. (2012). Kinetic analysis reveals successive steps leading to miRNA-mediated silencing in mammalian cells. EMBO Rep.

Bjerling, P., Silverstein, R.A., Thon, G., Caudy, A., Grewal, S., and Ekwall, K. (2002). Functional divergence between histone deacetylases in fission yeast by distinct cellular localization and in vivo specificity. Molecular and cellular biology *22*, 2170-2181.

Blobel, G. (1985). Gene gating: a hypothesis. Proc Natl Acad Sci U S A *82*, 8527-8529.

Brennecke, J., Aravin, A.A., Stark, A., Dus, M., Kellis, M., Sachidanandam, R., and Hannon, G.J. (2007). Discrete small RNA-generating loci as master regulators of transposon activity in Drosophila. Cell *128*, 1089-1103.

Brickner, D.G., Ahmed, S., Meldi, L., Thompson, A., Light, W., Young, M., Hickman, T.L., Chu, F., Fabre, E., and Brickner, J.H. (2012). Transcription factor binding to a DNA zip code controls interchromosomal clustering at the nuclear periphery. Developmental cell *22*, 1234-1246.

Brickner, J.H., and Walter, P. (2004). Gene recruitment of the activated INO1 locus to the nuclear membrane. PLoS biology *2*, e342.

Brodersen, P., Sakvarelidze-Achard, L., Bruun-Rasmussen, M., Dunoyer, P., Yamamoto, Y.Y., Sieburth, L., and Voinnet, O. (2008). Widespread translational inhibition by plant miRNAs and siRNAs. Science *320*, 1185-1190.

Brower-Toland, B., Findley, S.D., Jiang, L., Liu, L., Yin, H., Dus, M., Zhou, P., Elgin, S.C., and Lin, H. (2007). Drosophila PIWI associates with chromatin and interacts directly with HP1a. Genes & development *21*, 2300-2311.

Buhler, M., Haas, W., Gygi, S.P., and Moazed, D. (2007). RNAi-dependent and -independent RNA turnover mechanisms contribute to heterochromatic gene silencing. Cell *129*, 707-721.

Buhler, M., Spies, N., Bartel, D.P., and Moazed, D. (2008). TRAMP-mediated RNA surveillance prevents spurious entry of RNAs into the Schizosaccharomyces pombe siRNA pathway. Nat Struct Mol Biol *15*, 1015-1023.

Buhler, M., Verdel, A., and Moazed, D. (2006). Tethering RITS to a nascent transcript initiates RNAi- and heterochromatin-dependent gene silencing. Cell *125*, 873-886.

Buker, S.M., Iida, T., Buhler, M., Villen, J., Gygi, S.P., Nakayama, J., and Moazed, D. (2007). Two different Argonaute complexes are required for siRNA generation and heterochromatin assembly in fission yeast. Nat Struct Mol Biol *14*, 200-207.

Burkhart, K.B., Guang, S., Buckley, B.A., Wong, L., Bochner, A.F., and Kennedy, S. (2011). A pre-mRNA-associating factor links endogenous siRNAs to chromatin regulation. PLoS genetics *7*, e1002249.

Cam, H.P., Noma, K., Ebina, H., Levin, H.L., and Grewal, S.I. (2008). Host genome surveillance for retrotransposons by transposon-derived proteins. Nature *451*, 431-436.

Cam, H.P., Sugiyama, T., Chen, E.S., Chen, X., FitzGerald, P.C., and Grewal, S.I. (2005). Comprehensive analysis of heterochromatin- and RNAi-mediated epigenetic control of the fission yeast genome. Nat Genet *37*, 809-819.

Cao, X., and Jacobsen, S.E. (2002). Role of the arabidopsis DRM methyltransferases in de novo DNA methylation and gene silencing. Current biology : CB *12*, 1138-1144.

Capelson, M., Liang, Y., Schulte, R., Mair, W., Wagner, U., and Hetzer, M.W. (2010). Chromatin-bound nuclear pore components regulate gene expression in higher eukaryotes. Cell *140*, 372-383.

Carmell, M.A., Girard, A., van de Kant, H.J., Bourc'his, D., Bestor, T.H., de Rooij, D.G., and Hannon, G.J. (2007). MIWI2 is essential for spermatogenesis and repression of transposons in the mouse male germline. Developmental cell *12*, 503-514.

Carmichael, J.B., Stoica, C., Parker, H., McCaffery, J.M., Simmonds, A.J., and Hobman, T.C. (2006). RNA interference effector proteins localize to mobile cytoplasmic puncta in Schizosaccharomyces pombe. Traffic *7*, 1032-1044.

Carthew, R.W., and Sontheimer, E.J. (2009). Origins and Mechanisms of miRNAs and siRNAs. Cell *136*, 642-655.

Casolari, J.M., Brown, C.R., Komili, S., West, J., Hieronymus, H., and Silver, P.A. (2004). Genome-wide localization of the nuclear transport machinery couples transcriptional status and nuclear organization. Cell *117*, 427-439.

Cernilogar, F.M., Onorati, M.C., Kothe, G.O., Burroughs, A.M., Parsi, K.M., Breiling, A., Lo Sardo, F., Saxena, A., Miyoshi, K., Siomi, H*., et al.* (2011). Chromatin-associated RNA interference components contribute to transcriptional regulation in Drosophila. Nature *480*, 391-395.

Chen, D., Toone, W.M., Mata, J., Lyne, R., Burns, G., Kivinen, K., Brazma, A., Jones, N., and Bahler, J. (2003). Global transcriptional responses of fission yeast to environmental stress. Mol Biol Cell *14*, 214-229.

Chen, E.S., Zhang, K., Nicolas, E., Cam, H.P., Zofall, M., and Grewal, S.I. (2008). Cell cycle control of centromeric repeat transcription and heterochromatin assembly. Nature *451*, 734-737.

Cheng, C.Y., Vogt, A., Mochizuki, K., and Yao, M.C. (2010). A domesticated piggyBac transposase plays key roles in heterochromatin dynamics and DNA cleavage during programmed DNA deletion in Tetrahymena thermophila. Molecular biology of the cell *21*, 1753-1762.

Chung, W.J., Okamura, K., Martin, R., and Lai, E.C. (2008). Endogenous RNA interference provides a somatic defense against Drosophila transposons. Current biology : CB *18*, 795-802.

Colmenares, S.U., Buker, S.M., Buhler, M., Dlakic, M., and Moazed, D. (2007). Coupling of double-stranded RNA synthesis and siRNA generation in fission yeast RNAi. Mol Cell *27*, 449-461.

Czech, B., Malone, C.D., Zhou, R., Stark, A., Schlingeheyde, C., Dus, M., Perrimon, N., Kellis, M., Wohlschlegel, J.A., Sachidanandam, R., *et al.* (2008). An endogenous small interfering RNA pathway in Drosophila. Nature *453*, 798-802.

D'Angelo, M.A., Gomez-Cavazos, J.S., Mei, A., Lackner, D.H., and Hetzer, M.W. (2012). A change in nuclear pore complex composition regulates cell differentiation. Developmental cell *22*, 446-458.

Dieppois, G., Iglesias, N., and Stutz, F. (2006). Cotranscriptional recruitment to the mRNA export receptor Mex67p contributes to nuclear pore anchoring of activated genes. Molecular and cellular biology *26*, 7858-7870.

Djupedal, I., Kos-Braun, I.C., Mosher, R.A., Soderholm, N., Simmer, F., Hardcastle, T.J., Fender, A., Heidrich, N., Kagansky, A., Bayne, E., *et al.* (2009). Analysis of small RNA in fission yeast; centromeric siRNAs are potentially generated through a structured RNA. The EMBO journal *28*, 3832-3844.

Djupedal, I., Portoso, M., Spahr, H., Bonilla, C., Gustafsson, C.M., Allshire, R.C., and Ekwall, K. (2005). RNA Pol II subunit Rpb7 promotes centromeric transcription and RNAi-directed chromatin silencing. Genes Dev *19*, 2301-2306.

Djuranovic, S., Nahvi, A., and Green, R. (2012). miRNA-mediated gene silencing by translational repression followed by mRNA deadenylation and decay. Science *336*, 237-240.

Drinnenberg, I.A., Weinberg, D.E., Xie, K.T., Mower, J.P., Wolfe, K.H., Fink, G.R., and Bartel, D.P. (2009). RNAi in budding yeast. Science *326*, 544-550.

El-Shami, M., Pontier, D., Lahmy, S., Braun, L., Picart, C., Vega, D., Hakimi, M.A., Jacobsen, S.E., Cooke, R., and Lagrange, T. (2007). Reiterated WG/GW motifs form functionally and evolutionarily conserved ARGONAUTE-binding platforms in RNAi-related components. Genes & development *21*, 2539-2544.

Elkayam, E., Kuhn, C.D., Tocilj, A., Haase, A.D., Greene, E.M., Hannon, G.J., and Joshua-Tor, L. (2012). The Structure of Human Argonaute-2 in Complex with miR-20a. Cell.

Emmerth, S., Schober, H., Gaidatzis, D., Roloff, T., Jacobeit, K., and Buhler, M. (2010). Nuclear retention of fission yeast dicer is a prerequisite for RNAi-mediated heterochromatin assembly. Developmental cell *18*, 102-113.

Eshaghi, M., Lee, J.H., Zhu, L., Poon, S.Y., Li, J., Cho, K.H., Chu, Z., Karuturi, R.K., and Liu, J. (2010). Genomic binding profiling of the fission yeast stress-activated MAPK Sty1 and the bZIP transcriptional activator Atf1 in response to H2O2. PloS one *5*, e11620.

Fagegaltier, D., Bouge, A.L., Berry, B., Poisot, E., Sismeiro, O., Coppee, J.Y., Theodore, L., Voinnet, O., and Antoniewski, C. (2009). The endogenous siRNA pathway is involved in heterochromatin formation in Drosophila. Proceedings of the National Academy of Sciences of the United States of America *106*, 21258-21263.

Filion, G.J., van Bemmel, J.G., Braunschweig, U., Talhout, W., Kind, J., Ward, L.D., Brugman, W., de Castro, I.J., Kerkhoven, R.M., Bussemaker, H.J., *et al.* (2010). Systematic protein location mapping reveals five principal chromatin types in Drosophila cells. Cell *143*, 212-224.

Fire, A., Xu, S., Montgomery, M.K., Kostas, S.A., Driver, S.E., and Mello, C.C. (1998). Potent and specific genetic interference by double-stranded RNA in Caenorhabditis elegans. Nature *391*, 806-811.

Fischer, T., Cui, B., Dhakshnamoorthy, J., Zhou, M., Rubin, C., Zofall, M., Veenstra, T.D., and Grewal, S.I. (2009). Diverse roles of HP1 proteins in heterochromatin assembly and functions in fission yeast. Proc Natl Acad Sci U S A *106*, 8998-9003.

Fischle, W., Tseng, B.S., Dormann, H.L., Ueberheide, B.M., Garcia, B.A., Shabanowitz, J., Hunt, D.F., Funabiki, H., and Allis, C.D. (2005). Regulation of HP1-chromatin binding by histone H3 methylation and phosphorylation. Nature *438*, 1116-1122.

Fukagawa, T., Nogami, M., Yoshikawa, M., Ikeno, M., Okazaki, T., Takami, Y., Nakayama, T., and Oshimura, M. (2004). Dicer is essential for formation of the heterochromatin structure in vertebrate cells. Nat Cell Biol *6*, 784-791.

Gerace, E.L., Halic, M., and Moazed, D. (2010). The methyltransferase activity of Clr4Suv39h triggers RNAi independently of histone H3K9 methylation. Molecular cell *39*, 360-372.

Ghazal, G., Gagnon, J., Jacques, P.E., Landry, J.R., Robert, F., and Elela, S.A. (2009). Yeast RNase III triggers polyadenylation-independent transcription termination. Molecular cell *36*, 99-109.

Ghildiyal, M., Seitz, H., Horwich, M.D., Li, C., Du, T., Lee, S., Xu, J., Kittler, E.L., Zapp, M.L., Weng, Z*., et al.* (2008). Endogenous siRNAs derived from transposons and mRNAs in Drosophila somatic cells. Science *320*, 1077-1081.

Ghildiyal, M., and Zamore, P.D. (2009). Small silencing RNAs: an expanding universe. Nature reviews Genetics *10*, 94-108.

Gibbings, D.J., Ciaudo, C., Erhardt, M., and Voinnet, O. (2009). Multivesicular bodies associate with components of miRNA effector complexes and modulate miRNA activity. Nature cell biology *11*, 1143-1149.

Grishok, A., Sinskey, J.L., and Sharp, P.A. (2005). Transcriptional silencing of a transgene by RNAi in the soma of C. elegans. Genes & development *19*, 683-696.

Grishok, A., Tabara, H., and Mello, C.C. (2000). Genetic requirements for inheritance of RNAi in C. elegans. Science *287*, 2494-2497.

Guang, S., Bochner, A.F., Burkhart, K.B., Burton, N., Pavelec, D.M., and Kennedy, S. (2010). Small regulatory RNAs inhibit RNA polymerase II during the elongation phase of transcription. Nature *465*, 1097-1101.

Guang, S., Bochner, A.F., Pavelec, D.M., Burkhart, K.B., Harding, S., Lachowiec, J., and Kennedy, S. (2008). An Argonaute transports siRNAs from the cytoplasm to the nucleus. Science *321*, 537-541.

Guelen, L., Pagie, L., Brasset, E., Meuleman, W., Faza, M.B., Talhout, W., Eussen, B.H., de Klein, A., Wessels, L., de Laat, W*., et al.* (2008). Domain organization of human chromosomes revealed by mapping of nuclear lamina interactions. Nature *453*, 948-951.

Guertin, M.J., Petesch, S.J., Zobeck, K.L., Min, I.M., and Lis, J.T. (2010). Drosophila heat shock system as a general model to investigate transcriptional regulation. Cold Spring Harbor symposia on quantitative biology *75*, 1-9.

Gullerova, M., Moazed, D., and Proudfoot, N.J. (2011). Autoregulation of convergent RNAi genes in fission yeast. Genes & development *25*, 556-568.

Gullerova, M., and Proudfoot, N.J. (2008). Cohesin complex promotes transcriptional termination between convergent genes in S. pombe. Cell *132*, 983-995.

Gunawardane, L.S., Saito, K., Nishida, K.M., Miyoshi, K., Kawamura, Y., Nagami, T., Siomi, H., and Siomi, M.C. (2007). A slicer-mediated mechanism for repeat-associated siRNA 5' end formation in Drosophila. Science *315*, 1587-1590.

Halic, M., and Moazed, D. (2010). Dicer-independent primal RNAs trigger RNAi and heterochromatin formation. Cell *140*, 504-516.

Hamilton, A.J., and Baulcombe, D.C. (1999). A species of small antisense RNA in posttranscriptional gene silencing in plants. Science *286*, 950-952.

Hammond, S.M., Boettcher, S., Caudy, A.A., Kobayashi, R., and Hannon, G.J. (2001). Argonaute2, a link between genetic and biochemical analyses of RNAi. Science *293*, 1146-1150.

Hansen, K.R., Ibarra, P.T., and Thon, G. (2006). Evolutionary-conserved telomere-linked helicase genes of fission yeast are repressed by silencing factors, RNAi components and the telomere-binding protein Taz1. Nucleic Acids Res *34*, 78-88.

Hayashi, A., Ishida, M., Kawaguchi, R., Urano, T., Murakami, Y., and Nakayama, J. (2012). Heterochromatin protein 1 homologue Swi6 acts in concert with Ers1 to regulate RNAi-directed heterochromatin assembly. Proceedings of the National Academy of Sciences of the United States of America *109*, 6159-6164.

Heitz, E. (1928). Das Heterochromatin der Moose. Jahrbuch der Wissenschaftlichen Botanik *69*, 762-818.

Herr, A.J., Jensen, M.B., Dalmay, T., and Baulcombe, D.C. (2005). RNA polymerase IV directs silencing of endogenous DNA. Science *308*, 118-120.

Hiriart, E., Vavasseur, A., Touat-Todeschini, L., Yamashita, A., Gilquin, B., Lambert, E., Perot, J., Shichino, Y., Nazaret, N., Boyault, C*., et al.* (2012). Mmi1 RNA surveillance machinery directs RNAi complex RITS to specific meiotic genes in fission yeast. The EMBO journal *31*, 2296-2308.

Hirota, T., Lipp, J.J., Toh, B.H., and Peters, J.M. (2005). Histone H3 serine 10 phosphorylation by Aurora B causes HP1 dissociation from heterochromatin. Nature *438*, 1176-1180.

Huang, H., Gao, Q., Peng, X., Choi, S.Y., Sarma, K., Ren, H., Morris, A.J., and Frohman, M.A. (2011). piRNA-associated germline nuage formation and spermatogenesis require MitoPLD profusogenic mitochondrial-surface lipid signaling. Developmental cell *20*, 376-387.

Iida, T., Nakayama, J., and Moazed, D. (2008). siRNA-mediated heterochromatin establishment requires HP1 and is associated with antisense transcription. Mol Cell *31*, 178-189.

Janowski, B.A., Huffman, K.E., Schwartz, J.C., Ram, R., Nordsell, R., Shames, D.S., Minna, J.D., and Corey, D.R. (2006). Involvement of AGO1 and AGO2 in mammalian transcriptional silencing. Nature structural & molecular biology *13*, 787-792.

Janowski, B.A., Younger, S.T., Hardy, D.B., Ram, R., Huffman, K.E., and Corey, D.R. (2007). Activating gene expression in mammalian cells with promoter-targeted duplex RNAs. Nat Chem Biol *3*, 166-173.

Jia, S., Noma, K., and Grewal, S.I. (2004). RNAi-independent heterochromatin nucleation by the stress-activated ATF/CREB family proteins. Science *304*, 1971-1976.

Kalverda, B., and Fornerod, M. (2010). Characterization of genome-nucleoporin interactions in Drosophila links chromatin insulators to the nuclear pore complex. Cell Cycle *9*, 4812-4817.

Kalverda, B., Pickersgill, H., Shloma, V.V., and Fornerod, M. (2010). Nucleoporins directly stimulate expression of developmental and cell-cycle genes inside the nucleoplasm. Cell *140*, 360-371.

Kaneko, H., Dridi, S., Tarallo, V., Gelfand, B.D., Fowler, B.J., Cho, W.G., Kleinman, M.E., Ponicsan, S.L., Hauswirth, W.W., Chiodo, V.A*., et al.* (2011). DICER1 deficit induces Alu RNA toxicity in age-related macular degeneration. Nature *471*, 325-330.

Kanellopoulou, C., Muljo, S.A., Kung, A.L., Ganesan, S., Drapkin, R., Jenuwein, T., Livingston, D.M., and Rajewsky, K. (2005). Dicer-deficient mouse embryonic stem cells are defective in differentiation and centromeric silencing. Genes Dev *19*, 489-501.

Kanoh, J., Sadaie, M., Urano, T., and Ishikawa, F. (2005). Telomere binding protein Taz1 establishes Swi6 heterochromatin independently of RNAi at telomeres. Curr Biol *15*, 1808-1819.

Kapranov, P., Willingham, A.T., and Gingeras, T.R. (2007). Genome-wide transcription and the implications for genomic organization. Nat Rev Genet *8*, 413-423.

Kataoka, K., and Mochizuki, K. (2011). Programmed DNA elimination in Tetrahymena: a small RNA-mediated genome surveillance mechanism. Adv Exp Med Biol *722*, 156-173.

Kato, H., Goto, D.B., Martienssen, R.A., Urano, T., Furukawa, K., and Murakami, Y. (2005). RNA polymerase II is required for RNAi-dependent heterochromatin assembly. Science *309*, 467-469.

Kawamura, Y., Saito, K., Kin, T., Ono, Y., Asai, K., Sunohara, T., Okada, T.N., Siomi, M.C., and Siomi, H. (2008). Drosophila endogenous small RNAs bind to Argonaute 2 in somatic cells. Nature *453*, 793-797.

Keller, C., Adaixo, R., Stunnenberg, R., Woolcock, K.J., Hiller, S., and Buhler, M. (2012). HP1(Swi6) Mediates the Recognition and Destruction of Heterochromatic RNA Transcripts. Molecular cell *47*, 215-227.

Keller, C., Woolcock, K., Hess, D., and Buhler, M. (2010). Proteomic and functional analysis of the noncanonical poly(A) polymerase Cid14. RNA *16*, 1124-1129.

Kim, D.H., Villeneuve, L.M., Morris, K.V., and Rossi, J.J. (2006). Argonaute-1 directs siRNA-mediated transcriptional gene silencing in human cells. Nature structural & molecular biology *13*, 793-797.

Kim, M., Krogan, N.J., Vasiljeva, L., Rando, O.J., Nedea, E., Greenblatt, J.F., and Buratowski, S. (2004). The yeast Rat1 exonuclease promotes transcription termination by RNA polymerase II. Nature *432*, 517-522.

Kind, J., and van Steensel, B. Genome-nuclear lamina interactions and gene regulation. Curr Opin Cell Biol *22*, 320-325.

Klattenhoff, C., Xi, H., Li, C., Lee, S., Xu, J., Khurana, J.S., Zhang, F., Schultz, N., Koppetsch, B.S., Nowosielska, A*., et al.* (2009). The Drosophila HP1 homolog Rhino is required for transposon silencing and piRNA production by dual-strand clusters. Cell *138*, 1137-1149.

Klenov, M.S., Lavrov, S.A., Stolyarenko, A.D., Ryazansky, S.S., Aravin, A.A., Tuschl, T., and Gvozdev, V.A. (2007). Repeat-associated siRNAs cause chromatin silencing of retrotransposons in the Drosophila melanogaster germline. Nucleic acids research *35*, 5430-5438.

Kloc, A., Zaratiegui, M., Nora, E., and Martienssen, R. (2008). RNA interference guides histone modification during the S phase of chromosomal replication. Curr Biol *18*, 490-495.

Kuramochi-Miyagawa, S., Watanabe, T., Gotoh, K., Totoki, Y., Toyoda, A., Ikawa, M., Asada, N., Kojima, K., Yamaguchi, Y., Ijiri, T.W., *et al.* (2008). DNA methylation of retrotransposon genes is regulated by Piwi family members MILI and MIWI2 in murine fetal testes. Genes & development *22*, 908-917.

Kurshakova, M.M., Krasnov, A.N., Kopytova, D.V., Shidlovskii, Y.V., Nikolenko, J.V., Nabirochkina, E.N., Spehner, D., Schultz, P., Tora, L., and Georgieva, S.G. (2007). SAGA and a novel Drosophila export complex anchor efficient transcription and mRNA export to NPC. The EMBO journal *26*, 4956-4965.

LaCava, J., Houseley, J., Saveanu, C., Petfalski, E., Thompson, E., Jacquier, A., and Tollervey, D. (2005). RNA degradation by the exosome is promoted by a nuclear polyadenylation complex. Cell *121*, 713-724.

Lachner, M., O'Carroll, D., Rea, S., Mechtler, K., and Jenuwein, T. (2001). Methylation of histone H3 lysine 9 creates a binding site for HP1 proteins. Nature *410*, 116-120.

Lau, P.W., Guiley, K.Z., De, N., Potter, C.S., Carragher, B., and MacRae, I.J. (2012). The molecular architecture of human Dicer. Nature structural & molecular biology *19*, 436-440.

Lavoie, M., Ge, D., and Abou Elela, S. (2012). Regulation of conditional gene expression by coupled transcription repression and RNA degradation. Nucleic acids research *40*, 871-883.

Lee, Y., Ahn, C., Han, J., Choi, H., Kim, J., Yim, J., Lee, J., Provost, P., Radmark, O., Kim, S., *et al.* (2003). The nuclear RNase III Drosha initiates microRNA processing. Nature *425*, 415-419.

Lee, Y., Kim, M., Han, J., Yeom, K.H., Lee, S., Baek, S.H., and Kim, V.N. (2004a). MicroRNA genes are transcribed by RNA polymerase II. The EMBO journal *23*, 4051-4060.

Lee, Y.S., Nakahara, K., Pham, J.W., Kim, K., He, Z., Sontheimer, E.J., and Carthew, R.W. (2004b). Distinct roles for Drosophila Dicer-1 and Dicer-2 in the siRNA/miRNA silencing pathways. Cell *117*, 69-81.

Lee, Y.S., Pressman, S., Andress, A.P., Kim, K., White, J.L., Cassidy, J.J., Li, X., Lubell, K., Lim do, H., Cho, I.S., *et al.* (2009). Silencing by small RNAs is linked to endosomal trafficking. Nature cell biology *11*, 1150-1156.

Lengronne, A., Katou, Y., Mori, S., Yokobayashi, S., Kelly, G.P., Itoh, T., Watanabe, Y., Shirahige, K., and Uhlmann, F. (2004). Cohesin relocation from sites of chromosomal loading to places of convergent transcription. Nature *430*, 573-578.

Lewis, B.P., Shih, I.H., Jones-Rhoades, M.W., Bartel, D.P., and Burge, C.B. (2003). Prediction of mammalian microRNA targets. Cell *115*, 787-798.

Li, C.F., Henderson, I.R., Song, L., Fedoroff, N., Lagrange, T., and Jacobsen, S.E. (2008). Dynamic regulation of ARGONAUTE4 within multiple nuclear bodies in Arabidopsis thaliana. PLoS genetics *4*, e27.

Li, C.F., Pontes, O., El-Shami, M., Henderson, I.R., Bernatavichute, Y.V., Chan, S.W., Lagrange, T., Pikaard, C.S., and Jacobsen, S.E. (2006a). An ARGONAUTE4-containing nuclear processing center colocalized with Cajal bodies in Arabidopsis thaliana. Cell *126*, 93-106.

Li, L.C., Okino, S.T., Zhao, H., Pookot, D., Place, R.F., Urakami, S., Enokida, H., and Dahiya, R. (2006b). Small dsRNAs induce transcriptional activation in human cells. Proceedings of the National Academy of Sciences of the United States of America *103*, 17337-17342.

Light, W.H., Brickner, D.G., Brand, V.R., and Brickner, J.H. (2010). Interaction of a DNA zip code with the nuclear pore complex promotes H2A.Z incorporation and INO1 transcriptional memory. Molecular cell *40*, 112-125.

Liu, F., Bakht, S., and Dean, C. (2012). Cotranscriptional role for Arabidopsis DICER-LIKE 4 in transcription termination. Science *335*, 1621-1623.

Lucchetta, E.M., Carthew, R.W., and Ismagilov, R.F. (2009). The endo-siRNA pathway is essential for robust development of the Drosophila embryo. PloS one *4*, e7576.

Ma, J.B., Yuan, Y.R., Meister, G., Pei, Y., Tuschl, T., and Patel, D.J. (2005). Structural basis for 5'-end-specific recognition of guide RNA by the A. fulgidus Piwi protein. Nature *434*, 666-670.

Macrae, I.J., Zhou, K., Li, F., Repic, A., Brooks, A.N., Cande, W.Z., Adams, P.D., and Doudna, J.A. (2006). Structural basis for double-stranded RNA processing by Dicer. Science *311*, 195-198.

Malone, C.D., Anderson, A.M., Motl, J.A., Rexer, C.H., and Chalker, D.L. (2005). Germ line transcripts are processed by a Dicer-like protein that is essential for developmentally programmed genome rearrangements of Tetrahymena thermophila. Molecular and cellular biology *25*, 9151-9164.

Matzke, M., Kanno, T., Daxinger, L., Huettel, B., and Matzke, A.J. (2009). RNA-mediated chromatin-based silencing in plants. Current opinion in cell biology *21*, 367-376.

Menon, B.B., Sarma, N.J., Pasula, S., Deminoff, S.J., Willis, K.A., Barbara, K.E., Andrews, B., and Santangelo, G.M. (2005). Reverse recruitment: the Nup84 nuclear pore subcomplex mediates Rap1/Gcr1/Gcr2 transcriptional activation. Proceedings of the National Academy of Sciences of the United States of America *102*, 5749-5754.

Mochizuki, K., and Gorovsky, M.A. (2005). A Dicer-like protein in Tetrahymena has distinct functions in genome rearrangement, chromosome segregation, and meiotic prophase. Genes & development *19*, 77-89.

Morris, K.V., Chan, S.W., Jacobsen, S.E., and Looney, D.J. (2004). Small interfering RNA-induced transcriptional gene silencing in human cells. Science *305*, 1289-1292.

Morris, K.V., Santoso, S., Turner, A.M., Pastori, C., and Hawkins, P.G. (2008). Bidirectional transcription directs both transcriptional gene activation and suppression in human cells. PLoS genetics *4*, e1000258.

Moshkovich, N., and Lei, E.P. (2010). HP1 recruitment in the absence of argonaute proteins in Drosophila. PLoS genetics *6*, e1000880.

Moshkovich, N., Nisha, P., Boyle, P.J., Thompson, B.A., Dale, R.K., and Lei, E.P. (2011). RNAi-independent role for Argonaute2 in CTCF/CP190 chromatin insulator function. Genes & development *25*, 1686-1701.

Motamedi, M.R., Hong, E.J., Li, X., Gerber, S., Denison, C., Gygi, S., and Moazed, D. (2008). HP1 proteins form distinct complexes and mediate heterochromatic gene silencing by nonoverlapping mechanisms. Mol Cell *32*, 778-790.

Motamedi, M.R., Verdel, A., Colmenares, S.U., Gerber, S.A., Gygi, S.P., and Moazed, D. (2004). Two RNAi complexes, RITS and RDRC, physically interact and localize to noncoding centromeric RNAs. Cell *119*, 789-802.

Murchison, E.P., Partridge, J.F., Tam, O.H., Cheloufi, S., and Hannon, G.J. (2005). Characterization of Dicer-deficient murine embryonic stem cells. Proceedings of the National Academy of Sciences of the United States of America *102*, 12135-12140.

Nagai, S., Dubrana, K., Tsai-Pflugfelder, M., Davidson, M.B., Roberts, T.M., Brown, G.W., Varela, E., Hediger, F., Gasser, S.M., and Krogan, N.J. (2008). Functional targeting of DNA damage to a nuclear pore-associated SUMO-dependent ubiquitin ligase. Science *322*, 597-602.

Nakanishi, K., Weinberg, D.E., Bartel, D.P., and Patel, D.J. (2012). Structure of yeast Argonaute with guide RNA. Nature *486*, 368-374.

Nicolas, E., Yamada, T., Cam, H.P., Fitzgerald, P.C., Kobayashi, R., and Grewal, S.I. (2007). Distinct roles of HDAC complexes in promoter silencing, antisense suppression and DNA damage protection. Nat Struct Mol Biol *14*, 372-380.

Noma, K., Sugiyama, T., Cam, H., Verdel, A., Zofall, M., Jia, S., Moazed, D., and Grewal, S.I. (2004). RITS acts in cis to promote RNA interference-mediated transcriptional and post-transcriptional silencing. Nat Genet *36*, 1174-1180.

Nonaka, N., Kitajima, T., Yokobayashi, S., Xiao, G., Yamamoto, M., Grewal, S.I., and Watanabe, Y. (2002). Recruitment of cohesin to heterochromatic regions by Swi6/HP1 in fission yeast. Nat Cell Biol *4*, 89-93.

Noto, T., Kurth, H.M., Kataoka, K., Aronica, L., DeSouza, L.V., Siu, K.W., Pearlman, R.E., Gorovsky, M.A., and Mochizuki, K. (2010). The Tetrahymena argonaute-binding protein Giw1p directs a mature argonaute-siRNA complex to the nucleus. Cell *140*, 692-703.

Okamura, K., Ishizuka, A., Siomi, H., and Siomi, M.C. (2004). Distinct roles for Argonaute proteins in small RNA-directed RNA cleavage pathways. Genes & development *18*, 1655-1666.

Okamura, K., and Lai, E.C. (2008). Endogenous small interfering RNAs in animals. Nature reviews Molecular cell biology *9*, 673-678.

Olovnikov, I., Aravin, A.A., and Fejes Toth, K. (2012). Small RNA in the nucleus: the RNA-chromatin ping-pong. Current opinion in genetics & development *22*, 164-171.

Olsson, I., and Bjerling, P. (2011). Advancing our understanding of functional genome organisation through studies in the fission yeast. Curr Genet *57*, 1-12.

Pak, J., and Fire, A. (2007). Distinct populations of primary and secondary effectors during RNAi in C. elegans. Science *315*, 241-244.

Pal-Bhadra, M., Leibovitch, B.A., Gandhi, S.G., Rao, M., Bhadra, U., Birchler, J.A., and Elgin, S.C. (2004). Heterochromatic silencing and HP1 localization in Drosophila are dependent on the RNAi machinery. Science *303*, 669-672.

Pane, A., Jiang, P., Zhao, D.Y., Singh, M., and Schupbach, T. (2011). The Cutoff protein regulates piRNA cluster expression and piRNA production in the Drosophila germline. The EMBO journal *30*, 4601-4615.

Pardo, M., and Nurse, P. (2005). The nuclear rim protein Amo1 is required for proper microtubule cytoskeleton organisation in fission yeast. J Cell Sci *118*, 1705-1714.

Partridge, J.F., DeBeauchamp, J.L., Kosinski, A.M., Ulrich, D.L., Hadler, M.J., and Noffsinger, V.J. (2007). Functional separation of the requirements for establishment and maintenance of centromeric heterochromatin. Mol Cell *26*, 593-602.

Pontes, O., Li, C.F., Costa Nunes, P., Haag, J., Ream, T., Vitins, A., Jacobsen, S.E., and Pikaard, C.S. (2006). The Arabidopsis chromatin-modifying nuclear siRNA pathway involves a nucleolar RNA processing center. Cell *126*, 79-92.

Provost, P., Silverstein, R.A., Dishart, D., Walfridsson, J., Djupedal, I., Kniola, B., Wright, A., Samuelsson, B., Radmark, O., and Ekwall, K. (2002). Dicer is required for chromosome segregation and gene silencing in fission yeast cells. Proceedings of the National Academy of Sciences of the United States of America *99*, 16648-16653.

Rangan, P., Malone, C.D., Navarro, C., Newbold, S.P., Hayes, P.S., Sachidanandam, R., Hannon, G.J., and Lehmann, R. (2011). piRNA production requires heterochromatin formation in Drosophila. Current biology : CB *21*, 1373-1379.

Rea, S., Eisenhaber, F., O'Carroll, D., Strahl, B.D., Sun, Z.W., Schmid, M., Opravil, S., Mechtler, K., Ponting, C.P., Allis, C.D.*, et al.* (2000). Regulation of chromatin structure by site-specific histone H3 methyltransferases. Nature *406*, 593-599.

Rhoades, M.W., Reinhart, B.J., Lim, L.P., Burge, C.B., Bartel, B., and Bartel, D.P. (2002). Prediction of plant microRNA targets. Cell *110*, 513-520.

Robb, G.B., Brown, K.M., Khurana, J., and Rana, T.M. (2005). Specific and potent RNAi in the nucleus of human cells. Nature structural & molecular biology *12*, 133-137.

Robert, V.J., Sijen, T., van Wolfswinkel, J., and Plasterk, R.H. (2005). Chromatin and RNAi factors protect the C. elegans germline against repetitive sequences. Genes & development *19*, 782-787.

Roguev, A., Bandyopadhyay, S., Zofall, M., Zhang, K., Fischer, T., Collins, S.R., Qu, H., Shales, M., Park, H.O., Hayles, J.*, et al.* (2008). Conservation and rewiring of functional modules revealed by an epistasis map in fission yeast. Science *322*, 405-410.

Rondon, A.G., Mischo, H.E., Kawauchi, J., and Proudfoot, N.J. (2009). Fail-safe transcriptional termination for protein-coding genes in S. cerevisiae. Molecular cell *36*, 88-98.

Rougemaille, M., Braun, S., Coyle, S., Dumesic, P.A., Garcia, J.F., Isaac, R.S., Libri, D., Narlikar, G.J., and Madhani, H.D. (2012). Ers1 links HP1 to RNAi. Proceedings of the National Academy of Sciences of the United States of America.

Rougemaille, M., Shankar, S., Braun, S., Rowley, M., and Madhani, H.D. (2008). Ers1, a rapidly diverging protein essential for RNA interference-dependent heterochromatic silencing in Schizosaccharomyces pombe. J Biol Chem *283*, 25770-25773.

Sanso, M., Vargas-Perez, I., Quintales, L., Antequera, F., Ayte, J., and Hidalgo, E. (2011). Gcn5 facilitates Pol II progression, rather than recruitment to nucleosome-depleted stress promoters, in Schizosaccharomyces pombe. Nucleic acids research *39*, 6369-6379.

Schirle, N.T., and MacRae, I.J. (2012). The crystal structure of human Argonaute2. Science *336*, 1037-1040.

Schoenfelder, S., Sexton, T., Chakalova, L., Cope, N.F., Horton, A., Andrews, S., Kurukuti, S., Mitchell, J.A., Umlauf, D., Dimitrova, D.S.*, et al.* (2010). Preferential associations between co-regulated genes reveal a transcriptional interactome in erythroid cells. Nature genetics *42*, 53-61.

Schwartz, J.C., Younger, S.T., Nguyen, N.B., Hardy, D.B., Monia, B.P., Corey, D.R., and Janowski, B.A. (2008). Antisense transcripts are targets for activating small RNAs. Nature structural & molecular biology *15*, 842-848.

Seong, K.H., Li, D., Shimizu, H., Nakamura, R., and Ishii, S. (2011). Inheritance of stress-induced, ATF-2-dependent epigenetic change. Cell *145*, 1049-1061.

Shanker, S., Job, G., George, O.L., Creamer, K.M., Shaban, A., and Partridge, J.F. (2010). Continuous requirement for the Clr4 complex but not RNAi for centromeric heterochromatin assembly in fission yeast harboring a disrupted RITS complex. PLoS genetics *6*, e1001174.

Shav-Tal, Y., Darzacq, X., Shenoy, S.M., Fusco, D., Janicki, S.M., Spector, D.L., and Singer, R.H. (2004). Dynamics of single mRNPs in nuclei of living cells. Science *304*, 1797-1800.

Shirayama, M., Seth, M., Lee, H.C., Gu, W., Ishidate, T., Conte, D., Jr., and Mello, C.C. (2012). piRNAs Initiate an Epigenetic Memory of Nonself RNA in the C. elegans Germline. Cell *150*, 65-77.

Shiu, P.K., Zickler, D., Raju, N.B., Ruprich-Robert, G., and Metzenberg, R.L. (2006). SAD-2 is required for meiotic silencing by unpaired DNA and perinuclear localization of SAD-1 RNA-directed RNA polymerase. Proceedings of the National Academy of Sciences of the United States of America *103*, 2243-2248.

Sijen, T., Fleenor, J., Simmer, F., Thijssen, K.L., Parrish, S., Timmons, L., Plasterk, R.H., and Fire, A. (2001). On the role of RNA amplification in dsRNA-triggered gene silencing. Cell *107*, 465-476.

Sijen, T., Steiner, F.A., Thijssen, K.L., and Plasterk, R.H. (2007). Secondary siRNAs result from unprimed RNA synthesis and form a distinct class. Science *315*, 244-247.

Simmer, F., Buscaino, A., Kos-Braun, I.C., Kagansky, A., Boukaba, A., Urano, T., Kerr, A.R., and Allshire, R.C. (2010). Hairpin RNA induces secondary small interfering RNA synthesis and silencing in trans in fission yeast. EMBO Rep *11*, 112-118.

Sinkkonen, L., Hugenschmidt, T., Berninger, P., Gaidatzis, D., Mohn, F., Artus-Revel, C.G., Zavolan, M., Svoboda, P., and Filipowicz, W. (2008). MicroRNAs control de novo DNA methylation through regulation of transcriptional repressors in mouse embryonic stem cells. Nature structural & molecular biology *15*, 259-267.

Siomi, M.C., Sato, K., Pezic, D., and Aravin, A.A. (2011). PIWI-interacting small RNAs: the vanguard of genome defence. Nature reviews Molecular cell biology *12*, 246-258.

Song, J.J., Smith, S.K., Hannon, G.J., and Joshua-Tor, L. (2004). Crystal structure of Argonaute and its implications for RISC slicer activity. Science *305*, 1434-1437.

Strome, S., Powers, J., Dunn, M., Reese, K., Malone, C.J., White, J., Seydoux, G., and Saxton, W. (2001). Spindle dynamics and the role of gamma-tubulin in early Caenorhabditis elegans embryos. Molecular biology of the cell *12*, 1751-1764.

Sugiyama, T., Cam, H., Verdel, A., Moazed, D., and Grewal, S.I. (2005). RNA-dependent RNA polymerase is an essential component of a self-enforcing loop coupling heterochromatin assembly to siRNA production. Proc Natl Acad Sci U S A *102*, 152-157.

Sugiyama, T., Cam, H.P., Sugiyama, R., Noma, K., Zofall, M., Kobayashi, R., and Grewal, S.I. (2007). SHREC, an effector complex for heterochromatic transcriptional silencing. Cell *128*, 491-504.

Szittya, G., Silhavy, D., Molnar, A., Havelda, Z., Lovas, A., Lakatos, L., Banfalvi, Z., and Burgyan, J. (2003). Low temperature inhibits RNA silencing-mediated defence by the control of siRNA generation. The EMBO journal *22*, 633-640.

Taddei, A. (2007). Active genes at the nuclear pore complex. Current opinion in cell biology *19*, 305-310.

Taddei, A., Hediger, F., Neumann, F.R., Bauer, C., and Gasser, S.M. (2004). Separation of silencing from perinuclear anchoring functions in yeast Ku80, Sir4 and Esc1 proteins. EMBO J *23*, 1301-1312.

Taddei, A., Schober, H., and Gasser, S.M. (2010). The budding yeast nucleus. Cold Spring Harb Perspect Biol *2*, a000612.

Taddei, A., Van Houwe, G., Hediger, F., Kalck, V., Cubizolles, F., Schober, H., and Gasser, S.M. (2006). Nuclear pore association confers optimal expression levels for an inducible yeast gene. Nature *441*, 774-778.

Tanizawa, H., Iwasaki, O., Tanaka, A., Capizzi, J.R., Wickramasinghe, P., Lee, M., Fu, Z., and Noma, K. (2010). Mapping of long-range associations throughout the fission yeast genome reveals global genome organization linked to transcriptional regulation. Nucleic acids research *38*, 8164-8177.

Teixeira, A., Tahiri-Alaoui, A., West, S., Thomas, B., Ramadass, A., Martianov, I., Dye, M., James, W., Proudfoot, N.J., and Akoulitchev, A. (2004). Autocatalytic RNA cleavage in the human beta-globin pre-mRNA promotes transcription termination. Nature *432*, 526-530.

Ting, A.H., Schuebel, K.E., Herman, J.G., and Baylin, S.B. (2005). Short double-stranded RNA induces transcriptional gene silencing in human cancer cells in the absence of DNA methylation. Nature genetics *37*, 906-910.

Vaistij, F.E., Jones, L., and Baulcombe, D.C. (2002). Spreading of RNA targeting and DNA methylation in RNA silencing requires transcription of the target gene and a putative RNA-dependent RNA polymerase. Plant Cell *14*, 857-867.

van Bemmel, J.G., Pagie, L., Braunschweig, U., Brugman, W., Meuleman, W., Kerkhoven, R.M., and van Steensel, B. (2010). The insulator protein SU(HW) fine-tunes nuclear lamina interactions of the Drosophila genome. PloS one *5*, e15013.

van Steensel, B., and Henikoff, S. (2000). Identification of in vivo DNA targets of chromatin proteins using tethered dam methyltransferase. Nat Biotechnol *18*, 424-428.

Vanacova, S., Wolf, J., Martin, G., Blank, D., Dettwiler, S., Friedlein, A., Langen, H., Keith, G., and Keller, W. (2005). A new yeast poly(A) polymerase complex involved in RNA quality control. PLoS biology *3*, e189.

Vastenhouw, N.L., Fischer, S.E., Robert, V.J., Thijssen, K.L., Fraser, A.G., Kamath, R.S., Ahringer, J., and Plasterk, R.H. (2003). A genome-wide screen identifies 27 genes involved in transposon silencing in C. elegans. Current biology : CB *13*, 1311-1316.

Verdel, A., Jia, S., Gerber, S., Sugiyama, T., Gygi, S., Grewal, S.I., and Moazed, D. (2004). RNAi-mediated targeting of heterochromatin by the RITS complex. Science *303*, 672-676.

Volpe, T.A., Kidner, C., Hall, I.M., Teng, G., Grewal, S.I., and Martienssen, R.A. (2002). Regulation of heterochromatic silencing and histone H3 lysine-9 methylation by RNAi. Science *297*, 1833-1837.

Wang, S.W., Stevenson, A.L., Kearsey, S.E., Watt, S., and Bahler, J. (2008a). Global role for polyadenylation-assisted nuclear RNA degradation in posttranscriptional gene silencing. Mol Cell Biol *28*, 656-665.

Wang, Y., Juranek, S., Li, H., Sheng, G., Tuschl, T., and Patel, D.J. (2008b). Structure of an argonaute silencing complex with a seed-containing guide DNA and target RNA duplex. Nature *456*, 921-926.

Wang, Y., Sheng, G., Juranek, S., Tuschl, T., and Patel, D.J. (2008c). Structure of the guide-strand-containing argonaute silencing complex. Nature *456*, 209-213.

Wassenegger, M., Heimes, S., Riedel, L., and Sanger, H.L. (1994). RNA-directed de novo methylation of genomic sequences in plants. Cell *76*, 567-576.

Watanabe, T., Chuma, S., Yamamoto, Y., Kuramochi-Miyagawa, S., Totoki, Y., Toyoda, A., Hoki, Y., Fujiyama, A., Shibata, T., Sado, T., *et al.* (2011). MITOPLD is a mitochondrial protein essential for nuage formation and piRNA biogenesis in the mouse germline. Developmental cell *20*, 364-375.

Weinberg, D.E., Nakanishi, K., Patel, D.J., and Bartel, D.P. (2011). The inside-out mechanism of Dicers from budding yeasts. Cell *146*, 262-276.

Weinberg, M.S., Villeneuve, L.M., Ehsani, A., Amarzguioui, M., Aagaard, L., Chen, Z.X., Riggs, A.D., Rossi, J.J., and Morris, K.V. (2006). The antisense strand of small interfering RNAs directs histone methylation and transcriptional gene silencing in human cells. RNA *12*, 256-262.

Weinmann, L., Hock, J., Ivacevic, T., Ohrt, T., Mutze, J., Schwille, P., Kremmer, E., Benes, V., Urlaub, H., and Meister, G. (2009). Importin 8 is a gene silencing factor that targets argonaute proteins to distinct mRNAs. Cell *136*, 496-507.

Welker, N.C., Habig, J.W., and Bass, B.L. (2007). Genes misregulated in C. elegans deficient in Dicer, RDE-4, or RDE-1 are enriched for innate immunity genes. RNA *13*, 1090-1102.

Welker, N.C., Maity, T.S., Ye, X., Aruscavage, P.J., Krauchuk, A.A., Liu, Q., and Bass, B.L. (2011). Dicer's helicase domain discriminates dsRNA termini to promote an altered reaction mode. Molecular cell *41*, 589-599.

West, S., Gromak, N., and Proudfoot, N.J. (2004). Human 5' --> 3' exonuclease Xrn2 promotes transcription termination at co-transcriptional cleavage sites. Nature *432*, 522-525.

White, S.A., and Allshire, R.C. (2008). RNAi-mediated chromatin silencing in fission yeast. Curr Top Microbiol Immunol *320*, 157-183.

Wierzbicki, A.T., Haag, J.R., and Pikaard, C.S. (2008). Noncoding transcription by RNA polymerase Pol IVb/Pol V mediates transcriptional silencing of overlapping and adjacent genes. Cell *135*, 635-648.

Wilhelm, B.T., Marguerat, S., Watt, S., Schubert, F., Wood, V., Goodhead, I., Penkett, C.J., Rogers, J., and Bahler, J. (2008). Dynamic repertoire of a eukaryotic transcriptome surveyed at single-nucleotide resolution. Nature *453*, 1239-1243.

Win, T.Z., Draper, S., Read, R.L., Pearce, J., Norbury, C.J., and Wang, S.W. (2006). Requirement of fission yeast Cid14 in polyadenylation of rRNAs. Molecular and cellular biology *26*, 1710-1721.

Woolcock, K.J., Gaidatzis, D., Punga, T., and Buhler, M. (2011). Dicer associates with chromatin to repress genome activity in Schizosaccharomyces pombe. Nature structural & molecular biology *18*, 94-99.

Woolcock, K.J., Stunnenberg, R., Gaidatzis, D., Hotz, H.R., Emmerth, S., Barraud, P., and Buhler, M. (2012). RNAi keeps Atf1-bound stress response genes in check at nuclear pores. Genes & development *26*, 683-692.

Wyers, F., Rougemaille, M., Badis, G., Rousselle, J.C., Dufour, M.E., Boulay, J., Regnault, B., Devaux, F., Namane, A., Seraphin, B., *et al.* (2005). Cryptic pol II transcripts are degraded by a nuclear quality control pathway involving a new poly(A) polymerase. Cell *121*, 725-737.

Xie, Z., Johansen, L.K., Gustafson, A.M., Kasschau, K.D., Lellis, A.D., Zilberman, D., Jacobsen, S.E., and Carrington, J.C. (2004). Genetic and functional diversification of small RNA pathways in plants. PLoS biology *2*, E104.

Yamada, T., Fischle, W., Sugiyama, T., Allis, C.D., and Grewal, S.I. (2005). The nucleation and maintenance of heterochromatin by a histone deacetylase in fission yeast. Mol Cell *20*, 173-185.

Yamane, K., Mizuguchi, T., Cui, B., Zofall, M., Noma, K., and Grewal, S.I. (2011). Asf1/HIRA facilitate global histone deacetylation and associate with HP1 to promote nucleosome occupancy at heterochromatic loci. Molecular cell *41*, 56-66.

Ye, R., Wang, W., Iki, T., Liu, C., Wu, Y., Ishikawa, M., Zhou, X., and Qi, Y. (2012). Cytoplasmic Assembly and Selective Nuclear Import of Arabidopsis ARGONAUTE4/siRNA Complexes. Molecular cell *46*, 859-870.

Yekta, S., Shih, I.H., and Bartel, D.P. (2004). MicroRNA-directed cleavage of HOXB8 mRNA. Science *304*, 594-596.

Yigit, E., Batista, P.J., Bei, Y., Pang, K.M., Chen, C.C., Tolia, N.H., Joshua-Tor, L., Mitani, S., Simard, M.J., and Mello, C.C. (2006). Analysis of the C. elegans Argonaute family reveals that distinct Argonautes act sequentially during RNAi. Cell *127*, 747-757.

Yuan, Y.R., Pei, Y., Ma, J.B., Kuryavyi, V., Zhadina, M., Meister, G., Chen, H.Y., Dauter, Z., Tuschl, T., and Patel, D.J. (2005). Crystal structure of A. aeolicus argonaute, a site-specific DNA-guided endoribonuclease, provides insights into RISC-mediated mRNA cleavage. Molecular cell *19*, 405-419.

Zaratiegui, M., Castel, S.E., Irvine, D.V., Kloc, A., Ren, J., Li, F., de Castro, E., Marin, L., Chang, A.Y., Goto, D.*, et al.* (2011a). RNAi promotes heterochromatic silencing through replication-coupled release of RNA Pol II. Nature *479*, 135-138.

Zaratiegui, M., Vaughn, M.W., Irvine, D.V., Goto, D., Watt, S., Bahler, J., Arcangioli, B., and Martienssen, R.A. (2011b). CENP-B preserves genome integrity at replication forks paused by retrotransposon LTR. Nature *469*, 112-115.

Zhang, H., and Zhu, J.K. (2011). RNA-directed DNA methylation. Curr Opin Plant Biol *14*, 142-147.

Zhang, K., Mosch, K., Fischle, W., and Grewal, S.I. (2008). Roles of the Clr4 methyltransferase complex in nucleation, spreading and maintenance of heterochromatin. Nat Struct Mol Biol *15*, 381-388.

Zofall, M., Fischer, T., Zhang, K., Zhou, M., Cui, B., Veenstra, T.D., and Grewal, S.I. (2009). Histone H2A.Z cooperates with RNAi and heterochromatin factors to suppress antisense RNAs. Nature *461*, 419-422.

Zofall, M., Yamanaka, S., Reyes-Turcu, F.E., Zhang, K., Rubin, C., and Grewal, S.I. (2012). RNA elimination machinery targeting meiotic mRNAs promotes facultative heterochromatin formation. Science *335*, 96-100.

Zullo, J.M., Demarco, I.A., Pique-Regi, R., Gaffney, D.J., Epstein, C.B., Spooner, C.J., Luperchio, T.R., Bernstein, B.E., Pritchard, J.K., Reddy, K.L.*, et al.* (2012). DNA sequence-dependent compartmentalization and silencing of chromatin at the nuclear lamina. Cell *149*, 1474-1487.

Acknowledgments

First and foremost, I would like to thank Marc for being an all-round great supervisor, not only scientifically, but also professionally and personally. His continual support, encouragement and enthusiasm have helped me to make the most of my PhD and given me a springboard into the next step of my career. Second, I thank all members, past and present, of the Bühler lab for making it such a friendly, collaborative and fun place to work. In particular, I want to thank those with whom I directly collaborated: Rieka for all the microscopy work relating to Dicer and heat shock, Claudia for the Cid14 collaboration, and Kasia for the great collaboration towards the end of the project. I thank Yukiko for always having good experimental advice, and both her and Nathalie for keeping the lab so well organised. I am indebted to the FMI technology platforms, in particular the functional genomics facility for hybridisation and scanning of many microarrays, and the bioinformatics facility. For the latter, I am enormously grateful to Dimos for setting up the DamID analysis initially and teaching me how to analyse the datasets myself. In addition, Hans-Rudolf always provided bioinformatics support and created the new-and-improved *S. pombe* genome annotation. Rabih Murr proofread the thesis and gave helpful suggestions from the perspective of someone outside the *S. pombe* RNAi field. Finally, I thank the other members of my thesis committee, Dirk Schübeler and Bas van Steensel, for taking the time to fulfil this role and for their helpful suggestions, and particularly Bas for flying from Amsterdam for the meetings.

Appendix

nature structural & molecular biology

Dicer associates with chromatin to repress genome activity in *Schizosaccharomyces pombe*

Katrina J Woolcock, Dimos Gaidatzis, Tanel Punga & Marc Bühler

In the fission yeast *S. pombe*, the RNA interference (RNAi) pathway is required to generate small interfering RNAs (siRNAs) that mediate heterochromatic silencing of centromeric repeats. Here, we demonstrate that RNAi also functions to repress genomic elements other than constitutive heterochromatin. Using DNA adenine methyltransferase identification (DamID), we show that the RNAi proteins Dcr1 and Rdp1 physically associate with some euchromatic genes, noncoding RNA genes and retrotransposon long terminal repeats, and that this association is independent of the Clr4 histone methyltransferase. Physical association of RNAi with chromatin is sufficient to trigger a silencing response but not to assemble heterochromatin. The mode of silencing at the newly identified RNAi targets is consistent with a co-transcriptional gene silencing model, as proposed earlier, and functions with trace amounts of siRNAs. We anticipate that similar mechanisms could also be operational in other eukaryotes.

S. pombe contains single genes encoding the RNAi proteins Argonaute, Dicer and RNA-dependent RNA polymerase (*ago1*$^+$, *dcr1*$^+$ and *rdp1*$^+$, respectively). Deletion of any of these genes results in loss of heterochromatic gene silencing, markedly reduced levels of histone H3 Lys9 (H3K9) methylation (H3K9me) at centromeric repeat regions, and defects in chromosome segregation[1,2]. *S. pombe* expresses endogenous siRNAs, most of which correspond to heterochromatic regions and are found single stranded in an Ago1-containing complex, called the RNA-induced transcriptional silencing complex (RITS; consisting of Ago1, Chp1 and Tas3)[3,4]. Current models for RNAi-mediated heterochromatin formation in *S. pombe* propose that noncoding transcripts from repetitive elements are processed by Dcr1 into siRNAs, which guide the RITS complex to chromatin via complementary base-pairing of the Ago1-bound siRNA with the nascent RNA[4,5]. Subsequently this leads to recruitment of CLRC, a protein complex that contains the sole *S. pombe* H3K9 methyltransferase Clr4 (ref. 6). H3K9me further stabilizes binding of RITS to chromatin via its subunit Chp1 and provides binding sites for the heterochromatin proteins Swi6 and Chp2. RITS can also recruit the RNA-directed RNA polymerase complex (RDRC; consisting of Rdp1, Cid12 and Hrr1), generating more double-stranded RNA substrates for Dcr1 and amplifying the process[7,8]. Notably, it is assumed that this entire process occurs *in cis* on chromatin. This is directly supported by chromatin immunoprecipitation (ChIP) experiments that demonstrate a physical association of Ago1 and Rdp1 with chromatin[1,9]. However, attempts to cross-link Dcr1 to centromeric heterochromatin have failed[1]. Therefore, definitive proof for the *cis* model has been lacking, and the available data do not allow us to rule out the possibility that siRNA processing could occur off chromatin[10].

Although siRNAs are essential for proper heterochromatin assembly at centromeric repeats, they function poorly in *de novo* formation of heterochromatin at ectopic sites[5,11–13]. Furthermore, the accumulation of siRNAs and the methylation of H3K9 are mutually dependent processes in *S. pombe*, and the physical association of Ago1 with chromatin is lost in Clr4-deficient cells[7,9,14,15]. Notably, low levels of H3K9me persist at centromeres in RNAi-deficient cells, and genetic and biochemical analysis of the requirements for establishment and maintenance of centromeric heterochromatin have provided evidence that low levels of H3K9me play a crucial role in the initial steps of heterochromatin formation[1,16,17]. It has therefore been proposed that a siRNA-independent mechanism provides some low levels of H3K9me at centromeric repeats to allow the initial recruitment of the RNAi machinery to centromeres. This would then trigger a positive feedback loop to promote more efficient Clr4 recruitment and thus high levels of H3K9me and siRNAs[18]. How Clr4 is initially recruited to centromeres is debated. This process could be mediated by Dcr1-independent small RNAs, as recently proposed[19]. Alternatively, Clr4 might also be recruited via yet-to-be-identified *cis*-acting nucleation sites, as has been demonstrated for other heterochromatic loci in *S. pombe*[20].

In addition to its role in heterochromatin formation at centromeric repeats, the RNAi pathway has recently been implicated in the transient recruitment of the HP1 homolog Swi6 to some convergent gene pairs (CGPs)[21]. It is proposed that inefficient transcription termination at the studied CGPs leads to overlapping transcription in the G1 phase of the cell cycle, creating a double-stranded substrate for Dcr1. The resulting siRNAs would then target the RITS complex to the intergenic region, leading to H3K9 methylation and Swi6 binding. Swi6 in turn recruits cohesin, which ensures proper transcription termination for the remainder of the cell cycle. So far, this mechanism has been demonstrated only for a few gene pairs, and it remains unclear how widespread it is among CGPs across the whole *S. pombe* genome.

Here, we use DamID to probe the fission yeast genome for interactions with RNAi and heterochromatin proteins in a cell cycle–independent

Friedrich Miescher Institute for Biomedical Research, Basel, Switzerland. Correspondence should be addressed to M.B. (marc.buehler@fmi.ch).

Received 28 April; accepted 20 September; published online 12 December 2010; doi:10.1038/nsmb.1935

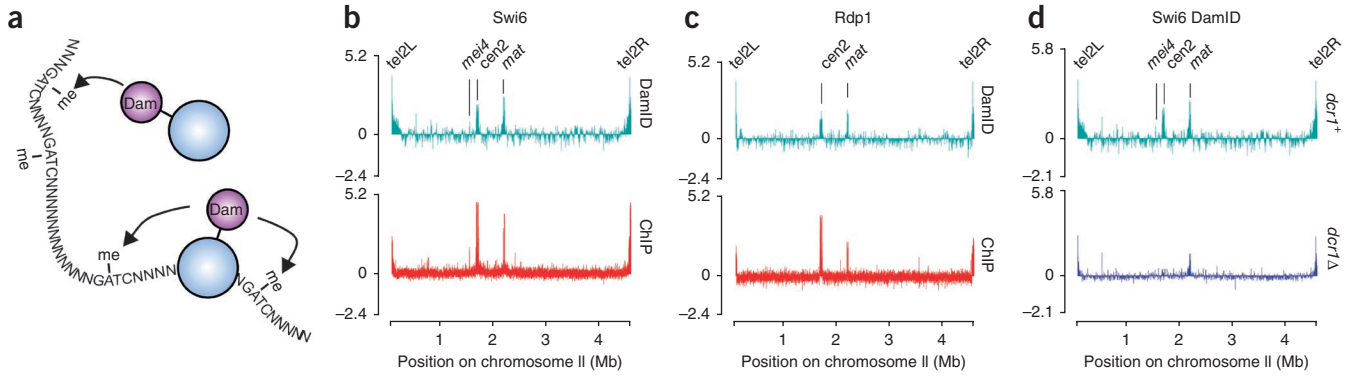

Figure 1 Identification of previously known and novel Swi6 and Rdp1 binding sites by DamID. (**a**) In DamID, a fusion protein consisting of a protein of interest and DNA adenine methyltransferase (Dam) from *Escherichia coli* is expressed at very low levels. On interaction of the fusion protein with chromatin, Dam methylates the N^6 position of adenine in the sequence context GATC. Thus, Dam leaves G^6mATC marks close to the genomic binding sites, which can be mapped by a methylation-specific PCR protocol (**Supplementary Fig. 1**). (**b**,**c**) Swi6 and Rdp1 maps for chromosome II as determined by DamID or ChIP-on-chip. (**d**) DamID map of Swi6 interactions for chromosome II in wild-type and *dcr1Δ* cells. For the DamID maps, the signal was averaged over every 500 probes. *y* axes are on $\log_2$ scale; *x* axes indicate position on chromosome II.

manner. We demonstrate that Swi6 can be recruited to a few but not all CGPs via the RNAi pathway, and we show for the first time that Dcr1 physically associates with chromatin, providing direct evidence for RNAi-mediated heterochromatin formation *in cis* at centromeric repeats. Unexpectedly, in the absence of H3K9 methylation, Dcr1, and to a certain extent Rdp1, can still associate with chromatin. On the basis of our results we propose that pre-existing H3K9 methylation is dispensable for siRNA generation, but not for proper loading of siRNAs onto Ago1, a process that ensures high levels of siRNAs and robust H3K9 methylation at centromeric repeats. In the absence of H3K9 methylation, Rdp1 and Dcr1 can still function on chromatin to trigger RNA decay but fail to accumulate high levels of siRNAs, a silencing mode that is consistent with a co-transcriptional gene silencing (CTGS) model, as proposed earlier[5,22].

RESULTS

Interactions of Swi6 and Rdp1 with the *S. pombe* genome

Previous genome-wide studies of RNAi-dependent heterochromatin formation in *S. pombe* have mainly used the ChIP technique to map interactions of proteins with chromatin[9,23], and deep sequencing technologies to identify sites of siRNA production[19,24,25]. Notably, *S. pombe* has an extended G2 phase, and as many of these studies used asynchronous cultures, they could have missed the association of proteins with chromatin or the production of small RNAs outside G2. Furthermore, attempts to immunoprecipitate certain components of the pathway with heterochromatin have failed[1,26], perhaps owing to insufficient sensitivity of the ChIP technique to detect indirect or weak interactions of proteins with chromatin. Similarly, even deep sequencing may be unable to detect small RNAs of very low abundance or stability. To address these problems, we took advantage of DamID[27], a highly sensitive chromatin profiling technique that is well suited to capture even transient protein-chromatin interactions that might occur during the cell cycle (**Fig. 1a** and **Supplementary Fig. 1**).

We first tested Swi6 and Rdp1, two proteins that are fully functional when fused to Dam (**Supplementary Fig. 2**) and for which genome-wide chromatin association profiles have been determined using ChIP in combination with microarrays (ChIP-on-chip)[9]. We hybridized samples from three independent DamID experiments to *S. pombe* tiling arrays from Affymetrix. A first analysis of the data revealed that DamID is a reliable method to detect both stable and transient Swi6 associations with the *S. pombe* genome (**Fig. 1** and data not shown). Comparing our data with the ChIP-on-chip data showed that DamID revealed all known major heterochromatic sites as well as their association with Rdp1 (**Fig. 1b**,**c**). As expected, Dcr1 was only partially required for Swi6 association with subtelomeric regions (as assessed by pseudogenes, most of which are located in subtelomeres) and the mating type locus, whereas Swi6 association with centromeric repeats was greatly affected in *dcr1Δ* cells (**Fig. 1d** and **Supplementary Fig. 3**). To investigate whether the DamID approach reveals so-far-unknown heterochromatic regions, we looked for regions that were enriched in the DamID but not in the ChIP-on-chip data and that were not located near known heterochromatic regions (**Supplementary Table 1**). This revealed a list of 28 elements for Swi6 and 11 elements for Rdp1 (**Supplementary Tables 2** and **3**). Notably, most of the newly identified Swi6-associated loci seem to be dependent on Dcr1, and many are part of a CGP and/or found near a noncoding RNA (ncRNA) gene.

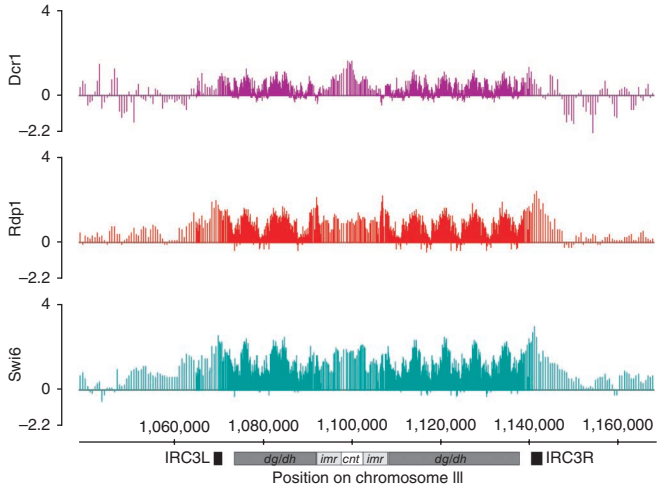

Figure 2 Dcr1 physically associates with centromeric chromatin. Dcr1, Rdp1 and Swi6 DamID maps for the centromeric region of chromosome III with flanking internal repeat elements (IRC3L/R), outermost repeats (*dg*/*dh*), innermost repeats (*imr*) and central core domain (*cnt*). The signal was averaged over every 50 probes. *y* axes are on $\log_2$ scale; *x* axes indicate position on chromosome III.

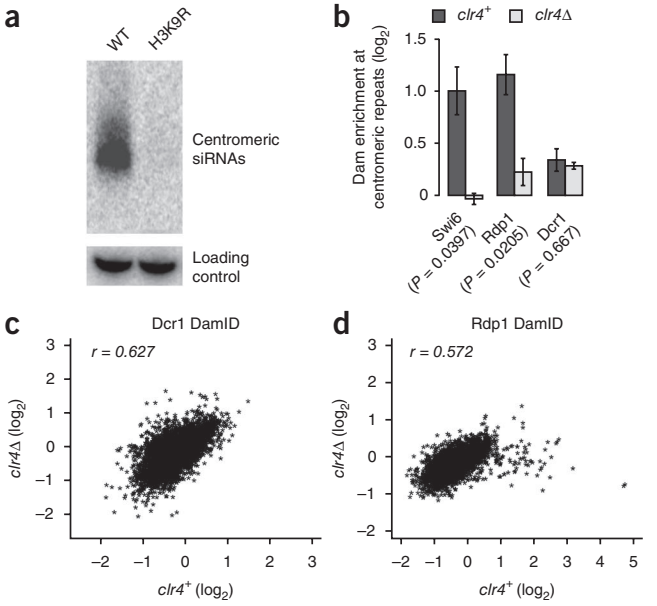

Figure 3 Clr4 dependency of Dcr1 or Rdp1 association with chromatin. (**a**) Northern blot for centromeric siRNAs in wild-type and heterochromatin-defective (H3K9R) cells. snoR69 serves as a loading control. (**b**) Swi6, Rdp1 and Dcr1 enrichment at centromeric repeat elements in wild-type and heterochromatin-defective (*clr4*Δ) cells. Error bars represent the s.e.m. ($n = 3$). *P* values were generated using the Student's *t*-test. (**c**,**d**) Comparisons of DamID signal quantified at annotated features across the genome in wild-type and heterochromatin-defective (*clr4*Δ) cells. Each axis shows the average of three independent biological replicates. (**c**) Dcr1 association is Clr4-independent across the whole genome. (**d**) Rdp1 association depends on Clr4 at some loci but not at others.

Dcr1 associates with chromatin independently of Clr4

A major advantage of using DamID is that it allows the detection of indirect protein-chromatin associations[28]. ChIP is inefficient in detecting interactions of proteins that do not bind to chromatin directly but rather bind via other proteins or chromatin-associated RNAs. For example, an association of Dcr1 with pericentromeric heterochromatin has so far not been demonstrated by ChIP[1], although current models propose that Dcr1 generates siRNAs *in cis* on centromeric chromatin[29]. We therefore set out to test whether Dam–Dcr1 would reveal any association with chromatin. Indeed, Dcr1 was revealed to be associated with centromeric repeats (**Fig. 2**), providing the first direct evidence that the entire RNAi machinery operates *in cis* to promote the assembly of centromeric heterochromatin.

An intriguing feature of the *S. pombe* RNAi pathway is that Clr4 is necessary for the accumulation of high siRNA levels. Consistent with previous studies[5,14,15,19], centromeric siRNA levels were drastically reduced when H3K9 methylation was prevented by either deleting *clr4*$^+$ or mutating H3K9 to H3R9 (**Fig. 3a** and data not shown), suggesting that Dcr1 might be recruited to centromeric repeats in a heterochromatin-dependent manner to generate siRNAs. DamID allowed us to test this model directly by comparing Dcr1 profiles in wild-type and *clr4Δ* cells. Unexpectedly, we found that Dcr1 still associated with centromeric repeats in *clr4Δ* cells (**Fig. 3b**). Notably, this pattern of Clr4 independence is seen throughout the genome for Dcr1 (**Fig. 3c**). Moreover, Rdp1 binding to centromeric repeats was significantly ($P = 0.0205$) reduced but not completely lost in *clr4Δ* cells (**Fig. 3b**,**d**). Therefore, the low centromeric siRNA levels observed in heterochromatin-deficient cells cannot be explained by the absence of the siRNA-processing machinery at centromeric repeats.

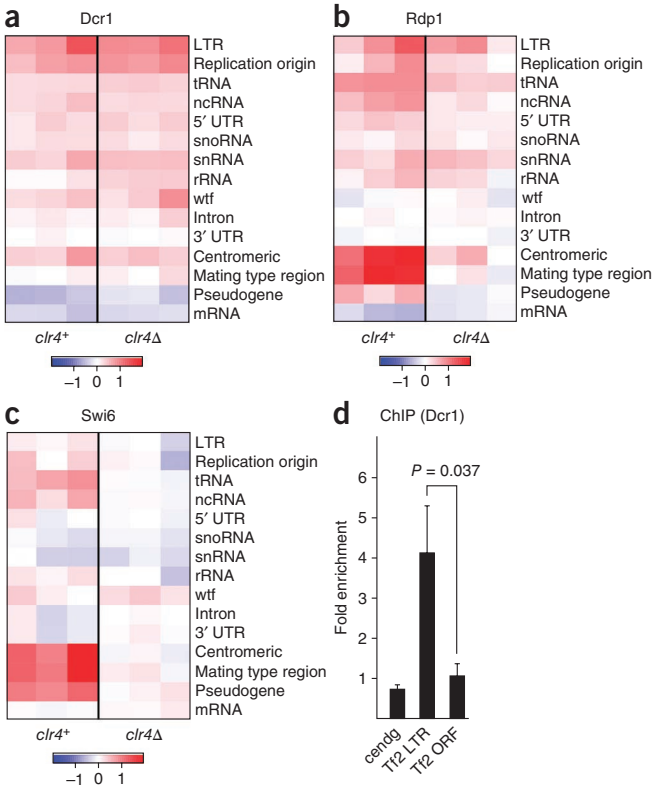

RNAi machinery contributes to long terminal repeat silencing

Having shown that Dcr1 directly associates with its known targets, we looked for other putative Dcr1-associated loci and found that it also associates with some euchromatic regions, including ncRNA genes and long terminal repeats (LTRs) (**Fig. 4a**). In total, we found 128 elements to be associated with Dcr1, 53 of them LTRs and 30 of them ncRNA genes (**Supplementary Table 4**). There are 13 full-length copies of the Tf2 LTR retrotransposon in the *S. pombe* genome, and ~250 solo LTRs or LTR fragments[30]. Using only unique probes and extending the LTR sequences by 200 bp on either side showed that ~65% of LTRs are associated with Dcr1. Unlike for centromeric repeats, we were able to confirm Dcr1 association with LTRs by ChIP (**Fig. 4**), suggesting that Dcr1 is more tightly associated with LTRs than centromeric repeat DNA.

Similar to what we saw for Dcr1, we also found Rdp1 to be associated with LTRs (**Fig. 4b**). In contrast to Dcr1, the dependency of Rdp1 binding on Clr4 differs between different genomic regions (**Figs. 3b**,**d** and **4b**). The association of Rdp1 with LTRs is independent of Clr4. Notably, those genomic features, such as LTRs, that show Clr4-independent Rdp1 binding are also those enriched in the Dcr1 DamID (**Fig. 4a**,**b**), suggesting that Rdp1 and Dcr1 may have a joint role in regulating these loci independently of heterochromatin. Indeed, transcripts originating from retrotransposon LTRs[31] were upregulated

Figure 4 Enrichment of Dam fusion proteins at different genomic features. (**a**–**c**) Dcr1, Rdp1 and Swi6 enrichments ($\log_2$) at the indicated genomic features in wild-type and heterochromatin-deficient (*clr4*Δ) cells. For all experiments, three biological replicates are shown. (**d**) ChIP experiment confirming physical association of Dcr1 with LTRs. The fold enrichment of Dcr1-TAP compared to a nontagged control, and normalized to actin and input, is shown. Error bars represent s.e.m. ($n = 3$). *P* value was generated using the Student's *t*-test; cendg, centromeric repeat element.

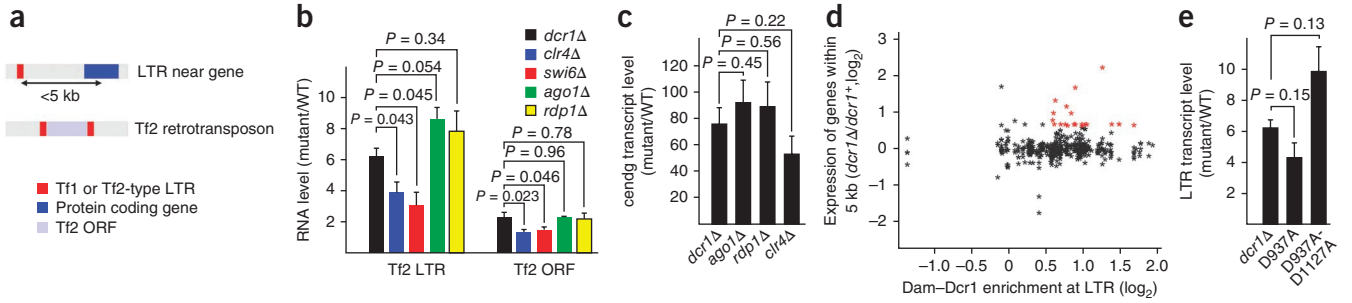

Figure 5 The *S. pombe* RNAi machinery contributes to LTR repression. (**a**) Schematic representation of LTRs and their position relative to protein coding genes (dark blue) or Tf2 retrotransposon ORFs (light blue). (**b**) Tf2 LTR and ORF transcript levels in the indicated mutant strains. (**c**) Dcr1, Ago1, Rdp1 and Clr4 are equally important for repression of centromeric repeats (cendg). (**d**) Genes within 5 kb of an LTR (measured from the middle of the gene to the middle of the LTR) were assessed for expression in Dcr1-deficient cells and for Dcr1 association with the nearby LTR. Genes whose expression was at least 1.5-fold increased in a *dcr1*Δ mutant and whose nearby LTR had at least 1.4-fold enrichment in the DamID data are highlighted in red and listed in **Supplementary Table 5**. (**e**) Tf2 LTR transcript levels in different *dcr1* mutants. D937A and D1127A are mutated sites in the RNaseIII catalytic centers of Dcr1. (**b**,**c**,**e**) RNA levels were normalized to actin and represented as fold increase compared to wild type. Error bars represent s.e.m., $n = 6$ biological replicates for *dcr1*Δ, $n = 3$ biological replicates for all other mutants. *P* values were generated using the Student's *t*-test.

in *dcr1Δ* and *rdp1Δ* cells (**Fig. 5a**,**b**). Similarly, LTR silencing was also affected in cells lacking the third fission yeast RNAi protein Ago1, implicating the *S. pombe* RNAi machinery in LTR repression (**Fig. 5b**). Notably, LTR derepression was significantly lower ($P = 0.043$ and $P = 0.045$, respectively) in *clr4*Δ or *swi6*Δ cells than in RNAi-deficient cells (**Fig. 5b**), suggesting that the conventional RNAi-mediated heterochromatin assembly pathway contributes only partly to their silencing. Consistent with this, Swi6 was not enriched at LTRs (**Fig. 4c** and data not shown). This is in contrast to the pattern for centromeric repeats, which are highly enriched for Swi6 and for which silencing is not significantly different ($P > 0.05$) between *clr4*Δ or RNAi-deficient cells (**Figs. 4c** and **5c**). Notably, silencing of Tf2 retrotransposon open reading frames (ORFs) was only slightly affected in RNAi and heterochromatin-deficient cells (**Fig. 5b**). Therefore, it seems likely that RNAi functions redundantly with other pathways to silence transposable elements in *S. pombe*[32,33].

Finally, it has previously been proposed that LTRs could regulate the expression of nearby genes in *S. pombe*, which led us to speculate that LTRs could function to create a local concentration of Dcr1, facilitating degradation of transcripts produced at nearby genes (**Fig. 5a**). However, comparing the enrichment of Dam–Dcr1 at LTRs with the expression of nearby genes in *dcr1*Δ cells did not reveal an overall positive correlation (**Fig. 5d**). Therefore, repression of nearby genes is unlikely to be a general feature of dispersed solo LTRs in *S. pombe*, although at this point we cannot rule out that some specific genes (**Supplementary Table 5**) are under direct control of LTRs and their associated RNAi proteins.

LTR silencing functions with trace amounts of siRNAs

A key feature of all RNAi-related pathways known to date is the presence of small RNAs that guide proteins of the Argonaute-Piwi family to their targets[34,35]. These mediate target RNA degradation, translational repression, or methylation of histone tails or DNA[36–38]. Therefore, the presence of siRNAs is a good criterion to define RNAi-mediated regulation. Because LTR silencing is dependent on all three *S. pombe* RNAi proteins (**Fig. 5b**), we expected to see substantial amounts of Dcr1-dependent siRNAs originating from Dcr1-associated LTRs and ncRNAs. However, we were not able to detect such siRNAs by northern blot techniques (data not shown). Even deep sequencing of total small RNAs or Ago1-bound small RNAs revealed only very few reads mapping to these sites (**Table 1**). Notably, although mutations in the RNase III domains of Dcr1, which abolish the processing of double-stranded RNAs into siRNAs, had the same effect on LTR silencing as deleting the *dcr1*$^+$ gene (**Fig. 5e**), only 29 out of 3×10^6 reads that map to the *S. pombe* genome could be uniquely assigned to LTRs (**Table 1**). These results demonstrate that siRNAs must be generated at LTRs, but that they are of extremely low abundance. Notably, these trace amounts of siRNAs seem to be sufficient to trigger a

Table 1 Small RNAs sequenced from wild-type and *dcr1Δ* cells

	Ago1-bound small RNAs				Total small RNAs			
	Wild type		*dcr1Δ*		Wild type		*dcr1Δ*	
	Reads	%	Reads	%	Reads	%	Reads	%
rRNA	1,705,697	56.72	4,883,712	91.57	52,742	55.51	226,615	69.97
tRNA	32,115	1.07	258,906	4.85	30,300	31.89	80,781	24.94
snRNA	728	0.02	5,669	0.11	418	0.44	1,798	0.56
snoRNA	650	0.02	1,994	0.04	283	0.30	909	0.28
3′ UTR	5,948	0.20	46,313	0.87	234	0.25	774	0.24
5′ UTR	2,982	0.10	1,998	0.04	129	0.14	164	0.05
mRNA	23,320	0.78	100,589	1.89	2,835	2.98	9,499	2.93
Intron	1,113	0.04	4,753	0.09	408	0.43	964	0.30
Centromeric	1,204,754	40.06	18,191	0.34	7,072	7.44	1,333	0.41
Mating type region	17,528	0.58	61	0.00	62	0.07	9	0.00
Replication origin	18	0.00	156	0.00	4	0.00	3	0.00
Pseudogene	1,247	0.04	138	0.00	23	0.02	25	0.01
LTR	29	0.00	471	0.01	11	0.01	22	0.01
wtf	19	0.00	154	0.00	152	0.16	70	0.02
ncRNA	11,296	0.38	10,078	0.19	341	0.36	915	0.28
Total	3,007,444	100	5,333,183	100	95,014	100	323,881	100

Weighted number of small RNA reads for different genomic features from deep sequencing of Ago1-bound small RNAs[19] or total small RNAs in wild-type and *dcr1Δ*. The number of reads for total small RNAs is lower, as barcoding was used to sequence several samples in one lane. snRNA, small nuclear RNA; snoRNA, small nucleolar RNA; UTR, untranslated region; wtf, with Tf2-type LTRs.

silencing response but function poorly in establishing a heterochromatic domain (**Figs. 4c** and **5b**,**e**). Similar to centromeric siRNAs in heterochromatin-deficient cells, the very low abundance of LTR siRNAs cannot be explained by the absence of the siRNA-processing machinery because both Rdp1 and Dcr1 are physically associated with LTRs (**Fig. 4a**,**b**). Therefore, we speculate that it may be Ago1 loading rather than siRNA biogenesis that depends on H3K9 methylation. We assume that unloaded siRNAs are prone to degradation, which would explain their low abundance in the absence of H3K9me.

DISCUSSION

In this study, we used DamID to probe the fission yeast genome for interactions with RNAi and heterochromatin proteins in a cell cycle–independent manner. Our findings provide new insights into the order of events during RNAi-mediated heterochromatin assembly and directly implicate RNAi proteins in repressing genomic elements other than the well-characterized centromeric repeats. Below, we discuss the implications of these findings for our understanding of nuclear RNAi.

RNAi-dependent Swi6 recruitment

The main function of the RNAi pathway in *S. pombe* was long thought to be assembly and maintenance of a heterochromatic structure at centromeric repeats. More recently, it has been demonstrated that RNAi also plays a key role in the transient recruitment of Swi6 to CGPs in the G1 phase or early S phase of the cell cycle[21]. Consistent with those results, we found Dcr1-dependent association of Swi6 with additional CGPs. However, on a genome-wide scale, Swi6 associates with only a few CGPs and shows no preference for association with CGPs when compared to other intergenic regions (data not shown), suggesting that Swi6 recruitment is unlikely to be a general or specific feature of CGPs in *S. pombe*.

Notably, our results revealed that there is a general agreement between the Dcr1-dependency of Swi6 binding to chromatin and association of such sites with Dcr1 itself. For example, Swi6 association with centromeres and ncRNAs requires Dcr1, and Dcr1 is associated with these regions. In contrast, Swi6 binding to the mating type region and telomeres is only partially dependent on Dcr1 (refs. 39,40), and Dcr1 does not associate with these regions. However, this does not apply for CGPs. Although Swi6 binding to CGPs is generally Dcr1-dependent, association of Dcr1 itself with these loci is not always observed (**Supplementary Table 2**), suggesting that RNAi does not necessarily need to act on chromatin to recruit Swi6 to CGPs. Consistent with this, RNAi proteins appeared to be largely excluded from CGPs on a genome-wide scale (**Supplementary Fig. 4**). We note that this does not rule out that the RNAi machinery may also function off chromatin to regulate the abundance of transcripts originating from CGPs on a truly post-transcriptional level[11] without recruiting Swi6, an intriguing possibility that deserves further study.

Heterochromatin-dependent accumulation of siRNAs

A remarkable observation in studies of RNAi in *S. pombe* is that the abundance of centromeric siRNAs depends on Clr4 or any of its associated proteins[7,14,15]. Unexpectedly, we found that Clr4 is dispensable for the association of Dcr1 and, partially, Rdp1 with centromeric repeats. These proteins were also found at euchromatic regions in the *S. pombe* genome, further demonstrating that H3K9 methylation is not a prerequisite for the association of the siRNA biogenesis machinery with chromatin. Based on these results, we favor a model in which efficient loading onto Ago1 rather than the biogenesis of siRNAs depends on H3K9me. We propose that Rdp1- and Dcr1-bound loci are poised for heterochromatin assembly, but that this is prevented by inefficient loading of Ago1 if H3K9 methylation is low or absent. If H3K9 methylation levels at such sites reach a certain threshold, this would then trigger a self-enforcing positive feedback mechanism in which siRNA-loaded RITS stably binds to the target locus via interactions with nascent RNA as well as methylated H3K9. This would lead to the recruitment of more Rdp1 and thereby activate siRNA amplification, eventually resulting in high levels of H3K9 methylation. This model predicts that alternative Clr4 recruitment mechanisms exist, which have yet to be identified. We note that ATF-CREB family proteins could serve this function at the mating type locus, where they have been shown to act in a parallel mechanism to the RNAi pathway to establish heterochromatin[39]. In summary, our data are consistent with a model in which some pre-existing H3K9 methylation is required for triggering an siRNA amplification loop, which is essential for efficient heterochromatin formation[8,36]. This may explain why siRNAs function poorly in *de novo* formation of heterochromatin *in trans*[5,11–13]. Notably, we provide evidence that Dcr1 and Rdp1 can function to degrade RNA in association with chromatin outside constitutive heterochromatin. This is consistent with a co-transcriptional gene silencing (CTGS) mechanism, as proposed earlier for heterochromatin silencing[5,22].

In contrast to yeast and plants, there is little evidence for a direct role of RNAi in gene silencing at the level of chromatin in other eukaryotes. Notably, this study demonstrates that even highly sensitive deep sequencing approaches may fail to identify all possible direct targets of the RNAi pathway. In addition, if CTGS were the only conserved function of RNAi in the nucleus of higher eukaryotes, attempts to find RNAi-dependent histone or DNA modifications in human cells could fail. Our results are opening up new avenues to address these issues, and we believe that approaches similar to those used in this study will disclose regions of other genomes that are under direct control of the RNAi pathway.

METHODS

Methods and any associated references are available in the online version of the paper at http://www.nature.com/nsmb/.

Accession codes. NCBI Gene Expression Omnibus: All datasets are deposited under accession number GSE24360.

Note: Supplementary information is available on the Nature Structural & Molecular Biology website.

ACKNOWLEDGMENTS

We thank H. Grosshans, A. Peters, F. Mohn and all members of the Bühler lab for critical comments on the manuscript; A.H. Brand for plasmids; B. van Steensel for advice; and H.-R. Hotz for bioinformatics support. We also thank the genomics facility of the Friedrich Miescher Institute for Biomedical Research for array hybridizations. This work was supported by the Swiss National Science Foundation and the Novartis Research Foundation.

AUTHOR CONTRIBUTIONS

K.J.W. and M.B. designed the research. K.J.W. designed and conducted experiments. D.G. wrote R scripts for data analysis. K.J.W. and D.G. analyzed the DamID data. T.P. conducted experiments. M.B. and K.J.W. analyzed the results and wrote the manuscript.

COMPETING FINANCIAL INTERESTS

The authors declare no competing financial interests.

Published online at http://www.nature.com/nsmb/.
Reprints and permissions information is available online at http://npg.nature.com/reprintsandpermissions/.

1. Volpe, T.A. *et al.* Regulation of heterochromatic silencing and histone H3 lysine-9 methylation by RNAi. *Science* **297**, 1833–1837 (2002).

2. Volpe, T. *et al.* RNA interference is required for normal centromere function in fission yeast. *Chromosome Res.* **11**, 137–146 (2003).
3. Reinhart, B.J. & Bartel, D.P. Small RNAs correspond to centromere heterochromatic repeats. *Science* **297**, 1831 (2002).
4. Verdel, A. *et al.* RNAi-mediated targeting of heterochromatin by the RITS complex. *Science* **303**, 672–676 (2004).
5. Bühler, M., Verdel, A. & Moazed, D. Tethering RITS to a nascent transcript initiates RNAi- and heterochromatin-dependent gene silencing. *Cell* **125**, 873–886 (2006).
6. Bayne, E.H. *et al.* Stc1: A critical link between RNAi and chromatin modification required for heterochromatin integrity. *Cell* **140**, 666–677 (2010).
7. Motamedi, M.R. *et al.* Two RNAi complexes, RITS and RDRC, physically interact and localize to noncoding centromeric RNAs. *Cell* **119**, 789–802 (2004).
8. Sugiyama, T., Cam, H., Verdel, A., Moazed, D. & Grewal, S.I. RNA-dependent RNA polymerase is an essential component of a self-enforcing loop coupling heterochromatin assembly to siRNA production. *Proc. Natl. Acad. Sci. USA* **102**, 152–157 (2005).
9. Cam, H.P. *et al.* Comprehensive analysis of heterochromatin- and RNAi-mediated epigenetic control of the fission yeast genome. *Nat. Genet.* **37**, 809–819 (2005).
10. Emmerth, S. *et al.* Nuclear retention of fission yeast dicer is a prerequisite for RNAi-mediated heterochromatin assembly. *Dev. Cell* **18**, 102–113 (2010).
11. Sigova, A., Rhind, N. & Zamore, P.D. A single Argonaute protein mediates both transcriptional and posttranscriptional silencing in *Schizosaccharomyces pombe*. *Genes Dev.* **18**, 2359–2367 (2004).
12. Iida, T., Nakayama, J. & Moazed, D. siRNA-mediated heterochromatin establishment requires HP1 and is associated with antisense transcription. *Mol. Cell* **31**, 178–189 (2008).
13. Simmer, F. *et al.* Hairpin RNA induces secondary small interfering RNA synthesis and silencing in trans in fission yeast. *EMBO Rep.* **11**, 112–118 (2010).
14. Noma, K. *et al.* RITS acts in cis to promote RNA interference-mediated transcriptional and post-transcriptional silencing. *Nat. Genet.* **36**, 1174–1180 (2004).
15. Hong, E.J., Villén, J., Gerace, E.L., Gygi, S.P. & Moazed, D. A cullin E3 ubiquitin ligase complex associates with Rik1 and the Clr4 histone H3–K9 methyltransferase and is required for RNAi-mediated heterochromatin formation. *RNA Biol.* **2**, 106–111 (2005).
16. Sadaie, M., Iida, T., Urano, T. & Nakayama, J. A chromodomain protein, Chp1, is required for the establishment of heterochromatin in fission yeast. *EMBO J.* **23**, 3825–3835 (2004).
17. Partridge, J.F. *et al.* Functional separation of the requirements for establishment and maintenance of centromeric heterochromatin. *Mol. Cell* **26**, 593–602 (2007).
18. Partridge, J.F. Centromeric chromatin in fission yeast. *Front. Biosci.* **13**, 3896–3905 (2008).
19. Halic, M. & Moazed, D. Dicer-independent primal RNAs trigger RNAi and heterochromatin formation. *Cell* **140**, 504–516 (2010).
20. Bühler, M. & Gasser, S.M. Silent chromatin at the middle and ends: lessons from yeasts. *EMBO J.* **28**, 2149–2161 (2009).
21. Gullerova, M. & Proudfoot, N.J. Cohesin complex promotes transcriptional termination between convergent genes in S. pombe. *Cell* **132**, 983–995 (2008).
22. Bühler, M. RNA turnover and chromatin-dependent gene silencing. *Chromosoma* **118**, 141–151 (2009).
23. Sadaie, M. *et al.* Balance between distinct HP1 proteins controls heterochromatin assembly in fission yeast. *Mol. Cell. Biol.* **23**, 6973–6988 (2008).
24. Bühler, M., Spies, N., Bartel, D.P. & Moazed, D. TRAMP-mediated RNA surveillance prevents spurious entry of RNAs into the *Schizosaccharomyces pombe* siRNA pathway. *Nat. Struct. Mol. Biol.* **15**, 1015–1023 (2008).
25. Djupedal, I. *et al.* Analysis of small RNA in fission yeast; centromeric siRNAs are potentially generated through a structured RNA. *EMBO J.* **28**, 3832–3844 (2009).
26. Buker, S.M. *et al.* Two different Argonaute complexes are required for siRNA generation and heterochromatin assembly in fission yeast. *Nat. Struct. Mol. Biol.* **14**, 200–207 (2007).
27. van Steensel, B. & Henikoff, S. Identification of *in vivo* DNA targets of chromatin proteins using tethered dam methyltransferase. *Nat. Biotechnol.* **18**, 424–428 (2000).
28. Bianchi-Frias, D. *et al.* Hairy transcriptional repression targets and cofactor recruitment in *Drosophila*. *PLoS Biol.* **2**, E178 (2004).
29. Bühler, M. & Moazed, D. Transcription and RNAi in heterochromatic gene silencing. *Nat. Struct. Mol. Biol.* **14**, 1041–1048 (2007).
30. Bowen, N.J., Jordan, I.K., Epstein, J.A., Wood, V. & Levin, H.L. Retrotransposons and their recognition of pol II promoters: a comprehensive survey of the transposable elements from the complete genome sequence of *Schizosaccharomyces pombe*. *Genome Res.* **13**, 1984–1997 (2003).
31. Mourier, T. & Willerslev, E. Large-scale transcriptome data reveals transcriptional activity of fission yeast LTR retrotransposons. *BMC Genomics* **11**, 167 (2010).
32. Cam, H.P., Noma, K., Ebina, H., Levin, H.L. & Grewal, S.I. Host genome surveillance for retrotransposons by transposon-derived proteins. *Nature* **451**, 431–436 (2008).
33. Anderson, H.E. *et al.* The fission yeast HIRA histone chaperone is required for promoter silencing and the suppression of cryptic antisense transcripts. *Mol. Cell. Biol.* **18**, 5158–5167 (2009).
34. Peters, L. & Meister, G. Argonaute proteins: mediators of RNA silencing. *Mol. Cell* **26**, 611–623 (2007).
35. Ghildiyal, M. & Zamore, P.D. Small silencing RNAs: an expanding universe. *Nat. Rev. Genet.* **10**, 94–108 (2009).
36. Moazed, D. Small RNAs in transcriptional gene silencing and genome defence. *Nature* **457**, 413–420 (2009).
37. Law, J.A. & Jacobsen, S.E. Establishing, maintaining and modifying DNA methylation patterns in plants and animals. *Nat. Rev. Genet.* **11**, 204–220 (2010).
38. Chapman, E.J. & Carrington, J.C. Specialization and evolution of endogenous small RNA pathways. *Nat. Rev. Genet.* **8**, 884–896 (2007).
39. Jia, S., Noma, K. & Grewal, S.I. RNAi-independent heterochromatin nucleation by the stress-activated ATF/CREB family proteins. *Science* **304**, 1971–1976 (2004).
40. Kanoh, J., Sadaie, M., Urano, T. & Ishikawa, F. Telomere binding protein Taz1 establishes Swi6 heterochromatin independently of RNAi at telomeres. *Curr. Biol.* **15**, 1808–1819 (2005).

ONLINE METHODS

Strains and plasmids. Fission yeast strains (grown at 30 °C in YES medium, MP Biomedicals no. 4101-532) and plasmids used in this study are described in **Supplementary Tables 6** and **7**. All strains were constructed following a standard PCR-based protocol[41] or by random spore analysis. DamMyc was cloned from pNDamMyc using XhoI and AscI into expression vectors pJR-L-3x or pJR-L-81x for high or low expression of the fusion, respectively[42]. For expression of unfused Dam, a stop codon was introduced after the Myc sequence. The protein of interest was inserted at the C terminus of DamMyc using ApaI and SmaI restriction sites. For PCR-based insertion of the fusion protein into the yeast genome, the whole sequence, including nmt1(81×) promoter and terminator, was cloned into plasmid pFA6a-kanMX6 (ref. 41) using In-Fusion PCR Cloning (Clontech) with PacI and BglII sites. This plasmid was used for PCR-based insertion of the construct into the *leu1* locus. Primer sequences used for cloning are available upon request. Constructs on plasmids and in yeast strains were confirmed by sequencing.

DamID. Strains expressing either unfused Dam or Dam fusion proteins were grown to OD_{600} = 0.4. Approximately 5.3×10^7 cells were harvested, washed once with water and flash frozen in liquid nitrogen. Cells were spheroplasted in 500 µl spheroplast buffer (1.2 M sorbitol, 100 mM $KHPO_4$, pH 7.5, 0.5 mg ml^{-1} Zymolyase (Zymo Research), 1 mg ml^{-1} lysing enzyme from *Trichoderma harzianum* (Sigma)). Genomic DNA was isolated using the DNeasy Blood and Tissue Kit (Qiagen). The DamID protocol was carried out as previously described[43], except that dUTP was included in the PCR reaction to allow fragmentation and labeling using the GeneChip Whole Transcript Double-Stranded DNA Terminal Labeling Kit (Affymetrix). The fragmented and labeled DNA was hybridized to GeneChip *S. pombe* Tiling 1.0FR Arrays (Affymetrix).

RNA isolation, cDNA synthesis and quantitative RT-PCR. Done as described previously[10]. Primer pairs used for PCR reactions can be found in **Supplementary Table 8**.

Statistical analysis. All *P* values were generated using the Student's *t*-test (two-tailed distribution, two-sample unequal variance). All error bars show the s.e.m., where *n* is at least three independent biological replicates.

Chromatin immunoprecipitation and northern blotting. Dcr1-TAP ChIP was done as described[5] except that cross-linking was done with 3% fresh formaldehyde. Sheep anti-mouse IgG Dynabeads (Invitrogen) were used. Centromeric siRNAs were isolated and detected by northern blotting as described previously[5].

Expression profiling. Previously published datasets were used for expression analysis of *dcr1Δ* cells[10].

Normalization of the tiling array data from DamID experiments. All tiling arrays were processed in R[44,45], using bioconductor[46] and the packages tilingArray[47] and preprocessCore. The arrays were RMA background corrected, quantile normalized and $\log_2$ transformed on the oligo level, using the following command: expr <- log2(normalize.quantiles(rma.background.correct(exprs(read Cel2eSet(filenames,rotated = TRUE))))). Contrasts were computed on the oligo level by subtracting respective columns of expression.

Reannotation of the Affymetrix *S. pombe* Tiling 1.0FR Array. The sequences of the 1174792 perfect-match oligos were extracted from the BPMAP file Sp20b_M_v04.bpmap (http://www.affymetrix.com/estore/browse/products.jsp?navMode=34000&productId=131500&navAction=jump&aId=productsNav#1_3) using the readBpmap function from the affxparser package. Alignment to the *S. pombe* genome (8 May 2009, http://www.sanger.ac.uk/Projects/S_pombe/) was done by using the software bowtie (version 0.9.9.1)[48], allowing for up to 100 matches per oligo.

Correcting a bias caused by variable fragment size between GATC restriction sites. While inspecting oligo level contrasts in a genome browser, we noticed enrichment breakpoints coinciding with GATC restriction sites (**Supplementary Fig. 1c**). We therefore speculated that during sample preparation, certain fragment sizes might be depleted or enriched. Plotting the fragment sizes between two GATC restriction sites against the average enrichment in the corresponding fragment confirmed this observation on a genome-wide scale (**Supplementary Fig. 1d**). We speculated that this resulted from small differences in the sample preparation process, probably during the step of size selection. In addition to fragment size–dependent mean enrichment or depletion, we noticed discontinuity of the contrast variability coinciding with GATC restriction sites. We plotted the fragment sizes between two GATC restriction sites against the s.d. of the enrichment in the corresponding fragment and observed discontinuities on a genome-wide level (**Supplementary Fig. 1d**). Both observed effects are highly unlikely to be of biological origin because they are tightly correlated to the fragment size between GATC restriction sites. Therefore, we designed software that would at least partially reverse the bias and correct the initial data. For every contrast independently, the corrector walks through all the fragments (between GATCs) and adjusts the mean and the s.d. of all the oligos that are located within the fragment. The adjustment is dependent on fragment size, and the extent of correction is determined from the lowess fit of the corresponding contrast. In more detail, for a given fragment size, the value of the lowess smoother is evaluated and compared to the average level of the given contrast. The corrector therefore does not modulate the overall mean or the variability of the contrasts. **Supplementary Figure 1c** shows the result of the corrector for one genomic locus.

***S. pombe* genome annotation.** The *S. pombe* annotation file pombe_160708.gff was downloaded from http://www.sanger.ac.uk/Projects/S_pombe/ and used to compile annotation categories for rRNA, tRNA, snRNA, snoRNA, 3′ UTR, 5′ UTR, mRNA, intron, centromeric, telomeric, mating type region, replication origin, pseudogene, LTR, wtf ('with Tf2-type LTRs') and ncRNA. Intergenic regions were generated from the mRNA annotation, not considering any regions interrupted by rRNA, tRNA, centromeric, snRNA, snoRNA and mating type region. Using the tiling arrays, we computed (differential) expression values for either individual features (for example, a transcript) or whole annotation categories by averaging enrichment values for all the oligos overlapping the respective regions. In the case of individual feature quantification, we considered only features covered by at least 50 oligos.

Reannotation of various publicly available datasets. Publicly available datasets[9,10,19] were downloaded and remapped to the *S. pombe* genome (8 May 2009) and reannotated based on the categories described above.

Deep sequencing. For Ago1-bound small RNAs, previously published data were downloaded and reannotated as above[19]. For total small RNAs, sample libraries were prepared and analyzed as previously described[10].

41. Bähler, J. *et al.* Heterologous modules for efficient and versatile PCR-based gene targeting in *Schizosaccharomyces pombe*. *Yeast* **14**, 943–951 (1998).
42. Moreno, M.B., Duran, A. & Ribas, J.C. A family of multifunctional thiamine-repressible expression vectors for fission yeast. *Yeast* **16**, 861–872 (2000).
43. Vogel, M.J., Peric-Hupkes, D. & van Steensel, B. Detection of *in vivo* protein-DNA interactions using DamID in mammalian cells. *Nat. Protoc.* **2**, 1467–1478 (2007).
44. The R Development Core Team. R: A language and environment for statistical computing. ⟨http://cran.r-project.org⟩ (2004).
45. Ihaka, R. & Gentleman, R.R. A language for data analysis and graphics. *J. Comput. Graph. Statist.* **5**, 299–314 (1996).
46. Gentleman, R.C. *et al.* Bioconductor: open software development for computational biology and bioinformatics. *Genome Biol.* **5**, R80 (2004).
47. Huber, W., Toedling, J. & Steinmetz, L.M. Transcript mapping with high-density oligonucleotide tiling arrays. *Bioinformatics* **22**, 1963–1970 (2006).
48. Langmead, B., Trapnell, C., Pop, M. & Salzberg, S.L. Ultrafast and memory-efficient alignment of short DNA sequences to the human genome. *Genome Biol.* **10**, R25 (2009).

doi:10.1038/nsmb.1935

SUPPLEMENTARY INFORMATION

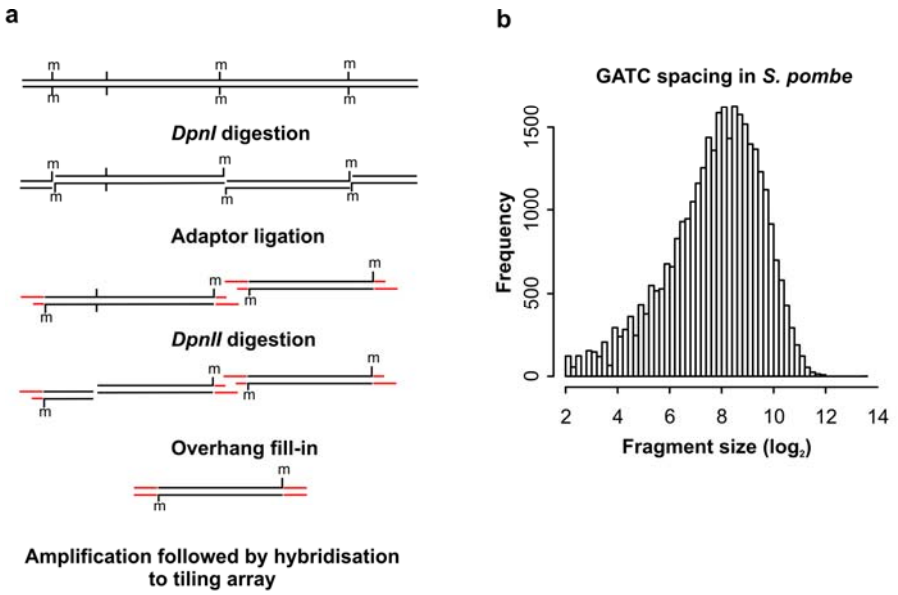

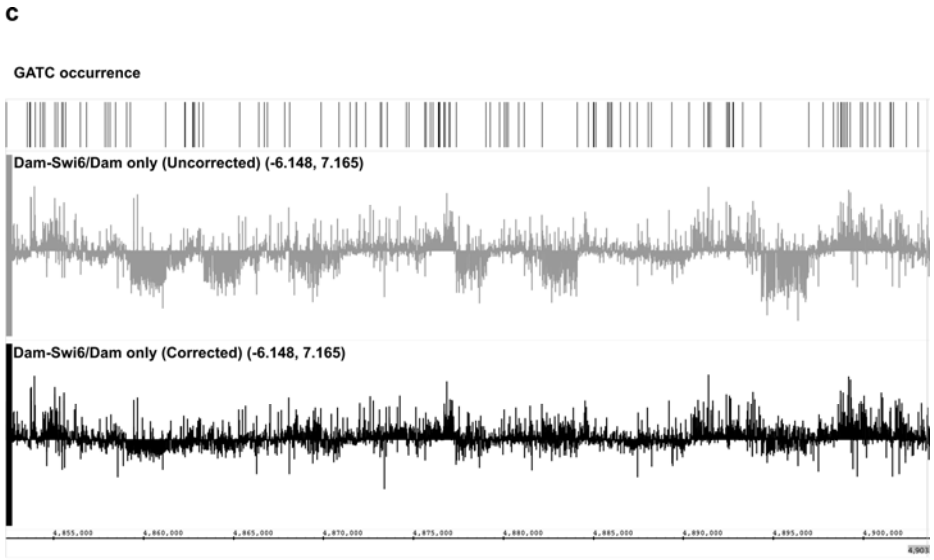

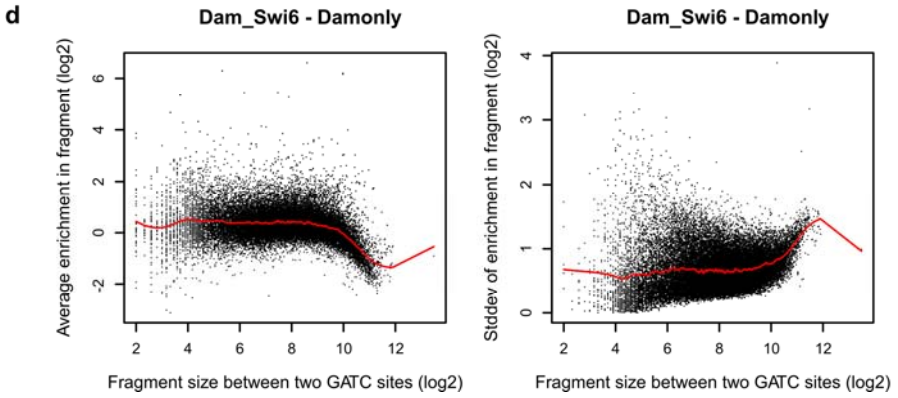

Figure S1. Establishment of DamID (DNA adenine methyltransferase identification) in *S. pombe*. DamID is based on the expression of a fusion protein consisting of a protein of interest and DNA adenine methyltransferase (Dam) from *E. coli*[1,2]. On interaction of the fusion protein with chromatin, Dam methylates the N^6-position of adenine in the sequence context GATC. Thus, Dam leaves $G^{6m}ATC$ marks close to the genomic binding sites, which can be mapped by a methylation-specific PCR protocol. Because methylation is a covalent modification, DamID is well-suited to capture even very transient protein-chromatin interactions that might occur during the cell cycle. Furthermore, the Dam will methylate DNA even if the interaction of the fusion protein with chromatin is indirect. (**a**) To detect sequences that were methylated by the fusion proteins, genomic DNA is isolated and cut between GA^{me} and TC nucleotides with the methylation-sensitive restriction enzyme *DpnI*. A double-stranded adaptor oligo with a 32 bp 5' overhang, which ensures directional ligation, is then ligated to the blunt ends. After cutting unmethylated GATCs with *DpnII*, adapter-ligated DNA fragments are amplified by PCR using adapter-specific primers with 5' TC nucleotides (to exclude non-specific ligation products). dUTP was included in the PCR reaction to allow fragmentation and labelling using the GeneChip Whole Transcript Double-Stranded DNA Terminal Labelling Kit (Affymetrix). Finally, the fragmented and labelled DNA was hybridised to GeneChip *S. pombe* Tiling 1.0FR Arrays (Affymetrix). (**b**) GATC-GATC fragment size distribution for the *S. pombe* genome. (**c,d**) Correcting a bias caused by variable GATC fragment sizes. Plotting the fragment sizes between two GATC restriction sites against the average enrichment in the corresponding fragment on a genome-wide scale reveals that certain fragment sizes might be depleted or enriched during sample preparation (**d**, left panel). In addition to fragment size-dependent mean enrichment/depletion, we noticed discontinuity of the contrast variability coinciding with GATC restriction sites (**d**, right panel). Both observed effects are highly unlikely to be of biological origin because they are tightly correlated to the fragment size between GATC restriction sites. Therefore, we designed a software that corrects the initial data (see Online Methods). The result of the corrector for one genomic locus is shown in **c**.

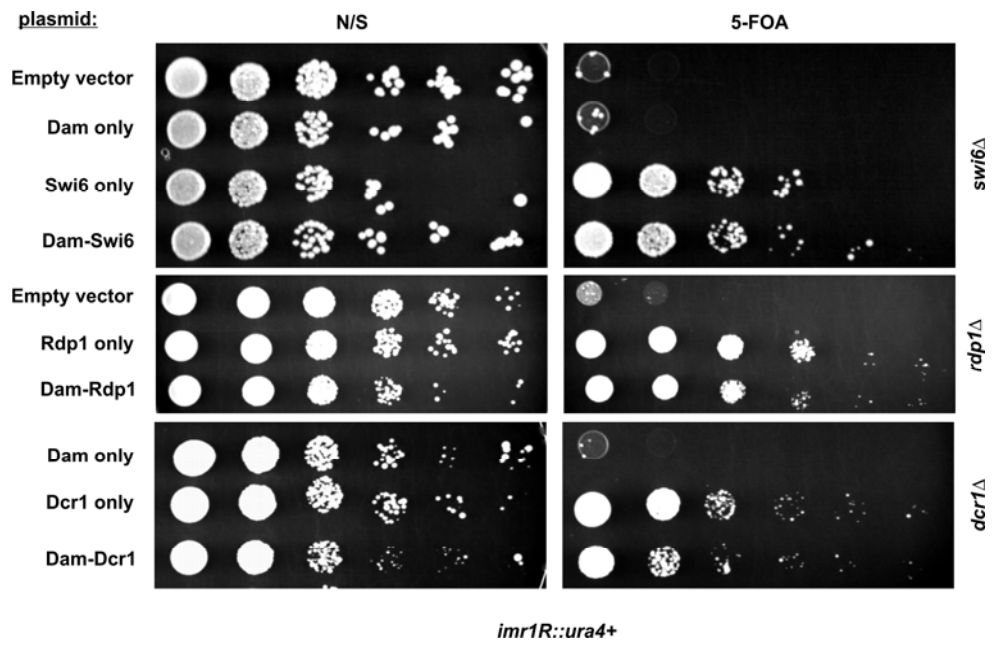

Figure S2. Functionality of Dam fusion proteins. Silencing assays confirm the ability of the Dam fusion proteins to rescue the silencing defect in the corresponding mutants. Serial 10-fold dilutions of the strains indicated on the right transformed with the plasmids indicated on the left were spotted on PMGc –leu plates (nonselective, N/S) or on PMGc –leu plates containing 2 mg ml^{-1} 5-FOA. Growth on 5-FOA indicates efficient silencing of the centromeric *imr1R::ura4*$^{+}$ reporter. Note that for the actual DamID experiments, the Dam fusion proteins were expressed at very low levels in addition to the endogenous, unfused protein.

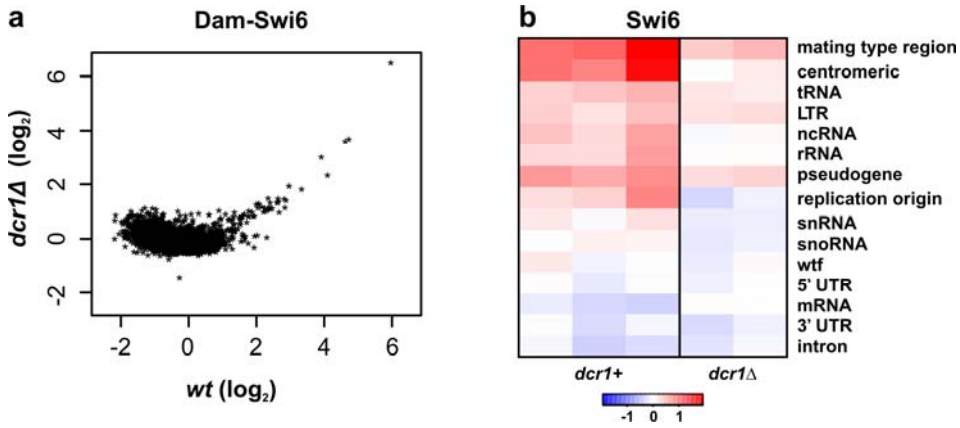

Figure S3. Swi6 association with chromatin in *dcr1⊿* cells. (**a**) To investigate the role of the RNAi pathway in Swi6 localization, we compared Dam-Swi6 profiles obtained from *dcr1*$^{+}$ and *dcr1⊿* backgrounds. As expected, this analysis revealed RNAi-dependent as well as RNAi-independent sites. (**b**) Swi6 enrichments (log_2) at the indicated genomic features in wild-type and *dcr1*Δ cells. Three and two biological replicates have been performed for WT and *dcr1⊿* strains, respectively.

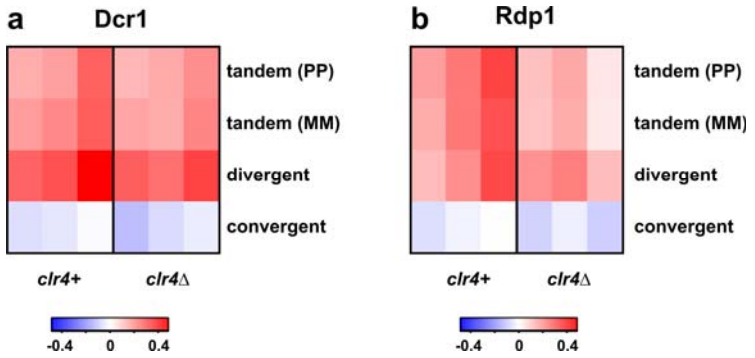

Figure S4. RNAi proteins appear to be largely excluded from CGPs on a genome-wide scale. (**a**) Dcr1 enrichments (log_2) at the four classes of intergenic regions in wild-type and *clr4*Δ cells. Three biological replicates are shown for each strain. MM and PP (minus/minus and plus/plus) indicate the orientation of tandem genes. (**b**) Rdp1 enrichments (log_2) at the four classes of intergenic regions in wild-type and *clr4*Δ cells. Three biological replicates are shown for each strain. MM and PP (minus/minus and plus/plus) indicate the orientation of tandem genes**.**

Table S1. Regions of constitutive heterochromatin

Heterochromatic region	Chromosome	Start	End
Telomeric1L	1	1	50000
Telomeric1R	1	5510000	5579133
Telomeric2L	2	1	50000
Telomeric2R	2	4480000	4539804
Telomeric3L	3	1	40000
Telomeric3R	3	2425000	2452883
Centromeric1	1	3700000	3870000
Centromeric2	2	1580000	1670000
Centromeric3	3	1040000	1200000
Mating type region	2	2100000	2150000

Major heterochromatic regions with some extension to ensure that novel sites identified from the DamID data do not result from methylation by Dam fusion protein binding to nearby heterochromatic regions.

Table S2. Novel Swi6-associated loci

Feature	Dam-Swi6 (log_2)		Swi6 ChIP (log_2)	Dam-Dcr1 (log_2)
	dcr1+	*dcr1*Δ		
SPBPB2B2.02	1.266621681	-0.022903266	0.22070635	0.5876396
SPAC13A11.03	1.247052975	0.300104609	0.25643665	0.151431188
SPNCRNA.197	1.173856755	-0.06786726	-0.2710698	0.501524993
SPNCRNA.279	1.129665062	0.04127715	-0.0864296	0.556387235
SPBC19C2.07	1.111015163	-0.222406315	0.21940964	0.38906384
SPBPB2B2.04*	1.099250773	-0.107754397	0.15387857	-0.086087212
SPAC23E2.03c	1.032393317	0.129163949	0.26652809	0.140016041
SPAC27D7.11c	1.014538632	-0.0947493	0.16694791	0.484248522
SPAC227.16c	0.970910911	-0.110333958	-0.0719933	0.631237116
SPBPB2B2.05	0.970112588	0.065271928	0.3392878	-0.414691622
SPBC19C2.04c	0.963255303	-0.191450909	0.46052083	-0.060563741
SPNCRNA.532	0.960384436	0.046281359	0.02111018	0.05171897
SP□CRNA.168	0.956261927	-0.137817348	-0.2968082	0.614459775
SPAC869.08	0.948295049	0.721026999	0.39284101	-0.356402345
SPBC14F5.04c	0.941786449	-0.161276795	0.21773268	0.734211716
SPAC869.05c	0.916961546	0.130233563	0.17242578	-0.657978447
SPNCRNA.145	0.908651294	-0.149164936	-0.4926407	0.866290854
SPAC1F8.03c	0.901326331	0.047000152	0.12299647	-0.691886634
SPCC553.10	0.891801019	-0.076048337	0.2138203	0.451001961
SPAC1834.03c	0.887827731	-0.304995936	-0.0373482	0.664834577
SPNCRNA.399	0.8654731	-0.304190403	-0.0874251	0.717631838
SPBC359.02	0.853663447	-0.249680576	-0.195947	0.514928651
SPNCRNA.296	0.847781713	-0.340362566	-0.3423216	0.940978153
SPBPB2B2.01	0.844524264	0.242268479	0.40006994	-0.181109807
unknown_620	0.831949575	-0.315108294	-0.0399484	0.943168828
unknown_3798	0.80768859	-0.466368227	-0.3692244	0.644035178
unknown_3802	0.80768859	-0.466368227	-0.3692244	0.644035178
SPBC1815.01	0.803424125	-0.030706663	0.12664465	0.279539263

Features enriched in the Dam-Swi6 data (>0.8, log_2 scale), not enriched in the Swi6 ChIP-on-chip data (<0.6, log_2 scale), and not located near major heterochromatic regions (Supplementary Table S1). There have been previous suggestions that Swi6 is involved in silencing meiotic genes[3] and perhaps genes upregulated in meiosis in this list represent further such examples. Genes highlighted in grey have been shown to be upregulated at least 4-fold in meiosis[3]. *Pseudogene. Features annotated as unknown are LTRs.

Table S3. Novel Rdp1-associated loci

Feature	Dam-Rdp1 (log_2)
SPBPB21E7.09	2.09799
SPAC17A2.11	1.668033
SPBC32F12.11	0.917882
unknown_620	0.889006
SPBC354.12	0.880252
unknown_3829	0.845338
SPBC119.02	0.836566
SPCC1672.09	0.820059
SPAC19A8.07c	0.814912
SPNCRNA.332	0.811095
unknown_531	0.806447

Features enriched in the Dam-Rdp1 data (>0.8, log_2 scale), not enriched in the Rdp1 ChIP-chip data (<0.6, log_2 scale), and not located near major heterochromatic regions (Supplementary Table S1). Features annotated as unknown are LTRs.

Table S4. Dcr1-associated loci

Feature	Dam-Dcr1 (log_2)	Feature	Dam-Dcr1 (log_2)	Feature	Dam-Dcr1 (log_2)
SPAC17A2.11	1.246964	**SPAC7D4.09c**	0.737494	**unknown_3063**	0.666806
SPNCRNA.387	1.143789	**unknown_1719**	0.735387	**SPAC1834.03c**	0.664835
SPCC24B10.20	1.090641	**unknown_2818**	0.735113	**unknown_1639**	0.662543
SPNCRNA.469	1.054236	**SPBC14F5.04c**	0.734212	**SPAC1687.17c**	0.661774
SPAC57A10.03	1.03911	**SPBC23G7.11**	0.733575	**unknown_619**	0.657924
SPNCRNA.439	1.014889	**SPCC63.12c**	0.730904	**unknown_780**	0.657456
SPNCRNA.472	1.005094	**SPNCRNA.421**	0.730431	**SPNCRNA.155**	0.656766
SPBC4F6.04	0.981193	**SPNCRNA.525**	0.728069	**SPNCRNA.237**	0.653962
SPCC1259.07	0.974006	**unknown_1431**	0.721326	**unknown_3593**	0.652254
SPBC409.21	0.964686	**unknown_1697**	0.719434	**SPBC685.05**	0.652148
unknown_620	0.943169	**unknown_2548**	0.719113	**unknown_698**	0.651785
SPNCRNA.296	0.940978	**SPNCRNA.399**	0.717632	**SPAC343.12**	0.650878
SPNCRNA.332	0.924709	**unknown_13**	0.715096	**SPNCRNA.221**	0.650563
SPNCRNA.415	0.904669	**unknown_1886**	0.711988	**unknown_1885**	0.647831
SPNCRNA.379	0.887773	**unknown_699**	0.710248	**SPAC105.02c**	0.647665
SPNCRNA.175	0.884519	**SPAPB15E9.01c**	0.709698	**SPAC521.02**	0.647019
SPNCRNA.145	0.866291	**unknown_1360**	0.707601	**unknown_2541**	0.646898
SPAC18B11.09c	0.862558	**SPNCRNA.411**	0.706481	**SPAC18B11.08c**	0.645914
SPBC1D7.01	0.860722	**SPNCRNA.431**	0.703951	**unknown_1315**	0.645199
unknown_531	0.835815	**unknown_3449**	0.702362	**unknown_3798**	0.644035
SPBC1703.11	0.832071	**unknown_3831**	0.701926	**unknown_3802**	0.644035
SPBC1685.03	0.826125	**unknown_4387**	0.699969	**SPAC343.02**	0.642145
SPBC19C2.12	0.819405	**unknown_2542**	0.699859	**unknown_3465**	0.641222
SPAC57A10.11c	0.818052	**unknown_4386**	0.699277	**unknown_1961**	0.639982
SPNCRNA.131	0.817684	**unknown_1522**	0.696831	**SPNCRNA.233**	0.635686
SPAC23D3.01	0.817057	**unknown_3451**	0.69633	**unknown_1358**	0.635191

SPNCRNA.194	0.811847	**SPBC1685.13**	0.695668	**SPAC13C5.02**	0.631373
SPAC22H12.01c	0.792662	**Tf2-7**	0.695058	**SPAC227.16c**	0.631237
unknown_1916	0.783729	**unknown_2490**	0.688903	**unknown_2103**	0.631186
SPBC19C2.13c	0.777821	**SPAC2F3.02**	0.688141	**SPAC222.03c**	0.631117
SPNCRNA.478	0.775839	**SPCC417.02**	0.685889	**unknown_4173**	0.630443
SPBC651.06	0.775208	**unknown_4174**	0.685775	**SPAC15F9.01c**	0.630107
SPNCRNA.322	0.773464	**SPNCRNA.217**	0.681086	**unknown_1223**	0.627735
SPAC19G12.06c	0.77256	**unknown_1749**	0.675744	**SPNCRNA.277**	0.625973
SPCC1494.02c	0.772505	**SPNCRNA.190**	0.674626	**SPNCRNA.385**	0.614742
unknown_4480	0.765607	**unknown_2817**	0.673732	**SPNCRNA.168**	0.61446
SPCC1753.03c	0.764799	**unknown_197**	0.673159	**SPAPB1E7.11c**	0.612076
unknown_1520	0.763412	**unknown_1274**	0.672967	**unknown_2167**	0.60741
unknown_3464	0.755937	**unknown_230**	0.672292	**SPBC1709.19c**	0.60623
SPNCRNA.442	0.746347	**SPCC1450.06c**	0.671318	**SPNCRNA.69**	0.605496
unknown_1784	0.741609	**unknown_3839**	0.670541	**unknown_1963**	0.604434
unknown_1273	0.741253	**unknown_1429**	0.669648	**SPAC5D6.09c**	0.600758
SPBC1718.05	0.740688	**SPBC342.06c**	0.667307		

List of features with Dam-Dcr1 association >0.6 (log_2, average of 3 biological replicates)

Table S5. Genes near a Dcr1-associated LTR that are upregulated in *dcr1*Δ cells

Gene		nearby LTR	description
SPAC13D1.01c	Tf2-7	Tf2-7	retrotransposable element
SPAC167.08	Tf2-2	unknown_1358	retrotransposable element
SPAC26A3.13c	Tf2-4	unknown_2817	retrotransposable element
SPAC26F1.04c	etr1	unknown_4372	enoyl-[acyl-carrier protein] reductase
SPAC27E2.08	Tf2-6	unknown_3465	retrotransposable element
SPAC2E1P3.03c	Tf2-3	unknown_2541	retrotransposable element
SPAC513.07		unknown_2541	flavonol reductase/cinnamoyl-CoA reductase family
SPAPB15E9.03c	Tf2-5	unknown_3449	retrotransposable element
SPAPJ691.02		Tf2-7	yippee-like protein
SPBC1289.14		unknown_3829	adducin
SPBC1289.17	Tf2-11	unknown_3831	retrotransposable element
SPBC16A3.02c		unknown_3704	mitochondrial peptidase (predicted)
SPBC1E8.04	Tf2-10-pseudo	unknown_1522	retrotransposable element: pseudo
SPBC215.11c		unknown_3517	aldo/keto reductase, unknown biological role
SPBC24C6.09c		unknown_1867	phosphoketolase family protein (predicted)
SPBC9B6.02c	Tf2-9	unknown_1429	retrotransposable element
SPCC1020.14	Tf2-12	unknown_698	retrotransposable element
SPCC569.09		unknown_1963	sequence orphan
SPCC737.04		unknown_1452	S. pombe specific UPF0300 family protein 6
SPCPB16A4.06c		unknown_834	sequence orphan

Genes within 5 kb of an LTR (measured from the middle of the gene to the middle of the LTR) were assessed for expression in *dcr1*Δ cells and for Dcr1 association with the nearby LTR. The list shows those genes whose expression was at least 1.5-fold increased in a *dcr1*Δ mutant and whose nearby LTR had at least 1.4-fold enrichment in the DamID data. For the calculation of Dam-Dcr1 enrichment at LTRs, only unique probes were included and the LTRs were extended by 200 bp either side in order to minimize the influence of cross-hybridisation between closely related LTRs on the analysis.

Table S6. Strains used in this study

Strain	Genotype	Source
SPB47	*h-3.1/4.1Δ::his3+ h3.3/h4.3Δ::arg3+ ade6-210 otr1R(SphI)::ade6+*	1
SPB50	*h+ 3.2-K9R h3.1/h4.1Δ::his3+ h3.3/h4.3Δ::arg3+ ade6-210 otr1R(SphI)::ade6+*	1
SPB74	*h+ otr1R(SphI)::ura4+ ura4-DS/E leu1-32 ade6-M210*	2
SPB80	*h+ leu1-32 ura4-D18 ori1 ade6-216 imr1R(Nco1)::ura4+*	2
SPB81	*h+ leu1-32 ura4-D18 ori1 ade6-216 imr1R(Nco1)::ura4+ dcr1D::TAP-kan*	2
SPB82	*h+ leu1-32 ura4-D18 ori1 ade6-216 imr1R(Nco1)::ura4+ rdp1D::TAP-kan*	2
SPB88	*h+ leu1-32 ura4-D18 ori1 ade6-216 imr1R(Nco1)::ura4+ swi6D::nat*	2
SPB94	*h+ otr1R(SphI)::ura4+ ura4-DS/E leu1-32 ade6-M210 dcr1Δ::nat*	2
SPB95	*h+ otr1R(SphI)::ura4+ ura4-DS/E leu1-32 ade6-M210 clr4Δ::kan*	2
SPB96	*h+ otr1R(SphI)::ura4+ ura4-DS/E leu1-32 ade6-M210 swi6Δ::nat*	2
SPB147	*h+ leu1-32 ura4-D18 ori1 ade6-216 imr1R(Nco1)::ura4+ dcr1+::TAP*	2
SPB330	*h+ otr1R(SphI)::ura4+ ura4-DS/E ade6-M210 leu1Δ::nmt1(81x)-dam-myc-swi6-kan*	3
SPB380	*h+ otr1R(SphI)::ura4+ ura4-DS/E ade6-M210 leu1Δ::nmt1(81x)-dam-myc-kan*	3
SPB381	*h+ otr1R(SphI)::ura4+ ura4-DS/E ade6-M210 leu1Δ::nmt1(81x)-dam-myc-dcr1-kan*	3
SPB432	*h?, otr1R::ura4+ OR imr1R::ura4+ leu1Δ::nmt1(81x)-dam-myc-kan clr4Δ::nat*	3
SPB433	*h?, otr1R::ura4+ OR imr1R::ura4+ leu1Δ::nmt1(81x)-dam-myc-dcr1-kan clr4Δ::nat*	3
SPB482	*h+ otr1R(SphI)::ura4+ ura4-DS/E ade6-M210 leu1Δ::nmt1(81x)-dam-myc-kan clr4Δ::nat*	3
SPB483	*h+ otr1R(SphI)::ura4+ ura4-DS/E ade6-M210 leu1Δ::nmt1(81x)-dam-myc-swi6-kan clr4Δ::nat*	3
SPB491	*h+ otr1R(SphI)::ura4+ ura4-DS/E ade6-M210 leu1Δ::nmt1(81x)-dam-myc-swi6-kan dcr1Δ::hph*	3
SPB492	*h+ otr1R(SphI)::ura4+ ura4-DS/E ade6-M210 leu1Δ::nmt1(81x)-dam-myc-kan*	3
SPB494	*h+ otr1R(SphI)::ura4+ ura4-DS/E ade6-M210 leu1Δ::nmt1(81x)-dam-myc-rdp1-kan*	3
SPB624	*h+ leu1-32 ura4-D18 ori1 ade6-216 imr1R(Nco1)::ura4+ KAN/TAP::dcr1-D937A*	2
SPB676	*h+ leu1-32 ura4-D18 ori1 ade6-216 imr1R(Nco1)::ura4+ dcr1-D937A, D1127A-TAP-kan*	3
SPB709	*h+ otr1R(SphI)::ura4+ ura4-DS/E ade6-M210 leu1Δ::nmt1(81x)-dam-myc-dcr1-kan clr4Δ::nat*	3
SPB711	*h+ otr1R(SphI)::ura4+ ura4-DS/E ade6-M210 leu1Δ::nmt1(81x)-dam-myc-kan clr4Δ::nat*	3
SPB712	*h+ otr1R(SphI)::ura4+ ura4-DS/E ade6-M210 leu1Δ::nmt1(81x)-dam-myc-rdp1-kan clr4Δ::nat*	3
SPB763	*h+ otr1R(SphI)::ura4+ ura4-DS/E leu1-32 ade6-M210 rdp1Δ::kan*	3
SPB764	*h+ otr1R(SphI)::ura4+ ura4-DS/E leu1-32 ade6-M210 ago1Δ::kan*	3

1 = Robin Allshire[4], 2 = Danesh Moazed, 3 = This study

Table S7. Plasmids used in this study

Name	Common name
pMB85	pJR-3xL
pMB237	pJR-3xL-DamMyc(STOP)
pMB117	pREP-nmt1-Swi6
pMB421	pJR-3xL-Rdp1
pMB262	pJR-3xL-Dcr1
pMB259	pJR-3xL-DamMyc-Swi6
pMB257	pJR-3xL-DamMyc-Dcr1
pMB419	pJR-3xL-DamMyc-Rdp1
pMB399	pFA6a - 81xL - DamMyc(STOP)-kanMX6
pMB293	pFA6a - 81xL - DamMyc-Swi6-kanMX6
pMB452	pFA6a - 81xL - DamMyc-Rdp1-kanMX6
pMB314	pFA6a - 81xL - DamMyc-Dcr1-kanMX6

Table S8. Primers used for quantitative RT-PCR

Name	Sequence
Tf2 LTR for	CCTCGTTCCTCAGTTCAGTTATGA
Tf2 LTR rev	CGGTGAGTTTTCCTTGTGATCTATT
Tf2 ORF for	TTTTCGTGGTAGTTGACCGATTT
Tf2 ORF rev	TGCTCTGCTGTAATGGATTTCG
cendg for	AAGGAATGTGCCTCGTCAAATT
cendg rev	TGCTTCACGGTATTTTTTGAAATC
act1 for	TCCTCATGCTATCATGCGTCTT
act1 rev	CCACGCTCCATGAGAATCTTC
For ChIP:	
Tf2 LTR for	TGATAGGTAACATTATAACCCAGT
Tf2 LTR rev	ACGCAGTTTGGTATCTGATT
Tf2 ORF for	GGTAGGCAGTTTATGTGCTC
Tf2 ORF rev	AGAACAGCCTCGTATGGTAA

REFERENCES

1. van Steensel, B. & Henikoff, S. Identification of in vivo DNA targets of chromatin proteins using tethered dam methyltransferase. *Nat Biotechnol* **18**, 424-8 (2000).
2. van Steensel, B., Delrow, J. & Henikoff, S. Chromatin profiling using targeted DNA adenine methyltransferase. *Nat Genet* **27**, 304-8 (2001).
3. Mata, J., Lyne, R., Burns, G. & Bahler, J. The transcriptional program of meiosis and sporulation in fission yeast. *Nat Genet* **32**, 143-7 (2002).
4. Mellone, B.G. et al. Centromere silencing and function in fission yeast is governed by the amino terminus of histone H3. *Curr Biol* **13**, 1748-57 (2003).

RNAi keeps Atf1-bound stress response genes in check at nuclear pores

Katrina J. Woolcock, Rieka Stunnenberg, Dimos Gaidatzis, et al.

Genes Dev. published online March 19, 2012
Access the most recent version at doi:10.1101/gad.186866.112

RNAi keeps Atf1-bound stress response genes in check at nuclear pores

Katrina J. Woolcock,[1,2] Rieka Stunnenberg,[1,2] Dimos Gaidatzis,[1,2,3] Hans-Rudolf Hotz,[1,2,3] Stephan Emmerth,[1,2] Pierre Barraud,[4] and Marc Bühler[1,2,5]

[1]Friedrich Miescher Institute for Biomedical Research, 4058 Basel, Switzerland; [2]University of Basel, 4003 Basel, Switzerland; [3]Swiss Institute of Bioinformatics, 4058 Basel, Switzerland; [4]Institute of Molecular Biology and Biophysics, ETH Zürich, CH-8093 Zürich, Switzerland

RNAi pathways are prevalent throughout the eukaryotic kingdom and are well known to regulate gene expression on a post-transcriptional level in the cytoplasm. Less is known about possible functions of RNAi in the nucleus. In the fission yeast *Schizosaccharomyces pombe*, RNAi is crucial to establish and maintain centromeric heterochromatin and functions to repress genome activity by a chromatin silencing mechanism referred to as cotranscriptional gene silencing (CTGS). Mechanistic details and the physiological relevance of CTGS are unknown. Here we show that RNAi components interact with chromatin at nuclear pores to keep stress response genes in check. We demonstrate that RNAi-mediated CTGS represses stress-inducible genes by degrading mRNAs under noninduced conditions. Under chronic heat stress conditions, a Dicer thermoswitch deports Dicer to the cytoplasm, thereby disrupting CTGS and enabling expression of genes implicated in the acquisition of thermotolerance. Taken together, our work highlights a role for nuclear pores and the stress response transcription factor Atf1 in coordinating the interplay between the RNAi machinery and the *S. pombe* genome and uncovers a novel mode of RNAi regulation in response to an environmental cue.

[*Keywords*: RNAi; CTGS; NPC; stress response; thermoswitch; Atf1 transcription factor]

Supplemental material is available for this article.

Received January 7, 2012; revised version accepted February 24, 2012.

The fission yeast *Schizosaccharomyces pombe* has been an invaluable model to study the assembly of centromeric heterochromatin, which depends on the processing of long noncoding repeat RNAs into double-stranded siRNAs by Dcr1 (Volpe et al. 2002; Moazed 2009). Double-stranded siRNAs are found in the ARC chaperone complex (consisting of Ago1, Arb1, and Arb2), which is involved in siRNA maturation (Buker et al. 2007). Mature, single-stranded siRNAs are found in the RNA-induced transcriptional silencing complex (RITS; consisting of Ago1, Chp1, and Tas3) (Verdel et al. 2004) and function to target RITS to nascent chromatin-bound transcripts. Subsequently, this recruits Clr4, the enzyme that methylates histone H3 at Lys 9 (H3K9). H3K9 methylation, a hallmark of heterochromatin, is crucial to stabilize the association of RITS with chromatin via Chp1, triggering a self-enforcing positive feedback mechanism in which RITS recruits the Rdp1-containing RNA-directed RNA polymerase complex (RDRC) (Motamedi et al. 2004). This activates siRNA amplification, which eventually leads to high levels of H3K9 methylation and functional heterochromatin at centromeric repeats. Although this pathway has been investigated in great detail, the mechanisms by which the RNAi machinery is initially targeted to centromeric repeats have remained elusive (Halic and Moazed 2010; Shanker et al. 2010).

Whereas the involvement of RNAi in the assembly of centromeric heterochromatin is well established, additional roles remain ill-defined. Recently, we obtained evidence that the RNAi pathway might also function to repress genomic elements other than the well-studied regions of constitutive heterochromatin. We proposed a cotranscriptional gene silencing (CTGS) model, in which RNAi functions in direct association with euchromatin to trigger RNA decay (Woolcock et al. 2011). The physiological relevance of this mode of genome regulation and, similar to centromeric heterochromatin, how specific targeting of RNAi components to particular regions in the genome is achieved are not known.

Results

Nuclear RNA turnover proteins physically associate with the S. pombe *genome*

An inherent difficulty in studying the cross-talk between the RNAi machinery and chromatin has been that some

[5]**Corresponding author.**
E-mail marc.buehler@fmi.ch.
Article published online ahead of print. Article and publication date are online at http://www.genesdev.org/cgi/doi/10.1101/gad.186866.112.

RNAi components hardly cross-link to chromatin. A solution to this problem is DNA adenine methyltransferase identification (DamID), a highly sensitive method that allowed us to map Dcr1 interactions with the genome (Woolcock et al. 2011). To profile other RNA turnover proteins implicated in chromatin silencing, we produced and compared genome-wide binding maps for Dcr1, Rdp1, Ago1, Arb1, Cid14, Rrp6, and the heterochromatin protein $HP1^{Swi6}$ by DamID in combination with tiling arrays (Fig. 1A). Of the RNAi proteins, Ago1 and Rdp1 show a high enrichment at major heterochromatic regions, as observed for $HP1^{Swi6}$. Dcr1 is also enriched at centromeric heterochromatin but not at other heterochromatic loci. Surprisingly, Arb1 is not enriched at any region. Thus, whereas Dcr1, RITS, and RDRC operate in close proximity to heterochromatin, ARC is the only RNAi complex that seems to function further away (Fig. 1A).

The Cid14 nucleotidyltransferase and the RNA exosome have been recently suggested to be involved in siRNA 3′ end processing by untemplated nucleotide addition and trimming, respectively (Halic and Moazed 2010). Consistent with an involvement in siRNA maturation, Cid14 shows an enrichment similar to that observed for Dcr1 at centromeric heterochromatin (Fig. 1A). This indicates that siRNA maturation by the exosome and Cid14 is initiated in association with chromatin. Interestingly, the nucleus-specific 3′-to-5′ exoribonuclease Rrp6 is depleted at centromeres. Therefore, trimming of siRNAs is most likely mediated by another exonuclease, which is consistent with the observation that centromeric siRNA levels are drastically reduced in *cid14*Δ but not *rrp6*Δ cells (Buhler et al. 2007). In contrast to centromeric heterochromatin, Rrp6 is slightly enriched at the mating type locus and telomeres, which is in line with its role in RNAi-independent repression at these regions (Buhler et al. 2007).

Although not generally enriched in euchromatin, RNAi factors and Cid14 do associate with particular euchromatic loci. Except for Arb1, all RNAi proteins are enriched to similar levels at long terminal repeats (LTRs), consistent with an increase in RNA from LTRs in RNAi mutants (Fig. 1B; Woolcock et al. 2011). Similar profiles can be observed at regions coding for long intergenic noncoding RNAs (lincRNAs), snoRNAs, and snRNAs, as well as at replication origins. wtf and tf2 retrotransposons are exceptional, as they are specifically enriched by Dcr1 and Cid14 only (Fig. 1B).

Taken together, these DamID experiments provide a comprehensive data set for interactions of the *S. pombe* genome with nuclear RNA turnover proteins implicated in chromatin silencing. Importantly, we found that the core RNAi machinery associates with many noncoding regions of the genome and certain protein-coding genes.

Interactions between chromatin and the RNAi pathway occur at nuclear pores independently of Argonaute

A unifying feature of RNAi pathways is that Argonaute-containing complexes are guided to their respective targets by small RNAs. Coherent with this paradigm, a transcriptome surveillance mechanism in which Ago1 associates with random, Dcr1-independent RNA degradation products in *S. pombe* has been recently proposed (Halic and Moazed 2010). These small RNAs are referred to as primal RNAs (priRNAs) and may function to target Ago1 to chromatin independently of Dcr1 or the H3K9 methylation status. Subsequently, RDRC and Dcr1 would be recruited and the siRNA amplification loop started. Indeed, the high enrichment observed for Rdp1 at centromeres is strongly affected in ago*1*Δ, *dcr1*Δ, and *clr4*Δ cells (Fig. 2A), implicating H3K9 methylation and a functional RNAi pathway in the establishment of the positive feedback loop. However, although reduced, the association of Rdp1 with chromatin is not completely lost in ago*1*Δ, *dcr1*Δ, or *clr4*Δ cells (Fig. 2A). Similarly, the enrichment of Dcr1 with centromeres remains unaffected in ago*1*Δ, *rdp1*Δ, or *clr4*Δ cells (Fig. 2B). These results demonstrate that neither priRNAs nor H3K9 methylation is required for targeting Dcr1 and Rdp1 to centromeric chromatin initially. However, Clr4 stabilizes RITS and RDRC association with heterochromatin, and priRNAs might be required to prime the amplification of centromeric siRNAs.

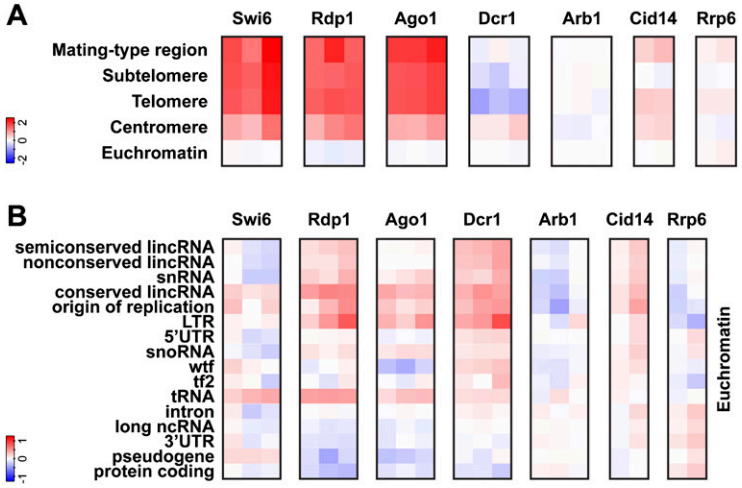

Figure 1. DamID for RNAi and nuclear surveillance components reveals association with genomic regions in both heterochromatin and euchromatin. (*A*) Enrichments ($\log_2$) at heterochromatic regions compared with euchromatin. (*B*) Enrichments ($\log_2$) at the indicated genomic features present in euchromatin. Individual columns represent biological replicates. (Tf2) Tf2 LTR retrotransposons; (wtf) with Tf2-type LTRs.

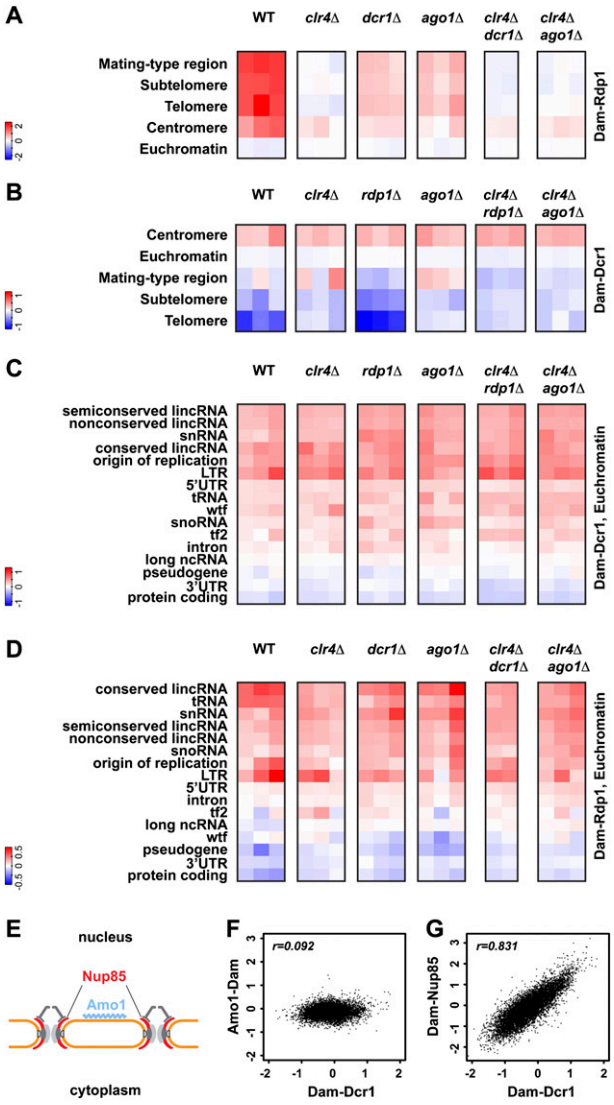

Figure 2. Interactions between chromatin and the RNAi pathway occur at NPCs, independently of small RNAs. (*A–D*) Rdp1 and Dcr1 enrichments ($\log_2$) in the mutant backgrounds indicated. Individual columns represent biological replicates. (*E*) Representation of Nup85 and Amo1 locations at the nuclear periphery. (*F,G*) Comparison of Dcr1 enrichments ($\log_2$) at individual features with Amo1 and Nup85 enrichments, respectively.

A requirement for priRNAs in actively targeting the RNAi machinery to euchromatic sites can also be ruled out because neither Dcr1 nor Rdp1 association with euchromatic loci was affected in *ago1*Δ cells (Fig. 2C,D). This raises the question of how RNAi components and specific regions of the genome are brought in close proximity, if not by small RNAs. Intriguingly, Dcr1 accumulates at the nuclear periphery in association with pores (Emmerth et al. 2010). Similarly, heterochromatin localizes at the nuclear periphery, prompting us to speculate that the interaction between RNAi components and the *S. pombe* genome might be orchestrated at the nuclear envelope. To test this hypothesis, we performed DamID for two nuclear peripheral proteins (Fig. 2E): Nup85, a scaffold nucleoporin and part of the Nup107–120 complex (Bai et al. 2004), and Amo1, which localizes to the nuclear rim in a punctate pattern that does not overlap with nuclear pore complex (NPC) components (Pardo and Nurse 2005). In contrast to Amo1, which does not strongly associate with specific regions of the genome, Nup85 is enriched at several genomic loci (Fig. 2F,G; Supplemental Fig. S1). Intriguingly, comparing the sites associated with Dcr1 or Nup85 revealed a strong correlation across the whole genome, demonstrating that NPCs preferentially associate with genomic loci that are also targets of Dcr1 (Fig. 2G). Furthermore, Ago1 seems to be largely dispensable for the association of Nup85 with the genome (Supplemental Fig. S1). These results strongly suggest that the interactions between chromatin and the RNAi pathway are coordinated by one or several components of the NPC and not by small RNAs. Because nuclear pore association of Dcr1 does not depend on a functional RNAi pathway or heterochromatin (Emmerth et al. 2010), Dcr1 is likely to interact with NPCs directly.

Dcr1 binds promoter regions and Atf1-bound genes at nuclear pores

Although genes as a class are not generally enriched in the DamID data (Fig. 1B), we noticed that certain genes are strongly enriched for RNAi components. We observed that Nup85, Dcr1, and Rdp1 are depleted from the intergenic region between convergent genes (Fig. 3A). In contrast, Dcr1 and Nup85 are enriched most highly at divergent intergenic regions and intermediately at tandem ones, suggesting that Dcr1 and Nup85 preferentially associate with promoter regions. This is confirmed by the profiles of the average DamID enrichment of Dcr1 and Nup85 1 kb on either side of the translation start site (Fig. 3B). Rdp1 shows a less-pronounced decrease in enrichment from the 5′ end to the 3′ end.

Intriguingly, we noticed that many of the genes with the highest enrichment for RNAi proteins are involved in responses to stressful conditions. RNAi components show a weak preference for induced core environmental stress response (CESR) genes (Chen et al. 2003) and a strong preference for genes that we refer to as bound by Atf1 under normal conditions (BANC; as judged by chromatin immunoprecipitation [ChIP]–chip data) (Fig. 3C–F; Eshaghi et al. 2010). Atf1 is a basic leucine zipper (bZIP) transcriptional activator and is constitutively bound to its targets (Kon et al. 1997). Upon stress, it becomes phosphorylated and causes an increase in transcription of most of its target genes (Lawrence et al. 2007). Importantly, $HP1^{Swi6}$ has no preference for BANCs, demonstrating that they are euchromatic (Supplemental Fig. S2). Finally, Nup85 shows a strong preference for BANCs, independently of Ago1, whereas Amo1 is depleted (Fig. 3G,H; Supplemental Fig. S2E). These results demonstrate that the RNAi machinery associates with protein-coding genes that are implicated in responses to stressful conditions. These genes are bound by the Atf1 transcription factor and colocalize with the RNAi machinery at NPCs, independently of small RNAs/Argonaute.

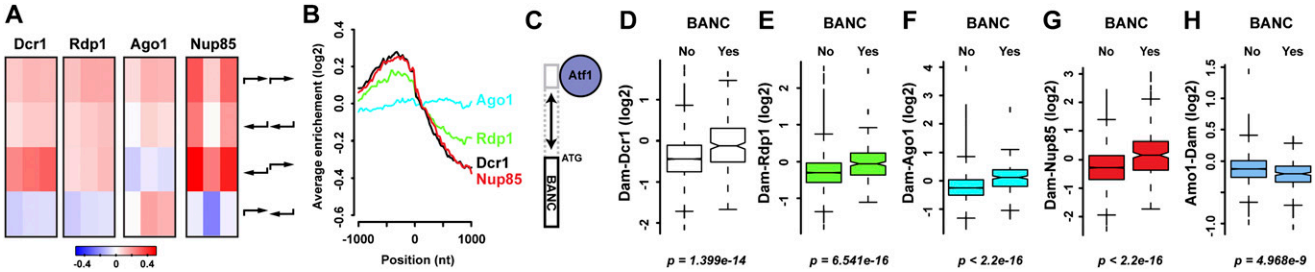

Figure 3. Promoter regions and genes associated with Atf1 colocalize with the RNAi machinery at NPCs. (*A*) Dcr1, Rdp1, Ago1, and Nup85 enrichments ($\log_2$) at tandem, divergent, and convergent intergenic regions. Individual columns represent biological replicates. (*B*) Average enrichments 1 kb on either side of the beginning of ORFs. One representative replicate is shown for each experiment. (*C*) BANCs are defined as having an Atf1 ChIP–chip peak under nonstressful conditions in their probable promoter regions (Eshaghi et al. 2010). (*D–H*) DamID enrichment ($\log_2$) at BANCs ("Yes"; 261 genes) compared with all other genes ("No"; 4715 genes).

RNAi contributes to repression of stress response genes

The physical association of the core RNAi machinery with stress response genes strongly suggests that RNAi is involved in cellular responses to environmental stress conditions. To test this hypothesis, we did expression profiling in strains lacking *dcr1*$^+$, *ago1*$^+$, or *rdp1*$^+$. Indeed, BANC genes are significantly up-regulated in all mutants (Fig. 4A–C). Importantly, they are not up-regulated in a *swi6Δ* mutant, confirming that the activation of BANC genes upon deletion of RNAi factors is not an indirect effect of losing heterochromatin, which can be considered a stressful condition (Fig. 4D). Ago1-bound small RNAs that are significantly enriched for BANCs compared with other genes further support the conclusion that the RNAi machinery is directly involved in repressing these loci (Fig. 4E). However, these small RNAs do not seem to be required for the organization of BANCs, Dcr1, and Rdp1 at NPCs, which is independent of Ago1, and their functional relevance is unclear. In summary, the RNAi machinery associates with BANC genes independently of small RNAs/Argonaute, although all three core components of the RNAi machinery are required for BANC repression.

To study the effect of stressful insults on expression of Atf1-bound genes in the absence or presence of RNAi, we chose heat shock as a paradigm and monitored expression of candidate heat-shock genes over time. Consistent with impaired repression of BANC genes in the absence of RNAi, heat-shock RNA levels in *dcr1Δ* cells, compared with wild type, are higher under noninduced conditions (Fig. 4F; data not shown). Interestingly, RNA polymerase 2 (RNAP2) occupancy changes at some but not all heat-shock genes in *dcr1Δ* cells (Fig. 4G; Supplemental Fig. S3). Thus, cotranscriptional degradation of RNA might feed back on RNAP2 at some genes. When grown at elevated temperatures, we observed that RNA levels of certain heat-shock genes decrease at a slower rate after their initial induction in *dcr1Δ* compared with wild-type cells (Fig. 4H,I; data not shown).

These results demonstrate that RNAi, when associated with BANCs, contributes to their repression under normal conditions. This regulation can occur on a truly cotranscriptional RNA decay level, although a regulatory effect on transcription at some genes cannot be ruled out at this point. We propose a model in which Atf1-bound stress response genes are recruited to NPCs and poised for rapid mRNA export, but kept in check by RNAi-mediated CTGS under normal conditions. Upon stress, strongly increased transcription rates simply overcome CTGS, with most transcripts escaping cotranscriptional degradation and accumulating to high levels. After a transient burst of transcription, CTGS contributes to the subsequent decrease in RNA levels.

This model predicts that the association of NPCs with Dcr1 and BANC genes is not disturbed under stressful conditions. Indeed, live-cell imaging of cells in which individual heat-shock genes have been tagged with the LacO/LacI-GFP system did not reveal significant delocalization of heat-shock genes (Fig. 5A,B). Similarly, the association of Dcr1 with NPCs was not affected under oxidative stress conditions or short exposure to elevated temperatures (Supplemental Fig. S4). By DamID, associations of Nup85 with the genome remained unchanged at elevated temperatures, as did Dcr1–genome associations under osmotic or oxidative stress conditions (Fig. 5C,D; Supplemental Fig. S5).

Dcr1 translocates to the cytoplasm under chronic heat stress conditions

In contrast to temporary heat-shock conditions, we observed a striking translocation of Dcr1 to the cytoplasm when cells were exposed to chronic heat stress (Fig. 6A). Consistent with this observation, DamID in the Dam–Dcr1 strain, but not the Dam-only strain, resulted in much lower DNA concentrations at the end of the protocol when performed at elevated temperatures (Fig. 6B), indicating that Dam–Dcr1 has left the nucleus and cannot further methylate DNA. Remarkably, Dcr1 protein levels are comparable at low and high temperatures (Supplemental Fig. S6), and perinuclear Dcr1 localization is restored within 1–2 h when cells are shifted back to 30°C after prolonged heat stress, hinting at a possible thermosensitive switch that regulates the nucleo–cytoplasmic distribution of Dcr1 (Fig. 6A).

We previously demonstrated a nucleo–cytoplasmic shuttling function for the dsRNA-binding domain (dsRBD)

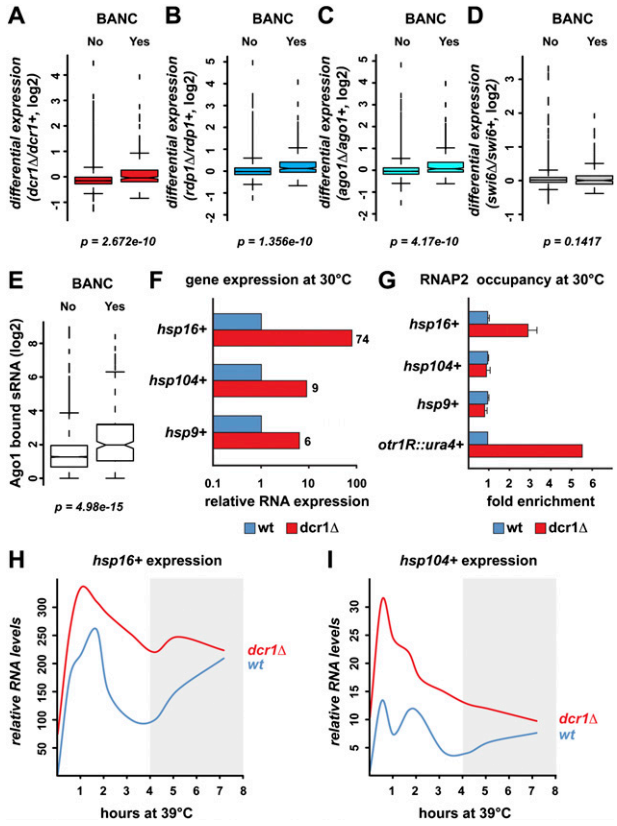

Figure 4. RNAi contributes to cotranscriptional degradation of BANCs. (*A–D*) Expression analysis by tiling arrays showing differential expression of BANCs ("Yes"; 261 genes) compared with all other genes ("No"; 4715 genes) in *dcr1Δ*, *rdp1Δ*, *ago1Δ*, and *swi6Δ*. (*E*) Small RNA deep-sequencing data (Halic and Moazed 2010) was reannotated to show the number of Ago1-bound sRNAs at BANCs compared with all other genes. (*F*) RNA levels of candidate heat-shock genes in *dcr1Δ* relative to wild-type cells at 30°C were determined by quantitative RT–PCR. Actin mRNA was used for normalization. (*G*) RNAP2 enrichment at candidate heat-shock genes in *dcr1Δ* relative to wild-type cells at 30°C. U6 snRNA was used for normalization. o*tr1R::ura4*$^+$ is located within centromeric heterochromatin and serves as a positive control. (*H,I*) RNA levels of candidate heat-shock genes were measured by quantitative RT–PCR in wild-type and *dcr1Δ* cells 0 min, 30 min, 1 h, 1 h 40 min, 2 h 10 min, 3 h 10 min, 4 h 10 min, 5 h 10 min, and 7 h 10 min after shifting to 39°C. RNA levels were normalized to actin and are represented as fold increase compared with wild-type at 30°C.

of Dcr1 (Emmerth et al. 2010). However, the physiological relevance of this property has remained mysterious. Intriguingly, the translocation phenotype as a response to chronic heat stress is reminiscent of Dcr1 alleles that harbor mutations in the dsRBD. These mutations either abolish the coordination of zinc, which aids proper folding of the dsRBD, or alter the protein–protein interaction surface required for nuclear retention (Fig. 6C; Barraud et al. 2011). Because the integrity of the dsRBD is crucial for nuclear retention of Dcr1, we monitored, by heteronuclear nuclear magnetic resonance (NMR), potential structural changes upon temperature increase. We noticed a global temperature instability of the domain, revealed by protein precipitation from ~35°C and progressive disappearance of NMR signals. Consistent with this observation, differential scanning fluorimetry (Niesen et al. 2007) revealed a melting temperature of 45°C for the domain (Fig. 6D). Interestingly, the initiation of the unfolding transition occurs around 34°C–38°C—the same temperature at which Dcr1 starts leaving the nucleus. Therefore, the Dcr1 translocation phenotype that we observed at temperatures >36°C can most likely be attributed to the temperature sensitivity of Dcr1's dsRBD.

We propose that the dsRBD of Dcr1 constitutes a thermoswitch that has nuclear retention and NPC interaction properties at temperatures up to 34°C (Emmerth et al. 2010; Barraud et al. 2011). At higher temperatures, the protein–protein interaction surface necessary for nuclear retention dissipates and the domain switches to a nuclear export promoter. As a result, RNAi no longer represses BANCs. Consistent with this, BANC genes are significantly up-regulated in Dcr1 mutants that cannot fold the dsRBD properly under normal conditions (Fig. 6E,F). We speculate that this thermoswitch might play an important role in activating chronic heat-shock pathways.

Discussion

This work points to a critical function for a key stress response transcription factor, Atf1, and nuclear pores in coordinating the interplay between the RNAi machinery and the *S. pombe* genome. That RNAi components colocalize with their targets independently of an Argonaute protein is unusual for RNAi–target interactions. For the establishment of RNAi-mediated CTGS, we foresee the requirement of a scaffold such as the NPC that brings the RNAi machinery and the target locus in close proximity. We propose a model in which transcription factors mediate the specific recruitment of genomic loci such as BANC genes to NPCs, where they meet the RNAi machinery (Fig. 7A). A scaffolding function similar to the one proposed here for NPCs might be attributed to endosomes, multivesicular bodies, or mitochondria in mammalian RNA silencing pathways (Gibbings et al. 2009; Huang et al. 2011; Watanabe et al. 2011).

Besides its crucial role in assembling noncoding repeats into heterochromatin, our work reveals that the *S. pombe* RNAi pathway also contributes to the regulation of protein-coding genes in response to environmental cues. Our results demonstrate that RNAi serves a general function to repress stress response genes. Although we cannot rule out a direct impact on transcription rates at some genes, we favor a CTGS model in which RNAi generally functions on a truly post- or cotranscriptional level by degrading newly synthesized RNA in association with its gene.

Whereas RNAi is involved in the regulation of heat-shock gene expression, the RNAi pathway itself is regulated in a unique temperature-dependent manner. Temperatures >34°C trigger a thermoswitch that deports Dcr1 to the cytoplasm. Importantly, although reversible, the kinetics of Dcr1 translocation to the cytoplasm is slow. Complete loss of perinuclear Dcr1 signal was only observed

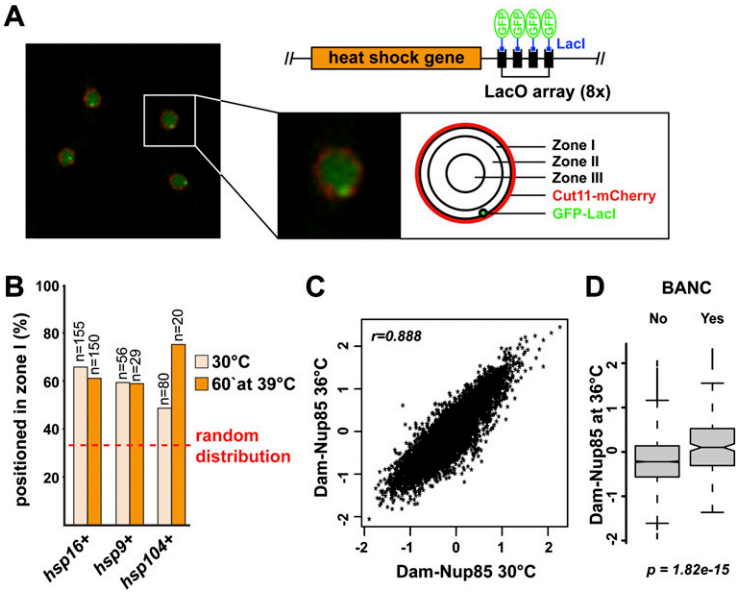

Figure 5. Genes associating with RNAi components do not change their nuclear localization upon temperature increase. (*A*) Summary of the LacO/LacI-GFP system used to analyze the location of individual heat-shock genes (Taddei et al. 2004). Live cells with GFP-LacI-marked *lacO::hsp16*$^+$ locus and the nuclear membrane marker mCherry-Cut11 were imaged at 30°C (single-plane confocal image). (*B*) Heat-shock gene localization was assigned to one of three concentric nuclear zones of equal area (shown in *A*). Percentage of cells with the GFP focus at the nuclear periphery (zone I) before and after a 1-h shift to 39°C is shown. (Dotted line) Random localization. (*C*) Comparison of the genome-wide Nup85 enrichment ($\log_2$) at 30°C and 36°C. (*D*) BANCs remain highly enriched for Nup85 at 36°C.

after several hours. This indicates that RNAi-mediated CTGS occurring at nuclear pores is only disrupted completely under chronic heat-shock conditions. Consistent with this idea, two heat-shock genes, *hsp104*$^+$ and *hsp16*$^+$, show reaccumulation of mRNA when incubated for >4 h at 39°C (Fig. 4H,I). Intriguingly, these genes have been implicated in the acquisition of thermotolerance (Yoshida and Tani 2005; Senechal et al. 2009), which requires mild pretreatment of cells with sublethal heat stress (Ribeiro et al. 1997). We speculate that transcription of certain genes is activated by mild heat shock, but the response is kept transient by RNAi-mediated CTGS, which remains functional for several hours (Fig. 7B). Upon prolonged incubation at elevated temperatures or recurrent heat shock, the Dcr1 thermoswitch could contribute to reactivation of such genes to help the cells tolerate temperatures that would otherwise be deadly (Fig. 7C). Interestingly, loss of silencing at centromeres after chronic heat stress amounts to a maximum increase in RNA of approximately fivefold, much less than the ~100-fold increase observed in *dcr1Δ* cells under normal conditions (data not shown), suggesting the existence of compensatory mechanisms that keep some regions repressed under chronic heat stress despite loss of Dcr1 from the nucleus.

Finally, we note that RNAi components have recently been implicated in heat-shock gene regulation in *Drosophila melanogaster* and that human Dicer has been demonstrated to physically interact with a nuclear pore protein (Ando et al. 2011; Cernilogar et al. 2011). This suggests that mechanisms similar to the ones described here might also be operational in animals.

Material and methods

Strains and plasmids

Fission yeast strains (grown at 30°C in YES medium; MP Biomedicals no. 4101-532) and plasmids used in this study are described in Supplemental Tables S1 and S2. All strains were constructed using a standard PCR-based protocol (Bahler et al. 1998). LacO repeats were inserted into the genome as described previously (Rohner et al. 2008). Constructs on plasmids and in yeast strains were confirmed by sequencing.

DamID

DamID was done as previously described (Woolcock et al. 2011). For DamID under stress conditions, the cells were grown to OD_{600} ~0.5, diluted again to OD_{600} = 0.08, and grown again to OD_{600} ~0.4. This should dilute out parental methylation so that the new methylation pattern reflects association of the fusion protein with the genome under the stress condition. Heat: 36°C; osmotic: cells grown in YES with 1 M sorbitol; oxidative: cells grown in YES with 0.5 mM H_2O_2.

S. pombe *genome annotation*

Two annotations sets ("chromosomal regions" and "genomic elements") were created and can be used in the form of GFF, BED, or Fasta files. The sequence of the genomic DNA is taken from the assembly "pombe_09052011.fasta" (downloaded from ftp://ftp.sanger.ac.uk/pub/yeast/pombe/GFF).

Chromosomal regions

The three chromosomes were split into centromere, euchromatin, subtelomere, telomere, and mating type regions using the coordinates described in Supplemental Table S4. The centromere ranges were taken from http://www.sanger.ac.uk/Projects/S_pombe/centromere.shtml. The mating type region and the chromosome ends were divided into regions of high H3K9me2 (telomeres and mating type region) and lower H3K9me2 (subtelomeres) enrichment based on published data (Cam et al. 2005).

For the Fasta files, the "mating_type_region" sequence fragment provided in the genomic DNA file was used instead of the region on chromosome 2. The euchromatin was extended to include the whole range from 1,644,747 to 4,497,199. The "Spmit" and the "telomeric_contig" sequences from the genomic DNA file were used as well.

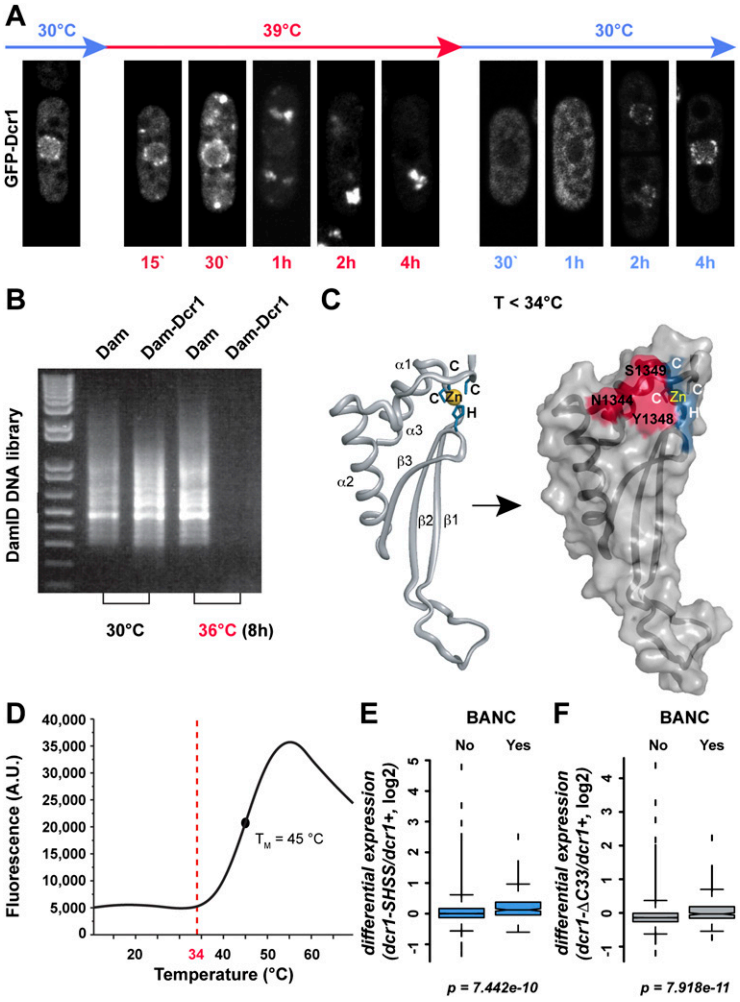

Figure 6. The dsRBD of Dcr1 loses nuclear retention properties at elevated temperatures. (*A*) Fluorescence microscopy of living cells expressing N-terminally tagged GFP-Dcr1. Cells were grown at 30°C, temperature was shifted to 39°C, and confocal images were taken at the indicated times (in red). The nuclear peripheral localization of Dcr1 is gradually lost and accumulates in bright foci in the cytoplasm, although some nuclear rim signal remains up to 4 h. Recovery of nuclear Dcr1 was monitored during 4 h after shifting the temperature from 39°C (cells having been at this temperature overnight) back to 30°C (in blue). (*B*) Much lower DamID library DNA concentrations are obtained for Dam–Dcr1 strains when performed at 36°C compared with 30°C (confirmed by at least four independent replicates). (*C*) Cartoon representation of the Dcr1 dsRBD is shown on the *left* (Barraud et al. 2011). Zinc-coordinating residues are indicated in blue, and the zinc ion is shown as a yellow sphere. Visualization of the dsRBD fold on the protein surface is shown on the *right*. The residues highlighted in red form a protein–protein interaction surface that is required to retain Dcr1 in the nucleus (Barraud et al. 2011). (*D*) Thermal unfolding of Dcr1's C-terminal domain shown in *C* monitored by differential scanning fluorimetry. (Dotted line) Temperature at which unfolding transition initiates. (*E*,*F*) Expression analysis by tiling array (Barraud et al. 2011) showing differential expression of BANCs compared with all other genes in a Dcr1 mutant in which the dsRBD can no longer coordinate a zinc ion and in a Dcr1 mutant lacking the C-terminal 33 amino acids, respectively. Both of these mutants are unable to fold the dsRBD properly and hence lose nuclear retention properties.

Genomic elements

Initial identification of elements is based on the features described in the GFF file "pombe_09052011.gff" (downloaded from ftp://ftp.sanger.ac.uk/pub/yeast/pombe/GFF).

The sequence ranges of the following features were taken directly from the GFF file. "rep_origin," "LTR," tRNA," "snRNA," and "snoRNA". "rRNA" was built from the rRNA features in the GFF file plus adding SPRRNA.25 (misc_feature). "pre_rRNA" was built from the "misc_feature" features in the GFF file, where the phrase "ribosomal RNA" was present in the attributes column. "pseudogene" was built from the mRNA and "misc_feature" features in the GFF file, where the word "pseudogene" was present in the attributes column, plus adding the mRNA features for SPAC23A1.20 and SPCC622.17. "repeats" was built from the "repeat_region" feature, where the words "wtf" and "tf2" were not present. Lists of "wtf" and "tf2" identifiers were built from the mRNA features in the GFF file, where the words "wtf" and "tf2," respectively, were present in the attributes column. Sequence regions derived from "pseudogenes," "wtf," and "tf2" elements were removed from the "unspliced_transcripts," "3UTR," and "5UTR" sets built from the mRNA, 3′ untranslated region (UTR), and 5′ UTR features, respectively. The same restrictions were applied to the "intron" set, in addition to the removal of "tRNA" intron sequences. "tf2" was built by adding the mRNA features from the "tf2" list to the "misc_feature" features in the GFF file, where the phrase "transpos" was present in the attributes column. The "misc_RNA" features were separated based on conservation between different fission yeasts (Rhind et al. 2011; Z Chen, N Rhind, pers. comm.). "conserved_lincR" were conserved in sequence and location. "semiconserved_lincR" were conserved in location with at least one other species. "nonconserved_lincR" were the remaining "intergenic ncRNA" from the work by Rhind et al. (2011). All remaining "misc_RNA" features (which included all "antisense ncRNA" from the work by Rhind et al. [2011]) were used for "longncRNA."

All resulting GFF files were used to create the BED and Fasta files. In addition, a Fasta file for "mRNA" (i.e., spliced transcripts) was built by combining the sequence for the 5′ UTR (if annotated), CDS (one or more per gene), and 3′ UTR (if annotated) features for each gene (after removing all features with identifiers present on the "pseudogene," "wtf," and "tf2" lists). The Fasta file for "wtf" was built from sequences of mRNA features from the "wtf" list, where no splicing (i.e., no intron was annotated) occurred. These sequence ranges were also used for the corresponding GFF and BED files. For the remaining identifiers, the sequence was built the same way as the "mRNA" file and was added to the Fasta file. Furthermore, all BED and Fasta files were split into four different files (e.g., "repeats.fa," "repeats_centromere.fa," "repeats_subtelomere.fa," and "repeats_telomere.fa") depending on whether the start of the original feature was within the "euchromatin," "centromere," "subtelomere," and

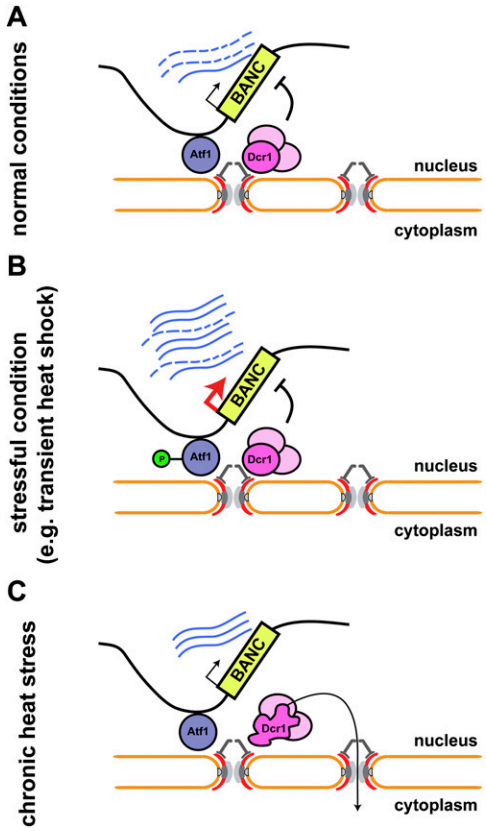

Figure 7. Proposed model for RNAi-mediated CTGS of Atf1-bound genes (BANCs) at nuclear pores. (*A*) The RNAi machinery colocalizes with BANCs at pores, contributing to their repression, presumably by degrading the nascent transcripts. (*B*) Upon stress, Atf1 becomes rapidly and transiently phosphorylated and causes strong transcriptional activation of BANCs. After a transient burst of transcription, CTGS remains active and contributes to the transient nature of the stress response. (*C*) After several hours at elevated temperatures, Dcr1 is lost from the nucleus, presumably due to unfolding of its dsRBD. This abrogates CTGS and causes the reaccumulation of some BANCs, which may be important for thermotolerance.

"telomere," respectively, region describe above. The features present on the "mating_type_region," "Spmit," and "telomeric_contig" sequences were ignored. The Fasta file for the mitochondrion (i.e., "Spmit") was added as one separate sequence.

DamID analysis

DamID analysis was done as previously described (Woolcock et al. 2011) but using the above annotation. Intergenic regions were generated as previously described (Woolcock et al. 2011), except that regions interrupted by an LTR were also excluded from the analysis to prevent the high enrichments found at LTRs from influencing the data. Profiles around translation start sites were as follows: For each transcript, we selected all of the uniquely mapping oligos that overlapped within a region of −1000 to 1000 from the start of the ORF. For each base, from the perspective of the translation start site, we calculated the mean enrichment and smoothed the resulting profiles with a lowess normalizer. Profiles from multiple samples were made comparable by subtracting their respective means.

Expression profiling

RNA isolation and processing were done as previously described (Emmerth et al. 2010). All tiling arrays were processed in R (Ihaka and Gentleman 1996) using bioconductor (Gentleman et al. 2004) and the packages tilingArray (Huber et al. 2006) and preprocessCore. The arrays were RMA background-corrected, quantile-normalized, and log2-transformed on the oligo level using the following command: expr < −log2(normalize.quantiles(rma.background.correct(exprs(readCel2eSet(filenames, rotated=TRUE))))). Oligo coordinates were intersected with the genome annotation and used to calculate average expression levels for individual genomic features (excluding those with <10 oligos) as well as broader annotation categories. In the latter case, multimapping oligos were counted only once per category (avoiding multiple counts from the same oligo).

Statistical analysis

Box plots and scatter plots were produced in R and show the average of at least two biological replicates for all experiments unless otherwise stated. All *P*-values were generated using the R command t.test.

RNA isolation, cDNA synthesis, and quantitative RT–PCR

RNA isolation, cDNA synthesis, and quantitative RT–PCR were done as previously described (Emmerth et al. 2010). Primer pairs used for PCR reactions can be found in Supplemental Table S3.

ChIP

PolII ChIP was performed as previously described (Buhler et al. 2006) using the 8GW16 antibody (Covance) and M-280 sheep anti-mouse IgG Dynabeads (Invitrogen). Primer pairs used for PCR reactions can be found in Supplemental Table S3.

Live fluorescence microscopy

Images were acquired with a LSM710 laser-scanning confocal microscope equipped with a multiline argon 458/488/514-nm (25-mW) laser and a Plan-Apochromat 63×/1,40 oil DIC M27 objective. Images were processed with ImageJ and Adobe Photoshop. In zoning assays, a second channel was added to visualize cut11-mCherry using the DPSS 561-nm (15-mW) laser. In addition, Z-stacks of 200-nm step size were taken and distance measurements of the foci were extracted using the plug-in "PointPicker" of ImageJ. Assignment of zones and statistical analysis was done as previously described (Taddei et al. 2004). The cells were imaged in a Ludin chamber coated with Lectin (BS-1, Sigma). For heat-shock conditions, the microscope was preheated to 39°C, cells were kept in a Ludin chamber, and pictures were acquired at different time points.

To monitor Dcr1 relocalization in response to temperature changes, cells expressing N-terminally GFP-tagged Dcr1 driven by the nmt1 (3×) promoter were grown in YES at 30°C or 39°C. After the respective temperature shift, aliquots from log phase cells were taken for each time point and spread onto agarose patches containing YES medium with 3% glucose. Images were acquired using 3.5% laser power (argon, 488 nm) with a gain of 700, a pinhole of 1.5 AU, and an averaging of 4. The microscope was preheated to 30°C for the recovery experiments and to 39°C in the case of heat induction.

NMR and differential scanning fluorimetry (DSF)

Protein samples for NMR and DSF were prepared as previously described (Barraud et al. 2011). NMR spectra were recorded with

a 0.2 mM ^{15}N-labeled sample at temperatures ranging from 298 K to 318 K in a buffer containing 25 mM NaPi (pH 7.0), 75 mM KCl, 2 mM DTT, and 10 mM $ZnCl_2$ on Bruker AVIII-500 MHz. Thermal unfolding was monitored in the same buffer conditions by DSF in the presence of SYPRO orange using a real-time PCR instrument (Bio-Rad CFX96). Excitation and emission wave lengths were 492 nm and 610 nm, respectively. Melting temperature value (T_M) was calculated using the first derivative of the unfolding transition.

Accession codes

All data sets were deposited under accession number GSE36214 (NCBI Gene Expression Omnibus).

Acknowledgments

We thank Yukiko Shimada and Nathalie Laschet for technical assistance, Laurent Gelman for assistance with light microscopy, Stéphane Thiry for hybridizing tiling arrays, Tim Roloff for help with quality control and archiving of the DamID data sets, Susan Gasser and Peter Meister for strains and plasmids, and Philip Knuckles for comments on the manuscript. Research in the laboratory of M.B. is supported by the Swiss National Science Foundation, the European Research Council, and the Gebert Rüf Stiftung. The Friedrich Miescher Institute for Biomedical Research is supported by the Novartis Research Foundation.

References

Ando Y, Tomaru Y, Morinaga A, Burroughs AM, Kawaji H, Kubosaki A, Kimura R, Tagata M, Ino Y, Hirano H, et al. 2011. Nuclear pore complex protein mediated nuclear localization of dicer protein in human cells. *PLoS ONE* **6:** e23385. doi: 10.1371/journal.pone.0023385.

Bahler J, Wu JQ, Longtine MS, Shah NG, McKenzie A 3rd, Steever AB, Wach A, Philippsen P, Pringle JR. 1998. Heterologous modules for efficient and versatile PCR-based gene targeting in *Schizosaccharomyces pombe*. *Yeast* **14:** 943–951.

Bai SW, Rouquette J, Umeda M, Faigle W, Loew D, Sazer S, Doye V. 2004. The fission yeast Nup107-120 complex functionally interacts with the small GTPase Ran/Spi1 and is required for mRNA export, nuclear pore distribution, and proper cell division. *Mol Cell Biol* **24:** 6379–6392.

Barraud P, Emmerth S, Shimada Y, Hotz HR, Allain FH, Buhler M. 2011. An extended dsRBD with a novel zinc-binding motif mediates nuclear retention of fission yeast Dicer. *EMBO J* **30:** 4223–4235.

Buhler M, Verdel A, Moazed D. 2006. Tethering RITS to a nascent transcript initiates RNAi- and heterochromatin-dependent gene silencing. *Cell* **125:** 873–886.

Buhler M, Haas W, Gygi SP, Moazed D. 2007. RNAi-dependent and -independent RNA turnover mechanisms contribute to heterochromatic gene silencing. *Cell* **129:** 707–721.

Buker SM, Iida T, Buhler M, Villen J, Gygi SP, Nakayama J, Moazed D. 2007. Two different Argonaute complexes are required for siRNA generation and heterochromatin assembly in fission yeast. *Nat Struct Mol Biol* **14:** 200–207.

Cam HP, Sugiyama T, Chen ES, Chen X, FitzGerald PC, Grewal SI. 2005. Comprehensive analysis of heterochromatin- and RNAi-mediated epigenetic control of the fission yeast genome. *Nat Genet* **37:** 809–819.

Cernilogar FM, Onorati MC, Kothe GO, Burroughs AM, Parsi KM, Breiling A, Sardo FL, Saxena A, Miyoshi K, Siomi H, et al. 2011. Chromatin-associated RNA interference components contribute to transcriptional regulation in *Drosophila*. *Nature* **480:** 391–395.

Chen D, Toone WM, Mata J, Lyne R, Burns G, Kivinen K, Brazma A, Jones N, Bahler J. 2003. Global transcriptional responses of fission yeast to environmental stress. *Mol Biol Cell* **14:** 214–229.

Emmerth S, Schober H, Gaidatzis D, Roloff T, Jacobeit K, Buhler M. 2010. Nuclear retention of fission yeast dicer is a prerequisite for RNAi-mediated heterochromatin assembly. *Dev Cell* **18:** 102–113.

Eshaghi M, Lee JH, Zhu L, Poon SY, Li J, Cho KH, Chu Z, Karuturi RK, Liu J. 2010. Genomic binding profiling of the fission yeast stress-activated MAPK Sty1 and the bZIP transcriptional activator Atf1 in response to H_2O_2. *PLoS ONE* **5:** e11620. doi: 10.1371/journal.pone.0011620.

Gentleman RC, Carey VJ, Bates DM, Bolstad B, Dettling M, Dudoit S, Ellis B, Gautier L, Ge Y, Gentry J, et al. 2004. Bioconductor: Open software development for computational biology and bioinformatics. *Genome Biol* **5:** R80. doi: 10.1186/gb-2004-5-10-r-80.

Gibbings DJ, Ciaudo C, Erhardt M, Voinnet O. 2009. Multivesicular bodies associate with components of miRNA effector complexes and modulate miRNA activity. *Nat Cell Biol* **11:** 1143–1149.

Halic M, Moazed D. 2010. Dicer-independent primal RNAs trigger RNAi and heterochromatin formation. *Cell* **140:** 504–516.

Huang H, Gao Q, Peng X, Choi SY, Sarma K, Ren H, Morris AJ, Frohman MA. 2011. piRNA-associated germline nuage formation and spermatogenesis require MitoPLD profusogenic mitochondrial-surface lipid signaling. *Dev Cell* **20:** 376–387.

Huber W, Toedling J, Steinmetz LM. 2006. Transcript mapping with high-density oligonucleotide tiling arrays. *Bioinformatics* **22:** 1963–1970.

Ihaka R, Gentleman R. 1996. R: A language for data analysis and graphics. *J Comput Graph Statist* **5:** 299–314.

Kon N, Krawchuk MD, Warren BG, Smith GR, Wahls WP. 1997. Transcription factor Mts1/Mts2 (Atf1/Pcr1, Gad7/Pcr1) activates the M26 meiotic recombination hotspot in *Schizosaccharomyces pombe*. *Proc Natl Acad Sci* **94:** 13765–13770.

Lawrence CL, Maekawa H, Worthington JL, Reiter W, Wilkinson CR, Jones N. 2007. Regulation of *Schizosaccharomyces pombe* Atf1 protein levels by Sty1-mediated phosphorylation and heterodimerization with Pcr1. *J Biol Chem* **282:** 5160–5170.

Moazed D. 2009. Small RNAs in transcriptional gene silencing and genome defence. *Nature* **457:** 413–420.

Motamedi MR, Verdel A, Colmenares SU, Gerber SA, Gygi SP, Moazed D. 2004. Two RNAi complexes, RITS and RDRC, physically interact and localize to noncoding centromeric RNAs. *Cell* **119:** 789–802.

Niesen FH, Berglund H, Vedadi M. 2007. The use of differential scanning fluorimetry to detect ligand interactions that promote protein stability. *Nat Protoc* **2:** 2212–2221.

Pardo M, Nurse P. 2005. The nuclear rim protein Amo1 is required for proper microtubule cytoskeleton organisation in fission yeast. *J Cell Sci* **118:** 1705–1714.

Rhind N, Chen Z, Yassour M, Thompson DA, Haas BJ, Habib N, Wapinski I, Roy S, Lin MF, Heiman DI, et al. 2011. Comparative functional genomics of the fission yeasts. *Science* **332:** 930–936.

Ribeiro MJ, Reinders A, Boller T, Wiemken A, De Virgilio C. 1997. Trehalose synthesis is important for the acquisition of thermotolerance in *Schizosaccharomyces pombe*. *Mol Microbiol* **25:** 571–581.

Rohner S, Gasser SM, Meister P. 2008. Modules for cloning-free chromatin tagging in *Saccharomyces cerevisae*. *Yeast* **25:** 235–239.

Senechal P, Arseneault G, Leroux A, Lindquist S, Rokeach LA. 2009. The *Schizosaccharomyces pombe* Hsp104 disaggregase is unable to propagate the [PSI] prion. *PLoS ONE* **4:** e6939. doi: 10.1371/journal.pone.0006939.

Shanker S, Job G, George OL, Creamer KM, Shaban A, Partridge JF. 2010. Continuous requirement for the Clr4 complex but not RNAi for centromeric heterochromatin assembly in fission yeast harboring a disrupted RITS complex. *PLoS Genet* **6:** e1001174. doi: 10.1371/journal.pgen.1001174.

Taddei A, Hediger F, Neumann FR, Bauer C, Gasser SM. 2004. Separation of silencing from perinuclear anchoring functions in yeast Ku80, Sir4 and Esc1 proteins. *EMBO J* **23:** 1301–1312.

Verdel A, Jia S, Gerber S, Sugiyama T, Gygi S, Grewal SI, Moazed D. 2004. RNAi-mediated targeting of heterochromatin by the RITS complex. *Science* **303:** 672–676.

Volpe TA, Kidner C, Hall IM, Teng G, Grewal SI, Martienssen RA. 2002. Regulation of heterochromatic silencing and histone H3 lysine-9 methylation by RNAi. *Science* **297:** 1833–1837.

Watanabe T, Chuma S, Yamamoto Y, Kuramochi-Miyagawa S, Totoki Y, Toyoda A, Hoki Y, Fujiyama A, Shibata T, Sado T, et al. 2011. MITOPLD is a mitochondrial protein essential for nuage formation and piRNA biogenesis in the mouse germline. *Dev Cell* **20:** 364–375.

Woolcock KJ, Gaidatzis D, Punga T, Buhler M. 2011. Dicer associates with chromatin to repress genome activity in *Schizosaccharomyces pombe*. *Nat Struct Mol Biol* **18:** 94–99.

Yoshida J, Tani T. 2005. Hsp16p is required for thermotolerance in nuclear mRNA export in fission yeast *Schizosaccharomyces pombe*. *Cell Struct Funct* **29:** 125–138.

SUPPLEMENTARY INFORMATION

RNA interference keeps Atf1-bound stress response genes in check at nuclear pores

Katrina J Woolcock, Rieka Stunnenberg, Dimos Gaidatzis, Hans-Rudolf Hotz, Stephan Emmerth, Pierre Barraud, and Marc Bühler

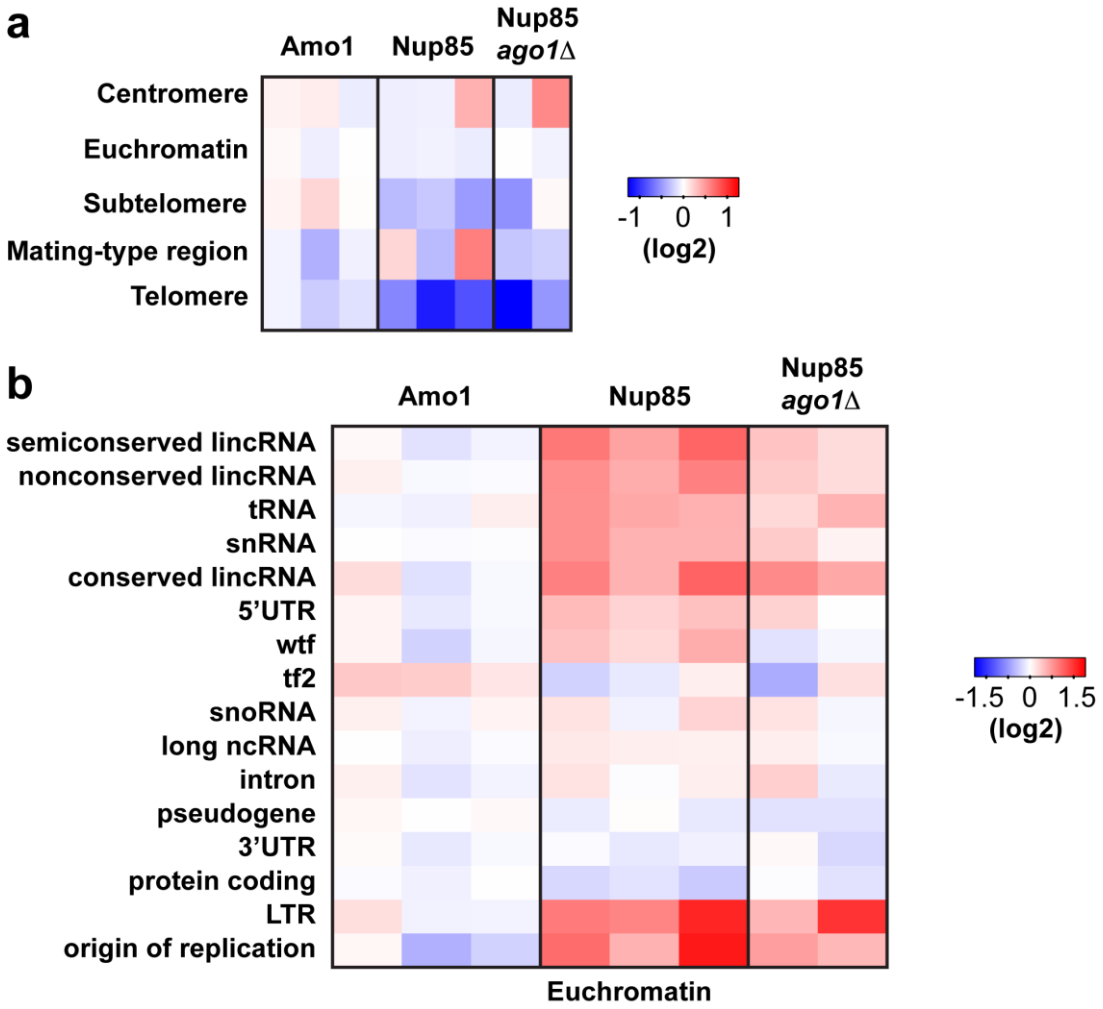

Figure S1. Nup85 interacts with several genomic regions, independently of Ago1, whereas Amo1 does not associate strongly with any class of features. (**a**) Enrichments (log_2) at heterochromatic regions compared to euchromatin. (**b**) Enrichments (log_2) at the indicated genomic features present in euchromatin. Individual columns represent biological replicates.

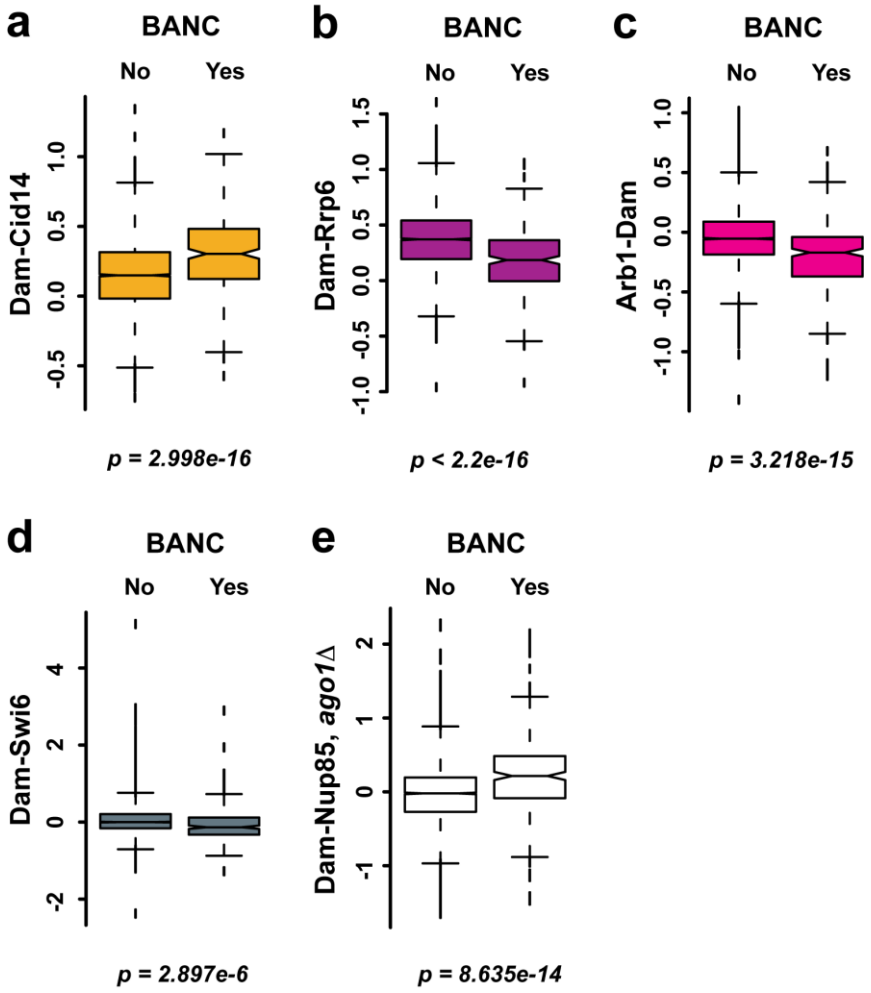

Figure S2. Cid14 is relatively enriched at BANCs, whereas Rrp6, Arb1 and Swi6 are relatively depleted. (**a**-**e**) DamID enrichment (log_2) at BANCs compared to all other genes. (**e**) Preferential association of BANCs with Nup85 is preserved in the absence of Ago1 (compare to Fig. 3G).

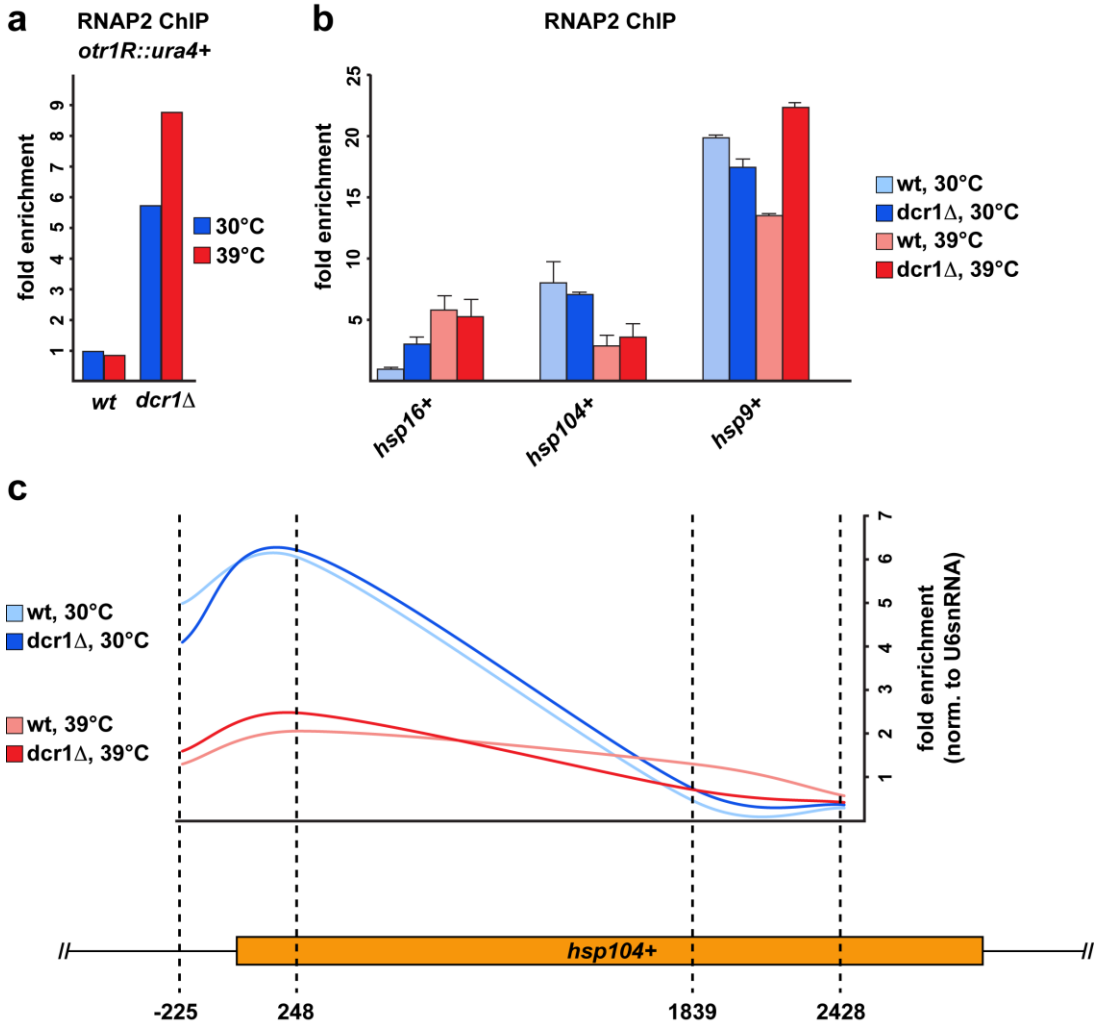

Figure S3. RNAi may influence RNAP2 occupancy on heat shock genes in some cases. (**a**) RNAP2 occupancy on the *ura4+* gene that has been inserted into centromeric heterochromatin (*otr1R::ura4+*). Because centromeric heterochromatin is disrupted in RNAi mutants, transcription of this gene becomes more active in the absence of Dcr1. (**b**) From the same samples as used in (a), the amount of RNAP2 at different heat shock genes was also determined. This result demonstrates that RNAi might be involved in transcriptional repression of *hsp16+* only (light and dark blue bars). Values are relative to the enrichment at *hsp16+* in wt at 30°C, which is set to 1. (**c**) *hsp104+* is shown as an example of heat shock gene regulation that might be mediated by promoter proximal pausing of RNAP2. Because wild-type and *dcr1Δ* cells are not different at normal or heat shock conditions, we conclude that RNAi does not contribute to RNAP2 pausing at this gene. Heat shock at 39°C was for 15 min.

Although transcription regulation at stress response genes in the presence or absence of RNAi will need to be studied in further detail and on a genome-wide scale, our data strongly support a model in which stress response genes are poised for rapid mRNA export at NPCs, but kept in check by RNAi-mediated co-transcriptional degradation (CTGS). Upon stress, strongly increased transcription rates simply overcome CTGS with most transcripts escaping co-transcriptional degradation and accumulating to high levels. After

a transient burst of transcription, CTGS contributes to the subsequent decrease in RNA levels.

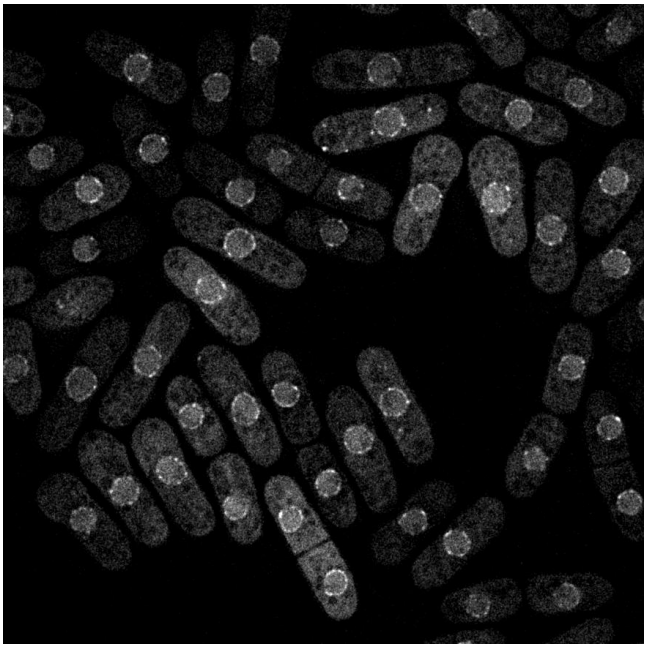

Figure S4. Dcr1 association with NPCs remains unaffected under oxidative stress conditions. Cells expressing N-terminally GFP tagged Dcr1 were grown to exponential phase and treated with 0.5 mM H_2O_2 for 15 min and then spread on agarose patches. Images were captured on a Delta Vision built of an Olympus IX70 widefield microscope equipped with a CoolSNAP HQ2/ICX285 camera. Image stacks were acquired with a Z-step size of 200 nm and deconvolved using the softworks (Delta Vision) software.

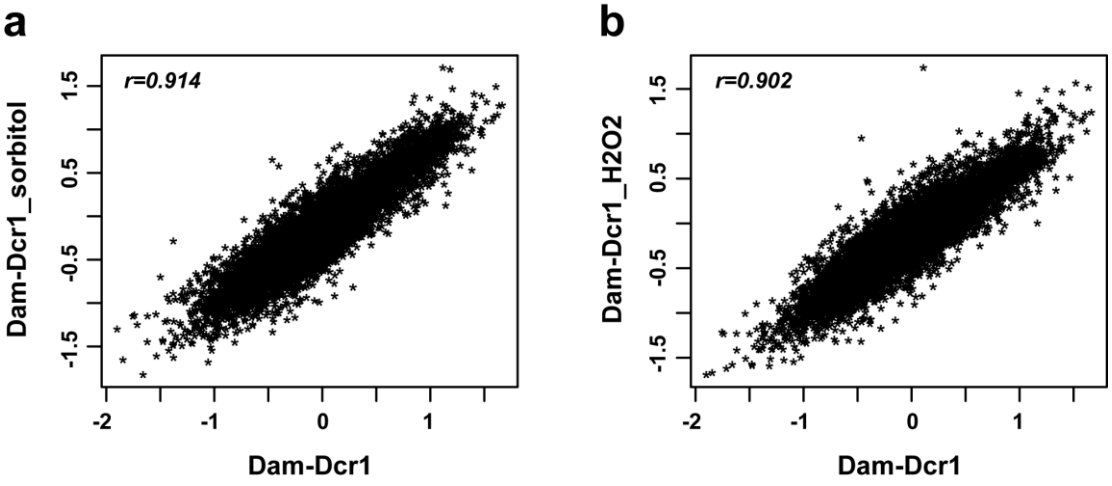

Figure S5. Dcr1 association with the genome does not change under conditions of osmotic or oxidative stress. (**a**-**b**) Dcr1 DamID for cells grown in normal YES compared to cells grown in YES with 1 M sorbitol or 0.5 mM H_2O_2, respectively. Only one replicate performed for each condition.

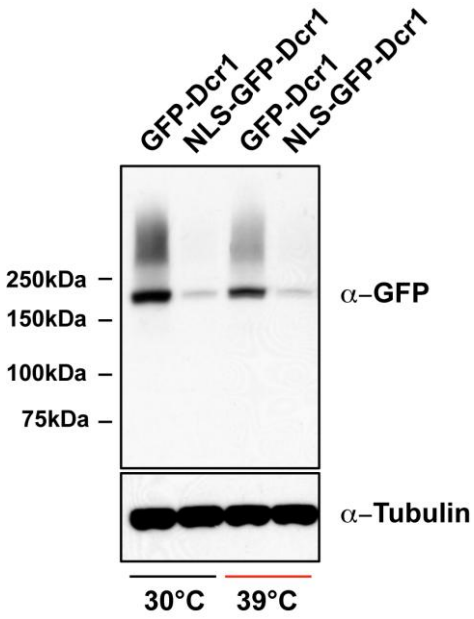

Figure S6. Dcr1 protein levels at normal and elevated temperatures. Western blot was performed with cells expressing GFP-tagged Dcr1 alleles. Cells were incubated at 30°C or 39°C for 8 hours, proteins extracted using TCA and separated on a NuPAGE® 4-12% Bis-Tris gel (Invitrogen). The following antibodies were used: GFP (Roche; 1:1000) and tubulin (Woods et al. 1989); 1:3000). This result demonstrates that total levels of Dcr1 are similar before and after translocation of Dcr1 to the cytoplasm (compare with Figure 6).

Supplementary Tables

Table S1. Strains used in this study

Strain	Genotype	Source
SPB492	*h+ otr1R(SphI)::ura4+ ura4-DS/E ade6-M210 leu1Δ::nmt1(81x)-dam-myc-kan*	1
SPB330	*h+ otr1R(SphI)::ura4+ ura4-DS/E ade6-M210 leu1Δ::nmt1(81x)-dam-myc-swi6-kan*	1
SPB381	*h+ otr1R(SphI)::ura4+ ura4-DS/E ade6-M210 leu1Δ::nmt1(81x)-dam-myc-dcr1-kan*	1
SPB494	*h+ otr1R(SphI)::ura4+ ura4-DS/E ade6-M210 leu1Δ::nmt1(81x)-dam-myc-rdp1-kan*	1
SPB926	*h+ otr1R(Sph1)::ura4+ ura4-DS/E ade6-M210 leu1Δ::nmt1(81x)-arb1-myc-dam-kan*	2
SPB927	*h+ otr1R(Sph1)::ura4+ ura4-DS/E ade6-M210 leu1Δ::nmt1(81x)-dam-myc-ago1-kan*	2
SPB1150	*h+ otr1R(SphI)::ura4+ ura4-DS/E ade6-M210 leu1Δ::nmt1(81x)-amo1-myc-dam-kan*	2
SPB1151	*h+ otr1R(SphI)::ura4+ ura4-DS/E ade6-M210 leu1Δ::nmt1(81x)-dam-myc-nup85-kan*	2
SPB435	*h+ leu1-32 ade6-M216 ura4Δ::nmt1(81x)-dam-myc-kan*	2
SPB436	*h+ leu1-32 ade6-M216 ura4Δ::nmt1(81x)-dam-myc-cid14-kan*	2
SPB437	*h+ leu1-32 ade6-M216 ura4Δ::nmt1(81x)-dam-myc-rrp6-kan*	2
SPB711	*h+ otr1R(SphI)::ura4+ ura4-DS/E ade6-M210 leu1Δ::nmt1(81x)-dam-myc-kan clr4Δ::nat*	1
SPB709	*h+ otr1R(SphI)::ura4+ ura4-DS/E ade6-M210 leu1Δ::nmt1(81x)-dam-myc-dcr1-kan clr4Δ::nat*	1
SPB851	*h+ otr1R(SphI)::ura4+ ura4-DS/E ade6-M210 leu1Δ::nmt1(81x)-dam-myc-dcr1-kan rdp1Δ::hph*	2
SPB852	*h+ otr1R(SphI)::ura4+ ura4-DS/E ade6-M210 leu1Δ::nmt1(81x)-dam-myc-dcr1-kan ago1Δ::hph*	2
SPB853	*h+ otr1R(SphI)::ura4+ ura4-DS/E ade6-M210 leu1Δ::nmt1(81x)-dam-myc-kan rdp1Δ::hph*	2
SPB854	*h+ otr1R(SphI)::ura4+ ura4-DS/E ade6-M210 leu1Δ::nmt1(81x)-dam-myc-kan ago1Δ::hph*	2
SPB855	*h+ otr1R(SphI)::ura4+ ura4-DS/E ade6-M210 leu1Δ::nmt1(81x)-dam-myc-kan clr4Δ::nat rdp1Δ::hph*	2
SPB856	*h+ otr1R(SphI)::ura4+ ura4-DS/E ade6-M210 leu1Δ::nmt1(81x)-dam-myc-kan clr4Δ::nat ago1Δ::hph*	2
SPB857	*h+ otr1R(SphI)::ura4+ ura4-DS/E ade6-M210 leu1Δ::nmt1(81x)-dam-myc-dcr1-kan clr4Δ::nat rdp1Δ::hph*	2
SPB858	*h+ otr1R(SphI)::ura4+ ura4-DS/E ade6-M210 leu1Δ::nmt1(81x)-dam-myc-dcr1-kan clr4Δ::nat ago1Δ::hph*	2
SPB712	*h+ otr1R(SphI)::ura4+ ura4-DS/E ade6-M210 leu1Δ::nmt1(81x)-dam-myc-rdp1-kan clr4Δ::nat*	1
SPB912	*h+ otr1R(SphI)::ura4+ ura4-DS/E ade6-M210 leu1Δ::nmt1(81x)-dam-myc-kan dcr1Δ::hph*	2
SPB913	*h+ otr1R(SphI)::ura4+ ura4-DS/E ade6-M210 leu1Δ::nmt1(81x)-dam-myc-rdp1-kan dcr1Δ::hph*	2
SPB914	*h+ otr1R(SphI)::ura4+ ura4-DS/E ade6-M210 leu1Δ::nmt1(81x)-dam-myc-rdp1-kan ago1Δ::hph*	2
SPB915	*h+ otr1R(SphI)::ura4+ ura4-DS/E ade6-M210 leu1Δ::nmt1(81x)-dam-myc-kan clr4Δ::nat dcr1Δ::hph*	2
SPB916	*h+ otr1R(SphI)::ura4+ ura4-DS/E ade6-M210 leu1Δ::nmt1(81x)-dam-myc-rdp1-kan clr4Δ::nat dcr1Δ::hph*	2
SPB917	*h+ otr1R(SphI)::ura4+ ura4-DS/E ade6-M210 leu1Δ::nmt1(81x)-dam-myc-rdp1-kan clr4Δ::nat ago1Δ::hph*	2

SPB1475	*h+ otr1R(SphI)::ura4+ ura4-DS/E ade6-M210 leu1Δ::nmt1(81x)-dam-myc-nup85-kan ago1Δ::hph*	2
SPB74	*h+ otr1R(SphI)::ura4+ ura4-DS/E leu1-32 ade6-M210*	3
SPB94	*h+ otr1R(SphI)::ura4+ ura4-DS/E leu1-32 ade6-M210 dcr1Δ::nat*	3
SPB96	*h+ otr1R(SphI)::ura4+ ura4-DS/E leu1-32 ade6-M210 swi6Δ::nat*	3
SPB763	*h+ otr1R(SphI)::ura4+ ura4-DS/E leu1-32 ade6-M210 rdp1Δ::kan*	2
SPB764	*h+ otr1R(SphI)::ura4+ ura4-DS/E leu1-32 ade6-M210 ago1Δ::kan*	2
SPB278	*h+ leu1-32 ura4-D18 ori1 ade6-216 imr1R(Nco1)::ura4+ Kan-nmt1(3x)-gfp::dcr1*	2
SPB1087	*h+ ura4- ade6- leu1-32 cut11::mCherry-Nat dis1-promoter-GFP-lacI::his7+ lacO(8x4)LexA(4x)::hsp16+*	2
SPB1199	*h+ ura4- leu1-32 dis1-promoter-GFP-lacI::his7+ lacO(8x4)LexA(4x)::hsp9+ cut11+::mCherry-natR*	2
SPB1200	*h+ ura4- leu1-32 dis1-promoter-GFP-lacI::his7+ lacO(8x4)LexA(4x)::hsp104+ cut11+::mCherry-natR*	2
SPB354	*h+ leu1-32 ura4-D18 ori1 ade6-216 imr1R(Nco1)::ura4+ Kan-nmt1(3x)-nls-gfp::dcr1*	

1 = (Woolcock et al.), 2 = This study, 3 = Danesh Moazed

Table S2. Plasmids used in this study

Name	Common name
pMB681	pFA6a - 81xL - arb1 - myc - dam - kanMX6
pMB682	pFA6a - 81xL - dam - myc - ago1 - kanMX6
pMB774	pFA6a - 81xL - amo1 - myc - dam - kanMX6
pMB798	pFA6a - 81xL - dam - myc - nup85 - kanMX6
pMB399	pFA6a - 81xL - dam - myc - kanMX6
pMB348	pFA6a - 81xL - dam - myc - cid14 - kanMX6
pMB349	pFA6a - 81xL - dam - myc - rrp6 - kanMX6
pMB308	placO(8x4)lexA(4x)-LEU2

Table S3. Primers used for quantitative RT-PCR

Name	Sequence
hsp16 for	AAAGCACCGAGGGTAACCAA
hsp16 rev	TGGTACGAGAGAATGAGCCAAA
hsp104 for	CGTGAATCTCAGCCCGAAGT
hsp104 rev	TCAACGCGGAGTTGTCGAA
hsp9 for	GAACAAGGCAAGGAGAAAATGACT
hsp9 rev	AATGGATTCCTTGGCCTTGTC
act1 for	TCCTCATGCTATCATGCGTCTT
act1 rev	CCACGCTCCATGAGAATCTTC
For ChIP:	
hsp16 for	GATTGATGCAGATCGCATTGAG
hsp16 rev	TTGGGCAAGGTGACAGTCAATA
hsp104 (-225) for	TCCTTTCCTTCCCATAGTAACATCAT
hsp104 (-225) rev	GTTGAGGATGCCGCAGGTA
hsp104 (248) for	CGCTTGCCTGCTCAGGAT
hsp104 (248) rev	TCGCACTTTCAGGTGACAGAGT
hsp104 (1839) for	CGTGCTGGTCTTTCTGATCCTA
hsp104 (1839) rev	CGGAAGGACCGCAAAACA
hsp104 (2428) for	GAGGTTCAGAAACGGCTTCAAT
hsp104 (2428) rev	GCTTCGTCGCTAACCTCGAT
hsp9 for	GAACAAGGCAAGGAGAAAATGACT
hsp9 rev	AATGGATTCCTTGGCCTTGTC
ura4 for	TACAAAATTGCTTCTTGGGCTCAT
ura4 rev	AGACCACGTCCCAAAGGTAAAC
U6 snRNA for	GATCTTCGGATCACTTTGGTCAA
U6 snRNA rev	TGTCGCAGTGTCATCCTTGTG

Table S4. Chromosomal regions

chromosome	start	end	region
1	1	19999	telomere
1	20000	35599	subtelomere
1	35600	3753686	euchromatin
1	3753687	3789420	centromere
1	3789421	5529999	euchromatin
1	5530000	5571499	subtelomere
1	5571500	5579133	telomere
2	1	15799	subtelomere
2	15800	1602263	euchromatin
2	1602264	1644746	centromere
2	1644747	2113999	euchromatin
2	2114000	2136999	mating type region
2	2137000	4497199	euchromatin
2	4497200	4516199	subtelomere
2	4516200	4539804	telomere
3	1	1070903	euchromatin
3	1070904	1137002	centromere
3	1137003	2452883	euchromatin

The coordinates are given in a 1-based notation.

References

Woods, A., Sherwin, T., Sasse, R., MacRae, T.H., Baines, A.J., and Gull, K. 1989. Definition of individual components within the cytoskeleton of Trypanosoma brucei by a library of monoclonal antibodies. *J Cell Sci* 93 (Pt 3): 491-500.

Woolcock, K.J., Gaidatzis, D., Punga, T., and Buhler, M. Dicer associates with chromatin to repress genome activity in Schizosaccharomyces pombe. *Nat Struct Mol Biol* 18(1): 94-99.

RNAi in fission yeast finds new targets and new ways of targeting at the nuclear periphery

Daniel Holoch and Danesh Moazed

Genes Dev. 2012 26: 741-745
Access the most recent version at doi:10.1101/gad.191155.112

PERSPECTIVE

RNAi in fission yeast finds new targets and new ways of targeting at the nuclear periphery

Daniel Holoch and Danesh Moazed[1]

Department of Cell Biology, Howard Hughes Medical Institute, Harvard Medical School, Boston, Massachusetts 02115, USA

RNAi in *Schizosaccharomyces pombe* is critical for centromeric heterochromatin formation. It has remained unclear, however, whether RNAi also regulates the expression of protein-coding loci. In the April 1, 2012, issue of *Genes & Development*, Woolcock and colleagues (pp. 683–667) reported an elegant mechanism for the conditional RNAi-mediated repression of stress response genes involving association with Dcr1 at the nuclear pore. Unexpectedly, the initial targeting of RNAi components to these genes does not require small RNA guides.

Not long after it was discovered as a mechanism of dsRNA-mediated post-transcriptional gene silencing (Fire et al. 1998), it became evident that RNAi also regulates the genome at the level of transcription and chromatin structure in a wide range of organisms. Roles for RNAi have been identified in DNA elimination in *Tetrahymena thermophila*, RNA-directed DNA methylation in plants, and transcriptional gene silencing in *Drosophila melanogaster*, *Caenorhabditis elegans*, and the fission yeast *Schizosaccharomyces pombe* (Moazed 2009). In principle, RNAi could identify target loci through direct base-pairing between its small RNA guides and DNA, but to date, only targeting via complementary RNA transcripts has been described. Consequently, RNAi-based regulation at the chromatin level is thought to involve the interaction of silencing proteins with nascent transcripts (Bühler and Moazed 2007; Lejeune and Allshire 2011). First described in *S. pombe*, this nascent transcript model is strongly supported by the finding that small RNAs can cause gene-specific arrest of elongating RNA polymerase II in *C. elegans* and RNA polymerase IV- and polymerase V-dependent DNA methylation in *Arabidopsis thaliana* (Wierzbicki et al. 2009; Guang et al. 2010).

Extensive evidence that nascent transcripts serve as targets of nuclear RNAi comes from studies in *S. pombe*, in which the genes encoding a Dicer dsRNA nuclease (*dcr1*$^+$), an Argonaute protein (*ago1*$^+$), and an RNA-directed RNA polymerase (*rdp1*$^+$) are each required for establishment and maintenance of centromeric heterochromatin (Volpe et al. 2002). Biochemical purifications showed that Ago1 acts within a chromatin-bound RNA-induced transcriptional silencing (RITS) complex (Verdel et al. 2004). Subsequent studies revealed that RITS interacts with noncoding centromeric transcripts and that artificially enforcing its binding to a nascent euchromatic RNA is sufficient to induce heterochromatic silencing of the corresponding locus (Motamedi et al. 2004; Bühler et al. 2006). Together, these results gave rise to the view that RNAi is recruited cotranscriptionally to its nuclear targets (Fig. 1A). Also consistent with this model are the observations that centromeric siRNA accumulation is disrupted in mutants of RNA polymerase II subunits or splicing factors (Djupedal et al. 2005; Bayne et al. 2008).

Although *S. pombe* has proved a uniquely powerful system for understanding RNAi-based silencing in the nucleus, the cotranscriptional gene silencing (CTGS) mechanism, suggested by the above studies, still presents several mysteries. Here, we focus in particular on two of them. First, in contrast to many other RNAi systems, it has been observed that *S. pombe* small RNAs alone do not robustly recruit the RNAi machinery to targeted loci, suggesting they must instead act in concert with other molecular signals (Fig. 1B). Second, the physiological regulation of protein-coding genes by RNAi in *S. pombe* has only recently begun to be appreciated.

A new study by Bühler and colleagues (Woolcock et al. 2012) offers exciting new insights into both of these questions. By probing the genome-wide localization of RNAi factors using the highly sensitive DNA adenine methyltransferase identification (DamID) technique, they uncover a role for RNAi in the regulation of a class of stress response genes associated with the DNA-binding protein Atf1 and nuclear pores. They present surprising and compelling evidence for small RNA-independent recruitment of RNAi components to their targets. Finally, they propose an attractive model that provides a structural basis for the conditional relocalization of Dcr1 and concomitant derepression of stress-inducible genes.

[*Keywords*: RNAi; CTGS; NPC; stress response; thermoswitch; Atf1 transcription factor]
[1]Corresponding author.
E-mail danesh@hms.harvard.edu.
Article is online at http://www.genesdev.org/cgi/doi/10.1101/gad.191155.112.

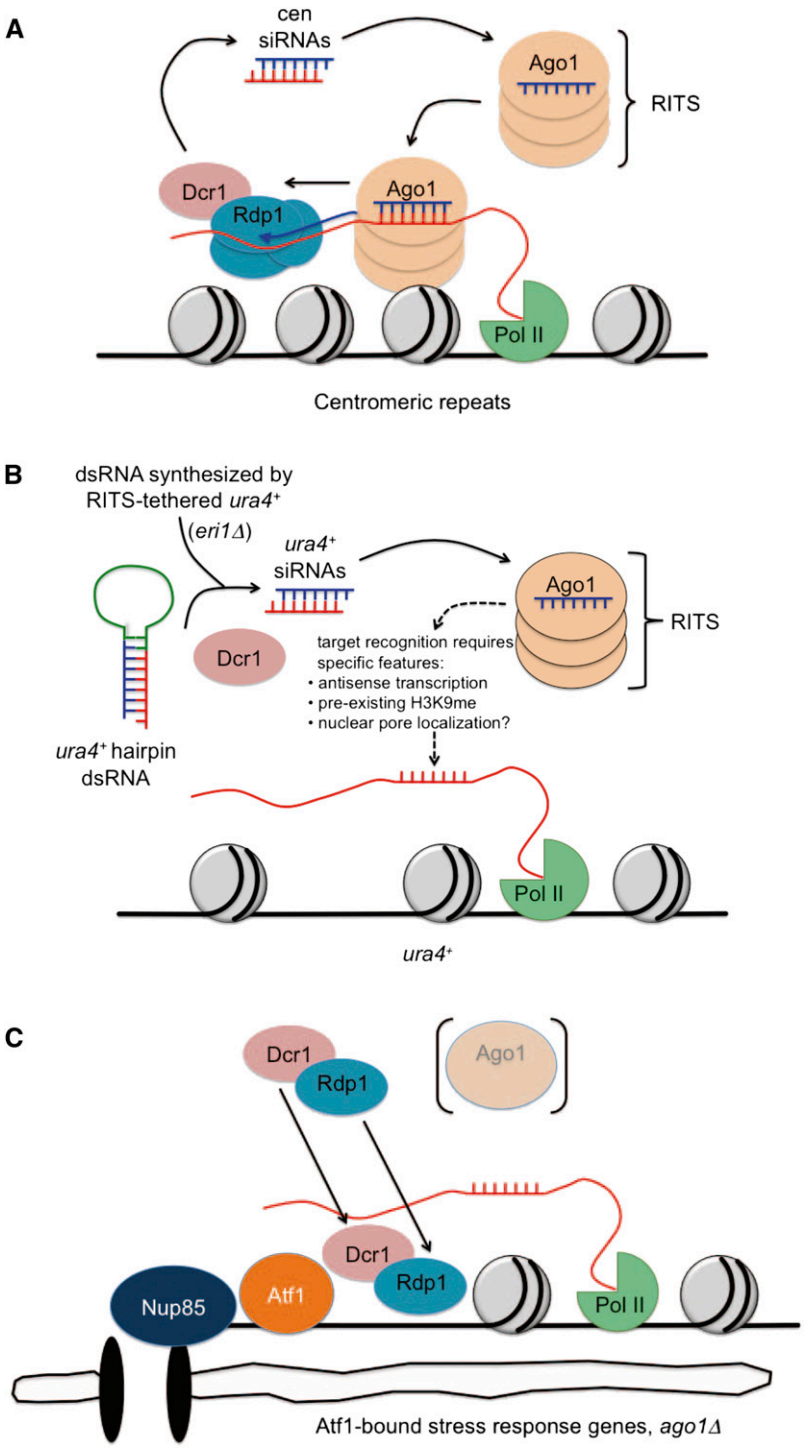

Figure 1. Models for target recognition by the *S. pombe* RNAi machinery. (*A*) At the robustly silenced centromeric repeats, siRNAs bound to the Ago1 subunit guide the RITS complex to complementary nascent RNA targets and corresponding sites on chromatin. RITS then promotes the recruitment of the RNA-dependent RNA polymerase complex (RDRC), containing Rdp1, and Dcr1. Small RNA guides are thus necessary for all targeting of the RNAi machinery to the centromeres. (*B*) Expression of *ura4*$^+$ hairpin transcripts or tethering of RITS to *ura4*$^+$ RNA yields large pools of Dcr1-dependent *ura4*$^+$ siRNAs that bind to the RITS complex, but the native *ura4*$^+$ locus is not targeted. Thus, small RNAs are not sufficient to trigger recruitment of the RNAi machinery to this gene. (*C*) The novel case of the Atf1-bound genes identified by Woolcock et al. (2012). Here, deletion of Ago1, the mediator of small RNA-guided sequence specificity, does not inhibit Dcr1 and Rdp1 recruitment to chromatin. Therefore, small RNAs are not necessary for the initial targeting of these loci.

Small RNAs and the recruitment of the RNAi machinery

In most organisms endowed with RNAi, short dsRNA molecules of ~20–25 nucleotides (nt) in length, often the products of a Dicer ribonuclease acting on endogenous or exogenous dsRNA substrates, are sufficient to trigger a sequence-specific silencing response (Meister and Tuschl 2004). Intriguingly, RNAi-mediated chromatin silencing in *S. pombe* stands in stark contrast to this rule. For example, high levels of hairpin-derived, Dcr1-dependent siRNAs directed against the *ura4*$^+$ gene are unable to elicit repression of the corresponding sequence in its native locus, despite being loaded into the RITS complex (Iida et al. 2008; Simmer et al. 2010). Instead, one or more other events are required to achieve hairpin-mediated silencing (see below). Similarly, when *ura4*$^+$ siRNAs are generated

by tethering RITS to *ura4* nascent transcripts, they fail to guide RITS to a second allele of *ura4* introduced on another chromosome unless the gene encoding the Eri1 ribonuclease is deleted (Bühler et al. 2006). Together, these results imply that siRNAs are not the only necessary determinants of RNAi targeting in *S. pombe*.

There are currently several clues as to what, in addition to small RNAs themselves, might trigger the initial recruitment of RNAi components (Fig. 1B). One possibility is that a minimal level of methylation of histone H3 on Lys 9 (H3K9me), a key heterochromatic signature, is obligatory to stabilize RITS for de novo silencing (Iida et al. 2008; Schalch et al. 2009). Such a requirement, and possibly other features, could make certain genomic loci more susceptible than others to small RNA-guided targeting of RNAi factors. Consistent with this notion are independent observations that displacing *ura4*$^+$ from its native locus can potentiate it for hairpin-mediated silencing (Iida et al. 2008; Simmer et al. 2010). Importantly, hairpin-programmed silencing seems to be favored by the presence of antisense transcription or pre-existing H3K9me at the targeted locus (Iida et al. 2008). A role for bidirectional transcription in targeting the RNAi machinery might also help explain why centromeric repeats are so robustly silenced. Indeed, the widespread presence of complementary transcripts appears to allow the repeats to be targeted by Ago1-bound primal RNAs even in the absence of Dcr1 (Halic and Moazed 2010).

The work of Woolcock et al. (2012) represents a sea change in our understanding of RNAi recruitment to chromatin. Extending previous DamID analyses that uncovered for the first time a physical association between Dcr1 and the genome (Woolcock et al. 2011), the new results show that, remarkably, binding of Dcr1 to both heterochromatin and euchromatin is unchanged in cells lacking Ago1 or Rdp1. Likewise, although Rdp1 association with heterochromatin requires Ago1 and Dcr1, consistent with previous chromatin immunoprecipitation data (Sugiyama et al. 2005), its euchromatic binding profile is very similar to that of Dcr1 and is also unchanged when Ago1 or Dcr1 is deleted. These findings reveal the existence of a mechanism for targeting components of the RNAi machinery to chromatin that is entirely distinct from previous models in that it does not rely on Ago1 or its small RNA guides (Fig. 1C). Until now, it has been taken for granted that small RNAs are indispensable, because deletion of Dcr1 abrogates the interactions of RITS and Rdp1 with one another and with centromeric repeats (Motamedi et al. 2004; Verdel et al. 2004; Sugiyama et al. 2005), but the DamID results from Woolcock et al. (2012) build a very different case for the euchromatic targets of RNAi and raise a host of new questions.

First, in addition to asking why siRNAs are not sufficient to recruit RNAi, we now are prompted to ask why they are not always necessary. In other words, if not siRNAs, what brings Dcr1 and Rdp1 to specific chromatin sites? The investigators attribute this phenomenon to the subnuclear colocalization of these proteins with targeted loci near the nuclear pore complex (NPC) (discussed below). It remains to be seen whether small RNA-independent targeting also occurs at loci not bound to nuclear pores. A second question regards the adaptive significance of this recruitment mechanism. Are Dcr1 and Rdp1 maintained at certain sites in order to keep the cell poised to preferentially amplify specific small RNA pools, or is the early timing of association prior to small RNA generation not critical for silencing itself? The investigators have uncovered an ideal system in which to study how physical targeting of RNAi might be uncoupled from repression and small RNA amplification.

The role of subcellular localization in regulating the activity of RNAi

Trafficking between the nucleus and cytoplasm has long been known to be instrumental in the cell's execution of RNAi. In the microRNA (miRNA) pathway, natively synthesized hairpin miRNA precursors undergo two successive processing steps in the nucleus and cytoplasm. The karyopherin Exportin 5 mediates their transport across the nuclear envelope and is essential for miRNA-dependent repression (Yi et al. 2003), and overexpression experiments suggest that it may be a limiting component of the pathway (Yi et al. 2005). In human cells, the Argonaute Ago2 has been shown to localize to the nucleus in an Importin 8-dependent manner, an activity that influences its ability to repress many targets, although the mechanism is not yet well defined (Weinmann et al. 2009). Not surprisingly, RNAi silencing pathways that operate specifically in the nucleus have also evolved ways of directing components to this compartment (for a review, see Ketting 2011). A notable example is the *C. elegans* Argonaute NRDE-3, which binds siRNAs in the cytoplasm and transports them to the nucleus, where it can silence corresponding genes undergoing transcription elongation (Guang et al. 2008, 2010). Analogously, the *Tetrahymena* Argonaute Twi1p binds to siRNAs in the cytoplasm and carries them into the nucleus with essential help from the binding protein Giw1p, which appears to sense successful conversion of siRNAs from a duplex to single-stranded form (Noto et al. 2010).

In *S. pombe* cells, siRNAs are currently only known to be generated and function within the nucleus. Nevertheless, Bühler and colleagues (Emmerth et al. 2010; Barraud et al. 2011) have reported that Dcr1 has the potential to shuttle between the nucleus and cytoplasm and that a C-terminal zinc coordination motif and a dsRNA-binding domain (dsRBD) orchestrate its nuclear retention. Within the nucleus, overexpressed Dcr1 resides in NPC-proximal foci, and deletion of the C terminus suggests that this localization is critical for heterochromatic silencing of the centromeric repeats (Emmerth et al. 2010). It has remained unclear, however, whether the nuclear retention mechanism is actively exploited by the cell to regulate Dcr1 activity or whether the apparent association of Dcr1 with the NPC is physiologically relevant.

In their new study, Woolcock et al. (2012) present significant advances on both of these fronts. First, their genome-wide DamID analyses reveal a very strong cor-

relation between the genomic sites bound by Dcr1 and the nucleoporin Nup85, but not Amo1, a perinuclear protein not associated with the NPC. The average Dcr1- and Nup85-binding positions relative to ORF start sites also match exquisitely well, with association occurring preferentially upstream. Together, these observations argue that the NPC-proximal localization of Dcr1 may guide it specifically to Nup85-bound target loci, bypassing Ago1 and small RNAs as determinants of sequence specificity (see above). A second major insight into Dcr1 subcellular localization comes from differential scanning fluorimetry experiments in which the dsRBD critical for nuclear retention unfolds at high temperatures. Consistent with a previous mutational analysis of the dsRBD (Barraud et al. 2011), subjecting live cells to the temperatures that compromised the dsRBD structure also abrogated nuclear retention of overexpressed Dcr1. Although indirect effects are not ruled out, the data support an elegant model in which the effects of heat shock on Dcr1 structure tip the balance toward cytoplasmic localization, with important consequences for silencing. In addition to the regulation of stress-inducible genes associated with NPCs (see below), this might also help explain an old observation that the canonical centromeric targets of Dcr1 are derepressed at high temperatures (Allshire et al. 1994).

RNAi-mediated silencing of protein-coding genes in fission yeast

Although the molecular mechanisms of RNAi are widely conserved, its cellular roles are tremendously varied across species (Ketting 2011). One peculiarity of RNAi in *S. pombe* has been its apparent lack of protein-coding targets. Until recently, RNAi in fission yeast was not known to function outside the assembly of constitutive heterochromatin domains. Interestingly, convergent protein-coding gene pairs have been found to produce overlapping readthrough transcripts specifically in the short G1 stage of the *S. pombe* cell cycle. Transient heterochromatin develops in the corresponding intergenic regions in a manner that requires *ago1*$^+$ and *dcr1*$^+$, suggesting that dsRNA may form and trigger RNAi-dependent regulation of these loci (Gullerova and Proudfoot 2008). As it turns out, many genes encoding RNAi components belong to convergent gene pairs, and their expression is autoregulated by this mechanism in a manner that is also critical for their role in centromeric silencing (Gullerova et al. 2011). In a distinct mechanism, Woolcock et al. (2012) identify as novel physiological targets of RNAi the class of genes bound by the stress response transcription factor Atf1. DamID shows that these loci are associated with NPCs and, under normal growth conditions, Dcr1, Rdp1, and Ago1. Importantly, expression analysis indicates that Dcr1, Rdp1, and Ago1 are all required for their repression. In at least some cases, RNA polymerase II occupancy is not affected by *dcr1*$^+$ deletion, implying that repression occurs by both transcriptional gene silencing and CTGS. As a plausible mechanism for release of these genes from RNAi repression during heat shock, the investigators suggest cytoplasmic export of Dcr1 by temperature-induced structural changes in its C terminus (see above), and the genes are indeed constitutively derepressed in mutants of the Dcr1 C terminus.

Intriguing differences stand out between the autoregulation of RNAi genes and the RNAi-mediated repression of Atf1-bound genes. First, autoregulated RNAi genes belong to convergent gene pairs; it is therefore their 3′ ends that are targeted by the RNAi and heterochromatin components (Gullerova et al. 2011). In contrast, Atf1-bound genes are bound by the RNAi machinery predominantly at their promoters (Woolcock et al. 2012). This suggests that the mechanism repressing the latter genes intervenes earlier in the process of transcription to generate a dsRNA signal. A second, related difference is that silencing at convergent gene pairs relies on Dcr1 and Ago1, but not Rdp1, contrary to Atf1-bound loci (Gullerova et al. 2011; Woolcock et al. 2012). Thus, whereas overlapping transcripts themselves are a sufficient source of dsRNA for regulation of convergent genes, stress-inducible genes seem to require Rdp1 to synthesize the dsRNA trigger, presumably using a nascent transcript as a template. Silencing of the Atf1-bound genes resembles centromeric silencing in this regard, but paradoxically, heterochromatin is absent, as Swi6 is not enriched at these loci, and the H3K9 methyltransferase Clr4 is not required for Dcr1 and Rdp1 binding (Woolcock et al. 2012). However, the Clr4 enzymatic activity was recently shown to contribute to centromeric siRNA generation independently of H3K9 (Gerace et al. 2010), so the possibility remains to be tested that it might participate in euchromatic RNAi as well.

Life beyond post-transcriptional gene silencing

Despite its widespread conservation, the RNAi machinery has been lost in certain organisms such as *Saccharomyces cerevisiae* (Drinnenberg et al. 2009). In the evolution of *S. pombe*, RNAi was retained but acts primarily at the chromatin level. Mechanistically, the *S. pombe* variant of RNAi stands apart from canonical post-transcriptional gene silencing, which potently targets protein-coding genes for repression with the mere presence of dsRNA. *S. pombe* instead features transcriptional and cotranscriptional silencing pathways with intricate targeting requirements and a role mainly in repressing noncoding repeats. In this context, the regulation of Atf1-bound stress-inducible genes, whose initial physical targeting is surprisingly independent of small RNAs, represents a novel adaptive role for RNAi. In future studies, it will be interesting to see whether silencing within this broad class of genes occurs by a uniform mechanism. The new data (Woolcock et al. 2012) hint at the possibility that both transcriptional gene silencing and CTGS may be at work, depending on the locus. Given the absence of heterochromatin, this suggests the action of another transcriptional repression pathway yet to be determined. Additionally, the noncanonical poly(A) polymerase Cid14, which targets aberrant transcripts for exosomal degradation, is also enriched at these genes (Woolcock et al. 2012), so RNAi-independent RNA processing might also be involved. These and other new

questions raised by this important work await further study.

Acknowledgments

We thank the National Institutes of Health (D.M.) and the National Science Foundation (graduate research fellowship to D.H.) for support. D.M. is an Investigator of the Howard Hughes Medical Institute.

References

Allshire RC, Javerzat JP, Redhead NJ, Cranston G. 1994. Position effect variegation at fission yeast centromeres. *Cell* **76:** 157–169.

Barraud P, Emmerth S, Shimada Y, Hotz H, Allain FH, Bühler M. 2011. An extended dsRBD with a novel zinc-binding motif mediates nuclear retention of fission yeast Dicer. *EMBO J* **30:** 4223–4235.

Bayne EH, Portoso M, Kagansky A, Kos-Braun IC, Urano T, Ekwall K, Alves F, Rappsilber J, Allshire RC. 2008. Splicing factors facilitate RNAi-directed silencing in fission yeast. *Science* **322:** 602–606.

Bühler M, Moazed D. 2007. Transcription and RNAi in heterochromatic gene silencing. *Nat Struct Mol Biol* **14:** 1041–1048.

Bühler M, Verdel A, Moazed D. 2006. Tethering RITS to a nascent transcript initiates RNAi- and heterochromatin-dependent gene silencing. *Cell* **125:** 873–886.

Djupedal I, Kos-Braun IC, Mosher RA, Söderholm N, Simmer F, Hardcastle TJ, Fender A, Heidrich N, Kagansky A, Bayne E, et al. 2005. RNA Pol II subunit Rpb7 promotes centromeric transcription and RNAi-directed chromatin silencing. *Genes Dev* **19:** 2301–2306.

Drinnenberg IA, Weinberg DE, Xie KT, Mower JP, Wolfe KH, Fink GR, Bartel DP. RNAi in budding yeast. 2009. *Science* **326:** 544–550.

Emmerth S, Schober H, Gaidatzis D, Roloff T, Jacobeit K, Bühler M. 2010. Nuclear retention of fission yeast Dicer is a prerequisite for RNAi-mediated heterochromatin assembly. *Dev Cell* **18:** 102–113.

Fire A, Xu S, Montgomery MK, Kostas SA, Driver SE, Mello CC. 1998. Potent and specific genetic interference by double-stranded RNA in *Caenorhabditis elegans*. *Nature* **391:** 806–811.

Gerace EL, Halic M, Moazed D. 2010. The methyltransferase activity of $Clr4^{Suv39h}$ triggers RNAi independently of histone H3K9 methylation. *Mol Cell* **39:** 360–372.

Guang S, Bochner AF, Pavelec DM, Burkhart KB, Harding S, Lachowiec J, Kennedy S. 2008. An Argonaute transports siRNAs from the cytoplasm to the nucleus. *Science* **321:** 537–541.

Guang S, Bochner AF, Burkhart KB, Burton N, Pavelec DM, Kennedy S. 2010. Small regulatory RNAs inhibit RNA polymerase II during the elongation phase of transcription. *Nature* **465:** 1097–1101.

Gullerova M, Proudfoot NJ. 2008. Cohesin complex promotes transcriptional termination between convergent genes in *S. pombe*. *Cell* **132:** 983–995.

Gullerova M, Moazed D, Proudfoot NJ. 2011. Autoregulation of convergent RNAi genes in fission yeast. *Genes Dev* **25:** 556–568.

Halic M, Moazed D. 2010. Dicer-independent primal RNAs trigger RNAi and heterochromatin formation. *Cell* **140:** 504–516.

Iida T, Nakayama J, Moazed D. 2008. siRNA-mediated heterochromatin establishment requires HP1 and is associated with antisense transcription. *Mol Cell* **31:** 178–189.

Ketting RF. 2011. The many faces of RNAi. *Dev Cell* **20:** 148–161.

Lejeune E, Allshire RC. 2011. Common ground: Small RNA programming and chromatin modifications. *Curr Opin Cell Biol* **23:** 258–265.

Meister G, Tuschl T. 2004. Mechanisms of gene silencing by double-stranded RNA. *Nature* **431:** 343–349.

Moazed D. 2009. Small RNAs in transcriptional gene silencing and genome defence. *Nature* **457:** 413–420.

Motamedi MR, Verdel A, Colmenares SU, Gerber SA, Gygi SP, Moazed D. 2004. Two RNAi complexes, RITS and RDRC, physically interact and localize to noncoding centromeric RNAs. *Cell* **119:** 789–802.

Noto T, Kurth HM, Kataoka K, Aronica L, Desouza LV, Siu KM, Pearlman RE, Gorovsky MA, Mochizuki K. 2010. The *Tetrahymena* argonaute-binding protein Giw1p directs a mature argonaute-siRNA complex to the nucleus. *Cell* **140:** 692–703.

Schalch T, Job G, Noffsinger VJ, Shanker S, Kuscu C, Joshua-Tor L, Partridge JF. 2009. High-affinity binding of Chp1 chromodomain to K9 methylated histone H3 is required to establish centromeric heterochromatin. *Mol Cell* **34:** 36–46.

Simmer F, Buscaino A, Kos-Braun IC, Kagansky A, Boukaba A, Urano T, Kerr AR, Allshire RC. 2010. Hairpin RNA induces secondary small interfering RNA synthesis and silencing in *trans* in fission yeast. *EMBO Rep* **11:** 112–118.

Sugiyama T, Cam HP, Verdel A, Moazed D, Grewal SI. 2005. RNA-dependent RNA polymerase is an essential component of a self-enforcing loop coupling heterochromatin assembly to siRNA production. *Proc Natl Acad Sci* **102:** 152–157.

Verdel A, Jia S, Gerber S, Sugiyama T, Gygi S, Grewal SI, Moazed D. 2004. RNAi-mediated targeting of heterochromatin by the RITS complex. *Science* **303:** 672–676.

Volpe TA, Kidner C, Hall IM, Teng G, Grewal SI, Martienssen RA. 2002. Regulation of heterochromatic silencing and histone H3 lysine-9 methylation by RNAi. *Science* **297:** 1833–1837.

Weinmann L, Höck J, Ivacevic T, Ohrt T, Mütze J, Schwille P, Kremmer E, Benes V, Urlaub H, Meister G. 2009. Importin 8 is a gene silencing factor that targets Argonaute proteins to distinct mRNAs. *Cell* **136:** 496–507.

Wierzbicki AT, Ream TS, Haag JR, Pikaard CS. 2009. RNA polymerase V transcription guides ARGONAUTE4 to chromatin. *Nat Genet* **41:** 630–634.

Woolcock KJ, Gaidatzis D, Punga T, Bühler M. 2011. Dicer associates with chromatin to repress genome activity in *Schizosaccharomyces pombe*. *Nat Struct Mol Biol* **18:** 94–99.

Woolcock KJ, Stunnenberg R, Gaidatzis D, Hotz HR, Emmerth S, Barraud P, Bühler M. 2012. RNAi keeps Atf1-bound stress response genes in check at nuclear pores. *Genes Dev* **26:** 683–692.

Yi R, Qin Y, Macara IG, Cullen BR. 2003. Exportin-5 mediates the nuclear export of pre-microRNAs and short hairpin RNAs. *Genes Dev* **17:** 3011–3016.

Yi R, Doehle BP, Qin Y, Macara IG, Cullen BR. 2005. Overexpression of exportin 5 enhances RNA interference mediated by short hairpin RNAs and microRNAs. *RNA* **11:** 220–226.

Proteomic and functional analysis of the noncanonical poly(A) polymerase Cid14

CLAUDIA KELLER, KATRINA WOOLCOCK, DANIEL HESS, and MARC BÜHLER
Friedrich Miescher Institute for Biomedical Research, Maulbeerstrasse 66, CH-4058 Basel, Switzerland

ABSTRACT

The fission yeast Cid14 protein belongs to a family of noncanonical poly(A) polymerases which have been implicated in a broad range of biological functions. Here we describe an extensive Cid14 protein–protein interaction network and its biochemical dissection. Cid14 most stably interacts with the zinc-knuckle protein Air1 to form the Cid14–Air1 complex (CAC). Providing a link to ribosomal RNA processing, Cid14 sediments with 60S ribosomal subunits and copurifies with 60S assembly factors. In contrast, no physical link to chromatin has been identified, although gene expression profiling revealed that efficient silencing of a few heterochromatic genes depends on Cid14 and/or Air1.

Keywords: TRAMP; CAC; heterochromatin silencing; ribosome biogenesis; poly(A) polymerase; Cid14

INTRODUCTION

Proper gene expression requires polyadenylation of most eukaryotic mRNA 3′ ends by the canonical poly(A) polymerase (PAP), which has been shown to be important for RNA export, translation, and RNA stabilization. Besides the canonical PAP, eukaryotic cells possess noncanonical PAPs, which have been implicated in a broad range of biological processes and are conserved from yeast to humans. The fission yeast *Schizosaccharomyces pombe* encodes six noncanonical PAPs: Cid1, Cid11, Cid12, Cid13, Cid14, and Cid16 (Stevenson and Norbury 2006). Although initially classified as noncanonical PAPs, some of these enzymes have been demonstrated to add U residues (Kwak and Wickens 2007; Rissland et al. 2007). Cid14 is a nuclear enzyme which preferentially adds purines to RNA substrates in vitro, functions in ribosomal RNA (rRNA) processing and heterochromatic gene silencing, and is required for faithful chromosome segregation, proper siRNA generation by the RNA interference (RNAi) pathway, and maintenance of genomic integrity of the ribosomal DNA (rDNA) locus (Win et al. 2006; Bühler et al. 2007, 2008; Wang et al. 2008; Bühler 2009).

Cid14 is a functional ortholog of the two noncanonical PAPs, Trf4p/5p, found in the distantly related budding yeast *Saccharomyces cerevisiae* (Win et al. 2006). Both Trf4p and Trf5p are found together with predicted zinc-knuckle proteins Air1p/2p and the helicase Mtr4p in complexes termed TRAMP4 (Trf4p–Air1p/2p–Mtr4p; LaCava et al. 2005; Vanacova et al. 2005; Wyers et al. 2005) and TRAMP5 (Trf5p–Air1p–Mtr4p; Houseley and Tollervey 2006). The TRAMP complexes are considered to be cofactors of the yeast nuclear exosome that functions to process or degrade RNAs (Mitchell et al. 1997; Mitchell and Tollervey 2000).

Here we report the existence of a single TRAMP-like complex in *S. pombe*, consisting of Mtr4, Cid14, and Air1. Whereas Air1 and Cid14 form a stable complex, the association with Mtr4 is weak and occurs only in the presence of both Cid14 and Air1. Moreover, Cid14 sediments with 60S ribosomal subunits and copurifies with 60S assembly factors, providing a link to its role in ribosomal RNA processing. Previously we have shown that efficient silencing of transgene insertions at heterochromatic loci depends on Cid14 (Bühler et al. 2007). Here we demonstrate that silencing of a few endogenous heterochromatic genes depends on Cid14. In contrast to the factors implicated in ribosome biogenesis, no components have been identified that would link Cid14 to chromatin. Therefore, we propose that Cid14 functions off chromatin to control gene expression.

RESULTS AND DISCUSSION

Cid14 stably associates with the zinc-knuckle protein Air1

Previously, we have shown that Cid14 copurifies with a large number of proteins, including ribosomal proteins

Reprint requests to: Marc Bühler, Friedrich Miescher Institute for Biomedical Research, Maulbeerstrasse 66, CH-4058 Basel, Switzerland; e-mail: marc.buehler@fmi.ch; fax: 41-61-697-39-76.

Article published online ahead of print. Article and publication date are at http://www.rnajournal.org/cgi/doi/10.1261/rna.2053710.

(RPs) and two proteins that are homologs of the budding yeast Mtr4p and Air1p/2p (Bühler et al. 2007). To better characterize this protein–protein interaction network, we revisited affinity chromatography under various conditions. We started our analysis by tandem affinity purifications of fully functional C-terminally TAP-tagged Cid14 (Cid14-TAP; Bühler et al. 2007) at different salt concentrations followed by analysis of the purification by SDS polyacrylamide gel electrophoresis and mass spectrometry. LC-MS/MS analysis of tryptic digests of protein mixtures of Cid14-TAP and control purifications revealed that Cid14 copurifies specifically with Air1 (*SPBP35G2.08c*), Mtr4 (*SPAC6F12.16c*), and a large number of RPs at 150 mM NaCl (Fig. 1A,D). Association with Mtr4 and RPs was gradually lost with increasing NaCl concentrations or upon treatment with RNase I (Fig. 1B,D). The only detectable interaction preserved at 500 mM NaCl was with Air1 (Fig. 1A,D; Supplemental Table S1). Thus, Cid14 and Air1 form a stable complex, independently of Mtr4. We refer to this complex as Cid14–Air1 Complex (CAC). Similarly, Trf4p has been shown to stably associate with either Air1p or Air2p in *S. cerevisiae*. Interestingly, this interaction is necessary for PAP activity (Vanacova et al. 2005; Wyers et al. 2005). In contrast, Cid14 shows PAP activity independently of Air1 (Bühler et al. 2007).

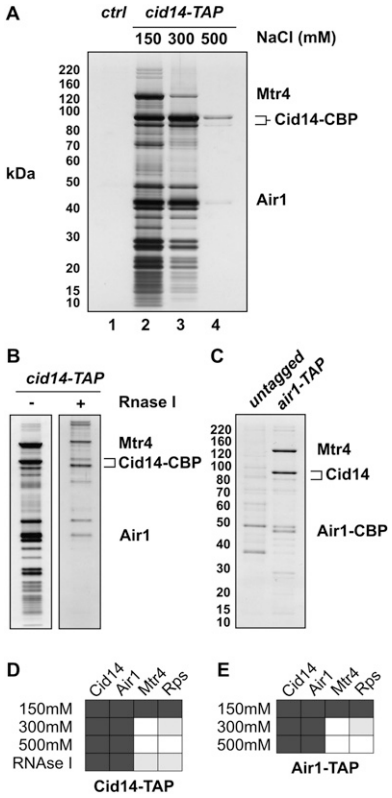

FIGURE 1. Cid14 interacts with Air1, Mtr4, and ribosomal proteins. (*A*) Silver-stained gel showing Cid14-TAP purifications under increasing salt conditions. The positions of Mtr4 (126 kDa), Cid14-CBP (83 kDa), a Cid14 degradation product, Air1 (35 kDa), and a molecular weight marker (*left*) are indicated. CBP, calmodulin binding peptide. (*B*) Silver-stained gel showing an RNase-treated Cid14-TAP purification. Five-hundred units of RNase I were added after the TEV-cleavage reaction for 1 h at RT. (*C*) Silver-stained gel showing an Air1-TAP purification (150 mM NaCl). (*D*,*E*) Table summarizing the LC-MS/MS results of the TAP purifications under various conditions (see also Supplemental Table S1). TAP elutions were TCA-precipitated and processed for LC-MS/MS analysis. RPs, ribosomal proteins. Black, gray, and white boxes indicate peptides that are, respectively, of high abundance, medium abundance, or absent in LC-MS/MS.

Mtr4, Cid14, and Air1 form a TRAMP-like complex in *S. pombe*

At low salt concentrations, Cid14 reproducibly copurified with Mtr4 and Air1, suggesting that a TRAMP-like complex also exists in *S. pombe*. To verify this, we constructed a strain expressing a C-terminally TAP-tagged Air1 protein (Air1-TAP). Affinity purification followed by mass spectrometry identified Cid14 and Mtr4 as Air1-interacting proteins, as well as RPs (Fig. 1C). Mtr4 and RP association was also sensitive to high salt concentrations (Fig. 1E and data not shown). Similarly, 500 mM NaCl washes have been demonstrated to dissociate Mtr4p from Trf4p, Trf5p, and Air2p in *S. cerevisiae* (LaCava et al. 2005). RNAse treatment of the Cid14-TAP complex bound to IgG beads prior to release by TEV cleavage did not abolish the recovery of Air1 and Mtr4 (Fig. 1B), whereas binding of RPs, in particular 40S ribosomal proteins, was reduced (Fig. 1B,D; Supplemental Table S1). This makes it unlikely that Mtr4, Cid14, and Air1 interact via substrate RNAs. Based on these results, we conclude that a TRAMP-like complex does exist in *S. pombe*.

In *S. cerevisiae*, Trf4p can either interact with Air1p or Air2p, suggesting the existence of two TRAMP complexes containing either Air1p or Air2p associated with Trf4p and Mtr4p (Wyers et al. 2005). Although *S. pombe* encodes for more than one Air1p/2p homolog, we consistently identified Air1 by LC-MS/MS from Cid14-TAP purifications (Supplemental Table S1). To rule out that a related zinc-knuckle protein could substitute in the absence of Air1, we purified Cid14-TAP expressed in *air1Δ* cells. These purifications did not reveal any other Air1 homologs associating with Cid14 (Fig. 2C,E; Supplemental Table S1). Thus, Air1 is the sole zinc-knuckle protein interacting with Cid14. Furthermore, we purified Air1-TAP from *cid14Δ* cells and found no other Cid14 homologs copurifying with Air1 (Fig. 2D). In conclusion, the association of CAC with Mtr4 represents the only TRAMP-like complex in *S. pombe*. Importantly, Cid14-TAP purifications from *air1Δ* cells revealed that Mtr4 no longer interacts with Cid14 in the absence of Air1 (Fig. 2C,E). This may suggest that Air1 mediates the interaction with Mtr4. However, Mtr4 was also lost when we purified Air1-TAP from *cid14Δ* cells (Fig. 2D,E). Therefore, an intact CAC complex is required for TRAMP formation in fission yeast.

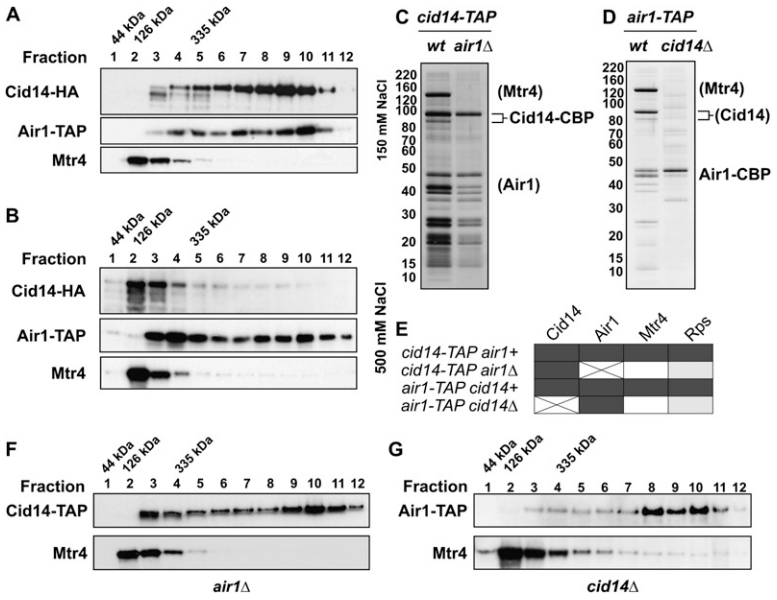

FIGURE 2. Cid14 resides in high and low molecular weight complexes. (*A*) Sucrose gradient fractionation under low salt conditions (150 mM NaCl). Individual fractions from sucrose density gradients were analyzed by Western blotting with antibodies recognizing Cid14-HA, Air1-TAP, or Mtr4. (*B*) Sucrose gradient fractionation under high salt conditions (500 mM NaCl). The analysis was performed as in *A*. (*C*) Silver-stained gel showing Cid14-TAP purifications performed with wild-type and *air1Δ* cells. (*D*) Silver-stained gel showing Air1-TAP purifications performed with wild-type and *cid14Δ* cells. (*C*,*D*) Salt concentration was 150 mM. (*E*) Table summarizing LC-MS/MS results of TAP purifications shown in *C* and *D*. Black, gray, and white boxes indicate peptides that are of high abundance, medium abundance, and absent in LC-MS/MS, respectively. (*F*,*G*) *S. pombe* lysates from *cid14-TAP air1Δ* and *air1-TAP cid14Δ* cells were separated by sucrose density gradient centrifugation. (*A*,*B*,*F*,*G*) *S. pombe* total cell lysates were loaded onto an 18%–54% sucrose gradient and protein complexes were separated by ultracentrifugation at 39,000 rpm for 18 h.

Cid14 associates with 60S ribosomal subunits and assembly factors

The results described above show that Cid14 resides in at least two biochemically distinct protein complexes, CAC and TRAMP. Importantly, Cid14 has previously been shown by gel filtration experiments to be part of a complex much larger than CAC and TRAMP (Win et al. 2006). Consistently, sucrose gradient fractionation indicated that Cid14 is part of both low and high molecular weight protein assemblies (Fig. 2A). We observed the same for Air1, but not Mtr4. Mtr4 sedimented mainly in fraction 2, which represents its own molecular weight of ~126 kDa (Fig. 2A,B). Thus, Mtr4 seems unlikely to be a stable component of any larger protein assemblies. Furthermore, only a small fraction of the Mtr4 population seems to be associated with CAC to form *sp*TRAMP, similar to what has also been described for Mtr4p in *S. cerevisiae* (LaCava et al. 2005).

The high number of copurifying RPs and the sedimentation of Cid14 in high molecular weight fractions is indicative of an association with ribosomes. Interestingly, Cid14 has been reported to be involved in 25S rRNA processing (Win et al. 2006), suggesting that Cid14 might interact with ribosomal proteins during assembly of the large ribosomal subunit. Therefore, we performed ribosome fractionation on sucrose gradients ranging from 10% to 50% by centrifugation for 15 h followed by Western blotting to detect Cid14-TAP. Consistent with its known role in 25S rRNA processing, Cid14 was mainly detected in fractions representing the 60S large ribosomal subunit (Fig. 3A). Importantly, five proteins known to be involved in 60S biogenesis could be identified by LC-MS/MS after reducing the complexity of our Cid14-TAP purification by SDS-PAGE separation and performing the tryptic digest on individual gel bands (Fig. 3B). Thus, we conclude that the higher molecular weight Cid14 complex represents a 60S ribosomal subunit assembly protein–protein interaction network.

Silencing of a few endogenous heterochromatic genes depends on Cid14

Previously we have shown that efficient silencing of transgene insertions at heterochromatic loci depends on Cid14 (Buhler et al. 2007). However, it remained to be tested to what extent Cid14 also functions in heterochromatic silencing of endogenous genes and whether this depends on an intact TRAMP complex. Therefore, we hybridized total RNA isolated from wild-type, *cid14Δ*, and *air1Δ* cells to affymetrix tiling arrays. Taking the average of two biological replicates and using a cutoff of 1.5-fold, 149 and 323 genes were shown to be up-regulated in *cid14Δ* and *air1Δ* cells, respectively, while 73 and 86 were down-regulated (Fig. 4A,B). Interestingly, the genes differentially expressed in *cid14Δ* and *air1Δ* cells overlapped only partially, suggesting that Air1 and Cid14 can also function outside the CAC or TRAMP complexes (Fig. 4A,D). Consistent with this, we noticed that both Cid14 and Air1 associated with high molecular weight protein assemblies independently of each other (Fig. 2F,G).

Comparing the expression in *cid14Δ* to previously published H3K9me2 and $HP1^{Swi6}$ ChIP-on-chip data (Cam et al. 2005) revealed that only a small set of heterochromatic genes was up-regulated in *cid14Δ* (Fig. 4E; Supplemental Table S2). The majority of these are subtelomeric genes, as previously described (Wang et al. 2008). Importantly, not all of these heterochromatic genes were up-regulated in *air1Δ* cells, suggesting that an intact CAC and/or TRAMP complex is not always necessary to

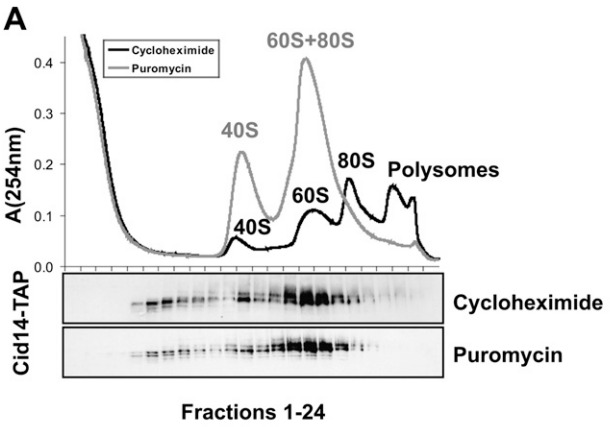

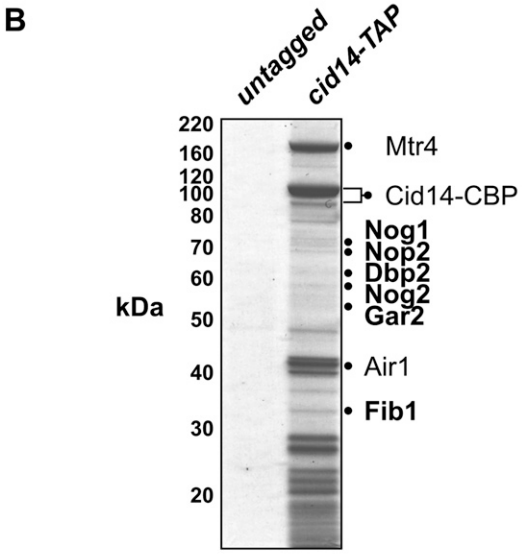

Protein	GeneDB	kDa	%	#	function
Nop2	SPBP8B7.20c	68.9	7	3	60S biogenesis
Nog1	SPBC651.01c	72.8	10	5	60S biogenesis
Gar2	SPAC140.02	53	12	4	40S
Dbp2	SPBP8B7.16c	61.5	4	2	60S
"Nog2"	SPAC6F6.03c	59.9	4	2	60S
Fib1	SPBC2D10.10c	32	12	3	40S/60S

FIGURE 3. Cid14 associates with 60S ribosomal subunits and 60S ribosome assembly factors. (*A*) Sedimentation behavior of Cid14-TAP in 10%–50% ribosome sucrose gradients. UV profile (OD at 254 nm) with ribosomal subunits, mono- and polysomes is indicated. Samples were treated with cycloheximide to stabilize or puromycin to disrupt polysomes. Twenty-four fractions were collected and analyzed by Western blotting against Cid14-TAP. (*B*) Cid14-TAP and control purifications from 20 g of cells were separated by SDS-PAGE followed by Coomassie-staining. Bands were cut out and LC-MS/MS analysis was performed on in-gel processed samples. Positions of the bands and the corresponding proteins indentified by LC-MS/MS are indicated. %, percent sequence coverage; # number of unique peptides.

silence heterochromatin (Supplemental Table S2). Although future work on Air1 and its RNA binding properties will be required to rule out alternative functions, we speculate that Air1 functions as an RNA adaptor to support the association of Cid14 with its substrate. Depending on yet to be determined characteristics of a Cid14 substrate, Air1 might be more or less important for this.

Conclusions

Our findings that Cid14 associates with 60S ribosomal subunits and with proteins known to be involved in 60S biogenesis strongly suggest that Cid14 is directly involved in the assembly of pre-ribosomes. This is further supported

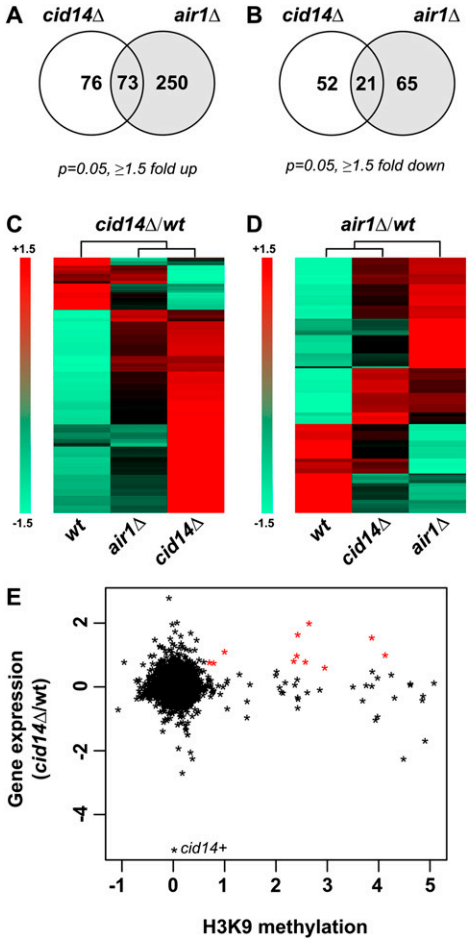

FIGURE 4. Differential gene expression in *cid14Δ* and *air1Δ* cells. (*A*,*B*) Venn diagrams showing the number of genes up- or down-regulated at least 1.5-fold in *cid14Δ* or *air1Δ* cells compared to wild type ($P = 0.05$) on *S. pombe* tiling arrays. Two biological replicates were analyzed. (*C*) Heatmap displaying the genes which were up- or down-regulated at least 1.5-fold ($P = 0.05$) in *cid14Δ* cells compared to wild type on *S. pombe* tiling arrays. (*D*) Heatmap displaying the genes which were up- or down-regulated at least 1.5-fold ($P = 0.05$) in *air1Δ* cells compared to wild type on *S. pombe* tiling arrays. (*C*,*D*) Artificially scaled expression values are shown for the strains indicated (−1.5 is set for the gene with the lowest expression and +1.5 is set for the gene with the highest expression). (*E*) Comparison of genes up-regulated in *cid14Δ* cells to previously published H3K9me2 ChIP-on-chip data (Cam et al. 2005). Asterisks in red indicate those genes that have a value >0.6 (log scale) in both the expression and ChIP experiments (listed in Supplemental Table S2).

by the nucleolar localization of Cid14 and its role in rRNA metabolism (Win et al. 2006; C Keller and M Bühler, unpubl.). Therefore, we propose that Cid14 is physically linked to ribosome biogenesis. Cid14 also functions in eliminating a variety of RNAs, amongst them transcripts originating from subtelomeric heterochromatin (this study; Bühler et al. 2007; Wang et al. 2008). In contrast to RPs and ribosome assembly factors, we were not able to identify proteins which could link Cid14 to heterochromatin physically. Therefore, we favor a model in which Cid14 recognizes and eliminates heterochromatic RNAs off chromatin. Finally, our biochemical and functional data suggest that Cid14 may at least partially function outside of an intact TRAMP complex. Future work will be required to elucidate substrate characteristics and requirements for Cid14 and/or the TRAMP complex.

MATERIALS AND METHODS

Strains and plasmids

Fission yeast strains used in this study are described in Supplemental Table S3 and were grown at 30°C in YES (Yeast Extract with Supplements). All strains were constructed following a standard PCR-based protocol (Bahler et al. 1998).

Tandem affinity purification

A 2-L culture of TAP-tagged *S. pombe* cells (OD at 600 nm ≈ 2) was pelleted, washed once in ice-cold PBS, resuspended in 1/4 pellet volume of lysis buffer (6 mM Na_2HPO_4, 4 mM $NaH_2PO_4•H_2O$, 1% NP-40, 150 mM NaCl, 2 mM EDTA, 1 mM EGTA, 50 mM NaF, 4 μg/mL leupeptin, 0.1 mM Na_3VO_4, 1 mM PMSF, 1× Protease Inhibitors Complete EDTA free [Roche]), and pelleted into N_2(l). Ten grams of cells were then disrupted by cryo-grinding with a Retsch MM 400 (3 × 3 min at 30 Hz). Sixteen milliliters of lysis buffer was added to the powder and stirred for ca. 15 min in the cold room. The salt concentration was now adjusted, if required. The lysate was spun for 25 min at 12,000 rpm (4°C). The supernatant was then incubated with 200 μL of IgG-Sepharose for 2 h at 4°C on a rocker. The beads were transferred to a column and washed three times with 10 mL of washing buffer (10 mM Tris-HCl [pH 8.0], 150 mM NaCl, 0.1% NP-40) and once with TEV-cleavage buffer (10 mM Tris-HCl [pH 8.0], 150 mM KOAc, 0.1% NP-40, 0.5 mM EDTA, 1 mM DTT). The TEV-cleavage reaction was performed using 50 U of acTEV (Invitrogen) in 1 mL of TEV-cleavage buffer for 1 h at 25°C. Where indicated, the RNase I (Ambion) treatment was subsequently performed for 1 h at RT using 500 U. The eluate was then transferred to a new column and the old column was washed out with 0.5 mL of TEV-c buffer. Three milliliters of Calmodulin-binding buffer (CAM-B: 10 mM Tris-HCl [pH 8.0], 150 mM NaCl, 1 mM $Mg[OAc]_2$, 1 mM imidazole, 2 mM $CaCl_2$, 10 mM β-mercaptoethanol), 4.5 μL of 1 M $CaCl_2$, and 150 μL of Calmodulin-Sepharose were added and incubated for 1 h at 4°C on a rocker. The beads were washed twice with 1.5 mL CAM-B (0.1% NP-40) and once with 1.5 mL CAM-B (0.02% NP-40). The purified proteins were eluted from the column using 1 mL of CAM-E (=CAM-B, but replacing the $CaCl_2$ with 10 mM EGTA). The eluate was split into two aliquots and each of them was TCA-precipitated. One pellet was resuspended in 1× LDS sample buffer and run on a 4%–12% NuPAGE gel (Invitrogen) using MOPS buffer followed by silver- or Coomassie-staining (Colloidal Blue Staining kit, Invitrogen). The other pellet was used for mass spectrometric analysis.

Sucrose density gradient centrifugation

The lysate was prepared as for the TAP purifications (0.5 g of cryo ground powder). After the high-speed spin, 300 μL of the lysate was loaded onto a 18%–54% sucrose gradient (buffered with 20 mM Tris-HCl [pH 7.5], 150 mM KCl, 1 mM DTT, 1 mM PMSF). Complexes were separated by ultracentrifugation for 18 h at 39,000 rpm (4°C) with an SW40 rotor (Beckman). The gradient was unloaded from the bottom with 70% sucrose. Twelve fractions of 1 mL were taken using a fraction collector while reading the absorbance at 254 nm with a UV reader. Twenty-eight microliters of the fractions was separated on a 4%–12% NuPAGE gel, blotted to nitrocellulose (1.5 h at 200 mA), and the proteins of interest were detected using the ECL system. Antibodies were used at 1:10,000 (α-PAP, Sigma), 1:20 (α-HA, FMI monoclonal antibody), 1:3000 (α-Mtr4, custom polyclonal, Eurogentec).

For the ribosome fractionation, 100 μg/mL cycloheximide or 1 mM puromycin was added to 250 mL of an exponentially growing *S. pombe* culture. The culture was incubated for another 10 min at 30°C and then pelleted. The cells were washed once and then resuspended in 0.5 mL of lysis buffer (20 mM Tris-HCl [pH 7.5], 150 mM KCl, 5 mM $MgCl_2$, 1 mM EGTA, 1 mM PMSF, 1× Protease Inhibitors Complete EDTA-free [Roche], 100 μg/mL Cycloheximide or 1 mM puromycin). For the puromycin treated sample, the $MgCl_2$ concentration in all buffers was reduced to 1 mM. One milliliter of glass beads was added and the cells were disrupted using a bead-beater (4 × 30 sec). The lysate was spun for 15 min at 16,000 rpm, 4°C, and then 300 μL of the supernatant was loaded onto a 10%–50% gradient, which was prepared as described above. The ultracentrifugation was carried out for 15 h at 27,000 rpm in a SW40 rotor (Beckman). In this case, 24 fractions of 0.5 mL were collected as described above.

Mass spectrometry

SDS-PAGE separated proteins and TCA-precipitated and acetone-washed protein pellets were reduced with TCEP, alkylated with iodoacetamide, and digested with trypsin. The generated peptides were analyzed by NanoLC-MSMS on a 4000Q Trap as described (Supplemental Table S1; Hess et al. 2008). The proteins were identified with Mascot searching Uniprot 15.6 (Perkins et al. 1999).

S. pombe tiling arrays and data analysis

RNA was isolated from cells collected at OD_{600} = 0.5 using the hot phenol method (Leeds et al. 1991). The isolated RNA was processed according to the GeneChip Whole Transcript (WT) Double-Stranded Target Assay Manual from Affymetrix using the GeneChip *S. pombe* Tiling 1.0FR. For analysis of the tiling arrays, an R-based script was used, which is available upon request. We used the genome and annotations from the *S. pombe* Genome

Project (http://www.sanger.ac.uk/Projects/S_pombe/). The oligos from the Affymetrix .BPMAP file were remapped using bowtie and the .GFF file was used to map them to the genes. The resulting .CDF file is available upon request. The expression data from *cid14Δ* was compared to ChIP-on-chip data for H3K9me2 (Cam et al. 2005) by plotting, for each annotated element, enrichment/input for the ChIP data against *cid14Δ*/wt for the expression data. The average of two biological replicates was taken for each data set.

SUPPLEMENTAL MATERIAL

Supplemental material can be found at http://www.rnajournal.org. Tiling array data are reposited at the Gene Expression Omnibus (http://www.ncbi.nlm.nih.gov/geo/), accession number GSE20905.

ACKNOWLEDGMENTS

We thank Nicolas Thomä and the members of the Bühler lab for helpful discussions and comments on the manuscript. We thank Ben Hurschler and the Grosshans laboratory for technical help with sucrose gradients, and Yukiko Shimada and Nathalie Laschet for technical support. This work was supported by the Swiss National Science Foundation (SNF) and the Novartis Research Foundation.

Received December 17, 2009; accepted February 19, 2010.

REFERENCES

Bahler J, Wu JQ, Longtine MS, Shah NG, McKenzie A III, Steever AB, Wach A, Philippsen P, Pringle JR. 1998. Heterologous modules for efficient and versatile PCR-based gene targeting in *Schizosaccharomyces pombe*. *Yeast* **14:** 943–951.

Bühler M. 2009. RNA turnover and chromatin-dependent gene silencing. *Chromosoma* **118:** 141–151.

Bühler M, Haas W, Gygi SP, Moazed D. 2007. RNAi-dependent and -independent RNA turnover mechanisms contribute to heterochromatic gene silencing. *Cell* **129:** 707–721.

Bühler M, Spies N, Bartel DP, Moazed D. 2008. TRAMP-mediated RNA surveillance prevents spurious entry of RNAs into the *Schizosaccharomyces pombe* siRNA pathway. *Nat Struct Mol Biol* **15:** 1015–1023.

Cam HP, Sugiyama T, Chen ES, Chen X, FitzGerald PC, Grewal SI. 2005. Comprehensive analysis of heterochromatin- and RNAi-mediated epigenetic control of the fission yeast genome. *Nat Genet* **37:** 809–819.

Hess D, Keusch JJ, Oberstein SAL, Hennekam RCM, Hofsteenge J. 2008. Peters Plus syndrome is a new congenital disorder of glycosylation and involves defective *O*-glycosylation of thrombospondin type 1 repeats. *J Biol Chem* **283:** 7354–7360.

Houseley J, Tollervey D. 2006. Yeast Trf5p is a nuclear poly(A) polymerase. *EMBO Rep* **7:** 205–211.

Kwak JE, Wickens M. 2007. A family of poly(U) polymerases. *RNA* **13:** 860–867.

LaCava J, Houseley J, Saveanu C, Petfalski E, Thompson E, Jacquier A, Tollervey D. 2005. RNA degradation by the exosome is promoted by a nuclear polyadenylation complex. *Cell* **121:** 713–724.

Leeds P, Peltz SW, Jacobson A, Culbertson MR. 1991. The product of the yeast UPF1 gene is required for rapid turnover of mRNAs containing a premature translational termination codon. *Genes Dev* **5:** 2303–2314.

Mitchell P, Tollervey D. 2000. Musing on the structural organization of the exosome complex. *Nat Struct Biol* **7:** 843–846.

Mitchell P, Petfalski E, Shevchenko A, Mann M, Tollervey D. 1997. The exosome: A conserved eukaryotic RNA processing complex containing multiple 3′→5′ exoribonucleases. *Cell* **91:** 457–466.

Perkins DN, Pappin DJ, Creasy DM, Cottrell JS. 1999. Probability-based protein identification by searching sequence databases using mass spectrometry data. *Electrophoresis* **20:** 3551–3567.

Rissland OS, Mikulasova A, Norbury CJ. 2007. Efficient RNA polyuridylation by noncanonical poly(A) polymerases. *Mol Cell Biol* **27:** 3612–3624.

Stevenson AL, Norbury CJ. 2006. The Cid1 family of noncanonical poly(A) polymerases. *Yeast* **23:** 991–1000.

Vanacova S, Wolf J, Martin G, Blank D, Dettwiler S, Friedlein A, Langen H, Keith G, Keller W. 2005. A new yeast poly(A) polymerase complex involved in RNA quality control. *PLoS Biol* **3:** e189. doi: 10.1371/journal.pbio.0030189.

Wang SW, Stevenson AL, Kearsey SE, Watt S, Bahler J. 2008. Global role for polyadenylation-assisted nuclear RNA degradation in posttranscriptional gene silencing. *Mol Cell Biol* **28:** 656–665.

Win TZ, Draper S, Read RL, Pearce J, Norbury CJ, Wang SW. 2006. Requirement of fission yeast Cid14 in polyadenylation of rRNAs. *Mol Cell Biol* **26:** 1710–1721.

Wyers F, Rougemaille M, Badis G, Rousselle JC, Dufour ME, Boulay J, Regnault B, Devaux F, Namane A, Seraphin B, et al. 2005. Cryptic pol II transcripts are degraded by a nuclear quality control pathway involving a new poly(A) polymerase. *Cell* **121:** 725–737.

Molecular Cell
Article

HP1^{Swi6} Mediates the Recognition and Destruction of Heterochromatic RNA Transcripts

Claudia Keller,[1,2] Ricardo Adaixo,[3] Rieka Stunnenberg,[1,2] Katrina J. Woolcock,[1,2] Sebastian Hiller,[3,*] and Marc Bühler[1,2,*]
[1]Friedrich Miescher Institute for Biomedical Research, Maulbeerstrasse 66, 4058 Basel, Switzerland
[2]University of Basel, Petersplatz 10, 4003 Basel, Switzerland
[3]Biozentrum, University of Basel, Klingelbergstrasse 70, 4056 Basel, Switzerland
*Correspondence: sebastian.hiller@unibas.ch (S.H.), marc.buehler@fmi.ch (M.B.)
DOI 10.1016/j.molcel.2012.05.009

SUMMARY

HP1 proteins are major components of heterochromatin, which is generally perceived to be an inert and transcriptionally inactive chromatin structure. Yet, HP1 binding to chromatin is highly dynamic and robust silencing of heterochromatic genes can involve RNA processing. Here, we demonstrate by a combination of in vivo and in vitro experiments that the fission yeast HP1^{Swi6} protein guarantees tight repression of heterochromatic genes through RNA sequestration and degradation. Stimulated by positively charged residues in the hinge region, RNA competes with methylated histone H3K9 for binding to the chromodomain of HP1^{Swi6}. Hence, HP1^{Swi6} binding to RNA is incompatible with stable heterochromatin association. We propose a model in which an ensemble of HP1^{Swi6} proteins functions as a heterochromatin-specific checkpoint, capturing and priming heterochromatic RNAs for the RNA degradation machinery. Sustaining a functional checkpoint requires continuous exchange of HP1^{Swi6} within heterochromatin, which explains the dynamic localization of HP1 proteins on heterochromatin.

INTRODUCTION

Heterochromatin is a distinct chromatin structure that is late replicating, gene poor, and rich in transposons or other parasitic genomic elements. Heterochromatic structures are required for proper centromere function, repression of recombination, sister chromatid cohesion, and the maintenance of telomere stability, and they also play an essential role in heritable gene silencing in a variety of organisms from yeast to humans (Grewal and Jia, 2007). One hallmark of heterochromatin is its association with members of the highly conserved heterochromatin protein 1 (HP1) family of proteins (James and Elgin, 1986). HP1 proteins consist of an N-terminal chromodomain (CD) and a structurally related C-terminal chromo shadow domain (CSD), separated by a hinge region. The CSD can mediate homodimerization of HP1 and binding to other proteins through a degenerate pentapeptide motif, PxVxL (Cowieson et al., 2000; Smothers and Henikoff, 2000). The CD binds the N-terminal tail of histone H3 when it is di- or trimethylated with high specificity but low affinity (Bannister et al., 2001; Jacobs and Khorasanizadeh, 2002; Jacobs et al., 2001; Lachner et al., 2001; Nielsen et al., 2002) and the hinge region has been implicated in nucleic acid binding (Muchardt et al., 2002). The fission yeast *Schizosaccharomyces pombe* contains two HP1 homologs, HP1^{Chp2} and HP1^{Swi6}, which both bind to methylated lysine 9 of histone H3 (H3K9) and are involved in heterochromatin silencing (Grewal and Jia, 2007). In contrast to other eukaryotes, *S. pombe* contains only a single member of the SUV39 histone methyltransferase family of proteins, Clr4, which is responsible for the methylation of H3K9 (Nakayama et al., 2001).

Heterochromatin is generally perceived to be a structurally rigid and static chromatin compartment that is inaccessible to the transcription machinery, yet several findings challenge this view. For example, the H3K9 methyl-binding affinity of HP1 proteins can be rather low, and their association with heterochromatin is surprisingly dynamic (Cheutin et al., 2004, 2003; Festenstein et al., 2003; Schalch et al., 2009). Furthermore, recent work has revealed that both RNAi-dependent and -independent RNA turnover mechanisms are crucial for the quiescence of heterochromatic sequences in *S. pombe*, indicating that silencing of heterochromatin does not occur exclusively at the transcriptional level (Bühler et al., 2007). Repression of marker genes when inserted into heterochromatin depends on the noncanonical poly(A) polymerase Cid14, which is thought to target the heterochromatic RNA for degradation via the RNA exosome and/or the RNAi pathway. Similarly, silencing of subtelomeric genes marked by H3K9 methylation also depends on Cid14 (Keller et al., 2010; Wang et al., 2008). Importantly, heterochromatic gene silencing is impaired in Cid14 mutant strains, yet heterochromatin remains intact (Bühler et al., 2007). Thus, some level of transcription within heterochromatin is possible, and pathways to cope with the unwanted heterochromatic RNA do exist (Bühler, 2009). However, the mechanism of specific recognition of heterochromatic transcripts and thus their targeting for the Cid14-dependent degradation has remained elusive.

HP1^{Swi6}, one of the two *S. pombe* heterochromatin proteins, is best known for its critical role in proper centromere function. In *swi6* mutant cells, centromeres lag on the spindle during anaphase, and chromosomes are lost at a high rate (Ekwall et al., 1995). This is associated with a failure in the recruitment of cohesin to pericentromeric heterochromatin (Bernard et al.,

2001; Nonaka et al., 2002). Thus, one function of HP1^{Swi6} is the attraction of a high concentration of cohesin to *S. pombe* centromeres, which guarantees proper chromosome segregation. HP1^{Swi6} has also been implicated in the recruitment of cohesin outside constitutive heterochromatin, thus regulating transcription termination between convergent gene pairs (Gullerova and Proudfoot, 2008). Besides cohesin subunits, HP1^{Swi6} also copurifies with a diverse set of other nuclear nonhistone proteins that are involved in a variety of nuclear functions such as chromatin remodelling and DNA replication (Fischer et al., 2009; Motamedi et al., 2008). Even though many of these interactions remain to be confirmed, HP1^{Swi6} may partner with many different factors and ensure genomic integrity. Apart from these functions, HP1^{Swi6} is also required for heterochromatic gene silencing, but on a mechanistic level this is poorly understood.

Here, we demonstrate that HP1^{Swi6} serves a general function linking transcription within heterochromatin to downstream RNA turnover. HP1^{Swi6} binds RNA via a molecular mechanism that involves the hinge region, the CD, and the N-terminal domain. Rather than tethering heterochromatic transcripts to chromatin, HP1^{Swi6} complexed with RNA dissociates from H3K9-methylated nucleosomes and escorts its associated RNAs to the RNA decay machinery. This detachment of HP1^{Swi6} from chromatin results from a competition mechanism that combines the interactions of RNA and methylated H3K9 to HP1^{Swi6} on the single-molecule level with dynamic exchange between the histone-bound and -unbound HP1^{Swi6} ensemble. Our results provide an explanation for the dynamic localization of HP1 proteins on heterochromatin and reveal insights into the role of RNA in the regulation of higher order chromatin structures.

RESULTS

Heterochromatic mRNA Transcripts Are Not Translated into Protein

Previous work revealed that the noncanonical polyA-polymerase Cid14 processes or eliminates a variety of RNA targets to control processes such as the maintenance of genomic integrity, meiotic differentiation, ribosomal RNA maturation, and heterochromatic gene silencing (Keller et al., 2010; Wang et al., 2008; Win et al., 2006). The effect of *cid14+* mutations on heterochromatin silencing has previously been studied using the *ura4+* reporter gene/5-FOA assay (Bühler et al., 2007). Because this assay does not allow a quantification of the resulting protein levels, and because it is also compromised by a general sensitivity of *cid14+* mutant cells to 5-FOA (Figure S1), we created reporter strains carrying a *gfp+* transgene inserted at the innermost centromeric repeat region (*imr1R::gfp+*) or at the *mat3M* locus (*mat3M::gfp+*) (Figure 1A). Consistent with previous results (Bühler et al., 2007), heterochromatic *gfp+* mRNA levels from centromeric locations increased significantly in *clr4Δ* and *dcr1Δ* cells, but only modestly in *cid14Δ* cells (Figure 1B), with no corresponding increase in GFP protein levels upon *cid14+* deletion (Figures 1C and S1A). Therefore, Cid14 plays a redundant role, if any at all, in the silencing of a reporter gene located in centromeric heterochromatin. In contrast, deleting the *cid14+* gene resulted in strongly elevated *gfp+* mRNA levels from the mating-type locus. Unexpectedly, however, this was not accompanied by a concomitant increase in GFP protein levels (Figures 1D and E).

To test whether mRNAs originating from heterochromatic genes engage in translation at all, we set out to profile their association with polyribosomes (Figure 1F). *S. pombe* cell lysates were separated on sucrose gradients and RNA was extracted from the individual fractions. The relative amount of a given mRNA in each fraction was then quantified by quantitative real-time RT-PCR (qRT-PCR). As expected, *act1+* mRNA was highly enriched, whereas the nuclear U6 snRNA was absent from the polysomal fractions (Figure 1F). When transcribed from its endogenous locus, mRNA encoded by the *ura4+* gene was also highly enriched in polysomes (data not shown). Similarly, *ura4+* mRNA originating from a *mat3M::ura4+* reporter was found in the polysomal fractions in the absence of the H3K9 methyltransferase Clr4. However, no considerable association with polysomes was observed for heterochromatic *ura4+* reporter mRNA in wild-type or *cid14Δ* cells (Figure 1F).

Thus, although heterochromatic mRNAs can be over 10-fold more abundant in *cid14Δ* cells than in wild-type cells, they are not translated into protein effectively.

HP1^{Swi6} Functions as an H3K9 Methylation-Specific Checkpoint to Assemble Translationally Incompetent Ribonucleoprotein Particles

Atypical processing of 5′ or 3′ ends of heterochromatic mRNAs could explain why heterochromatic mRNAs do not engage in translation. However, our analysis of mRNA termini revealed no major differences between heterochromatic and euchromatic transcripts (Figure S2 and data not shown), suggesting that heterochromatic mRNAs per se do not contain aberrant features that would signal their destruction or render them translationally inactive. Rather, transcripts emerging from heterochromatin are more likely to be channeled into the RNA decay pathway by the assembly of a heterochromatin-specific ribonucleoprotein particle (hsRNP). Therefore, we postulate the existence of an H3K9 methylation-specific checkpoint that would function on chromatin and assemble emerging transcripts into hsRNPs that are translationally incompetent and prone for degradation (Figure 2A).

Obvious candidates for proteins that could function as such a checkpoint are HP1 proteins, because they have been reported to have affinity for both H3K9-methylated histone H3 tails and RNA. Therefore, HP1 proteins might capture heterochromatic RNAs in an H3K9 methylation-specific manner. The *S. pombe* genome contains two HP1 homologs, HP1^{Chp2} and HP1^{Swi6}. Interestingly, even though HP1^{Swi6} is essential for the full repression of heterochromatin, its contribution to transcriptional gene silencing is minimal. Furthermore, heterochromatic RNAs have been observed to copurify with HP1^{Swi6} but not HP1^{Chp2} (Motamedi et al., 2008).

Therefore, we tested whether heterochromatic mRNAs would become translated in cells lacking HP1^{Swi6}. Consistent with the checkpoint model, GFP protein expression from the *mat3M::gfp+* allele was restored in *swi6Δ* and *swi6Δ cid14Δ* cells (Figure 2B). However, deletion of *swi6+* also resulted in a significant reduction in H3K9me2 at *mat3M::gfp+* (Figure 2C),

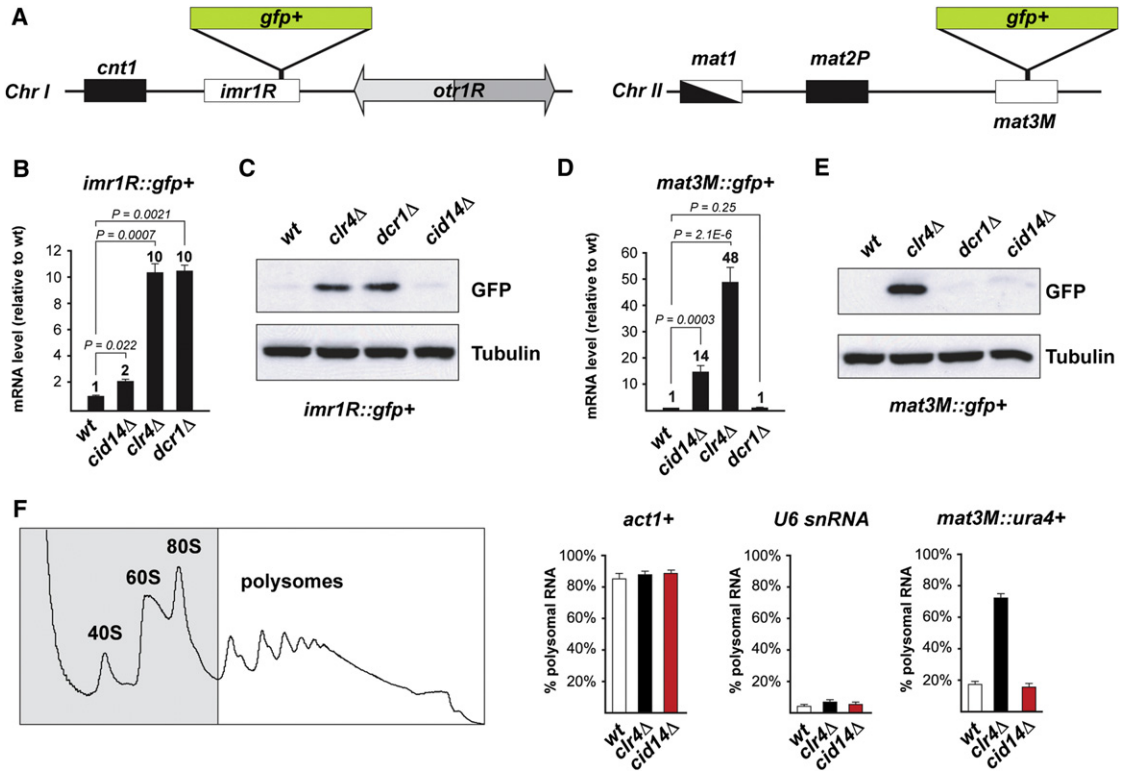

Figure 1. Heterochromatic mRNAs Are Not Translated into Protein

(A) Diagram representing DNA organization at the centromere of chromosome I and at the mating-type locus (chromosome II). cnt1, central core; imr1, innermost repeats; otr1, outermost repeat. *gfp+* reporter transgenes are driven by the *ura4+* promoter, whereas the ORF is followed by a natMX6 cassette (Tadh1 terminator).

(B) Quantitative real-time RT-PCR showing *gfp+* mRNA levels in *imr1R::gfp+* cells. Mean values normalized to *act1+* are shown (n = 3). Error bars represent SEM; p values were calculated using the Student's t test.

(C) Western blot showing GFP protein levels in *imr1R::gfp+* cells. Total protein from an equivalent number of cells was extracted by TCA. Tubulin served as a loading control.

(D) Quantitative real-time RT-PCR showing *gfp+* mRNA levels in *mat3M::gfp+* cells. Mean values normalized to *act1+* are shown (n = 14). Error bars represent SEM, p values were calculated using the Student's t test.

(E) Western blot showing GFP protein levels in *mat3M::gfp+* cells. Total protein from an equivalent number of cells was extracted by TCA. Tubulin served as a loading control.

(F) A representative polysome profile (OD 254 nm) with monosomal (fractions 1–5) and polysomal fractions (fractions 6–12 polysomal) is shown on the left. RNA levels were determined by quantitative real-time RT-PCR and the enrichment in the polysomal fraction was calculated as a percentage of the total. Error bars represent SEM. Act1+ RNA and U6 snRNA served as positive and negative controls, respectively.

not allowing us to definitely assign the checkpoint function to HP1Swi6. In contrast, deletion of *swi6+* or *cid14+* or both did not significantly lower H3K9 methylation levels at the subtelomeric *tlh1/2+* genes, yet resulted in a strong upregulation of the respective mRNAs (Figures 2D and 2E). Importantly, association of *tlh1/2+* mRNA with polysomes was only observed in cells lacking *swi6+* but not *cid14+* (Figure 2F). These results place HP1Swi6 upstream of Cid14 and directly support a model in which HP1Swi6 acts on H3K9-methylated nucleosomes and promotes the assembly of translationally incompetent hsRNPs.

HP1Swi6 Binds RNA via the Hinge Region

The above results implicate HP1Swi6 in the checkpoint model as the H3K9 methylation "reader," yet it was not clear whether HP1Swi6 itself or any of its interacting proteins could capture heterochromatic RNAs. Whereas RNA-binding affinity has been demonstrated for mammalian HP1α (Muchardt et al., 2002), it was not known whether fission yeast HP1Swi6 can bind RNA directly. We purified recombinant HP1Swi6 and performed electrophoretic mobility shift assays (EMSA) using various RNA and DNA probes. In these assays, recombinant HP1Swi6 bound efficiently to the different RNAs but only weakly to DNA (Figure 3B). Furthermore, RNA binding could be competed with unlabeled RNA probes (Figure S3). HP1Swi6 consists of four domains: An N-terminal domain (NTD, residues 1–74), which is presumably flexibly disordered; a chromodomain (CD, residues 75–139), which binds K9-methylated histone tails (Bannister et al., 2001); a hinge region (H, residues 140–264); and a C-terminal chromo shadow domain (CSD, residues 265–328) (Cowieson et al., 2000). The hinge region of mammalian HP1α has been implicated in RNA binding (Muchardt et al., 2002). To test whether the hinge region also confers RNA binding

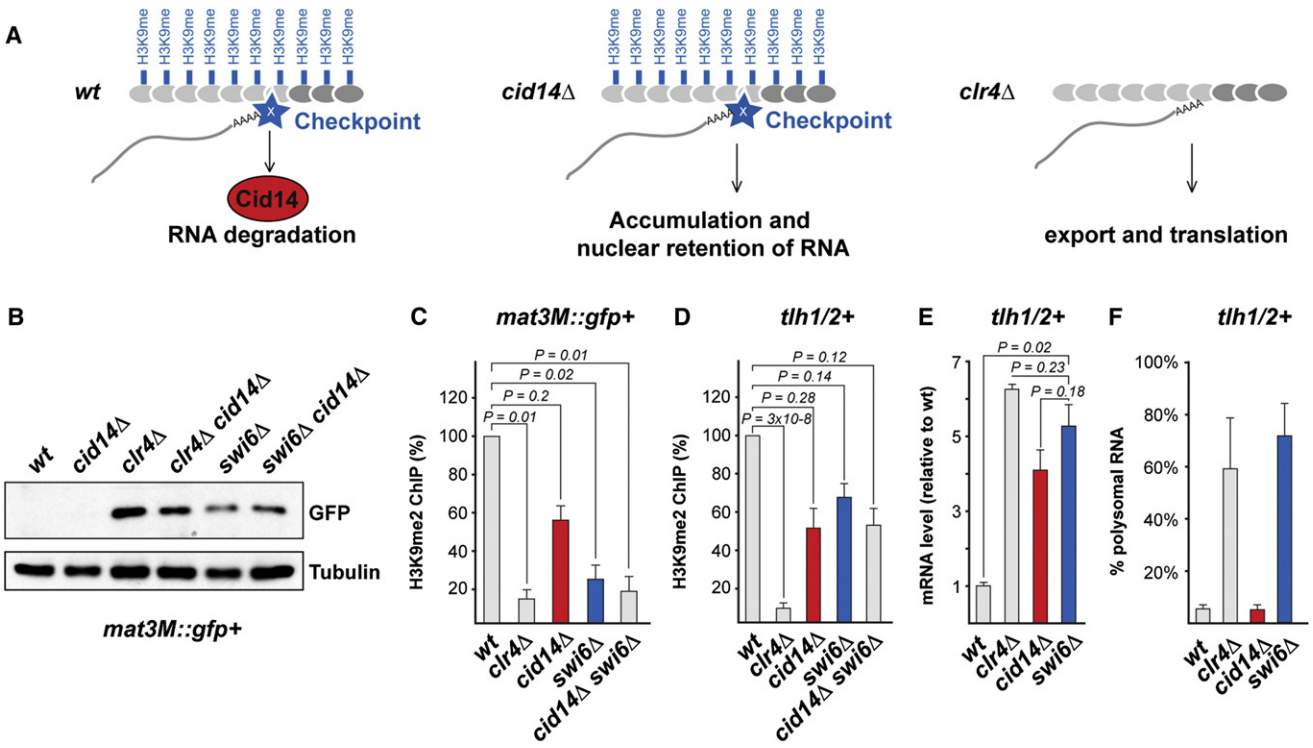

Figure 2. HP1Swi6 Prevents Translation of Heterochromatic RNAs

(A) Checkpoint model for the specific recognition of mRNA originating from heterochromatin. When H3K9 is unmethylated (*clr4Δ* or euchromatin), the checkpoint cannot assemble and mRNAs are exported and translated. In *WT* and *cid14Δ* cells, the checkpoint assembles on H3K9 methylated nucleosomes and captures heterochromatic mRNA transcripts. Eventually, these mRNAs are degraded in a Cid14-dependent manner. In the absence of Cid14 (*cid14Δ*), heterochromatic mRNAs accumulate but are not translated because they are retained by the checkpoint.

(B) Western blot showing GFP protein levels in *mat3M::gfp+* cells. Total protein from an equivalent number of cells was extracted by TCA. Tubulin served as a loading control.

(C and D) ChIP experiment showing that H3K9me2 levels at *mat3M::gfp+* are significantly reduced in *swi6Δ* and *cid14Δ swi6Δ* cells but not in *cid14Δ* cells. H3K9me2 levels at the telomeric *tlh1+* and *tlh2+* genes are not significantly reduced in *cid14Δ*, *swi6Δ*, and *cid14Δ swi6Δ* cells. Enrichment was determined by quantitative real-time PCR. Mean values normalized to *act1+* are shown (n = 4). Error bars represent SEM, p values were calculated using the Student's t test.

(E) *tlh1/2+* mRNA levels were determined by quantitative real-time RT-PCR. Mean values normalized to *act1+* are shown (n = 9). Error bars represent SEM, p values were calculated using the Student's t test.

(F) *tlh1/2+* mRNA associates with polysomes in *swi6Δ* but not in *cid14Δ* cells, although total mRNA levels are not significantly different in *swi6Δ* and *cid14Δ* cells (E). Enrichment of *tlh1/2+* mRNA in polysomal fractions of the indicated mutants was determined by polysome profiling as in Figure 1F. Error bars represent SEM.

properties to HP1Swi6, we purified recombinant CD, hinge, and CSD. In contrast to the CD and the CSD, the isolated hinge region was sufficient for strong RNA binding (Figure 3B). By using NMR chemical shift titrations monitored on amide resonances in the flexible hinge region, we determined the binding constant of full-length HP1Swi6 to a 20-mer RNA as 38 ± 13 μM (Figure 3C). These results demonstrate that HP1Swi6 is able to bind RNA alone and that the hinge region is substantially involved in this binding interaction.

Design of an HP1Swi6 Mutant that Affects RNA but Not H3K9me Binding

Because heterochromatin at certain loci disintegrates upon removal of the *swi6+* gene (Figure 2C), we aimed to develop an HP1Swi6 mutant with compromised RNA- but normal H3K9me-binding affinity. Therefore, we mutated the positively charged residues of the hinge region, 20 lysines and 5 arginines, to alanines (Figure 4A). For the resulting mutant protein, HP1Swi6-KR25A, RNA binding was indeed drastically reduced when compared to the wild-type protein (Figure 4B). For the subsequent use of the protein in vivo, we assessed the impact of these 25 mutations on protein architecture by solution NMR spectroscopy using recombinant HP1Swi6 and HP1Swi6-KR25A protein. Based on the full-length proteins and subconstructs thereof, we established complete sequence-specific resonance assignments for the isolated CD (residues 75–139) (Figure S4A), as well as domain-specific resonance assignments for the NTD, the hinge region, and the CSD of wild-type HP1Swi6. The chemical shift dispersion and intensities of the resonances in full-length HP1Swi6 indicated the CD and the CSD to be folded domains and the NTD and the hinge region to be flexibly unfolded polypeptide segments, as expected from predictions of the secondary structure. Analysis of the $^{13}C^{\alpha}$ and $^{13}C^{\beta}$ secondary chemical shifts of the isolated CD indicates three β-strands and one large α-helix at the C-terminal end of the domain (Figure S4E), which is well in agreement with the known

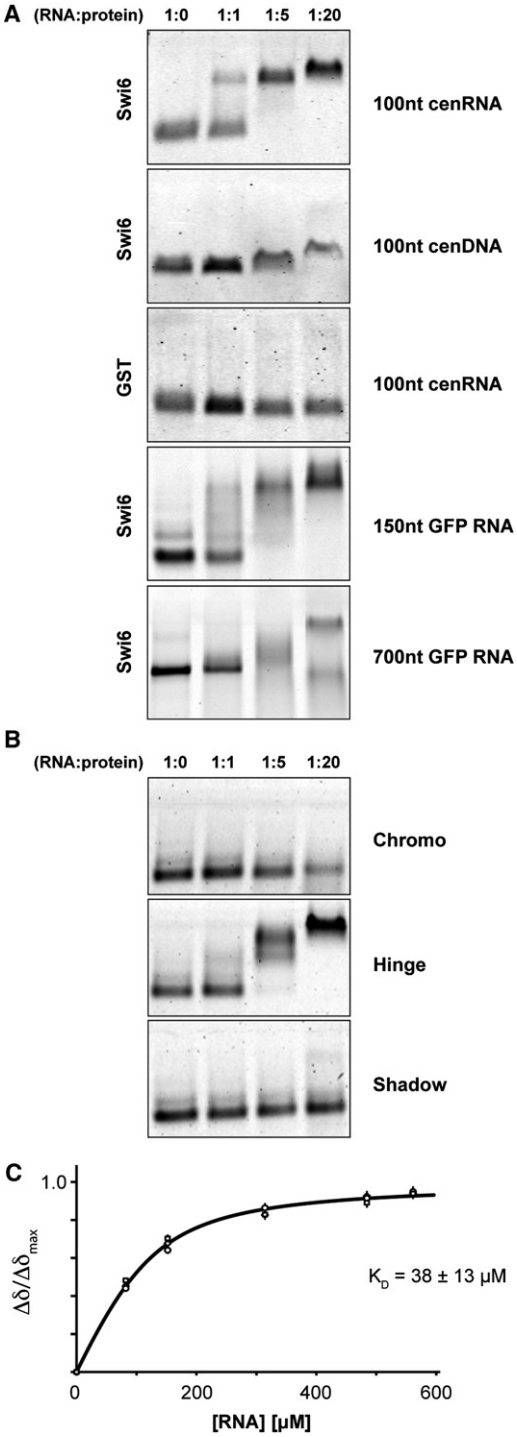

Figure 3. HP1^{Swi6} Is an RNA-Binding Protein

(A and B) Electrophoretic mobility shift assay (EMSA) using recombinant HP1^{Swi6}, HP1^{Swi6} subdomains or GST and different substrate nucleic acids (see Supplemental Information). RNA probes were labeled with fluorescein-UTP by in vitro transcription. DNA probes were produced by standard PCR. Protein-nucleic acid complexes were separated on 1.6%-TB agarose gels and the signal detected using a typhoon scanner.

(C) NMR chemical shift perturbation assay. The open circles are combined amide chemical shifts $\Delta\delta = \sqrt{0.04 \cdot \Delta\delta(^{15}\mathrm{N})^2 + \Delta\delta(^{1}\mathrm{H})^2}$ of three selected amide resonances plotted versus the RNA concentration. The line is the result of a nonlinear least-squares fit of a single binding curve to the data. The resulting dissociation constant K_D is indicated.

secondary structure elements in the homologous human chromobox homolog 3 (Kaustov et al., 2011). Importantly, 2D [^{15}N,^{1}H]-TROSY NMR spectra revealed the subspectra for the CD, the CSD, and the NTD, but not the hinge region of recombinant HP1^{Swi6}-KR25A, to be essentially identical to wild-type HP1^{Swi6} (Figures 4D and 4E). Thus, the 25 Lys and Arg to Ala mutations in the hinge region abolish RNA binding without affecting the global fold of the CD and CSD domains or having a structural effect on the unfolded NTD. Binding to methylated H3K9 is, therefore, expected to be maintained in the HP1^{Swi6}-KR25A mutant. This we could confirm by surface plasmon resonance (SPR) measurements (Figure 4C). The binding constants of wild-type and HP1^{Swi6}-KR25A to an immobilized peptide corresponding to residues 1–20 of a K9 trimethylated histone H3 tail (H3K9me3 peptide) (2.5 ± 0.5 μM and 7.8 ± 0.8 μM, respectively), were akin to and in correspondence with published values for the individual domains (Jacobs and Khorasanizadeh, 2002; Schalch et al., 2009).

Silencing but Not the Integrity of Heterochromatin Is Affected in the HP1^{Swi6} RNA-Binding Mutant

To study the functional relevance of RNA binding through the hinge region of HP1^{Swi6}, we replaced the endogenous *swi6+* open reading frame (ORF) with the HP1^{Swi6}-KR25A mutant ORF. Consistent with previous results that assigned a nuclear localization signal (NLS) function to the hinge region (Wang et al., 2000), we observed that the HP1^{Swi6}-KR25A protein localized mainly to the cytoplasm (Figure S5A and data not shown). Therefore, we added an N-terminal SV40 NLS to the wild-type and mutant HP1^{Swi6} alleles, which restored the characteristic heterochromatic foci in the nucleus and the specific association with RNA from heterochromatic regions (Figures 5A and S5B–S5F). Furthermore, in contrast to *swi6Δ* cells, neither NLS-HP1^{Swi6}- nor NLS-HP1^{Swi6}-KR25A-expressing cells were sensitive to thiabendazole (TBZ), showing that RNA binding to HP1^{Swi6} is not required for proper chromosome segregation (Figure 5B). Importantly, the H3K9 methylation defect observed at the *mat3M::gfp+* locus in *swi6Δ* cells (Figure 2C) was rescued by the *nls-swi6-KR25A* allele (Figure 5D). Similarly, H3K9 methylation within telomeric heterochromatin remained unaffected in *nls-swi6-KR25A* cells (Figures 5E and 5F).

These results demonstrate that neither H3K9 methylation nor recruitment of HP1^{Swi6} to heterochromatin depend on RNA binding through the hinge region of HP1^{Swi6}. However, silencing of heterochromatic genes was nonfunctional in *nls-swi6-KR25A* cells (Figures 5G–5J). Thus, RNA binding to HP1^{Swi6} is required for full repression of heterochromatic genes but dispensable for the integrity of heterochromatin. In summary, with *nls-swi6-KR25A* we created a separation-of-function allele of HP1^{Swi6} that fails to repress heterochromatic genes but still fulfills its architectural roles, with no impact on H3K9 methylation or chromosome segregation.

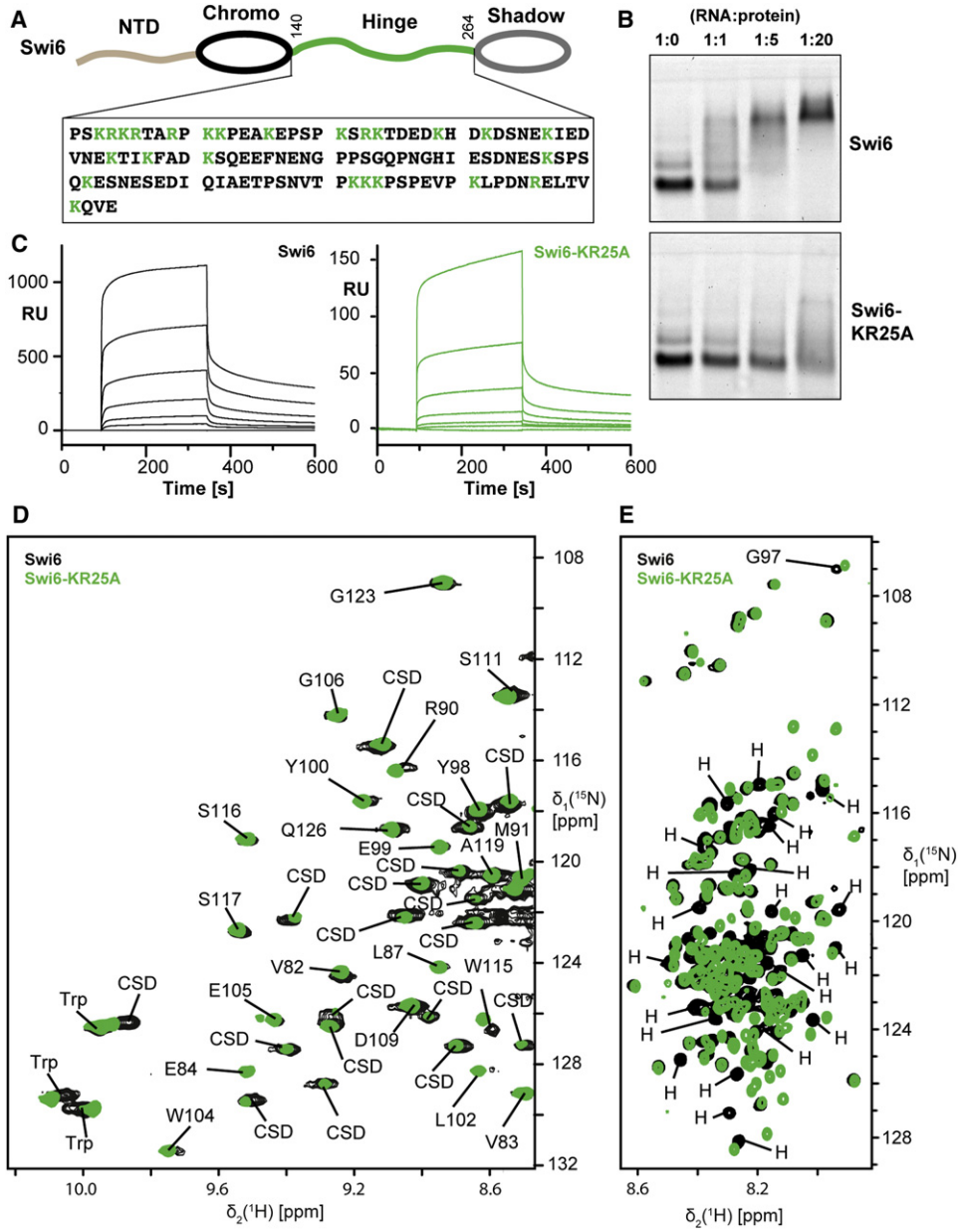

Figure 4. Characterization of HP1^{Swi6}-KR25A

(A) Domain architecture of HP1^{Swi6}. The two folded domains are indicated as ellipses, the two flexible domains as wavy lines. The amino acid sequence of the hinge region (residues 140–264) is given below. Lys and Arg residues that are mutated to Ala in the HP1^{Swi6}-KR25A protein are marked in green.

(B) EMSA showing that RNA binding of HP1^{Swi6}-KR25A is strongly impaired compared with the wild-type protein. A 100 nt centromeric RNA probe was used.

(C) SPR sensorgrams for binding of HP1^{Swi6} (black) and HP1^{Swi6}-KR25A (green) to an H3K9me3 surface. The protein concentrations are from bottom to top 0, 0.015, 0.047, 0.15, 0.43, 1.3, and 3.8 μM.

(D and E) Comparison of 2D [^{15}N,^{1}H]-TROSY correlation spectra of HP1^{Swi6} (black) and HP1^{Swi6}-KR25A (green). In (D), the downfield region of the spectrum is plotted at a low base level, showing mainly resonances from folded parts of the proteins. The sequence-specific resonance assignments for the CD and domain-specific assignments for the CSD (labeled "CSD") are indicated. In (E), the random-coil region of the same spectra are plotted at high base level, showing mainly resonances from the flexibly disordered NTD and hinge region. Domain-specific resonance assignments are shown for those resonances that are altered by the KR25A mutations. These are all located in the hinge region ("H"). The complete domain-specific resonance assignments are given in Figure S4.

HP1^{Swi6} Binding to K9 Methylated Histone H3 Is Highly Dynamic

Consistent with published results (Cheutin et al., 2004), fluorescence recovery after photobleaching (FRAP) experiments revealed that HP1^{Swi6} proteins are highly dynamic at the cellular ensemble level in vivo (Figure S5A). For proteins that are bound tightly to chromatin, recovery kinetics can be expected to be slow or not detectable, as observed for the telomere-binding

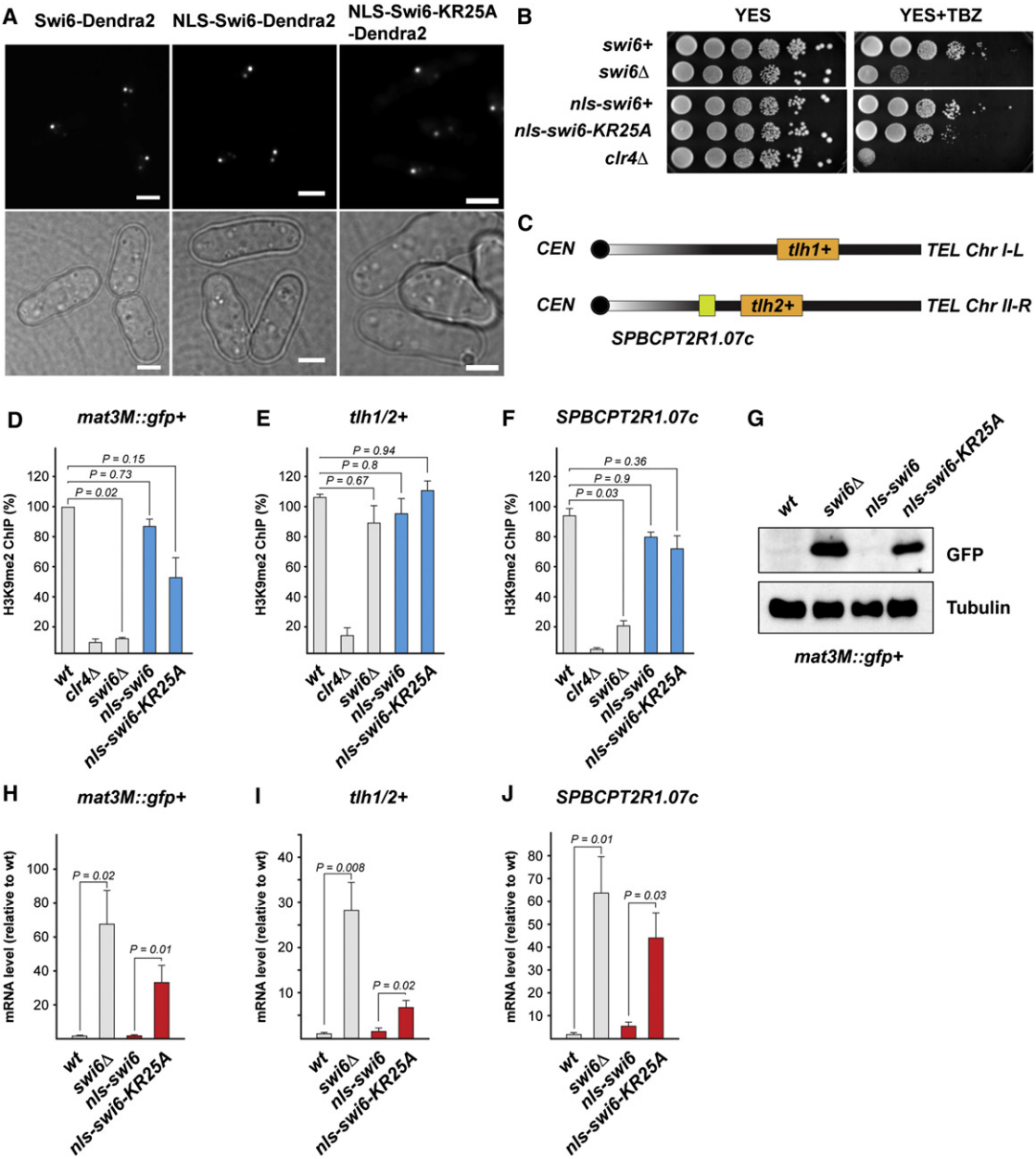

Figure 5. RNA Binding through the Hinge Region of HP1^{Swi6} Is Required for Silencing but Not Maintenance of Heterochromatin

(A) Microscopy of living *S. pombe* cells expressing C-terminally Dendra2-tagged HP1^{Swi6} variants driven from the endogenous promoter. Cells were grown in YES medium at 30°C. To restore nuclear localization of the HP1^{Swi6}-KR25A mutant (Figure S4), a SV40 NLS was added N-terminally. Scale bar = 2 μm.

(B) In contrast to *swi6*Δ cells, cells expressing the RNA-binding mutant NLS-HP1^{Swi6}-KR25A are not sensitive to thiabendazole (TBZ), indicating that chromosome segregation is normal. Cells were spotted on YES agar plates containing either 0 or 14 mg/l TBZ.

(C) Schematic diagram showing the location of three heterochromatic genes at the telomeres of chromosome I and II. *tlh1*+ and *tlh2*+ produce identical transcripts (Mandell et al., 2005). CEN, centromere; TEL, chromosome end.

(D–F) ChIP experiments demonstrating that H3K9me2 levels are not significantly reduced at *mat3M::gfp*+ (D), *tlh1/2*+ (E), and *SPBCPT2R1.07c* (F) in *nls-swi6*+ and *nls-swi6-KR25A* cells compared with wild-type cells. Mean values normalized to *act1*+ are shown (n = 4). Error bars represent SEM, p values were calculated using the Student's t test.

(G) Western blot showing GFP protein levels in *mat3M::gfp*+ cells. Total protein from an equivalent number of cells was extracted by TCA. Tubulin serves as a loading control.

(H–J) Quantitative real-time RT-PCR showing *mat3M::gfp*+ (I), *tlh1/2*+ (K), or SPBCPT2R1.07c (L) transcript levels in the respective mutants. Mean values normalized to *act1*+ are shown (n = 5). Error bars represent SEM, p values were generated using the Student's t test.

protein Taz1 (Figure S5B). This is not the case for HP1^{Swi6}, for which fluorescence recovered rapidly after photobleaching with an exponential lifetime of 1.8 ± 0.1 s (Figure S5C). This dynamic exchange of the HP1^{Swi6} ensemble from chromatin in vivo is qualitatively consistent with the rapid exchange dynamics we observed in NMR peptide titration experiments in vitro. We found that the resonances of the CD involved in H3K9me3 peptide binding underwent line broadening due to intermediate chemical exchange. This indicates kinetic on/off rates for the exchange between bound and unbound forms of individual HP1^{Swi6} molecules in the range of about 0.01–1.0 ms^{-1}, corresponding to lifetimes of 1–100 ms. These in vivo and in vitro data thus demonstrate the highly dynamic behavior of HP1^{Swi6} and rule out the possibility that individual HP1^{Swi6} molecules remain tightly bound to heterochromatin for minutes or longer. Therefore, HP1^{Swi6} alone cannot tether heterochromatic RNAs to chromatin.

Localization of the HP1^{Swi6} Interaction Sites with RNA and H3K9me

To obtain insight into the interactions of HP1^{Swi6} with RNA and methylated H3K9 at the atomic level, we used NMR chemical shift perturbation to identify residues structurally involved in these interactions. To this end, we monitored amide moiety chemical shifts, which are sensitive to structural changes of the polypeptide backbone. For the interaction of full-length HP1^{Swi6} with the H3K9me3 peptide, we observed chemical shift changes for 21 out of the 65 residues in the CD, as well as for one tryptophan side chain indole moiety (Figures 6A and 6B). The location of these residues in the amino acid sequence in HP1^{Swi6} corresponds to the location of the known binding pocket for the peptide in homologous domains (Jacobs and Khorasanizadeh, 2002; Kaustov et al., 2011; Nielsen et al., 2002). No significant chemical shift changes occurred for the backbone amide resonances of the CSD, but smaller chemical shift perturbations were observed for 8 residues of the N-terminal domain and 1 residue of the hinge region (Figure 6B). On the other hand, interaction with 20-mer-GFP RNA induced chemical shift changes for resonances of three different domains: 13 residues from the hinge region, 19 from the CD, and 10 from the N-terminal domain (Figures 6C and 6D). Furthermore, all resonances of the CD underwent line broadening at intermediate RNA concentrations due to intermediate exchange indicating kinetic on/off rate constants for RNA binding below about 1 ms^{-1}.

These data show that binding of RNA as well as binding of H3K9me3 peptide to HP1^{Swi6} occurs by a molecular mechanism that includes structural changes in three domains of HP1^{Swi6}. The observation that these interaction sites partially overlap thereby points toward the intriguing possibility that histone tail and RNA binding are not independent. Rather, these could be competitive processes, meaning that HP1^{Swi6} dissociates from H3K9-methylated nucleosomes when complexed with RNA. Consistent with this idea, steady-state competition assays using SPR showed competitive behavior (Figure 6E). At substoichiometric RNA:HP1^{Swi6} ratios, the initial SPR response increased. This can be rationalized by the dimeric nature of HP1^{Swi6} caused by its CSD, which leads to complexes with 2 RNA and 2 peptide-binding sites. At concentrations above stoichiometry, however, the SPR response decreased with increasing RNA concentration, indicating competition for the peptide surface. Importantly, the 20-mer GFP-RNA did not bind to the immobilized peptide surface in a control experiment under the same buffer conditions (Figure S6D). Furthermore, binding of the HP1^{Swi6} -KR25A mutant to H3K9me was insensitive and noncompetitive to the addition of RNA (Figures 6E and S6D).

In summary, our results implicate a mechanism by which RNA and methylated H3K9 compete for HP1^{Swi6} binding at the ensemble as well as the single-molecule level. Binding of RNA to HP1^{Swi6} structurally involves the hinge, the CD, and the NTD and impedes binding of HP1^{Swi6} to methylated H3K9. Thus, rather than tethering RNA to heterochromatin firmly, HP1^{Swi6} dynamically complexes with RNA and dissociates from H3K9-methylated nucleosomes.

Cid14 Functions in the Vicinity of Heterochromatin

The above results have established HP1^{Swi6} as a crucial constituent of hsRNPs, tagging RNAs as a result of their heterochromatic origin and priming them for degradation. Importantly, the dynamic properties of HP1^{Swi6} imply that the degradation of heterochromatic RNA originating from telomeres and the mating-type locus occurs off chromatin, but it is unclear whether Cid14 would join the hsRNP before or after dissociation from H3K9 methylated nucleosomes. If it would occur before dissociation from heterochromatin, it should be possible to crosslink Cid14 to telomeres or the mating-type locus. However, ChIP experiments did not show enrichment of Cid14 at these loci (data not shown), suggesting that Cid14 joins the HP1^{Swi6}/RNA complex only after dissociation from heterochromatin.

To test whether this still occurs in close proximity to heterochromatin, we employed the DNA adenine methyltransferase identification method (DamID, Figure 7A), a sensitive chromatin profiling technique that is suited to capture indirect or transient protein–chromatin interactions. We generated strains that express HP1^{Swi6} and Cid14 fused to the Dam DNA methyltransferase (Figure 7A; Woolcock et al., 2011) and assessed GATC methylation throughout the *S. pombe* genome using tiling arrays. As expected, HP1^{Swi6} was highly enriched at the mating-type locus, the centromeres, and the telomeric regions when compared to a Dam-only control (Figure 7B). Similarly, GATC methylation within the different heterochromatic regions was also observed for Dam-Cid14, demonstrating that Cid14 resides in close proximity to heterochromatin. Importantly, GATC methylation by Dam-Cid14 at the mating-type locus and telomeres is fully dependent on HP1^{Swi6} and not as strong as for Dam-HP1^{Swi6} (Figure 7C). This indicates that Cid14 joins hsRNPs after assembly and dissociation from heterochromatin at the mating-type region and the telomeres.

In conclusion, these results demonstrate that Cid14 resides in the vicinity of heterochromatin and that heterochromatic RNA originating from telomeres or the mating-type locus is delivered to Cid14 in a close spatial and temporal correlation to the dissociation of HP1^{Swi6} from H3K9-methylated nucleosomes. We speculate that the actual degradation of heterochromatic RNA might also occur near heterochromatin. The functional relevance of the HP1^{Swi6}-independent association of Cid14 with centromeric heterochromatin remains unknown.

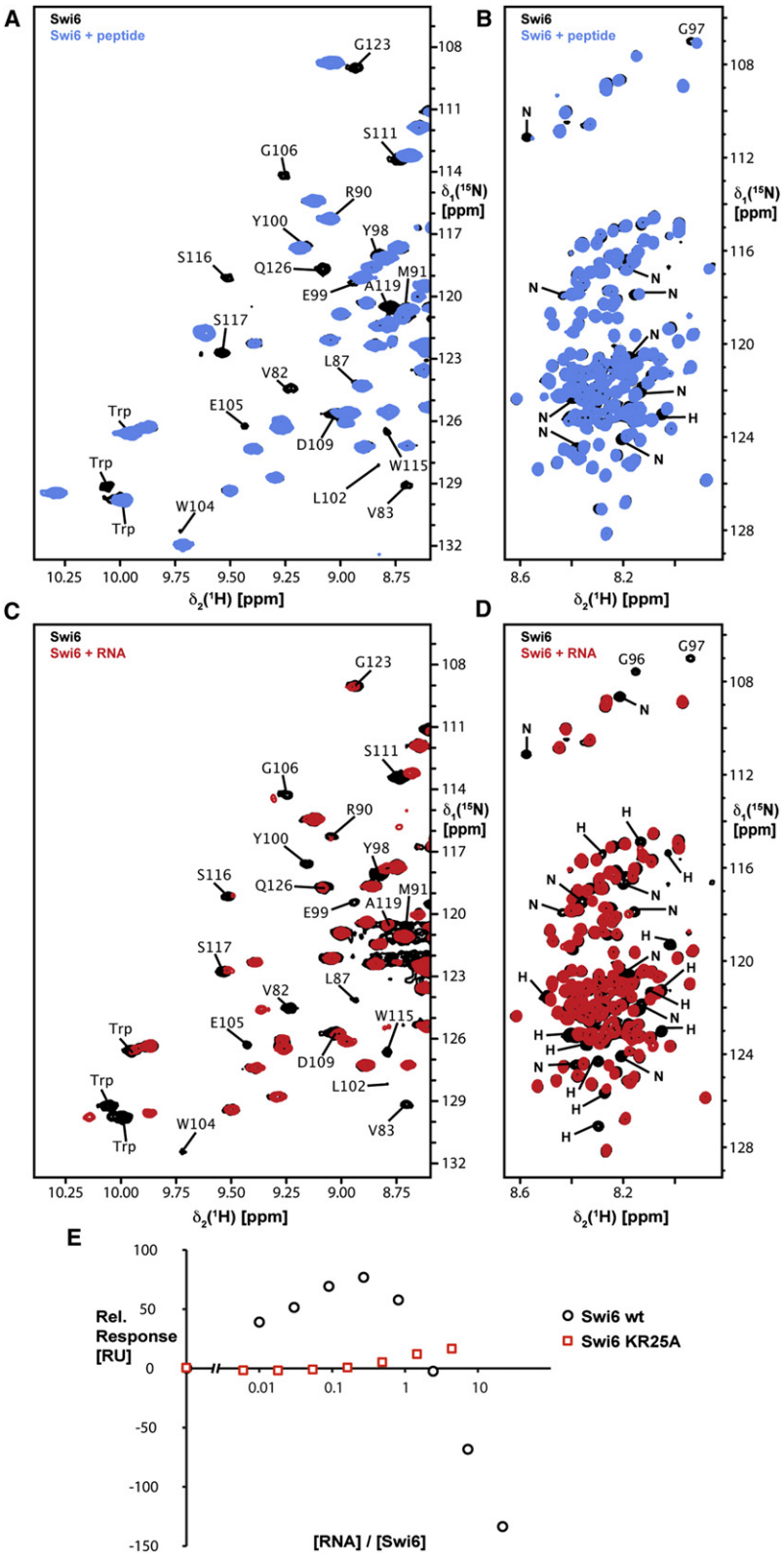

Figure 6. Localization and Competition of the HP1^{Swi6} Interactions

(A–D) Overlay of 2D [^{15}N,^{1}H]-TROSY correlation spectra of HP1^{Swi6}. The spectra are plotted in (A) and (C) at low base level, showing mainly resonance peaks from the two folded domains CD and CSD. The spectra are plotted in (B) and (D) at high base level, showing mainly resonances from the flexibly unfolded hinge and N-terminal domains. Residue type and number indicate sequence-specific resonance assignments for the CD. "H," "N," and "Trp" denote resonances from the hinge region, the NTD, and tryptophan side chains, respectively. (A and B) Black: HP1^{Swi6}; blue: 138 μM HP1^{Swi6} + 513 μM H3K9me3 peptide. (C and D) Black: HP1^{Swi6}; red: 95 μM HP1^{Swi6} + 560 μM RNA.

(E) SPR responses for competitive binding of H3K9me3 and RNA to HP1^{Swi6}. A constant concentration of 1 μM HP1^{Swi6} (black circles) or 5 μM HP1^{Swi6}-KR25A (red squares) with increasing concentrations of 20-mer GFP-RNA was injected to the H3K9me3 surface. The maximal SPR response after 200 s injection is plotted versus the RNA:protein concentration ratio. For each of the two proteins, the response in the absence of RNA was set to zero (raw data, see Figure S6D).

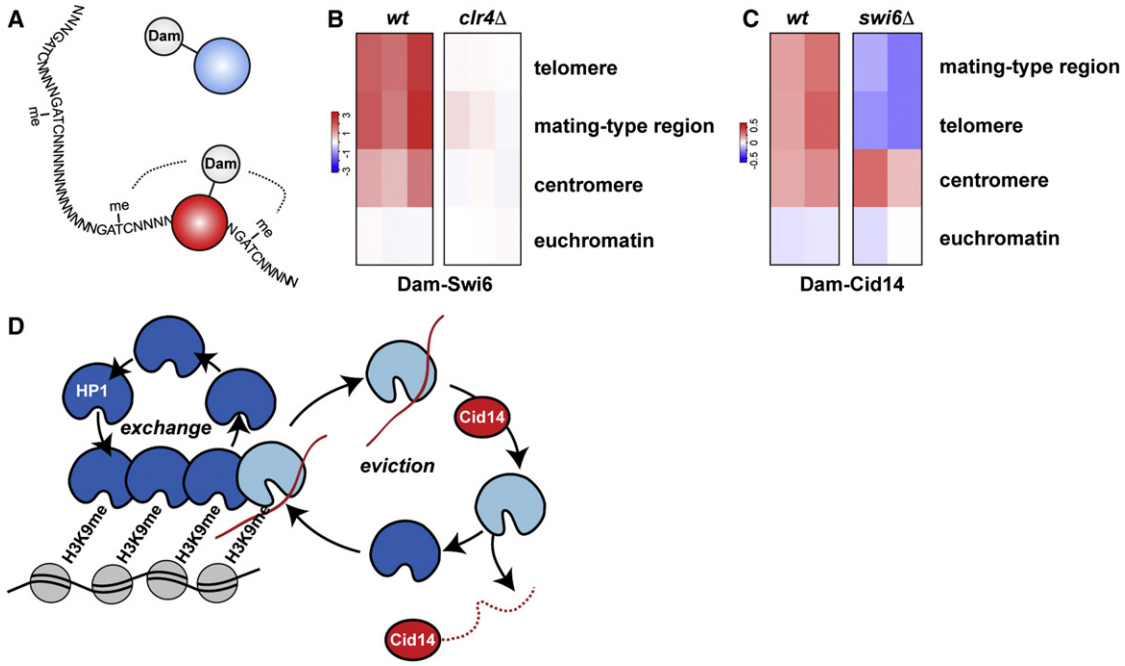

Figure 7. Cid14 Functions in the Vicinity of Heterochromatin

(A) In DamID, a Dam fusion protein is expressed at very low levels. On interaction of the fusion protein with chromatin (red), Dam methylates the adenine in the sequence context of GATC, which can be mapped by a methylation-specific PCR protocol.

(B and C) HP1^{Swi6} and Cid14 enrichments from DamID experiments (log_2) at chromosomal regions.

(D) Model for HP1^{Swi6}-mediated degradation of heterochromatic RNA. HP1^{Swi6} proteins associate with H3K9-methylated nucleosomes (gray) only transiently and readily exchange from heterochromatin (dark blue). This continuous exchange of HP1^{Swi6} prevents saturation of heterochromatin with RNA. In case transcription within heterochromatin occurs, HP1^{Swi6} binds the newly synthesized RNA (red) and dissociates from H3K9 methylated nucleosomes as a result of competition between RNA and the histone tail for HP1^{Swi6} binding (light blue). Subsequently, the RNA is passed on to Cid14 (red), which in turn initiates RNA degradation.

DISCUSSION

Association of HP1 Proteins with RNA

It was recognized earlier that proteins involved in chromatin regulation have the ability to bind RNA, although the functional relevance of this interaction has remained elusive. RNA binding was first demonstrated for the CDs of MOF and MSL-3, proteins involved in dosage compensation in *Drosophila* (Akhtar et al., 2000). For mammalian HP1α, the hinge region has been implicated in RNA binding (Muchardt et al., 2002). Here we demonstrate that HP1^{Swi6}, the fission yeast homolog of HP1α, can also bind RNA directly. Importantly, we have found that the interaction of HP1^{Swi6} with RNA mechanistically includes the hinge region, the CD, and the NTD, a property that could be easily overlooked when working with isolated domains. Therefore, it will be interesting to revisit the RNA-binding properties of other HP1 proteins, such as mammalian HP1α, β, or γ, by approaches similar to those in this study. It might be that different HP1 isoforms display important differences in their interaction with RNA, which could reveal novel insights into their functional diversification. It will also be very interesting to elucidate the structural basis of the RNA and peptide binding of HP1^{Swi6} at the atomic level, which should give additional insights into the biophysical nature of their competitive binding mechanism.

It has been speculated that the functional relevance of the RNA affinities of HP1α or the dosage compensation complex might be the targeting to chromatin by major satellite or roX noncoding RNAs, respectively (Akhtar et al., 2000; Maison et al., 2002, 2011). In such a model, RNA is proposed to be involved structurally in the assembly of a higher order chromatin structure by serving as a recruitment platform. This is unlikely to apply to *S. pombe* HP1^{Swi6}, as neither H3K9 methylation nor recruitment of HP1^{Swi6} to heterochromatin depends on RNA binding. In contrast, RNA bound to HP1^{Swi6} dissociates from chromatin as a result of exchange with the cellular HP1^{Swi6} ensemble and a decrease in affinity for methylated H3K9.

Stable Repression of Heterochromatin through RNA Sequestration and Degradation

The results of our work reinforce previous findings that heterochromatin is not always refractory to transcription, yet is tightly repressed. We demonstrate here that HP1^{Swi6} assures coupling between heterochromatin transcription and RNA turnover by serving as an H3K9 methylation-specific checkpoint. Based on the data presented, we propose a model for the action of the HP1^{Swi6} ensemble, which dynamically exchanges with the bulk in a maintenance cycle. Free RNA is captured in the eviction cycle and passed on to the degradation machinery. Constant flux of RNA-unbound HP1^{Swi6} from the bulk ensemble prevents

saturation of heterochromatin with RNA. Competition between RNA and methylated H3K9 for HP1^{Swi6} binding at the ensemble level guarantees that RNA-free HP1^{Swi6} is preferably recruited to heterochromatin, thereby sustaining a functional checkpoint on the H3K9-methylated nucleosome and ensuring constant turnover of heterochromatic RNAs (Figure 7C).

In our model, HP1^{Swi6} functions on chromatin to bind to and assemble emerging heterochromatic transcripts into special RNPs, which we refer to as hsRNPs. Thereby, HP1^{Swi6} guarantees specific and tight repression of heterochromatic genes on at least two levels. First, HP1^{Swi6} prevents protein synthesis by sequestration of mRNAs from ribosomes, most likely through nuclear retention. Thus, a heterochromatic mRNA remains repressed even in the absence of RNA degradation. This explains why classical PEV screens failed to recover RNA decay factors such as Cid14. Notably, Cid14 itself is involved in the processing of ribosomal RNA and also associates with 60S ribosomal proteins (Keller et al., 2010; Win et al., 2006), raising the possibility that loss of Cid14 might result in a general defect in translation. However, association of euchromatic mRNAs with polyribosomes, as well as protein expression levels, remain unaffected in *cid14Δ* cells (Figure 1 and data not shown), strongly arguing against such an indirect effect. Second, the HP1^{Swi6} ensemble ensures elimination of heterochromatic mRNAs by capturing the RNA at the site of transcription and escorting it to the degradation machinery. Rather than the classical features of an aberrant RNA, such as a truncated open reading frame or defective 5′ or 3′ ends, our data suggests that it is the physical association of a heterochromatic mRNA with HP1^{Swi6} that primes it for destruction. We note that artificial tethering of HP1^{Swi6} to a euchromatic mRNA does not result in RNA degradation (data not shown), suggesting that canonical mRNPs are immune to HP1^{Swi6}-mediated RNA turnover. Furthermore, since the kinetics of RNA binding to HP1^{Swi6} are fast, the hsRNPs may be stabilized by additional factors. However, at this point we can only speculate on such contributions by additional proteins or other molecules.

Concluding Remarks

In this study, we have discovered a function for one of the fission yeast HP1 proteins that provides the missing link between transcriptional origin and Cid14-dependent degradation of heterochromatic mRNAs. Our results highlight the role of RNA as a negative regulator of HP1^{Swi6} binding to chromatin and provide insights into the repression of heterochromatic domains at a posttranscriptional level. The high degree of conservation of HP1 proteins and heterochromatin-mediated gene silencing phenomena suggest that our findings may also apply to other eukaryotes.

Our work has revealed that HP1^{Swi6}, in addition to its role in proper centromere function, also guarantees tight repression of heterochromatic genes through RNA sequestration and degradation. Interestingly, the *Drosophila* HP1 protein Rhino has been linked recently to the piRNA pathway (Klattenhoff et al., 2009). In analogy to our checkpoint model, Rhino may bind the initial sense transcript at the heterochromatic transposon locus and subsequently escort it to the perinuclear "nuage" structure, where it can enter the ping-pong amplification cycle. Thus, rather than forming repressive chromatin, Rhino might specify the recognition and ensure efficient elimination of transposon RNA.

Finally, our results add another layer of complexity to the crosstalk between RNA and chromatin. In contrast to the emerging theme that RNA can serve as a scaffold to assemble, recruit, or guide chromatin-modifying complexes to their respective targets (Wang and Chang, 2011), we demonstrate that they may also function as "repellents." RNA-mediated eviction might be a possible mechanism that counteracts HP1 spreading along the chromatin fiber or the formation of ectopic heterochromatin. Importantly, neither coding potential nor stability is important for an RNA to function as a repellent, offering a possible molecular function for the many short-lived, low-abundant noncoding RNAs that are present in the eukaryotic cell.

EXPERIMENTAL PROCEDURES

Strains and Plasmids

Fission yeast strains and plasmids used in this study are described in Supplemental Information.

Western Blot and Polysome Profiling

Total proteins from exponentially growing cells were extracted using TCA and separated by SDS-PAGE. Antibodies for western blotting were used at the following concentrations: GFP (Roche; 1:3000), tubulin (Woods et al., 1989; 1:5000), Swi6 (Bioacademia; 1:10,000). Polysome profiling is described in Supplemental Information.

Chromatin Immunoprecipitation and Gene Expression Analysis

RNA isolation, cDNA synthesis, and quantitative RT-PCR was performed as described in Emmerth et al. (2010). Chromatin immunoprecipitation (ChIP) was performed as described in Bühler et al. (2006), using 2.5 μg of an antibody against dimethylated H3K9 (Kimura et al., 2008).

Electrophoretic Mobility Shift Assay (EMSA)

The desired amount of protein was diluted into 9 μl of 1 × electrophoretic mobility shift assay (EMSA) buffer (20 mM HEPES-KOH [pH 7.5], 100 mM KCl, 0.05% NP-40) and incubated for 10 min at RT. The substrate was added, incubated at 30°C for 30 min, and followed by gel electrophoresis (1.6% TB-agarose). Fluorescently labeled RNA was detected using a TyphoonTM 9400 Gel Scanner. RNA labeling is described in Supplemental Information.

Recombinant Protein Expression and Purification for NMR

Expression and purification was performed as described in Supplemental Information with the following modifications. Bacteria were grown in 6 l of M9 minimal medium containing ^{15}N-NH_4Cl as a nitrogen source. Induction was carried out using 0.5 mM IPTG. The lysate was incubated with 10 ml of glutathione-sepharose FF (GE). The protein was released from the glutathione-resin by TEV-cleavage o/n at 4°C using acTEV (Invitrogen). This was followed by Source15Q ion exchange chromatography (GE Healthcare). The purification was completed by size exclusion chromatography (Superdex 200; GE Healthcare) in 50 mM MES pH 6.5, 100 mM KCl, 5 mM DTT. The purified complex was concentrated to 100 μM by centrifugal filtration.

Solution NMR Spectroscopy and SPR

NMR experiments were performed on Bruker 800 MHz and 600 MHz spectrometers. The sequence-specific resonance assignments for the isolated HP1^{Swi6} CD (residues 75–139) were obtained from the two APSY-type experiments 4D APSY-HNCACB (15 projections) and 5D APSY-HNCOCACB (16 projections) (Gossert et al., 2011; Hiller et al., 2005, 2007) and subsequent automated backbone assignment by the algorithm MATCH (Volk et al., 2008). For SPR, samples were analyzed using a Biacore T-100 instrument (GE Healthcare). Further details are given in Supplemental Information.

DamID

DamID was carried out as previously published (Woolcock et al., 2011). Coordinates of heterochromatic regions are given in Supplemental Information.

ACCESSION NUMBERS

DamID data sets were deposited under accession number GSE36956 (NCBI Gene Expression Omnibus).

SUPPLEMENTAL INFORMATION

Supplemental Information includes six figures, Supplemental Experimental Procedures, Supplemental References, and five tables and can be found with this article online at doi:10.1016/j.molcel.2012.05.009.

ACKNOWLEDGMENTS

We are grateful to Yukiko Shimada, Nathalie Laschet, Sébastien Morin, Larisa Kapinos, and Alvar Gossert for technical assistance and discussions; Ben Hurschler and Helge Grosshans for help with polysome profiling; Tessi Iida for sharing protocols; Antoine Peters for peptides; the Nicolas Thomä lab, i.e., Andrea Scrima, Eric Fischer, and Mahamadou Faty, for technical advice and sharing awesome equipment; Laurent Gelman for assistance with FRAP analysis; and Heinz Gut and Hans-Rudolf Hotz for help with domain mappings and bioinformatics. Research in the lab of M.B. is supported by the Swiss National Science Foundation, the European Research Council, and the Gebert Rüf Stiftung. The Friedrich Miescher Institute for Biomedical Research is supported by the Novartis Research Foundation. Research in the lab of S.H. is supported by the Swiss National Science Foundation. R.A. acknowledges the Werner-Siemens Foundation.

Received: December 23, 2011
Revised: March 21, 2012
Accepted: May 3, 2012
Published online: June 7, 2012

REFERENCES

Akhtar, A., Zink, D., and Becker, P.B. (2000). Chromodomains are protein-RNA interaction modules. Nature *407*, 405–409.

Bannister, A.J., Zegerman, P., Partridge, J.F., Miska, E.A., Thomas, J.O., Allshire, R.C., and Kouzarides, T. (2001). Selective recognition of methylated lysine 9 on histone H3 by the HP1 chromo domain. Nature *410*, 120–124.

Bernard, P., Maure, J.F., Partridge, J.F., Genier, S., Javerzat, J.P., and Allshire, R.C. (2001). Requirement of heterochromatin for cohesion at centromeres. Science *294*, 2539–2542.

Bühler, M. (2009). RNA turnover and chromatin-dependent gene silencing. Chromosoma *118*, 141–151.

Bühler, M., Verdel, A., and Moazed, D. (2006). Tethering RITS to a nascent transcript initiates RNAi- and heterochromatin-dependent gene silencing. Cell *125*, 873–886.

Bühler, M., Haas, W., Gygi, S.P., and Moazed, D. (2007). RNAi-dependent and -independent RNA turnover mechanisms contribute to heterochromatic gene silencing. Cell *129*, 707–721.

Cheutin, T., McNairn, A.J., Jenuwein, T., Gilbert, D.M., Singh, P.B., and Misteli, T. (2003). Maintenance of stable heterochromatin domains by dynamic HP1 binding. Science *299*, 721–725.

Cheutin, T., Gorski, S.A., May, K.M., Singh, P.B., and Misteli, T. (2004). In vivo dynamics of Swi6 in yeast: evidence for a stochastic model of heterochromatin. Mol. Cell. Biol. *24*, 3157–3167.

Cowieson, N.P., Partridge, J.F., Allshire, R.C., and McLaughlin, P.J. (2000). Dimerisation of a chromo shadow domain and distinctions from the chromodomain as revealed by structural analysis. Curr. Biol. *10*, 517–525.

Ekwall, K., Javerzat, J.P., Lorentz, A., Schmidt, H., Cranston, G., and Allshire, R. (1995). The chromodomain protein Swi6: a key component at fission yeast centromeres. Science *269*, 1429–1431.

Emmerth, S., Schober, H., Gaidatzis, D., Roloff, T., Jacobeit, K., and Bühler, M. (2010). Nuclear retention of fission yeast dicer is a prerequisite for RNAi-mediated heterochromatin assembly. Dev. Cell *18*, 102–113.

Festenstein, R., Pagakis, S.N., Hiragami, K., Lyon, D., Verreault, A., Sekkali, B., and Kioussis, D. (2003). Modulation of heterochromatin protein 1 dynamics in primary Mammalian cells. Science *299*, 719–721.

Fischer, T., Cui, B., Dhakshnamoorthy, J., Zhou, M., Rubin, C., Zofall, M., Veenstra, T.D., and Grewal, S.I. (2009). Diverse roles of HP1 proteins in heterochromatin assembly and functions in fission yeast. Proc. Natl. Acad. Sci. USA *106*, 8998–9003.

Gossert, A.D., Hiller, S., and Fernández, C. (2011). Automated NMR resonance assignment of large proteins for protein-ligand interaction studies. J. Am. Chem. Soc. *133*, 210–213.

Grewal, S.I., and Jia, S. (2007). Heterochromatin revisited. Nat. Rev. Genet. *8*, 35–46.

Gullerova, M., and Proudfoot, N.J. (2008). Cohesin complex promotes transcriptional termination between convergent genes in S. pombe. Cell *132*, 983–995.

Hiller, S., Fiorito, F., Wüthrich, K., and Wider, G. (2005). Automated projection spectroscopy (APSY). Proc. Natl. Acad. Sci. USA *102*, 10876–10881.

Hiller, S., Wasmer, C., Wider, G., and Wüthrich, K. (2007). Sequence-specific resonance assignment of soluble nonglobular proteins by 7D APSY-NMR spectroscopy. J. Am. Chem. Soc. *129*, 10823–10828.

Jacobs, S.A., and Khorasanizadeh, S. (2002). Structure of HP1 chromodomain bound to a lysine 9-methylated histone H3 tail. Science *295*, 2080–2083.

Jacobs, S.A., Taverna, S.D., Zhang, Y., Briggs, S.D., Li, J., Eissenberg, J.C., Allis, C.D., and Khorasanizadeh, S. (2001). Specificity of the HP1 chromo domain for the methylated N-terminus of histone H3. EMBO J. *20*, 5232–5241.

James, T.C., and Elgin, S.C. (1986). Identification of a nonhistone chromosomal protein associated with heterochromatin in Drosophila melanogaster and its gene. Mol. Cell. Biol. *6*, 3862–3872.

Kaustov, L., Ouyang, H., Amaya, M., Lemak, A., Nady, N., Duan, S., Wasney, G.A., Li, Z., Vedadi, M., Schapira, M., et al. (2011). Recognition and specificity determinants of the human cbx chromodomains. J. Biol. Chem. *286*, 521–529.

Keller, C., Woolcock, K., Hess, D., and Bühler, M. (2010). Proteomic and functional analysis of the noncanonical poly(A) polymerase Cid14. RNA *16*, 1124–1129.

Kimura, H., Hayashi-Takanaka, Y., Goto, Y., Takizawa, N., and Nozaki, N. (2008). The organization of histone H3 modifications as revealed by a panel of specific monoclonal antibodies. Cell Struct. Funct. *33*, 61–73.

Klattenhoff, C., Xi, H., Li, C., Lee, S., Xu, J., Khurana, J.S., Zhang, F., Schultz, N., Koppetsch, B.S., Nowosielska, A., et al. (2009). The Drosophila HP1 homolog Rhino is required for transposon silencing and piRNA production by dual-strand clusters. Cell *138*, 1137–1149.

Lachner, M., O'Carroll, D., Rea, S., Mechtler, K., and Jenuwein, T. (2001). Methylation of histone H3 lysine 9 creates a binding site for HP1 proteins. Nature *410*, 116–120.

Maison, C., Bailly, D., Peters, A.H., Quivy, J.P., Roche, D., Taddei, A., Lachner, M., Jenuwein, T., and Almouzni, G. (2002). Higher-order structure in pericentric heterochromatin involves a distinct pattern of histone modification and an RNA component. Nat. Genet. *30*, 329–334.

Maison, C., Bailly, D., Roche, D., Montes de Oca, R., Probst, A.V., Vassias, I., Dingli, F., Lombard, B., Loew, D., Quivy, J.P., and Almouzni, G. (2011). SUMOylation promotes de novo targeting of HP1α to pericentric heterochromatin. Nat. Genet. *43*, 220–227.

Mandell, J.G., Bähler, J., Volpe, T.A., Martienssen, R.A., and Cech, T.R. (2005). Global expression changes resulting from loss of telomeric DNA in fission yeast. Genome Biol. *6*, R1.

Motamedi, M.R., Hong, E.J., Li, X., Gerber, S., Denison, C., Gygi, S., and Moazed, D. (2008). HP1 proteins form distinct complexes and mediate heterochromatic gene silencing by nonoverlapping mechanisms. Mol. Cell *32*, 778–790.

Muchardt, C., Guilleme, M., Seeler, J.S., Trouche, D., Dejean, A., and Yaniv, M. (2002). Coordinated methyl and RNA binding is required for heterochromatin localization of mammalian HP1alpha. EMBO Rep. *3*, 975–981.

Nakayama, J., Rice, J.C., Strahl, B.D., Allis, C.D., and Grewal, S.I. (2001). Role of histone H3 lysine 9 methylation in epigenetic control of heterochromatin assembly. Science *292*, 110–113.

Nielsen, P.R., Nietlispach, D., Mott, H.R., Callaghan, J., Bannister, A., Kouzarides, T., Murzin, A.G., Murzina, N.V., and Laue, E.D. (2002). Structure of the HP1 chromodomain bound to histone H3 methylated at lysine 9. Nature *416*, 103–107.

Nonaka, N., Kitajima, T., Yokobayashi, S., Xiao, G., Yamamoto, M., Grewal, S.I., and Watanabe, Y. (2002). Recruitment of cohesin to heterochromatic regions by Swi6/HP1 in fission yeast. Nat. Cell Biol. *4*, 89–93.

Schalch, T., Job, G., Noffsinger, V.J., Shanker, S., Kuscu, C., Joshua-Tor, L., and Partridge, J.F. (2009). High-affinity binding of Chp1 chromodomain to K9 methylated histone H3 is required to establish centromeric heterochromatin. Mol. Cell *34*, 36–46.

Smothers, J.F., and Henikoff, S. (2000). The HP1 chromo shadow domain binds a consensus peptide pentamer. Curr. Biol. *10*, 27–30.

Volk, J., Herrmann, T., and Wüthrich, K. (2008). Automated sequence-specific protein NMR assignment using the memetic algorithm MATCH. J. Biomol. NMR *41*, 127–138.

Wang, K.C., and Chang, H.Y. (2011). Molecular mechanisms of long noncoding RNAs. Mol. Cell *43*, 904–914.

Wang, G., Ma, A., Chow, C.M., Horsley, D., Brown, N.R., Cowell, I.G., and Singh, P.B. (2000). Conservation of heterochromatin protein 1 function. Mol. Cell. Biol. *20*, 6970–6983.

Wang, S.W., Stevenson, A.L., Kearsey, S.E., Watt, S., and Bähler, J. (2008). Global role for polyadenylation-assisted nuclear RNA degradation in posttranscriptional gene silencing. Mol. Cell. Biol. *28*, 656–665.

Win, T.Z., Draper, S., Read, R.L., Pearce, J., Norbury, C.J., and Wang, S.W. (2006). Requirement of fission yeast Cid14 in polyadenylation of rRNAs. Mol. Cell. Biol. *26*, 1710–1721.

Woods, A., Sherwin, T., Sasse, R., MacRae, T.H., Baines, A.J., and Gull, K. (1989). Definition of individual components within the cytoskeleton of Trypanosoma brucei by a library of monoclonal antibodies. J. Cell Sci. *93*, 491–500.

Woolcock, K.J., Gaidatzis, D., Punga, T., and Bühler, M. (2011). Dicer associates with chromatin to repress genome activity in Schizosaccharomyces pombe. Nat. Struct. Mol. Biol. *18*, 94–99.

Molecular Cell, Volume *47*

Supplemental Information

HP1^{Swi6} Mediates the Recognition and Destruction of Heterochromatic RNA Transcripts

Claudia Keller, Ricardo Adaixo, Rieka Stunnenberg, Katrina J. Woolcock, Sebastian Hiller, and Marc Bühler

Supplemental Data

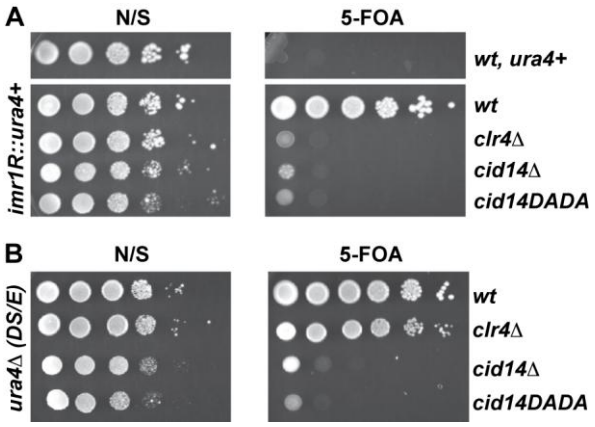

Figure S1, Related to Figure1. The Noncanonical PolyA-polymerase Cid14 Confers Resistance to 5-FOA

(A and B) Cells were spotted on PMG agar plates containing either 0 or 2 mg/L 5-FOA. The *ura4+* gene encodes orotidine 5'-phosphate decarboxylase, which converts 5-FOA to toxic 5-fluorouracil. Therefore, cells can only grow on 5-FOA containing medium if the *ura4+* gene is absent or silenced.

(A) Growth on 5-FOA containing medium indicates that the centromeric *ura4+* reporter (*imr1R::ura4+*) is efficiently silenced by heterochromatin. Deletion of the gene encoding the histone H3 methyltransferase Clr4 (*clr4*Δ) disrupts heterochromatin and silencing of *imr1R::ura4+* is lost. Similar to *clr4*Δ cells, cells lacking the *cid14+* gene or cells expressing a catalytically inactive Cid14 (*cid14DADA*) cannot grow on 5-FOA.

(B) Cells lacking a functional *ura4+* gene (*ura4DS/E*) grow on 5-FOA media in the absence of heterochromatin (*clr4*Δ), but not in the absence of Cid14 (*cid14*Δ) or if Cid14 has lost its polyadenylation activity (*cid14DADA).* Therefore, the inability of *imr1R::ura4+* cells to grow on 5-FOA when expressing *cid14*$^{+}$ mutants (A) is unlikely to result from defective heterochromatin silencing. Rather, 5-FOA is converted into 5-fluorouracil or another toxic substance by a *ura4+*-independent, endogenous pathway that becomes activated in the absence of Cid14. Alternatively, 5-FOA itself is toxic, but is usually degraded by an enzyme that is only expressed in the presence of functional Cid14.

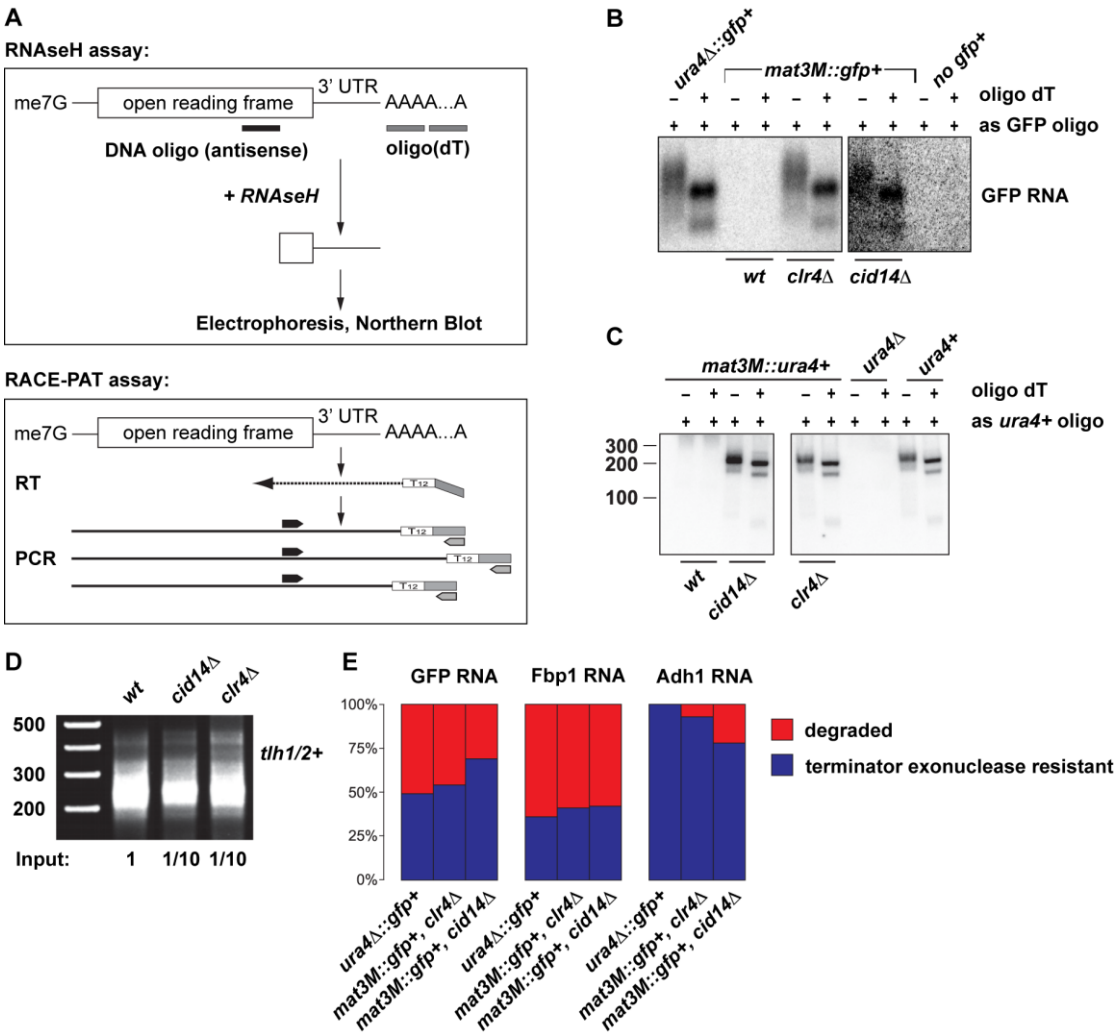

Figure S2, Related to Figure 2. Heterochromatic mRNAs Are Properly Processed

(A) Schematic diagram outlining RNAseH and RACE-PAT assays, which were used to assess the polyadenylation status of heterochromatic RNAs in different mutants.

(B) Evaluation of the polyadenylation status of heterochromatic *mat3M::gfp+* mRNAs by the RNaseH assay. Total RNA was separated on an agarose gel and transferred to a nylon membrane. GFP RNA was detected using specific ^{32}P-labelled DNA oligos. In the presence of oligodT (+oligodT), polyA tails are degraded by RNAseH. The appearance of two bands upon polyA tail removal is consistent with the presence of two major polyadenylation sites in the Tadh1 terminator present in this *gfp+* reporter. As expected, the distal site is used more frequently. The smear in the -oligodT lanes indicates the heterogenous polyA tail length of the GFP mRNA. Importantly, no major qualitative differences can be observed for euchromatic or heterochromatic GFP mRNAs in *wt, clr4Δ, or cid14Δ* cells.

(C) The polyadenylation status of heterochromatic *mat3M::ura4+* mRNAs was assessed as in B. Instead of agarose, polyacrylamide was used to separate RNAseH treated RNA.

(D) RACE-PAT assay to determine the polyadenylation state of *tlh1/2+* mRNAs. 1/10th of the RT reaction was used as input for the PCR in *cid14Δ* and *clr4Δ* cells.

(E) Total RNA was extracted from cells expressing either *gfp+* from a euchromatic (*ura4Δ::gfp+*) or heterochromatic (*mat3M::gfp+*) locus. The RNA was subsequently treated with terminator 5'-phosphate dependent exonuclease, which selectively degrades 5'-monophosphorylated RNA, while leaving 5'-me7G-capped RNA intact. The efficiency of the reaction was determined by comparing the amount of degraded 25S and 18S RNA (5'-monophosphorylated) versus 5S RNA (stable) on a Agilent Total RNA Nano Chip. The relative amount of a given RNA was quantified in untreated and exonuclease-treated samples by quantitative real-time RT-PCR. The terminator exonuclease resistant population reflects the relative amount of 5'-me7G-capped RNA.

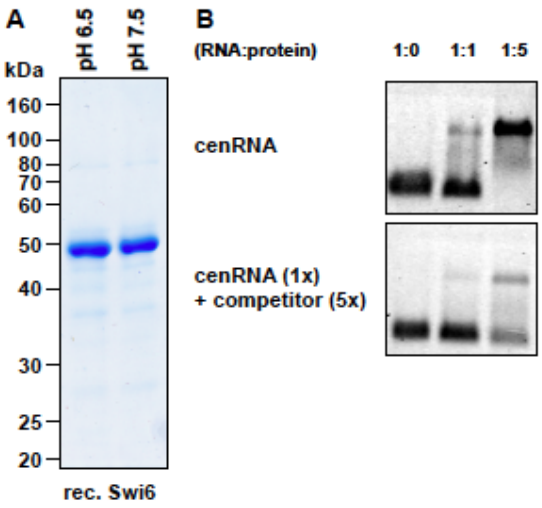

Figure S3, Related to Figure 3. HP1^{Swi6} Is an RNA-Binding Protein
(A) SDS-PAGE of the recombinant HP1^{Swi6} proteins that were used for NMR and SPR (pH 6.5), or EMSA (pH 7.5).
(B) EMSA demonstrating that binding of HP1^{Swi6} to a fluorescently labelled RNA probe can be competed by an unlabelled RNA probe.

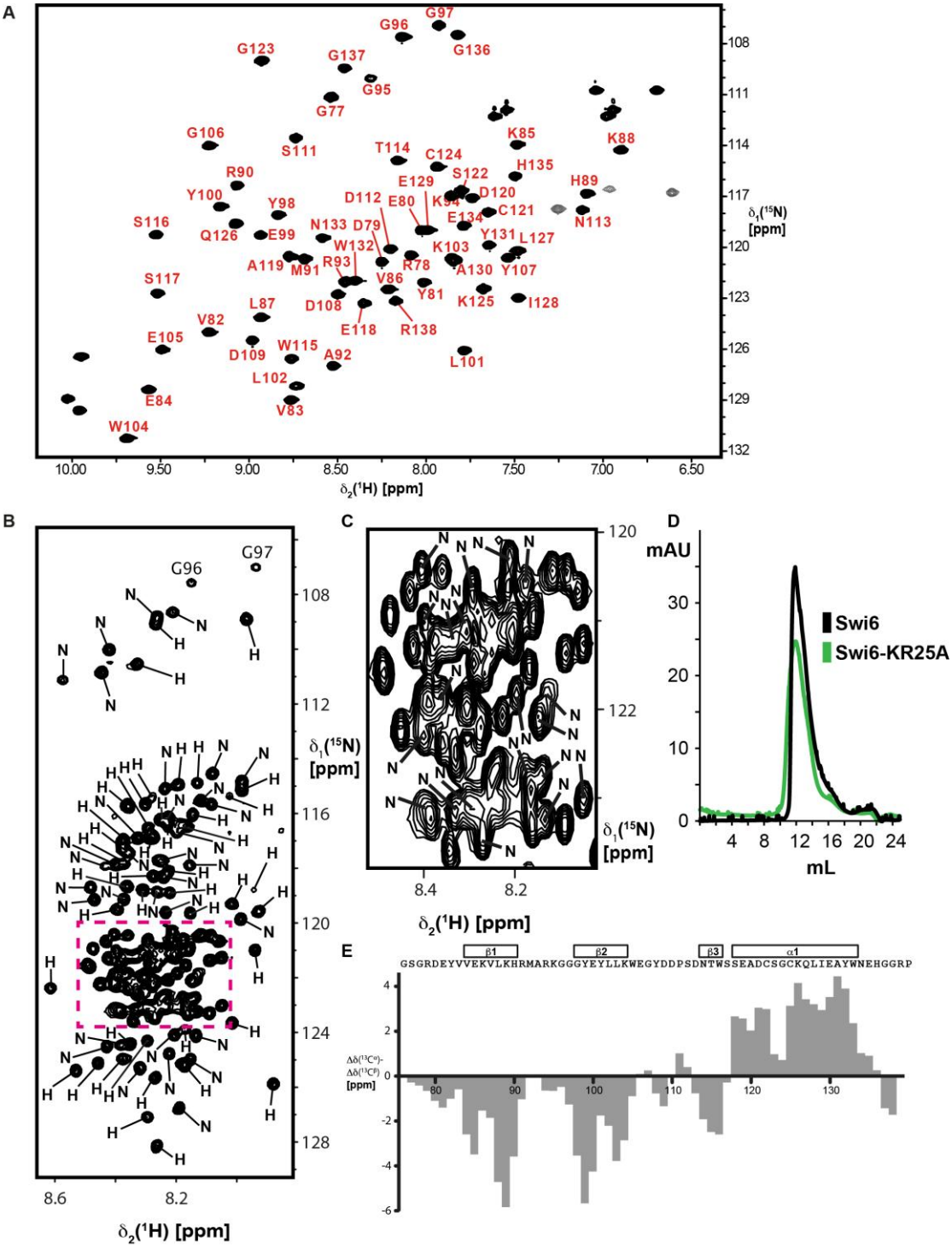

Figure S4, Related to Figure 4. Creation of a Mutant HP1^{Swi6} that Fails to Bind RNA but Keeps Its Other Molecular Properties

(A) 2D [^{15}N,^{1}H]-HSQC spectrum of the isolated CD (residues 75–139). Sequence-specific resonance assignments are indicated.

(B) Domain-specific assignments for the amide resonances arising from flexibly disordered segments of the polypeptide chain. On a 2D [^{15}N,^{1}H]-TROSY spectrum of full-length HP1^{Swi6}, the residues are identified which are part of the hinge region ("H") and the N-terminal domain ("N"). The part in red dashed lines is shown enlarged in (C).

(C) Enlargement of the central part of the spectrum (B). Resonances from the N-terminal domain are indicated "N". All other resonances belong to the hinge region.

(D) The chromatograms of $HP1^{Swi6}$ and $HP1^{Swi6}$-KR25A that were loaded onto a Superdex200 size exclusion column show that the KR25A mutation does not affect the dimeric state of protein.
(E) Secondary chemical shifts for the $^{13}C^{\alpha}$ and $^{13}C^{\beta}$ chemical shifts of the isolated CD (residues 75–139) relative to random coil values. Above the amino acid sequence of the domain, the secondary structure elements inferred from these shifts, three β-strands and one α-helix, are indicated.

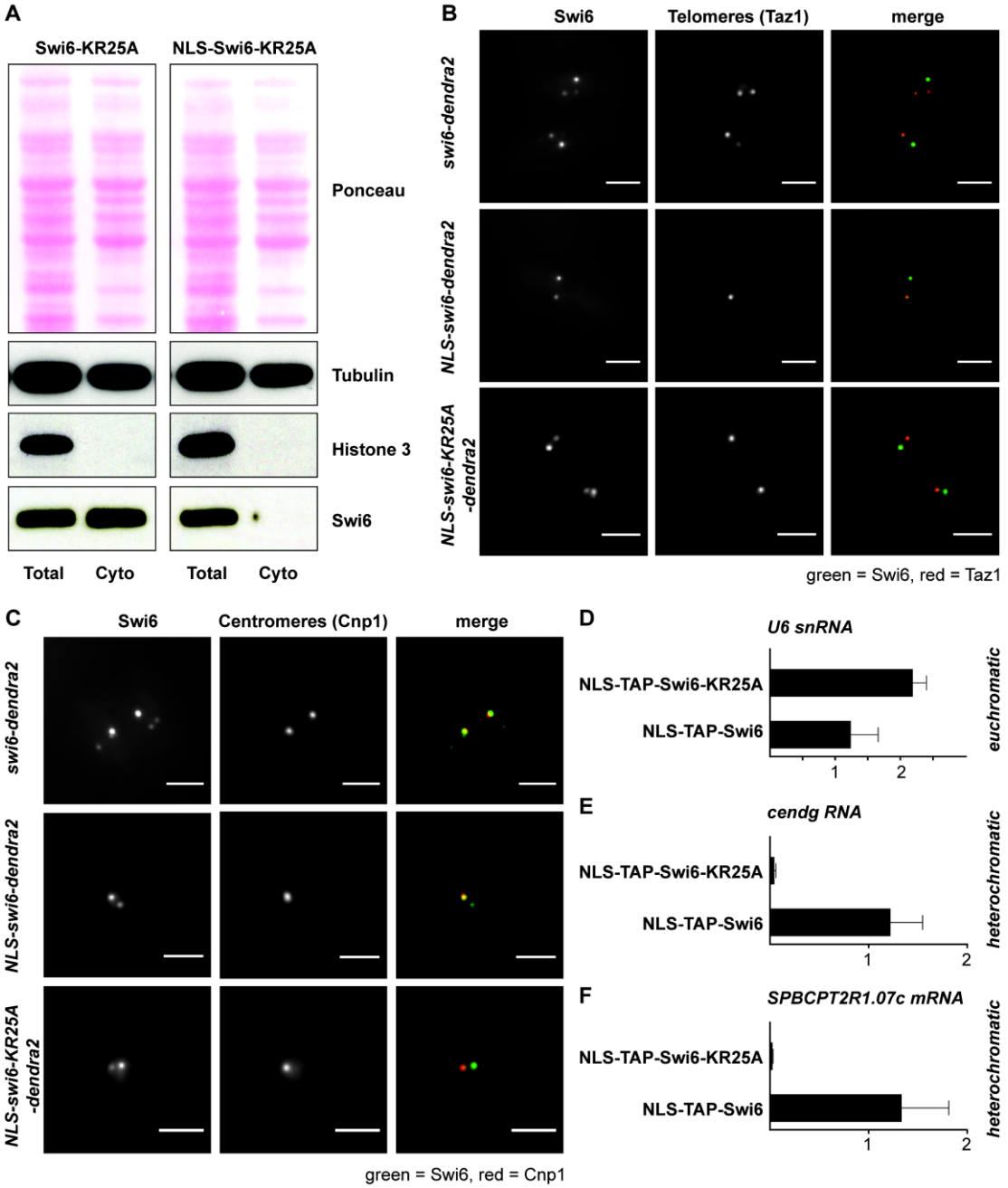

Figure S5, Related to Figure 5. RNA Binding through the Hinge Region of HP1^{Swi6} Is Required for Silencing but Not Maintenance of Heterochromatin

(A) Cells expressing HP1^{Swi6}-KR25A with or without an SV40 NLS were fractionated into total and cytoplasmic fractions. Proteins were separated by SDS-PAGE and detected by Western blot. Cytoplasmic Tubulin and nuclear Histone H3 serve as fractionation controls.

(B) Microscopy of living *S. pombe* cells co-expressing C-terminally Dendra2-tagged HP1^{Swi6} variants and C-terminally mCherry-tagged Taz1 driven from their endogenous promoters. Cells were grown in YES medium at 30°C. To restore nuclear localization of the HP1^{Swi6}-KR25A mutant (Figure S4), a SV40 NLS was added N-terminally.

(C) Microscopy of living *S. pombe* cells co-expressing C-terminally Dendra2-tagged HP1^{Swi6} variants and C-terminally mCherry-tagged Cnp1 driven from their endogenous promoters. Cells were grown in YES medium at 30°C. To restore nuclear localization of the HP1^{Swi6}-KR25A mutant (Figure S4), a SV40 NLS was added N-terminally.

(D-F) RIP experiment demonstrating that HP1^{Swi6} but not HP1^{Swi6}-KR25A interacts with heterochromatic RNA in vivo. TAP-tagged Swi6 was immunoprecipitated and the RNA was

isolated followed by cDNA synthesis. The amount of co-immunoprecipitated RNA was quantified by quantitative real-time RT-PCR and normalized to act1+ mRNA. The amount of RNA co-immunoprecipitated with $HP1^{Swi6}$-KR25A is shown relative to the amount of RNA that co-immunoprecipitates with $HP1^{Swi6}$. As a control for unspecific background RNA binding in this pulldown experiment, U6 snRNA levels were measured (D).

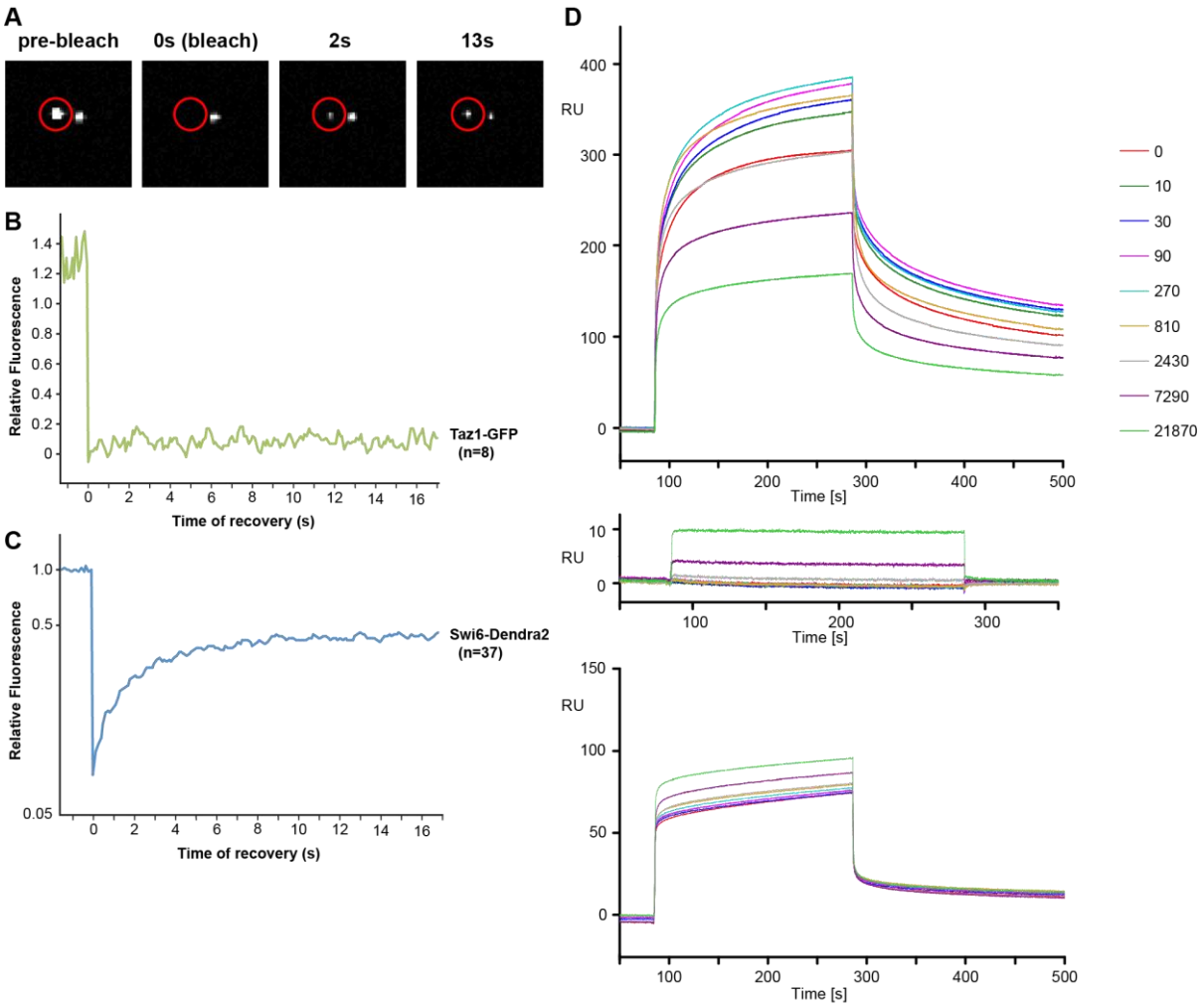

Figure S6, Related to Figure 6. Dynamic Exchange of HP1^{Swi6} from Chromatin on the Ensemble Level In Vivo and the Influence of RNA Binding on H3K9me Binding Properties

(A) Representative images of Fluorescence Recovery After Photobleaching (FRAP) performed with a cell expressing HP1^{Swi6}-Dendra2. Pictures were taken before, immediately after, 2 seconds after, and 13 seconds after photobleaching. Red circle indicates the heterochromatin focus subjected to photobleaching.

(B) FRAP analysis of cells expressing Taz1-GFP. Average relative fluorescence intensities of 8 bleached foci (cells) with a gliding time-average of 3 frames are shown.

(C) FRAP analysis of cells expressing HP1^{Swi6}-Dendra2. The fluorescence intensities were normalized to an unbleached focus in the same image. Average relative fluorescence intensities of 37 bleached foci (cells) with a gliding time-average of 3 frames are shown.

(D) SPR responses for competitive binding of H3K9me3 and RNA to HP1^{Swi6}. Top panel: A constant concentration of 1 µM HP1^{Swi6} with increasing concentrations of 20mer GFP-RNA was injected to an H3K9me3 surface for 200 s. The color code indicates the RNA concentrations in nM. Middle panel: same experiment without HP1^{Swi6}, showing that RNA does not bind to the peptide surface under the experimental conditions used. Bottom panel: same experiment as in the top panel but using 5 µM HP1^{Swi6} KR25A instead of 1 µM HP1^{Swi6} wild-type.

Supplemental Experimental Procedures

Strains and Plasmids

Fission yeast strains were grown at 30°C in YES. All strains were constructed following a PCR-based protocol (Bahler et al., 1998) or standard mating and sporulation. Point mutations were created using the QuickChange Lightning Site-directed mutagenesis kit (Stratagene).
The Swi6-KR25A hinge region fragment was created by gene synthesis (Integrated DNA Technologies, Inc.) and linked by a fusion PCR strategy to give rise to Swi6-KR25A. This was then cloned into a bacterial GST-expression vector. This plasmid was either transformed into bacteria for recombinant protein expression or used as a template for PCR-based gene targeting in *S. pombe*. All Swi6 mutant strains were created by transformation into a *swi6Δ::ura3+* (c.a.) strain (ORF deletion) followed by counterselection on 5-FOA. The Dendra2 protein sequence (Chudakov et al., 2007) was reverse translated *in silico* using yeast codons. The template for PCR-based gene targeting was created by gene synthesis (Integrated DNA Technologies, Inc.) followed by cloning into a pFA6a-link-plasmid series vector (Sheff and Thorn, 2004),
All strains were confirmed by sequencing. Plasmid sequences and detailed maps are available upon request.

Silencing Assays

Serial 10-fold dilutions of the strains indicated were plated on PMGc (nonselective, NS) or on PMGc plates containing 2 mg/mL 5-Fluoroorotic Acid. For ade6-reporter strains, the cells were spotted on YES, YE low ade (22.5 mg/L adenine). For TBZ assays, the cells were spotted on YES plates containing 14 µg/mL Thiabendazole (TBZ) (Sigma T5535).

RNA Probe Labelling for EMSA

DNA templates were generated by PCR on *S. pombe* genomic DNA using primers containing T7 polymerase promoter sequences. In-vitro transcription was performed using the T7 RNA polymerase MEGA script kit (Ambion). For the synthesis of labeled probes, a mix of 0.6 mM UTP and 0.4 mM Fluorescin-UTP (Roche, 2.5 mM) was used. The reaction was carried out for 1h at 37°C followed by a 15 min incubation with 1 µL Turbo DNaseI (37°C). The reaction was phenol-chloroform extracted and purified over G50 spin columns (Amersham) to remove unincorporated nucleotides.

Recombinant Protein Expression and Purification

Recombinant proteins were expressed as N-terminal GST-fusion proteins in Rosetta (BL21) bacteria. A 1L culture was grown in LB + antibiotics until OD_{600}=0.4. The cells were grown for another 2h at 20°C (OD_{600} around 0.6), followed by induction of expression of the GST-fusion proteins with 0.5 mM IPTG. The culture was grown o/n at 20°C. The cells were pelleted, washed and frozen in N_2(l). For protein purification, the cell pellet was resuspended in 5 pellet volumes of lysis buffer (25 mM Tris-HCl (pH 7.5), 500 mM NaCl, 1% Triton-X100 + Protease Inhibitors) and sonicated 6 x 30 sec at 50%. The lysate was spun at 16'000 rpm, 4°C for 30 minutes and cleared by filtration (0.45 µm). The extract was incubated with 1 mL of glutathione-agarose (Sigma) and rotated for 2h at 4°C. After 3 washes (25 mM Tris-HCl (pH 7.5), 500 mM NaCl, 0.1% Triton-X100) the protein was eluted using 50 mM reduced glutathione. The eluate was dialysed o/n into 50 mM HEPES (pH 7.5), 200 mM KCl, 10% Glycerol. This recombinant protein was used for EMSA.

Polysome Profiling

A detailed protocol for polysome profiling in *S. pombe* is available upon request. Briefly, 50 mL of cells were grown to an OD of 0.5-0.6. Cycloheximide was added to a final concentration of 100 µg/µL and the culture was incubated for another 10 min at 30°C. The cells were pelleted and flash frozen in N_2(l). Lysis was performed by bead-beating in 200 µL of lysis buffer and 500 µL glass beads followed by removing insoluble material by centrifugation. 140 OD_{260} were loaded onto a 15-60% sucrose gradient and separated by ultracentrifugation for 2h at 39'000 rpm (Beckman SW40 rotor). The gradient was unloaded from the bottom with 70% sucrose. Fractions were collected while monitoring the absorbance at 254 nm. RNA was isolated from the fractions using phenol-chloroform extraction followed by isopropanol precipitation. RNA recovery was determined by UV absorbance. cDNA was synthesized from 500 ng RNA using the Affinity Script Multiple Temperature cDNA synthesis kit (Stratagene)

and subsequently quantified by qRT-PCR. The data was analyzed as described in (Ding and Grosshans, 2009), calculating the RNA enrichment relative to the total amount of RNA in a given fraction.

mRNA Polyadenylation State Assays

The polyadenylation state of mRNAs was assayed by RACE-PAT or oligo(dT)/RNase H-Northern analysis as described in (Salles et al., 1999). To increase resolution in the RNAseH-Northern assay, an oligo (mb1314) that anneals 100 bp before the STOP codon of the GFP ORF was included in the RNaseH cleavage reaction. RNA was isolated from 50 mL of exponentially growing cells using the hot phenol method. 50 µg of total RNA was incubated with 2 uL mb1314 (100 µM) and with or without oligo dT (10 µL of 100 ng/µL) in a total volume of 68 µL. This was incubated at 65°C for 5 min and slowly cooled down to RT. 8 µL of 10 x buffer, 1 µL RNasIn Plus (Promega) and 1.5 µL RNaseH (New England Biolabs) were added followed by a 30 min incubation at 37°C. The RNA was phenol-chloform extracted followed by ethanol precipitation. The pellet was resuspended in 20 µL of 100% formamide, denatured and separated on a 2.4% MOPS-agarose gel. After capillary transfer in 20 x SSC to a positively charged nylon membrane and UV crosslinking, PNK-labelled oligos (mb1315/mb1316) were hybridized o/n at 35°C. The membrane was washed 3 x 15 min in 0.5 x SSC, 0.1% Triton-X100 at 35°C. Signal was detected using a Phosphorscreen.

5'-Dependent Terminator Exonuclease Assay

Total RNA was isolated using the hot phenol method. The RNA was subjected to DNase digestion using the Absolutely RNA Miniprep Kit (Stratagene). 1 µg RNA was treated with 1 µL of terminator 5'phosphate-dependent exonuclease (Epicentre) for 2h at 30°C. Control reactions were incubated for 2h at 30°C in the absence of the enzyme. The reaction was terminated by phenol-chloroform extraction followed by isopropanol precipitation.1/10th of the reaction was analyzed on a Agilent Bioanalyzer 2100 (Eukaryote Total RNA Nano Chip). 500 ng of RNA was used for cDNA synthesis and quantification by qRT-PCR.

Live Cell Imaging and FRAP Analysis

Imaging was performed on an Olympus IX81 microscope equipped with a Yokogawa CSU-X1 spinning disk, a UPlanFLN 40x/1.3 objective, a CascadeII camera (Photometrics, AZ), a 491nm laser line (Cobolt, Sweden), a Semrock Di01-T488/568 dichroic and a Semrock FF01-525/40-25 emission filter. All devices were piloted with the software Metamorph (Molecular Devices Inc, CA). For FRAP experiments, a UGA-40 module (Rapp-Optoelectronics, Hamburg) equipped with a 473nm laser line and a chroma Z405/473rpc-xt dichroic was installed on the setup. In Metamorph, image acquisition was done using the live replay menu with an exposure time of 100ms and binning 2 for the camera. The bleaching region was a diffraction-limited spot, bleach time was 20ms. The acquired images were analyzed using the open source Fiji software (Walter et al., 2010). The fluorescence intensities were normalized to an unbleached focus in the same image and pre-bleach intensities were averaged and set to 1. Growth conditions for live cell microscopy were described in (Emmerth et al., 2010). Images were acquired at room temperature.

Solution NMR Spectroscopy

The sequence-specific resonance assignments for the isolated HP1^{Swi6} CD (residues 75–140) were obtained using a 750 µM sample of [*U*-^{13}C,^{15}N]-labeled CD sample in 50 mM MES-KOH pH 6.5 buffer with 100 mM KCl, 5 mM DTT and 5%/95% D_2O/H_2O. The assignments were obtained from the two triple-resonance APSY-type experiments 4D APSY-HNCACB (15 projections) and 5D APSY-HNCOCACB (16 projections) (Gossert et al., 2010; Hiller et al., 2005; Hiller et al., 2007) and subsequent automated backbone assignment by the algorithm MATCH (Volk et al., 2008). These experiments were recorded at 25°C on a Bruker 600 MHz spectrometer equipped with a room-temperature triple-resonance probe in a total experiment time of 63 h. The assignments of the CD were transferred to full-length HP1^{Swi6} by a comparison of the [^{15}N,^{1}H]-correlation patterns, which were found to be highly similar (Figs. 4 & S4). The domain-specific resonance assignments of the NTD, the hinge region and the CSD were obtained by identifying the individual substracta from HP1^{Swi6} subconstructs: isolated CD, CD+hinge, CD+hinge+CSD, NTD+CD+hinge.

The NMR titration experiments were performed at 25°C on a Bruker 800 MHz spectrometer equipped with a cryogenic triple-resonance probe. 2D [^{15}N,^{1}H]-TROSY experiments

(Pervushin et al., 1997) of 50–120 μM samples of [*U*-^{15}N]-Swi6 in 50 mM MES-KOH pH 6.5 buffer with 100 mM KCl, 5 mM DTT and 5%/95% D_2O/H_2O were recorded. Typically, 1024 and 90 complex points were recorded in the direct and indirect dimension, respectively in total experiment times of 8–12 h for each spectrum. H3K9me3 peptide from a 1 mM stock solution or 20mer GFP-RNA from a 3 mM stock solution of the same buffer were added.

Surface Plasmon Resonance (SPR)
Samples were analyzed using a Biacore T-100 instrument (GE Healthcare). H3K9me3 peptide was covalently bound to a CM5 chip by amine coupling achieving a final density of 1985 RU. All measurements were recorded as subtracted sensorgrams relative to a flow channel with blank amine immobilisation. Sensorgrams were recorded at 25 °C and flow rate of 50μl min^{-1} using 25 mM NaP_i pH 7.0, 150 mM KCl, 5mM DTT, 0.1% P20, 62.5 μg ml^{-1} BSA and 5% Glycerol as running buffer. All samples were diluted in running buffer prior to injection. Each sample was injected for 200 sec and dissociation was recorded for 300 sec. A regeneration step was performed at the end of each cycle by injecting 5 mM NaOH for 30 sec followed by a stabilization period of 50 sec. For the determination of binding constants, increasing concentrations of HP1^{Swi6} or HP1^{Swi6}-KR25A were injected. For the competition assay, samples of 1 μM Swi6 with increasing amounts of RNA were injected.

Dam-ID
DamID was carried out as previously published (Woolcock et al., 2011). Average enrichment values were calculated for all the oligos overlapping the major heterochromatic regions: mating type locus (chromosome 2, 2114000-2137000), telomeres (chromosome 1, 1-20000 and 5571500-5579133; chromosome 2, 4516200-4539804), and centromeres (chromosome 1, 3753687-3789421, chromosome 2, 1602264-1644747, chromosome 3, 1070904-1137003).

RNA Immunoprecipitation (RIP)
RIP was performed essentially as described in (Gilbert and Svejstrup, 2006). IgG-dynabeads (expoxy-coupled) that have been pre-blocked using E.coli tRNA were used for the immunoprecipitation of the TAP-tagged proteins. An additional DNaseI-digestion step was included before the cDNA synthesis with random primers.

Supplemental References

Bahler, J., Wu, J.Q., Longtine, M.S., Shah, N.G., McKenzie, A., III, Steever, A.B., Wach, A., Philippsen, P., and Pringle, J.R. (1998). Heterologous modules for efficient and versatile PCR-based gene targeting in Schizosaccharomyces pombe. Yeast *14*, 943-951.

Chudakov, D.M., Lukyanov, S., and Lukyanov, K.A. (2007). Tracking intracellular protein movements using photoswitchable fluorescent proteins PS-CFP2 and Dendra2. Nat. Protocols *2*, 2024-2032.

Ding, X.C., and Grosshans, H. (2009). Repression of C. elegans microRNA targets at the initiation level of translation requires GW182 proteins. EMBO J. *28*, 213-222.

Emmerth, S., Schober, H., Gaidatzis, D., Roloff, T., Jacobeit, K., and Bühler, M. (2010). Nuclear retention of fission yeast dicer is a prerequisite for RNAi-mediated heterochromatin assembly. Dev. Cell *18*, 102-113.

Gilbert, C., and Svejstrup, J.Q. (2006). RNA immunoprecipitation for determining RNA-protein associations in vivo. Curr. Protoc. Mol. Biol. *Chapter 27*, Unit 27 24.

Gossert, A.D., Hiller, S., and Fernández, C. (2010). Automated NMR resonance assignment of large proteins for protein-ligand interaction studies. J. Am. Chem. Soc. *133*, 210-213.

Hiller, S., Fiorito, F., Wüthrich, K., and Wider, G. (2005). Automated projection spectroscopy (APSY). Proc. Natl. Acad. Sci. USA *102*, 10876-10881.

Hiller, S., Wasmer, C., Wider, G., and Wüthrich, K. (2007). Sequence-specific resonance assignment of soluble nonglobular proteins by 7D APSY-NMR spectroscopy. J. Am. Chem. Soc. *129*, 10823-10828.

Pervushin, K., Riek, R., Wider, G., and Wüthrich, K. (1997). Attenuated T_2 relaxation by mutual cancellation of dipole-dipole coupling and chemical shift anisotropy indicates an avenue to NMR structures of very large biological macromolecules in solution. Proc. Natl. Acad. Sci. USA *94*, 12366-12371.

Salles, F.J., Richards, W.G., and Strickland, S. (1999). Assaying the polyadenylation state of mRNAs. Methods *17*, 38-45.

Sheff, M.A., and Thorn, K.S. (2004). Optimized cassettes for fluorescent protein tagging in Saccharomyces cerevisiae. Yeast *21*, 661-670.

Volk, J., Herrmann, T., and Wüthrich, K. (2008). Automated sequence-specific protein NMR assignment using the memetic algorithm MATCH. J. Biomol. NMR *41*, 127-138.

Walter, T., Shattuck, D.W., Baldock, R., Bastin, M.E., Carpenter, A.E., Duce, S., Ellenberg, J., Fraser, A., Hamilton, N., Pieper, S*., et al.* (2010). Visualization of image data from cells to organisms. Nat. Methods *7*, S26-41.

Woolcock, K.J., Gaidatzis, D., Punga, T., and Bühler, M. (2011). Dicer associates with chromatin to repress genome activity in Schizosaccharomyces pombe. Nat. Struct. Mol. Biol. *18*, 94-99.

Supplemental Tables

Table S1. Plasmids

pMB247	pFA6a-Cid14DADA-TAP-hphMX6	Template for PCR based gene targeting (Creation of Cid14DADA::TAP allele)
pMB680	pGEX	empty n-term GST fusion vector with TEV and Thrombin cleavage site
pMB714	pGEX-Swi6	Swi6 purification (N-term GST, TEV and Thrombin cleavage site)
pMB715	pGEX-Swi6-KR25A	Swi6-KR25A purification (N-term GST, TEV and Thrombin cleavage site)
pMB776	pGEX-Swi6-CD	Swi6-Chromodomain purification (N-term GST, TEV and Thrombin cleavage site)
pMB768	pFA6a-link-Dendra2-hphMX	Template for PCR based gene targeting (C-term Dendra2 tagging)

Table S2. Primers for Real-Time PCR

		Forward Primer	***Reverse Primer***
cendg	mb549/mb550	AAGGAATGTGCCTCGTCAAATT	TGCTTCACGGTATTTTTTGAAATC
cendh	mb551/mb552	GTATTTGGATTCCATCGGTACTATGG	ACTACATCGACACAGAAAAGAAAACAA
gfp+	mb820/mb821	CGAAAGATCCCAACGAAAAGAG	TCCCAGCAGCTGTTACAAACTC
ura4+	mb553/554	TACAAAATTGCTTCTTGGGCTCAT	AGACCACGTCCCAAAGGTAAAC
tlh1/2+	mb682/683	CGTGTGCAAGCCGTCAAA	GCTCGAGTTGTGCTGAAATGTC
SPBCPT2R1.07c	mb3006/mb3007	TGGTGTTGCTCCAAAGTGTAGTGGA	GACAGTTGCCTCCGGTAAATGGATTC
Control Genes			
U6 snRNA	mb1281/mb1282	GATCTTCGGATCACTTTGGTCAA	TGTCGCAGTGTCATCCTTGTG
act1+	mb555/mb556	TCCTCATGCTATCATGCGTCTT	CCACGCTCCATGAGAATCTTC
fbp1+	mb557/mb558	CTGGCCAGCTTATTCAACTTCAT	GATTTCGTCGAGATCTTTTTTCATG

Table S3. Primers for RNaseH Assays

		Target	***Purpose***
mb1315	TTACAAACTCAAGAAGGACCATGTGGTCTCTC	GFP	probe
mb1316	TTTGTATAGTTCATCCATGCCATGTGTAATCCCA	GFP	probe
mb1314	GATTGTGTGGACAGGTAATGG	GFP	cleavage

Table S4. RNA Probes

		Length	***Purpose***
20-GFP-RNA	AUGGGUAAAGGAGAAGAACU	20nt	NMR
150-GFP-RNA	ggAGUAAAGGAGAAGAACUUUUCACUGGAGUUGUCCCAAUUCUUGUUGAAUUAGA UGGUGAUGUUAAUGGGCACAAAUUUUCUGUCAGUGGAGAGGGUGAAGGUGAUGC AACAUACGGAAAACUUACCCUUAAAUUUAUUUGCACUACUG	150nt	EMSA
700-GFP-RNA	ggAGUAAAGGAGAAGAACUUUUCACUGGAGUUGUCCCAAUUCUUGUUGAAUUAGA UGGUGAUGUUAAUGGGCACAAAUUUUCUGUCAGUGGAGAGGGUGAAGGUGAUGC AACAUACGGAAAACUUACCCUUAAAUUUAUUUGCACUACUGGAAAACUACCUGUU CCAUGGCCAACACUUGUCACUACUUUCACUUAUGGUGUUCAAUGCUUUUCAAGAU ACCCAGAUCAUAUGAAACGGCAUGACUUUUUCAAGAGUGCCAUGCCCGAAGGUUA UGUACAGGAAAGAACUAUAUUUUUCAAAGAUGACGGGAACUACAAGACACGUGCU GAAGUCAAGUUUGAAGGUGAUACCCUUGUUAAUAGAAUCGAGUUAAAAGGUAUUG AUUUUAAAGAAGAUGGAAACAUUCUUGGACACAAAUUGGAAUACAACUAUAACUC ACACAAUGUAUACAUCAUGGCAGACAAACAAAAGAAUGGAAUCAAAGUUAACUUCA AAAUUAGACACAACAUUGAAGAUGGAAGCGUUCAACUAGCAGACCAUUAUCAACA	711nt	EMSA

	AAAUACUCCAAUUGGCGAUGGCCCUGUCCUUUUACCAGACAACCAUUACCUGUCC ACACAAUCUGCCCUUUCGAAAGAUCCCAACGAAAAGAGAGACCACAUGGUCCUUC UUGAGUUUGUAACAGCUGCUGGGAUUACACAUGGCAUGGAUGAACUAUACAAA		
100-cen-RNA	ggCGUGCGAUCGGGCCGCGACUGGCCAUUUUCAAGGAUAUAUCGAAUCAAAUUUA GGUAUUGCUCUUCUUCUGUAUUUCUAUAUUCGGAGGAAGUAAAU	99nt	EMSA

Table S5. Strain Table

		Figure	Genotype	Source	Comment
spb28	wt	1	h+ leu1-32 ura4D18 oriI ade6-M216 imr1R(Nco1)::gfp+::natMX	*	gfp+ driven by ura4+ promoter
spb38	clr4Δ	1	h+ leu1-32 ura4D18 oriI ade6-M216 imr1R(Nco1)::gfp+::natMX clr4Δ::kanMX	*	gfp+ driven by ura4+ promoter
spb36	dcr1Δ	1	h+ leu1-32 ura4D18 oriI ade6-M216 imr1R(Nco1)::gfp+::natMX dcr1Δ::kanMX	*	gfp+ driven by ura4+ promoter
spb313	cid14Δ	1	h+ leu1-32 ura4D18 oriI ade6-M216 imr1R(Nco1)::gfp+::natMX cid14Δ::kanMX	*	gfp+ driven by ura4+ promoter
spb342	wt	1	h90 mat3M(EcoRV)::gfp+::natMX ura4-DS/E leu1-32 ade6-M210	*	gfp+ driven by ura4+ promoter
spb360	clr4Δ	1	h90 mat3M(EcoRV)::gfp+::natMX ura4-DS/E leu1-32 ade6-M210 clr4Δ::kanMX	*	gfp+ driven by ura4+ promoter
spb361	dcr1Δ	1	h90 mat3M(EcoRV)::gfp+::natMX ura4-DS/E leu1-32 ade6-M210 dcr1Δ::kanMX	*	gfp+ driven by ura4+ promoter
spb374	cid14Δ	1	h90 mat3M(EcoRV)::gfp+::natMX ura4-DS/E leu1-32 ade6-M210 cid14Δ::kanMX	*	gfp+ driven by ura4+ promoter
spb342	wt	2	h90 mat3M(EcoRV)::gfp+::natMX ura4-DS/E leu1-32 ade6-M210	*	gfp+ driven by ura4+ promoter
spb374	cid14Δ	2	h90 mat3M(EcoRV)::gfp+::natMX ura4-DS/E leu1-32 ade6-M210 cid14Δ::kanMX	*	gfp+ driven by ura4+ promoter
spb360	clr4Δ	2	h90 mat3M(EcoRV)::gfp+::natMX ura4-DS/E leu1-32 ade6-M210 clr4Δ::kanMX	*	gfp+ driven by ura4+ promoter
spb535	cid14Δ clr4Δ	2	h90 mat3M(EcoRV)::gfp+::natMX ura4- leu1-32 ade6- clr4D::hph cid14Δ::kanMX	*	gfp+ is driven by ura4+ promoter; ura4D18 or DS/E; ade6-M210 or 216
spb721	swi6Δ	2	h90 mat3M(EcoRV)::gfp+::natMX ura4-DS/E leu1-32 ade6-M210 swi6Δ::ura3+	*	gfp+ driven by ura4+ promoter
spb723	cid14Δ swi6Δ	2	h90 mat3M(EcoRV)::gfp+::natMX ura4-DS/E leu1-32 ade6-M210 swi6Δ::ura3+ cid14Δ::kan	*	gfp+ driven by ura4+ promoter
spb1071	swi6-Dendra2	4	h90 mat3M(EcoRV)::gfp+::natMX ura4-DS/E leu1-32 ade6-M210 swi6-Dendra2::hphMX	*	gfp+ driven by ura4+ promoter
spb1240	nls-swi6-Dendra2	4	h90 mat3M(EcoRV)::gfp+::natMX ura4-DS/E leu1-32 ade6-M210 nls-swi6-Dendra2::hphMX	*	gfp+ driven by ura4+ promoter
spb1241	nls-swi6-KR25A-Dendra2	4	h90 mat3M(EcoRV)::gfp+::natMX ura4-DS/E leu1-32 ade6-M210 nls-swi6-KR25A-Dendra2::hphMX	*	gfp+ driven by ura4+ promoter
spb342	wt	4	h90 mat3M(EcoRV)::gfp+::natMX ura4-DS/E leu1-32 ade6-M210	*	gfp+ driven by ura4+ promoter
spb360	clr4Δ	4	h90 mat3M(EcoRV)::gfp+::natMX ura4-DS/E leu1-32 ade6-M210 clr4Δ::kanMX	*	gfp+ driven by ura4+ promoter
spb939	swi6Δ	4	h90 mat3M(EcoRV)::gfp+::natMX ura4-DS/E leu1-32 ade6-M210 swi6Δ::ura3+ (ORF deletion only)	*	gfp+ driven by ura4+ promoter
spb1226	nls-swi6	4	h90 mat3M(EcoRV)::gfp+::natMX ura4-DS/E leu1-32 ade6-M210 nls-swi6	*	gfp+ driven by ura4+ promoter
spb1227	nls-swi6-KR25A	4	h90 mat3M(EcoRV)::gfp+::natMX ura4-DS/E leu1-32 ade6-M210 nls-swi6-KR25A	*	gfp+ driven by ura4+ promoter

spb435	dam	6	h+ leu1-32 ade6-M216 ura4Δ::nmt1(81x)-dam-myc-kan		
spb436	dam-cid14	6	h+ leu1-32 ade6-M216 ura4Δ::nmt1(81x)-dam-myc-cid14-kan		
spb1386	dam swi6Δ	6	h+ leu1-32 ade6-M216 ura4Δ::nmt1(81x)-dam-myc-kan swi6Δ::ura3+ (ORF deletion only)		
spb1387	dam-cid14 swi6Δ	6	h+ leu1-32 ade6-M216 ura4Δ::nmt1(81x)-dam-myc-cid14-kan swi6Δ::ura3+ (ORF deletion only)		

spb65	wt, ura4+	S1	972h-	1	
spb221	wt	S1	h- imr1R(Nco1)::gfp+::natMX	*	gfp+ driven by ura4+ promoter
spb295	clr4Δ	S1	h- imr1R(Nco1)::gfp+::natMX clr4Δ::kanMX	*	gfp+ driven by ura4+ promoter
spb294	cid14Δ	S1	h- imr1R(Nco1)::gfp+::natMX cid14Δ::kanMX	*	gfp+ driven by ura4+ promoter
spb373	cid14DADA	S1	h- imr1R(Nco1)::gfp+::natMX cid14DADA-TAP::hphMX	*	gfp+ driven by ura4+ promoter
spb342	wt	S1	h90 mat3M(EcoRV)::gfp+::natMX ura4-DS/E leu1-32 ade6-M210	*	gfp+ driven by ura4+ promoter
spb360	clr4Δ	S1	h90 mat3M(EcoRV)::gfp+::natMX ura4-DS/E leu1-32 ade6-M210 clr4Δ::kanMX	*	gfp+ driven by ura4+ promoter
spb374	cid14Δ	S1	h90 mat3M(EcoRV)::gfp+::natMX ura4-DS/E leu1-32 ade6-M210 cid14Δ::kanMX	*	gfp+ driven by ura4+ promoter
spb739	cid14DADA	S1	h90 mat3M(EcoRV)::gfp+::natMX ura4-DS/E leu1-32 ade6-M210 cid14DADA-TAP::hphMX	*	gfp+ driven by ura4+ promoter

spb29	wt, ura4+	S2	h+ otr1R(SphI)::ura4+ leu1-32 ade6-M210 ura4Δ::gfp::natMX	*	end. ura+ ORF replaced with gfp+
spb342	wt	S2	h90 mat3M(EcoRV)::gfp+::natMX ura4-DS/E leu1-32 ade6-M210	*	gfp+ driven by ura4+ promoter
spb360	clr4Δ	S2	h90 mat3M(EcoRV)::gfp+::natMX ura4-DS/E leu1-32 ade6-M210 clr4Δ::kanMX	*	gfp+ driven by ura4+ promoter
spb374	cid14Δ	S2	h90 mat3M(EcoRV)::gfp+::natMX ura4-DS/E leu1-32 ade6-M210 cid14Δ::kanMX	*	gfp+ driven by ura4+ promoter
spb76	no gfp	S2	h90 mat3M(EcoRV)::ura4+ ura4-DS/E leu1-32 ade6-M210	2	

spb342	wt	S5	h90 mat3M(EcoRV)::gfp+::natMX ura4-DS/E leu1-32 ade6-M210	*	gfp+ driven by ura4+ promoter
spb1055	swi6-KR25A	S5	h90 mat3M(EcoRV)::gfp+::natMX ura4-DS/E leu1-32 ade6-M210 swi6-KR25A	*	gfp+ driven by ura4+ promoter
spb1468	swi6-Dendra2 cnp1-mCherry	S5	h90 mat3M(EcoRV)::gfp+::natMX ura4-DS/E leu1-32 ade6-M210 swi6-Dendra2::hphMX cnp1-mCherry::kanMX	*	gfp+ driven by ura4+ promoter
spb1450	nls-swi6-Dendra2 cnp1-mCherry	S5	h90 mat3M(EcoRV)::gfp+::natMX ura4-DS/E leu1-32 ade6-M210 nls-swi6-Dendra2::hphMX cnp1-mCherry::kanMX	*	gfp+ driven by ura4+ promoter
spb1469	nls-swi6-KR25A-Dendra2 cnp1-mCherry	S5	h90 mat3M(EcoRV)::gfp+::natMX ura4-DS/E leu1-32 ade6-M210 nls-swi6-KR25A-Dendra2::hphMX cnp1-mCherry::kanMX	*	gfp+ driven by ura4+ promoter
spb1439	NLS-TAP-Swi6	S5	h90 mat3M(EcoRV)::gfp+::natMX ura4-DS/E leu1-32 ade6-M210 NLS-TAP-Swi6	*	gfp+ driven by ura4+ promoter
Spb1493	NLS-TAP-Swi6-KR25A	S5	h90 mat3M(EcoRV)::gfp+::natMX ura4-DS/E leu1-32 ade6-M210 NLS-TAP-Swi6-KR25A	*	gfp+ driven by ura4+ promoter

Source: *this study, [1]Charles Hoffmann, [2]Danesh Moazed

THE EMBO JOURNAL

Have you seen?

The EMBO Journal (2012) 31, 3237–3238 | © 2012 European Molecular Biology Organization | All Rights Reserved 0261-4189/12
www.embojournal.org

Silent decision: HP1 protein escorts heterochromatic RNAs to their destiny

Jie Ren and Robert A Martienssen*

Cold Spring Harbor Laboratory, Cold Spring Harbor, NY, USA
*Correspondence to: martiens@cshl.edu

The EMBO Journal (2012) **31,** 3237–3238. doi:10.1038/emboj.2012.172; Published online 15 June 2012

Heterochromatin is classically perceived to be refractory to transcription because of its compact structure. However, Keller *et al* (2012) now demonstrated that heterochromatic transcripts can accumulate even when heterochromatin is normally packaged. By tracking down the fate of these heterochromatic RNAs, they revealed a new post-transcriptional mechanism of silencing in heterochromatin that involves the dynamic turnover of HP1^{Swi6} between its free, chromatin-bound and RNA-bound forms. The latter form escorts heterochromatic RNA to degradation.

In eukaryotes, chromatin can be classified into two states: euchromatin, which is loosely packed and actively transcribed, and heterochromatin, which remains condensed during interphase. The compact structure of heterochromatin is critical for its widespread roles in chromosome integrity, stability and transposon silencing around centromeres and in other repeat-rich regions, such as subtelomeric regions.

Heterochromatin is relatively devoid of coding sequences, and reporter genes embedded are tightly repressed under most situations. The compact structure of heterochromatin was generally thought to be inert and refractory to transcription (Gasser and Cockell, 2001). However, HP1 (heterochromatin protein 1), which binds the conserved heterochromatin mark, histone H3 lysine 9 methylation (H3K9me) and serves as the structural basis for the condensed state of heterochromatin, undergoes very active turnover between the chromatin-bound and -free states (Cheutin *et al*, 2003; Maison and Almouzni, 2004). Furthermore, heterochromatin is not as 'silent' as initially thought, and undergoes substantial transcription. But the transcripts are quickly processed by RNA interference (RNAi), which utilizes 20- to 30-nt small RNA to guide cleavage or translational inhibition of target transcripts (Carmell and Hannon, 2004), and to release RNA polymerase II (Zaratiegui *et al*, 2011). RNA degradation also participates in this process, and its role is newly interpreted by Keller *et al* (2012).

Although the detailed mechanisms underlying the establishment and maintenance of heterochromatin vary in different species, the principles are conserved from yeast to human. Much work has been done in the fission yeast *Schizosaccharomyces pombe* to understand how the enzymes responsible for the deposition of heterochromatic marks are recruited to specific regions of the genome, and has revealed a complicated network of mechanisms both dependent and independent of RNAi (Buhler *et al*, 2007; Grewal and Jia, 2007). The involvement of RNA turnover in this network is known but not well understood.

Keller *et al* (2012) set out to understand the role of RNA degradation by tracking down the fate of heterochromatic transcripts. They used a *cid14* mutant, which has defects in polyadenylation-assisted RNA turnover (Wang *et al*, 2008) and observed accumulation of transcripts from reporter genes embedded in heterochromatic regions. Interestingly, such derepression is not accompanied by heterochromatin decondensation. They also found a discrepancy between mRNA and protein levels, suggesting that these reporter gene transcripts are assembled into translation-incapable

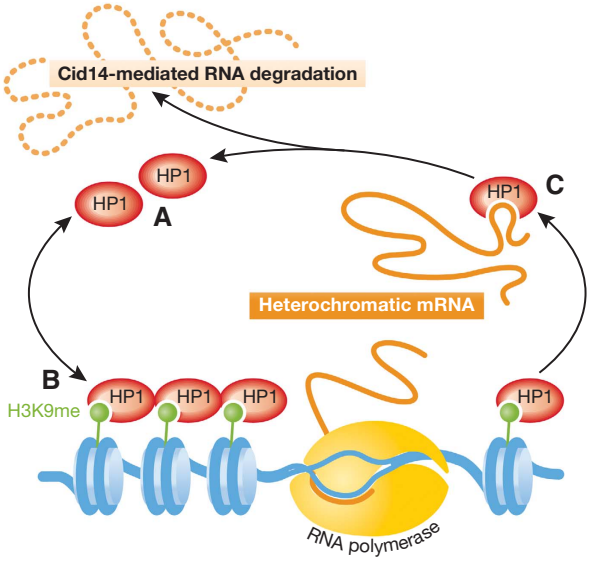

Figure 1 HP1^{Swi6} undergoes rapid turnover between its (**A**) free, (**B**) H3K9me-bound and (**C**) heterochromatic RNA-bound forms. The major structural component of heterochromatin, H3K9me-bound HP1^{Swi6} (**B**) exchanges dynamically with its free ensemble (**A**). Contrary to the classical view, RNA polymerase can get access to heterochromatin, but the transcripts are captured by HP1^{Swi6} (**C**) and escorted to Cid14-mediated RNA degradation. RNA competes with H3K9me for binding with HP1^{Swi6} and causes structural change to HP1^{Swi6}. Thus, both heterochromatin and HP1^{Swi6}–RNA association contributes to the tight repression of genes within heterochromatin.

ribonucleoprotein particles. The authors then hypothesized that Swi6, an HP1 homologue in *S. pombe*, may be central to these particles by targeting and escorting heterochromatic RNA for degradation, because of its dual affinity for both H3K9me and RNA (Motamedi *et al*, 2008). Keller *et al* (2012) confirmed $HP1^{Swi6}$–RNA association and further explored the structural basis of both interactions. They found that overlapping regions of $HP1^{Swi6}$ were important for both interactions, and demonstrated alternation between them and induced structural change of $HP1^{Swi6}$ after binding to either partner. Such alternation and structural change are important for $HP1^{Swi6}$ targeting RNA from heterochromatic regions, and may prevent $HP1^{Swi6}$ binding non-specifically to euchromatic mRNA. To explore the function of the newly identified $HP1^{Swi6}$–RNA association, the creation of a separation-of-function mutant was necessary, as $HP1^{Swi6}$ also has a structural role in heterochromatin. Guided by the structural information obtained for these interactions, the authors designed a mutant that abolishes RNA-binding, while not affecting heterochromatin structure, and indeed, observed that heterochromatic transcripts were no longer degraded, nor were they inhibited from being translated.

In summary, Keller *et al* (2012) have revealed another level of tight repression of heterochromatic genes through uncovering the dynamic turnover of $HP1^{Swi6}$ between its free, H3K9me-bound and RNA-bound forms (Figure 1). The structural component of heterochromatin, $HP1^{Swi6}$ serves as the unidentified link to capture heterochromatic transcripts onsite and escort them towards eventual degradation. Because of the high conservation of HP1, it is possible that a similar mechanism contributes to the tight repression of heterochromatin in higher eukaryotes.

Conflict of interest

The authors declare that they have no conflict of interest.

References

Buhler M, Haas W, Gygi SP, Moazed D (2007) RNAi-dependent and -independent RNA turnover mechanisms contribute to heterochromatic gene silencing. *Cell* **129:** 707–721

Carmell MA, Hannon GJ (2004) RNase III enzymes and the initiation of gene silencing. *Nat Struct Mol Biol* **11:** 214–218

Cheutin T, McNairn AJ, Jenuwein T, Gilbert DM, Singh PB, Misteli T (2003) Maintenance of stable heterochromatin domains by dynamic HP1 binding. *Science* **299:** 721–725

Gasser SM, Cockell MM (2001) The molecular biology of the SIR proteins. *Gene* **279:** 1–16

Grewal SI, Jia S (2007) Heterochromatin revisited. *Nat Rev Genet* **8:** 35–46

Keller C, Adaixo R, Stunnenberg R, Woolcock KJ, Hiller S, Bühler M (2012) HP1(Swi6) mediates the recognition and destruction of heterochromatic RNA transcripts. *Mol Cell* (advance online publication, 7 June 2012; doi:10.1016/j.molcel.2012.05.009)

Maison C, Almouzni G (2004) HP1 and the dynamics of heterochromatin maintenance. *Nat Rev Mol Cell Biol* **5:** 296–304

Motamedi MR, Hong EJ, Li X, Gerber S, Denison C, Gygi S, Moazed D (2008) HP1 proteins form distinct complexes and mediate heterochromatic gene silencing by nonoverlapping mechanisms. *Mol Cell* **32:** 778–790

Wang SW, Stevenson AL, Kearsey SE, Watt S, Bahler J (2008) Global role for polyadenylation-assisted nuclear RNA degradation in posttranscriptional gene silencing. *Mol Cell Biol* **28:** 656–665

Zaratiegui M, Castel SE, Irvine DV, Kloc A, Ren J, Li F, de Castro E, Marin L, Chang AY, Goto D, Cande WZ, Antequera F, Arcangioli B, Martienssen RA (2011) RNAi promotes heterochromatic silencing through replication-coupled release of RNA Pol II. *Nature* **479:** 135–138

Nature Reviews Molecular Cell Biology | AOP, published online 11 July 2012; doi:10.1038/nrm3400

CHROMATIN

RNA eviction by HP1

The formation of heterochromatin requires the conserved heterochromatin protein 1 (HP1), which can associate directly and dynamically with Lys9 trimethylated tails of histone H3 (H3K9me3). Bühler and colleagues find that, in fission yeast, this ensures local capture of heterochromatic mRNAs and their targeting for mRNA decay.

Although heterochromatin has traditionally been regarded as a region that is transcriptionally repressed, recent findings indicate that heterochromatin silencing can occur post-transcriptionally and that RNA processing is also important for this. For example, the non-canonical poly(A) polymerase Cid14 mediates heterochromatic mRNA processing. In this study, the authors first showed that, although loss of Cid14 results in higher levels of heterochromatic mRNAs, these are not translated into protein. They thus hypothesized that these mRNAs might be targeted into ribonucleoprotein particles that are refractory to translation.

In addition to having affinity for H3K9me3 tails, mammalian HP1 has been shown to bind RNA, suggesting that the HP1 homologue in fission yeast, $HP1^{Swi6}$, might have a role in diverting heterochromatic mRNAs away from the translation machinery. Indeed, in the absence of $HP1^{Swi6}$, heterochromatic mRNAs could be translated. Moreover, $HP1^{Swi6}$ was found to directly bind RNA *in vitro*, as previously observed in mammalian cells, and the hinge region of $HP1^{Swi6}$ is sufficient for this.

> “this ensures local capture of heterochromatic mRNAs and their targeting for mRNA decay”

So what is the role of $HP1^{Swi6}$ binding to mRNA? To answer this question, the authors constructed an HP1 protein that contained 25 mutations in the Lys and Arg residues of its hinge region ($HP1^{Swi6}$-KR25A) and thus could no longer bind RNA, although its overall protein folding was intact, as was its ability to bind an immobilized peptide corresponding to H3K9me3. Expression of $HP1^{Swi6}$-KR25A (fused with a nuclear localization sequence to ensure its localization to the nucleus) at the endogenous *swi6* locus revealed that, although RNA binding via the hinge region is not required for $HP1^{Swi6}$ association with heterochromatin or for the overall structural integrity of heterochromatin, the affinity of $HP1^{Swi6}$ for RNA is crucial for the repression of heterochromatic genes.

Next, the authors used fluorescence recovery after photobleaching (FRAP) experiments to confirm that the association of $HP1^{Swi6}$ with chromatin is dynamic *in vivo*. By using a nuclear magnetic resonance (NMR)-based assay they observed that binding of $HP1^{Swi6}$ to RNA and methylated H3K9 occurs through multiple domains. Interestingly, further biophysical analysis revealed that RNA and H3K9me3 binding are competitive processes; the authors therefore concluded that $HP1^{Swi6}$ association with heterochromatic RNAs actually triggers its release from heterochromatin owing to weakened H3K9me3 binding of $HP1^{Swi6}$ when bound by RNA. Finally, chromatin profiling analysis also placed Cid14 nearby to heterochromatin, suggesting that a rapid ‘hand-off’ of mRNA from $HP1^{Swi6}$ to Cid14 for processing might be possible.

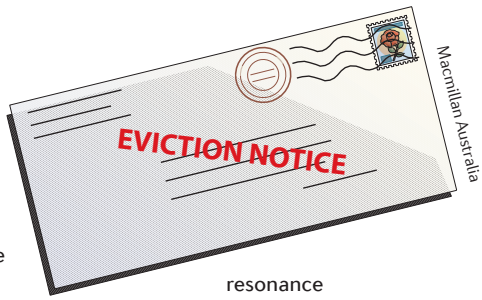

Macmillan Australia

Thus, although transcription can occur at heterochromatic loci, the methylation of Lys9 on histone H3 provides a local checkpoint through recruitment of $HP1^{Swi6}$. The association of $HP1^{Swi6}$ with locally transcribed heterochromatic mRNAs results in its dissociation from chromatin and targeting of mRNAs for decay.

Alison Schuldt

ORIGINAL RESEARCH PAPER Keller, C. *et al.* $HP1^{Swi6}$ mediates the recognition and destruction of heterochromatic RNA transcripts. *Mol. Cell* 7 Jun 2012 (doi:10.1016/j.molcel.2012.05.009)

mean gene expression levels that occur as cells change state. Deciphering the structure of gene expression noise and dynamics in the context of biological programs represents an emerging frontier in understanding how evolution shapes transcriptional programs, and it will be interesting to see how these concepts extend to metazoan cells.

REFERENCES

Blake, W.J., KAErn, M., Cantor, C.R., and Collins, J.J. (2003). Nature *422*, 633–637.

Blake, W.J., Balázsi, G., Kohanski, M.A., Isaacs, F.J., Murphy, K.F., Kuang, Y., Cantor, C.R., Walt, D.R., and Collins, J.J. (2006). Mol. Cell *24*, 853–865.

Cairns, B.R. (2009). Nature *461*, 193–198.

Core, L.J., and Lis, J.T. (2008). Science *319*, 1791–1792.

Elowitz, M.B., Levine, A.J., Siggia, E.D., and Swain, P.S. (2002). Science *297*, 1183–1186.

Locke, J.C., Young, J.W., Fontes, M., Hernández Jiménez, M.J., and Elowitz, M.B. (2011). Science *334*, 366–369.

Ozbudak, E.M., Thattai, M., Kurtser, I., Grossman, A.D., and van Oudenaarden, A. (2002). Nat. Genet. *31*, 69–73.

Suter, D.M., Molina, N., Gatfield, D., Schneider, K., Schibler, U., and Naef, F. (2011). Science *332*, 472–474.

Weinberger, L.S., Burnett, J.C., Toettcher, J.E., Arkin, A.P., and Schaffer, D.V. (2005). Cell *122*, 169–182.

Weinberger, L., Voichek, Y., Tirosh, I., Hornung, G., Amit, I., and Barkai, N. (2012). Mol. Cell *47*, this issue, 193–202.

Whitelaw, N.C., Chong, S., and Whitelaw, E. (2010). Dev. Cell *19*, 649–650.

Should I Stay or Should I Go? Chromodomain Proteins Seal the Fate of Heterochromatic Transcripts in Fission Yeast

Kevin M. Creamer[1,2] and Janet F. Partridge[1,2,*]
[1]Department of Biochemistry, St. Jude Children's Research Hospital, 262 Danny Thomas Place, Memphis, TN 38105, USA
[2]Integrated Program in Biomedical Sciences, University of Tennessee Health Science Center, 858 Madison Ave, Memphis, TN 38163, USA
*Correspondence: janet.partridge@stjude.org
http://dx.doi.org/10.1016/j.molcel.2012.07.007

In this issue of *Molecular Cell*, Ishida et al. (2012) and Keller et al. (2012) show distinct outcomes for heterochromatic RNAs that bind different chromodomain proteins; Chp1 tethers transcripts to centromeres, whereas Swi6^{HP1}-bound transcripts are evicted from chromatin and destroyed.

Posttranslational modification of histones and the proteins that recognize these changes coordinate the arrangement and utilization of chromatin. Heterochromatin is characterized by transcriptional silencing, histone hypoacetylation, and enrichment for methylation on K9 and K27 of histone H3. Silencing can occur via reduction in RNA polymerase access (transcriptional suppression) and through posttranscriptional destruction of RNA. Chromodomain proteins bind to H3K9me2/3- or K27me3-marked chromatin and recruit additional chromatin regulatory complexes that can reinforce and spread the heterochromatic signals. Despite being among the earliest-identified and best-known nonhistone proteins associated with heterochromatin, the mechanistic details of how chromodomain proteins such as HP1 (heterochromatin protein 1) act to silence transcription are poorly understood. Keller et al. (2012) provide evidence that the fission yeast HP1 homolog Swi6 directly captures heterochromatin-associated transcripts and targets them for degradation.

The fission yeast *S. pombe* harbors four chromodomain proteins that are known to recognize H3K9 methylation, including two HP1-like proteins, Swi6^{HP1} and Chp2^{HP1}, which have largely nonoverlapping activities that contribute to heterochromatic silencing. Chp2^{HP1} acts to silence heterochromatin at the transcriptional level. In contrast, Swi6^{HP1} has been implicated as associating with a variety of chromatin-modifying factors and, unlike Chp2^{HP1}, associates with RNA in vivo. Swi6^{HP1} is presumed to be largely involved in the co- or posttranscriptional processing of heterochromatic transcripts rather than acting as a barrier to prevent transcription itself (Motamedi et al., 2008).

Until recently, it was not known whether Swi6^{HP1} associates with RNA directly or through an intermediary protein. Keller et al. (2012) demonstrated that recombinant Swi6^{HP1}, like HP1 isoforms in other organisms (Muchardt et al., 2002), binds RNA directly in vitro primarily through the hinge domain, with contributions from other regions including the chromodomain. Mutation of positively charged residues within the hinge (Swi6-KR25A) disrupted the association of RNA with Swi6^{HP1} in vivo. The mutant protein was still capable of being recruited to heterochromatin by its affinity for H3K9

methylation (which was unaffected by these mutations), but was not competent for silencing. Thus, RNA-binding activity does not target Swi6^{HP1} to heterochromatin. Instead, binding of transcripts to Swi6^{HP1} appears to be an early step in their pathway to destruction.

What does Swi6^{HP1} do with RNA once estranged from chromatin? Keller et al. present evidence that Swi6^{HP1} prevents the translation of transcripts, possibly by retaining them in the nucleus, and instead "passes" transcripts into the exosome and RNAi degradation pathways (Figure 1). The authors note that there is no known biochemical feature of heterochromatic transcripts that signals for their destruction. They suggest a model where association with Swi6^{HP1} may "mark" the RNA for degradation. However, artificially tethering Swi6^{HP1} to transcripts is not sufficient to induce silencing. Therefore, while Swi6^{HP1} seems to act early in this pathway, much remains unclear, such as how Swi6^{HP1} feeds RNA into degradation pathways. What other factors, in addition to the Cid14 polyadenylase, contribute to this process?

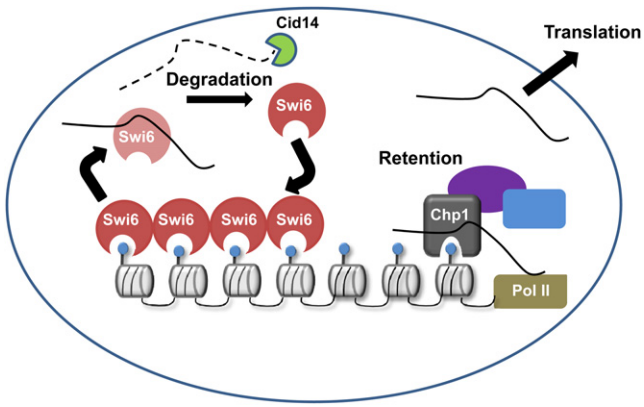

Figure 1. Alternative Fates for Heterochromatic Transcripts
Capture by Swi6^{HP1} leads to eviction from chromatin and degradation mediated by Cid14, capture by Chp1 or chromatin-bound Clr4^{Suv39} leads to retention on chromatin, and failure to be "caught" by chromodomain proteins allows exit from the nucleus and translation.

Perhaps the most intriguing finding of this work is that, contrary to prior speculation that Swi6^{HP1} may bind RNA and H3K9 methylation simultaneously and thus act as a tether of nascent transcripts to chromatin, RNA actually impedes the binding of Swi6^{HP1} to H3K9 methylation in vitro. This implies that binding to spurious transcripts disengages Swi6^{HP1} from chromatin, rather than stabilizing it. Furthermore, the authors convincingly argue against a role of Swi6^{HP1} as a structural component of heterochromatin by reaffirming its dynamic interaction with the chromosome.

In a contrasting study, Ishida et al. (2012) demonstrate that the two other H3K9me binding chromodomain proteins in fission yeast, Chp1 and Clr4^{Suv39}, the homolog of Suv39 proteins, have the propensity to bind RNA by their chromodomains. This activity is enhanced, however, or in the case of Clr4^{Suv39}'s chromodomain, only revealed, when the chromodomain is also bound to H3K9me2. Thus, for Chp1 and Clr4^{Suv39}, which are required for the establishment of heterochromatin, chromatin-bound proteins exhibit stronger RNA binding activity than the free forms, suggesting that the heterochromatin-bound proteins tether heterochromatic transcripts to heterochromatin (Figure 1).

Very interestingly, Ishida et al. generated two separation-of-function mutants in Chp1's chromodomain that accumulate centromeric transcripts to similar levels but which, viewed in the light of the Keller et al. results, exhibit distinct fates for the transcripts. One Chp1 mutant (αmut1), which associates with centromeric chromatin but is incapable of binding to RNA, allows efficient translation of centromeric heterochromatin reporter transcripts into protein. A second Chp1 mutant (W44A), which retains RNA binding activity but cannot bind H3K9me2, shows defective translation of reporter gene transcripts. This second mutant exhibits properties similar to those ascribed to Swi6 by Keller et al. (2012), raising the possibility that this mutant Chp1 is now functioning like Swi6, binding transcripts off chromatin and passing them on for destruction. Alternatively, mislocalization of Chp1 may allow Swi6 to bind centromeric transcripts.

Chromodomain proteins are present at all heterochromatic loci in fission yeast, but the cellular abundance and affinity for binding chromatin are distinct, which may set up competition between different proteins for binding to heterochromatic transcripts and result in different outcomes. Swi6 is more abundant than the other proteins and shows the lowest affinity for binding H3K9me2/3, whereas Chp1 is relatively rare and has high affinity for H3K9me (Schalch et al., 2009). Perhaps the fate of transcripts at different loci also differs—the Keller study focuses on the mating type and telomeres, whereas Ishida's study focuses on centromeres. Experiments designed to explain how the various chromodomain proteins cooperate to bind chromatin and RNA at different regions of the genome will be important for developing an integrated model for how they function.

The research of Keller and Ishida and colleagues raises questions about the role of chromodomain proteins in RNA binding and processing in fission yeast and higher eukaryotes alike. It seems likely that behaviors of various HP1 isoforms and chromodomain bearing proteins such as Polycomb can be partially explained by their differential ability to bind RNA and how this binding affects their canonical interaction with methylated histone H3 (Bernstein et al., 2006). Further complexity can be assumed because of the incorporation of many chromodomain proteins into larger complexes that include other RNA-binding and processing activities (Verdel et al., 2004; Hong et al., 2005). Recent research suggests that HP1 proteins can function within euchromatin to regulate splicing and elongation (Vakoc et al., 2005; Saint-André et al., 2011). It will be interesting to know whether there is similar interplay between RNA and chromatin binding in these instances.

REFERENCES

Bernstein, E., Duncan, E.M., Masui, O., Gil, J., Heard, E., and Allis, C.D. (2006). Mol. Cell. Biol. *26*, 2560–2569.

Hong, E.J., Villén, J., Gerace, E.L., Gygi, S.P., and Moazed, D. (2005). RNA Biol. *2*, 106–111.

Ishida, M., Shimojo, H., Hayashi, A., Kawaguchi, R., Ohtani, Y., Uegaki, K., Nishimura, Y., and Nakayama, J.-I. (2012). Mol. Cell *47*, this issue, 228–241.

Keller, C., Adaixo, R., Stunnenberg, R., Woolcock, K.J., Hiller, S., and Bühler, M. (2012). Mol. Cell *47*, this issue, 215–227.

Motamedi, M.R., Hong, E.J., Li, X., Gerber, S., Denison, C., Gygi, S., and Moazed, D. (2008). Mol. Cell *32*, 778–790.

Muchardt, C., Guilleme, M., Seeler, J.S., Trouche, D., Dejean, A., and Yaniv, M. (2002). EMBO Rep. *3*, 975–981.

Saint-André, V., Batsché, E., Rachez, C., and Muchardt, C. (2011). Nat. Struct. Mol. Biol. *18*, 337–344.

Schalch, T., Job, G., Noffsinger, V.J., Shanker, S., Kuscu, C., Joshua-Tor, L., and Partridge, J.F. (2009). Mol. Cell *34*, 36–46.

Vakoc, C.R., Mandat, S.A., Olenchock, B.A., and Blobel, G.A. (2005). Mol. Cell *19*, 381–391.

Verdel, A., Jia, S., Gerber, S., Sugiyama, T., Gygi, S., Grewal, S.I., and Moazed, D. (2004). Science *303*, 672–676.

TOR-tured Yeast Find a New Way to Stand the Heat

J. Ross Buchan,[1,2] Andrew P. Capaldi,[3] and Roy Parker[1,2,*]
[1]Howard Hughes Medical Institute
[2]Department of Chemistry and Biochemistry, University of Colorado Boulder, Boulder, CO 80309, USA
[3]Department of Molecular and Cellular Biology, University of Arizona, Tuscon, AZ 85721, USA
*Correspondence: roy.parker@colorado.edu
http://dx.doi.org/10.1016/j.molcel.2012.07.005

In this issue, Takahara and Maeda (2012) discover that together, Pbp1 and sequestration of the TORC1 complex in cytoplasmic mRNP stress granules provides a negative regulatory mechanism for TORC1 signaling during stress.

The TOR kinase, as part of TOR complex 1 (TORC1), is a central regulator of cell growth in eukaryotes with effects on cancer development, aging, and metabolism. In optimal conditions, TORC1 drives mass accumulation by promoting protein synthesis while repressing catabolic pathways such as autophagy (Figure 1A). However, in the absence of growth hormones, or during stress or starvation, TORC1 is inactivated, limiting growth. A key issue is how TORC1 is regulated. Several pathways stimulate TORC1 in response to growth factors, including the PI3 kinases, AKT, ERK, and the tuberous sclerosis proteins TSC1/TSC2, which are all regulators of tumor progression. Insight has also recently emerged into how TORC1 is controlled by stress and nutrients. For example, TORC1 is activated by small GTPases, called Rags, in part through recruitment to the vacuolar membrane (Figure 1A). Strikingly, the Rag GTPases are only activated when leucine levels are high as sensed by the leucyl transfer RNA synthase (Bonfils et al., 2012). In contrast, during stress or nitrogen starvation, another small GTPase located on the vacuolar membrane, Rho1, transiently binds to TORC1, releasing it from the membrane and triggering its inactivation (Yan et al., 2012) (Figure 1B). In this issue of *Molecular Cell*, work from Takahara and Maeda (2012) now suggest that TORC1 is also repressed during stress by sequestration into cytoplasmic messenger ribonucleoprotein (mRNP) aggregates known as stress granules (Figure 1B).

The authors first identify a link between stress granule formation and TOR when they find that in *Saccharomyces cerevisiae*, overexpression of Pbp1 suppresses growth defects caused by a hyperactive TOR allele and reduces the recovery of TOR activity during alleviation of nitrogen or glucose starvation. Pbp1 and its human ortholog Ataxin-2 both promote stress granule formation and have roles in regulating messenger RNA (mRNA) function (Nonhoff et al., 2007; Buchan et al., 2008). Stress granules are conserved cytoplasmic aggregates of nontranslating mRNPs in association with some translation initiation factors and mRNA binding proteins (Buchan and Parker, 2009). Stress granules are typically observed under conditions, such as stress, in which translation initiation is limited and nontranslating mRNPs accumulate and aggregate. The function of mRNP aggregation into stress granules is not fully understood, but it is suggested to regulate mRNA translation and degradation, as well as to affect signaling pathways. Such functions are consistent with stress granule formation correlating with better survival during stress (Kwon et al., 2007; Eisinger-Mathason et al., 2008).

Takahara and Maeda's main argument, that sequestration of TORC1 in stress granules is inhibitory for TORC1 function, is supported as follows: First, the authors show that Kog1 (a TORC1 subunit) and Tor1 can localize in stress granules and coimmunoprecipitate with Pbp1. Second, they demonstrate that the ability of Pbp1 to downregulate TOR signaling, coimmunoprecipitate with TORC1, and recruit TORC1 into stress granules depends on Pbp1's ability to self-associate, which is also necessary for Pbp1 to both localize within and promote assembly of stress granules. Third, kinetic analysis showed that recovery of TOR signaling after stress correlates with its exit from stress granules, while genetic and chemical approaches that alter stress granule